



HAL
open science

Shedding light on the mechanisms of tumor formation linked to BRCA2 using two known pathogenic variants

Anna Minello

► **To cite this version:**

Anna Minello. Shedding light on the mechanisms of tumor formation linked to BRCA2 using two known pathogenic variants. Cancer. Université Paris-Saclay, 2023. English. NNT : 2023UPASL135 . tel-04925290

HAL Id: tel-04925290

<https://theses.hal.science/tel-04925290v1>

Submitted on 2 Feb 2025

HAL is a multi-disciplinary open access archive for the deposit and dissemination of scientific research documents, whether they are published or not. The documents may come from teaching and research institutions in France or abroad, or from public or private research centers.

L'archive ouverte pluridisciplinaire **HAL**, est destinée au dépôt et à la diffusion de documents scientifiques de niveau recherche, publiés ou non, émanant des établissements d'enseignement et de recherche français ou étrangers, des laboratoires publics ou privés.

Shedding light on the mechanisms of tumor formation linked to BRCA2 using two known pathogenic variants

Mise en évidence des mécanismes de formation tumorale associés à BRCA2, en utilisant deux variants pathogènes connus

Thèse de doctorat de l'université Paris-Saclay

École doctorale n° 582 cancérologie : biologie - médecine - santé (CBMS)
Spécialité du doctorat: Sciences du cancer
Graduate School: Life Sciences and Health, Référent: Faculté de médecine

Thèse préparée dans l'unité de recherche **Intégrité du Génome, ARN et Cancer, (Université Paris-Saclay, CNRS)**, sous la direction de **Aura CARREIRA**, chercheuse

Thèse soutenue à Paris-Saclay, le 11 décembre 2023, par

Anna MINELLO

Composition du Jury

Membres du jury avec voix délibérative

Dominique STOPPA-LYONNET

Professeur des universités
Praticien hospitalier,
Institut Curie, Paris (FR)

Présidente

Josée GUIROUILH-BARBAT

Chercheuse statutaire,
Institut Cochin, Paris (FR)

Rapportrice & Examinatrice

Maaïke VREESWIJK

Associate professor,
Universiteit Leiden (NL)

Rapportrice & Examinatrice

Charles THEILLET

Directeur de recherche, Institut
de Recherche en Cancérologie
de Montpellier (FR)

Examineur

Filippo ROSSELLI

Directeur de recherche,
Institut Gustave Roussy, Paris (FR)

Examineur

Titre : Mise en évidence des mécanismes de formation tumorale associés à BRCA2, en utilisant deux variants pathogènes connus

Mots clés : Haploinsuffisance, BRCA2, Instabilité génomique, Suppresseur de tumeurs, Réparation de l'ADN - Formation de tumeurs

Résumé : L'intégrité du génome de la cellule eucaryote est constamment menacée par des lésions de l'ADN causées soit par des facteurs externes, soit par le métabolisme cellulaire. Ces dommages pouvant avoir des conséquences néfastes, les cellules disposent de divers mécanismes de réparation des dommages de l'ADN : parmi eux, la recombinaison homologue (HR) est l'un des plus importants, car elle effectue une réparation de haute-fidélité des cassures double brin de l'ADN (DSB), des liaisons croisées inter-brins (ICL) ainsi que des lésions de l'ADN générées pendant la réplication en utilisant une séquence identique (la chromatide sœur) comme modèle. BRCA2 est une protéine suppresseur de tumeurs essentielle au maintien de l'intégrité du génome grâce à son rôle clé dans la voie de la HR. Par conséquent, les mutations mono-alléliques héréditaires de BRCA2 prédisposent au cancer du sein et de l'ovaire. Alors que les effets délétères de la déficience de BRCA2 sont connus, notamment les défauts de la HR, le stress réplicatif et l'accumulation de ponts d'ADN simple brin (ssDNA gaps), les mécanismes de formation des tumeurs chez les porteurs de mutations de BRCA2 restent mal définis. L'inactivation de l'allèle sauvage (perte d'hétérozygotie, LOH) semble être cruciale pour la carcinogenèse des cellules mutées de BRCA2. Cependant, certains cancers conservent le deuxième allèle intact, suggérant une haplo-insuffisance de BRCA2. Pour répondre à cette question, nous avons édité génétiquement deux lignées cellulaires isogéniques épithéliales mammaires non tumorales, chacune portant un variant pathogène mono-allélique de BRCA2.

L'analyse par RNA-seq a révélé que le variant c.771-775del (del5) de BRCA2 avait un impact minimal sur l'expression génique tandis que le deuxième, le c.5946del (delT), entraînait des changements transcriptomiques substantiels, notamment la régulation négative de gènes liés à l'adhésion cellulaire. Les essais en soft-agar ont révélé que cette lignée avait une capacité accrue à former des colo-

nies de manière indépendante de l'ancrage, indiquant un phénotype invasif, en accord avec les changements d'expression génique observés. Les cellules portant le variant del5 présentaient des niveaux protéiques réduits à la fois de BRCA2 et de son effecteur clé, RAD51. Cette réduction corrèle avec des déficiences dans la réparation médiée par la HR et avec une sensibilité accrue aux inhibiteurs de PARP (PARPi) et au traitement à la Mitomycine C (MMC). De plus, les cellules +/-del5 ont accumulé des ssDNA gaps en réponse au stress réplicatif induit par le PARPi, suggérant une instabilité génomique persistante dans cette lignée.

Ensuite, pour comparer les deux variants dans un contexte tumoral, nous avons analysé, par séquençage complet du génome (WGS), des échantillons d'ADN de tumeurs mammaires primaires et de tissus non néoplasiques adjacents. De manière surprenante, malgré les différences observées dans les cellules porteuses de mutations hétérozygotes de BRCA2, nous avons observé des profils génomiques similaires, indicatifs d'une déficience en recombinaison homologue (HRD) dans les deux cohortes de tumeurs. De plus, lorsque nous avons analysé la proportion de tumeurs ayant subi une LOH de BRCA2, nous avons trouvé des fréquences différentes entre les deux cohortes, suggérant une pression sélective différente pour cet événement dans les tumeurs.

En conclusion, notre travail suggère que différents variants pathogènes mono-alléliques de BRCA2 conduisent à des profils transcriptomiques et phénotypiques différents. Ces disparités pourraient potentiellement expliquer la fréquence variable de LOH dans les tumeurs, tandis que leur signature mutationnelle est principalement attribuée à une HRD. Ceci pourrait avoir des implications cliniques significatives, affectant la réponse des tumeurs associées à BRCA2 aux traitements chimiothérapeutiques comme les PARPi, qui se sont avérés plus efficaces dans les cellules subissant une LOH de BRCA2.

Title: Shedding light on the mechanisms of tumor formation linked to BRCA2 using two known pathogenic variants

Keywords: Haploinsufficiency, BRCA2, Genomic instability, Tumor suppressor, DNA repair, Tumor formation

Abstract: The genome integrity of the eukaryotic cell is constantly threatened by DNA lesions, caused by external factors or endogenous by-products of cellular metabolism. As those damages could lead to harmful consequences, cells are provided with several DNA damage repair mechanisms: among them, homologous recombination (HR) is one of the most important as it operates a high-fidelity repair of DNA double-strand breaks (DSBs), inter-strand crosslinks (ICLs) and replicative DNA lesions using an identical sequence (the sister chromatid) as a template.

BRCA2 is a tumor suppressor protein essential for maintaining genome integrity, especially through its key role in the HR pathway. As such, inherited BRCA2 mono-allelic mutations confer predisposition to breast and ovarian cancer. While the deleterious effects of BRCA2 deficiency are known, including HR defects, replication stress, and ssDNA gaps accumulation, the mechanisms driving tumor formation in BRCA2 mutation carriers remains ill defined. The inactivation of the wild-type allele (loss of heterozygosity, LOH) appears to be crucial for BRCA2-mutated cell carcinogenesis. Nonetheless, some cancers retain an intact second allele, suggesting that cells with a BRCA2 mono-allelic mutation may display a distinct genome instability phenotype, thereby pointing to BRCA2 haploinsufficiency.

To address this question, we gene-edited two non-tumoral breast epithelial isogenic cell lines, each bearing a common truncating pathogenic mono-allelic BRCA2 variant.

Using RNA-seq analysis, we demonstrated that the c.771-775del (del5) variant had a minimal impact on gene expression whereas the c.5946del (delT) variant led to substantial transcriptomic changes, notably the downregulation of cell adhesion-related genes. Soft agar assays revealed an increased ability of the

latter to form colonies in an anchorage-independent manner, indicating an invasive phenotype, consistent with the gene expression changes observed.

In stark contrast, +/del5 cells exhibited reduced levels of both BRCA2 and its key downstream effector, RAD51. This correlated with deficiencies in HR-mediated repair and increased sensitivity to PARP inhibitors (PARPi) and Mitomycin C (MMC) treatment. Furthermore, +/del5 cells accumulated ssDNA gaps in response to replication stress induced by PARPi, suggesting an ongoing genomic instability in this clone.

Next, to compare the two variants in a tumor context, we analyzed the mutational pattern of DNA samples from primary breast tumors and non-neoplastic matched surrounding tissue bearing the same variants by Whole-Genome Sequencing (WGS). Surprisingly, despite the differences observed in cells with heterozygous BRCA2 mutations, we observed similar mutational profiles indicative of HR deficiency (HRD) in both sets of tumors. Interestingly, when we analyzed the proportion of tumors that underwent BRCA2 LOH, we found different frequencies between the two cohorts suggesting different selective pressure for this event to occur in the two sets of tumors.

In conclusion, our work suggests that different BRCA2 pathogenic variants in heterozygosity lead to different transcriptomic and phenotypic outcomes. These differences potentially explain the variable frequency of LOH in tumors while suggesting that HRD is a predominant driver of BRCA-mutated cancer. Our findings could have significant clinical implications, for example, in predicting the response of BRCA2-associated tumors to chemotherapeutic drugs like PARPi, shown to be more efficient in cells undergoing LOH.

INDEX

List of figures	12
Chapter 1 – Introduction.....	13
1. Challenges to genome stability.....	13
1.1. DNA damage	13
1.1.1. Sources of DNA damage.....	14
1.1.2. Repair of ssDNA damage	15
1.1.3. Single-strand break repair (SSBR).....	18
1.1.4. Double-Strand Break (DSB) repair	20
1.2. Replication stress	31
1.2.1. The eukaryotic DNA replication process.....	31
1.2.2. Source of replication stress	33
1.2.3. Mechanisms of resolution of replication stress.....	38
2. BRCA2, the custodian of genome integrity	42
2.1. The tumor suppressor BRCA2	42
2.2. BRCA2 structure, functional domains and interactors	43
2.3. BRCA2 functions	46
2.3.1. HR-dependent functions.....	46
2.3.2. Non-canonical functions	48
2.4. HR, FP, and GS in cancer therapy	49
2.5. BRCA2 variants and cancer predisposition	50
3. BRCA2 haploinsufficiency	53
3.1. The two-hit model and the BRCA paradox	53
3.2. Evidence of locus-specific LOH from BRCA-mutated tumors.....	54
3.3. Molecular evidence and mechanisms of BRCA2 haploinsufficiency.....	56
Chapter 2 – Objectives and Results.....	59
1. Hypothesis	59

2. Preliminary data.....	59
3. Objectives	62
4. Results	64
OBJECTIVE 1: Explore the impact of two different mono-allelic pathogenic variants of BRCA2 on the transcriptome of breast epithelial cells.....	64
OBJECTIVE 2: Functional characterization of BRCA2 +/-del5 and +/-delT breast epithelial cell lines	68
OBJECTIVE 3: Reveal the genomic changes induced by two different truncating variants in BRCA2-mutated tumors.....	80
Chapter 3 – Discussion	84
Perspectives.....	89
References.....	91
Material and Methods	115
Synthèse:	137
Appendix.....	139

“As you set out for Ithaka
hope your road is a long one,
full of adventure, full of discovery.
Laistrygonians, Cyclops,
wild Poseidon—you won’t encounter them
unless you bring them along inside your soul,
unless your soul sets them up in front of you.
Hope your road is a long one.
Keep Ithaka always in your mind.
Arriving there is what you’re destined for.
But don’t hurry the journey at all.
Better if it lasts for years,
so you’re old by the time you reach the island,
wealthy with all you’ve gained on the way,
not expecting Ithaka to make you rich.
Ithaka gave you the marvelous journey.”

Adapted from “Ithaka”, Costantino Kavafis

Acknowledgements

As my doctoral journey comes to an end, I would like to acknowledge to all those who contributed to make it possible. I am afraid the list is quite long.

Tout d'abord, je tiens à exprimer ma gratitude au ministère de l'Enseignement Supérieur pour la bourse de 3 ans et à la Fondation pour la Recherche Médicale (FRM) pour avoir financé ma dernière année.

Next, I would like to thank all the members of my PhD jury who kindly accepted the task of evaluating my work. A special acknowledgment goes to Dominique Stoppa-Lyonnet, who consistently offered valuable help to this project and advice during my thesis committees.

I want to express my gratitude to Aura, who trusted me with the responsibility of this research project. Aura, you have been understanding, always available to answer my questions, and an exceptional mentor, even despite the geographical distance in recent years. Thank you for the countless times you provided reassurance and relieved stress when things didn't go as planned. A big thank you is also due to all the current members of the Carreira team and to Jesus Gomez for his significant contributions to this PhD project. I cannot forget to mention Rady, the tornado of the lab. Daily life in Orsay became much more enjoyable with your presence, and the shared anecdotes we have created in and out of the lab are countless.

Thanks to all the former members of the team. It's a bit challenging to categorize some of you solely as colleagues. Tania, one of the kindest people I have met, with whom I felt instantly "a casa". Isaac, your availability toward others left a lasting impression on me, along with your expertise in handling proteins and your talent for inventing jokes. Jenny, thank you for always providing honest advice that I truly trust and for instilling me self-confidence. Comment ne pas mentionner Charlotte, une incroyable lab manager, toujours disponible, même maintenant qui es partie – à l'étage – mais continue à me prodiguer des conseils et à m'aider avec toutes mes péripéties cotidiennes.

Thanks to all the collaborators that contributed significantly to this project: the CRB of I. Curie, Anne-Vincent Salomon, Elodie Girard and Nicolas Servant, Matthias Altmeyer and Antonio Galarreta, Serena Nik-Zainal and Yasin Memari, Stefán Sigurðsson and Maria-Rose Bustos.

Depuis un an, je partage mon quotidien au lab avec de nouveaux collègues, Tristan, Thibaud et Kevin. Merci à vous pour les bons moments passés ensemble, pour votre disponibilité, et tous les fous rires. Géraldine, même si tu n'es pas vraiment nouvelle, je suis ravie de partager mon quotidien avec toi. Merci pour ta douceur et ta sensibilité, et pour tout ce que tu as fait pour moi même si je ne fais pas partie de ton équipe.

Un grand merci à Stephan Vagner, le directeur de l'UMR3348, qui a rendu possible l'achèvement de mon travail au sein de l'Unité. Naturellement, cela n'aurait pas été

possible sans Reini Luco, qui s'est montrée très accommodante en partageant des espaces avec moi. Merci aussi à la directrice adjointe Sarah Lambert, qui est également devenue ma superviseuse administrative. Merci à Sarah et Reini pour votre gentillesse et vos précieux conseils, scientifiques et non.

Comment ne pas remercier tous les membres de l'unité, que je considère depuis un an comme une grande équipe. Merci à toute l'équipe Lambert, avec une mention spéciale pour Kamila et Shrena : thank you for always welcoming me for nice discussions in your office ! Shrena, next to you I feel the funniest person in the world, and for this I will be forever grateful. Kamila, sharing these years with you has been an absolute pleasure. Your friendship has been a constant source of joy, laughter, and a safe space for sharing both highs and lows. Thanks for embracing spontaneity, ignoring judgment, and letting me be completely authentic—like our unforgettable adventure taking a train to explore Toulon!

Merci aux personnes qui ont rendu mes déjeuners très agréables : Pascale, tu n'es pas seulement une des personnes les plus drôles que je connaisse, mais avec Laurence, vous êtes des gestionnaires incroyables et très patientes. Merci à Anne, qui, entre autres, a significativement contribué à enrichir ma connaissance de la géographie de la France. Je voudrais également exprimer ma gratitude envers Laetitia et Charlène pour leur gentillesse et leur patience, et envers Joao, car il n'y a pas un jour où je suis rentré au laboratoire sans qu'avec son sourire et son « ça va ? » ne m'aient mis de bonne humeur. Je voudrais aussi remercier des anciens collègues : Aude, ton dynamisme et ta curiosité m'ont beaucoup inspiré, c'est probablement grâce à toi que j'ai postulé pour une thèse. Thanks to Daniele, Camille, Marie et Hatice who helped me growing as a scientist when I was just a "baby" M2.

Infine, l'ultima parte è destinata a tutto il mio inner circle e sarà scritta in italiano così "almeno capisco qualcosa della tesi" (cit.). Grazie mamma e papà per il vostro supporto quotidiano a distanza. Grazie a Giacomo, all'apparenza un life advisor molto serio e autorevole, ma ai miei occhi per sempre il mio fratellino. Grazie a tutta la mia grande famiglia italiana, zii, cugini: senza saperlo avete contribuito a rendere i soggiorni in Italia molto divertenti, e sì, le sagre sono state di grande aiuto. Grazie ad Alice e Martina: è incredibile come la nostra amicizia nata tra le esercitazioni in lab all'UniTS non solo non sia fermata ma continui più solida che mai, nonostante siamo sparpagliate per l'Europa. Sono molto fiera di noi. Grazie a Beatrice e Matteo, i miei real compagni fedeli fin dall'adolescenza, sempre al mio fianco a gioire per i bei momenti e cercare di ridere dei brutti. Grazie a Camilla per continuare a essere al mio fianco fin dai banchi del liceo. Grazie a Seed e gli altri amici del Doppio Diploma per aver reso il trasferimento a Parigi meno traumatico e ricco di bei ricordi. Merci à Christophe, pour sa compagnie avec ses podcast « Hondelatte raconte » pendant les trajets en RER. Et enfin, un merci particulier à l'autre, mon Christophe. Merci de croire en moi bien plus que je ne le fais moi-même, d'être mon plus grand soutien, ma source de « heuresité » même dans les moments les plus sombres. Je ne sais pas ce que l'avenir nous réserve, mais je suis certaine que je ne voudrais pas le vivre aux côtés de quelqu'un d'autre.

Abbreviations

53BP1: P53 Binding Protein 1

Alt-EJ: Alternative End Joining

AP: Apurinic/Apyrimidinic

APE1: AP Endonuclease 1

APLF: Aprataxin and PNK-Like Factor

ATM: Ataxia Telangiectasia-Mutated

ATR: Ataxia Telangiectasia and Rad3 Related

ATRIP: ATR-Interacting Protein

BARD1: BRCA1-Associated RING Domain 1

BER: Base excision repair

BIR: Break-Induced Replication

BLM: Bloom Syndrome Protein

BRCA1: Breast Cancer Susceptibility Protein 1

BRCA2: Breast Cancer Susceptibility Protein 2

C-DBD: C-Terminal DNA Binding Domain

CDK: Cyclin-dependent kinase

CFS: Common fragile sites

CMG: CDC45-MCM2-7-GINS complex

cNHEJ: Canonical Non-Homologous End Joining

CTD: C-Terminal Domain

CS: Cockayne Syndrome

CtIP: Ctbp-Interacting Protein

DDR: DNA Damage Response

DDT: DNA Damage Tolerance

DDX5: DEAD-Box Helicase 5

DEGs: Differentially Expressed Genes

dHJ: Double Holliday Junction

DMC1: DNA Meiotic Recombinase 1

DNA-PK: DNA-Dependent Protein Kinase

DPC: DNA protein crosslink

DSB: Double-Strand Break

dsDNA: Double-Stranded DNA

ER: Estrogen Receptor

ERCC: Excision Repair Cross Complementing –

EXO1: Exonuclease 1

FA: Fanconi Anemia

FEN1: Flap Structure-Specific Endonuclease 1

FP: Fork Protection

FR: Fork Reversal

GG-NER: global genome NER

GO: Gene Ontology

GS: Gaps Suppression

HD: Helical Domain

HER2: Human Epidermal growth factor Receptor 2

HR: Homologous Recombination

HRD: Homologous recombination deficiency

HU: Hydroxyurea

ICL: Inter-Strand Crosslink

IR: Ionizing Radiation

LOH: Loss Of Heterozygosity

LIG: Ligase

MCM: Minichromosome maintenance

MMC: Mitomycin C

MMR: Mismatch repair

MMS: Methyl methanesulfonate

MRN: MRE11-RAD50-NBS1 complex

MS: Microsatellite

N-DBD: N-Terminal DNA Binding Domain

NER: Nucleotide excision repair

NTD: N-Terminal Domain

NLS: Nuclear Localization Signal

OB Folds: Oligonucleotide /Oligosaccharide Binding Folds

PARG: PAR Glycohydrolase

PARP1: Poly ADP-Ribose Polymerase 1

PARPi: PARP Inhibitor

PARylation: Poly-ADP-Ribosylation

PCA: Principal Component Analysis

PCNA: Proliferation Cell Nuclear Antigen Protein

PLK1: Polo-Like Kinase 1

PNKP: Polynucleotide Kinase 3'-Phosphatase

PR: Progesterone Receptor

pre-RC: pre-replicative complex

RNAP II: Rna Polymerase II
RNR: Ribonucleotide Reductase
ROS: Reactive Oxygen Species
RF: Replication Fork
RPA: Replication Protein A

SBS: Single Base Substitution
SDSA: Synthesis Dependent Strand Annealing
SSA: Single-Strand Annealing
SSB: Single-strand break
ssDNA: Single-Stranded DNA

TC-NER: transcription-coupled NER
TDP1: Tyrosyl-DNA Phosphodiesterase 1
TFIIH: Transcription Initiation Factor IIH
TLS: Translesion Synthesis
TNBC: Triple-Negative Breast Cancer
TOP1: Topoisomerase 1
TOP1cc: TOP1 Cleavage Complexes
TS: Template Switching
TS: Tumor Suppressor

UV: Ultraviolet

WGS: Whole Genome Sequencing

XP: Xeroderma Pigmentosum
XRCC: X-Ray Repair Cross-Complementing

List of figures

Introduction

- Figure 1. Sources of DNA damage, related lesions, and their main repair pathways
- Figure 2. Mismatch Repair (MMR) and Base Excision Repair (BER) pathways
- Figure 3. Nucleotide Excision Repair (NER) and Single-Strand Break Repair (SSBR) pathways
- Figure 4: Detection, signaling, and consequences of DNA double-strand breaks (DSBs)
- Figure 5. Sub-pathways of homologous recombination
- Figure 6. Overview of the DSB repair pathways
- Figure 7. Overview of the eukaryotic DNA replication
- Figure 8. Sources of replication stress
- Figure 9. Inter-strand crosslink (ICL) repair pathway
- Figure 10. DNA damage tolerance (DDT) mechanisms at replication forks
- Figure 11. BRCA2 functional domains and main interacting partners
- Figure 12. Overview of BRCA2 HR-dependent and non-canonical functions
- Figure 13. Schematic of cancer risk depending on BRCA2 mutation location
- Figure 15. Overview of key findings supporting the BRCA2 haploinsufficiency hypothesis

Results and discussion

- Figure 1. Two different mono-allelic BRCA2 truncating pathogenic variants resulted in distinct transcriptomic profile
- Figure 2. The mono-allelic BRCA2 delT mutation induces deregulation of cell migration-related pathways in MCF10A cells
- Figure 3. Transcriptomic analysis of familial breast tumors bearing the BRCA2 delT mutation
- Figure 4. The BRCA2 +/-delT clone show increased cell invasion ability
- Figure 5. The +/-delT clone shows increased BRCA2 WT protein levels
- Figure 6. The +/-del5 clone shows increased sensitivity to PARPi and MMC treatment
- Figure 7. +/-del5 cells show HR defects and accumulate PARPi-induced ssDNA gaps
- Figure 8. Breast tumors bearing the BRCA2 delT or del5 variant show HRD mutational signature
- Figure 9. Breast tumors bearing the BRCA2 delT variant show increased frequency of locus-specific LOH
- Figure 10. Proposed model of tumorigenesis for distinct BRCA2 germline pathogenic variants

Chapter 1 – Introduction

Genome integrity maintenance is vital for cell survival, as its loss can result in genome instability, a hallmark of cancer (Hanahan & Weinberg, 2011). To avoid this scenario, eukaryotic cells are equipped with several mechanisms, sensing and repairing lesions that spontaneously generate. In this first chapter, I will delve into the sources of DNA damage and replication stress, which are closely connected as one can trigger the other, and how cells deal with them. Then I will focus on BRCA2, the central topic of my PhD project, describing its multifaceted role in genome integrity maintenance, including its functions at the replication fork and in DNA repair. Additionally, I will examine genetic mutations within the BRCA2 gene and their connection to an increased risk of cancer, particularly in breast cancer. Lastly, I will discuss about the mounting evidence pointing out BRCA2 haploinsufficiency, a concept that challenges conventional understanding of tumor formation related to germline mutations in this gene.

1. Challenges to genome stability

1.1. DNA damage

Maintaining genomic integrity is crucial for the survival of all organisms. DNA, carrying essential instructions for cellular functions, must be faithfully replicated to transmit error-free genetic material to the next generation of cells. However, eukaryotic cells encounter approximately 1×10^5 DNA lesions daily (Hoeijmakers, 2009), originating both from endogenous and exogenous sources and posing a threat for genomic stability. Consequently, cells have evolved the DNA damage response (DDR), an intricate cellular network that senses, signals, and promotes DNA repair, while also regulating cell-cycle progression and programmed cell death in cases of severe DNA damage (Harper & Elledge, 2007). DDR and DNA repair proteins coordinate in a tight spatio-temporal organization, ensuring the precise action of repair enzymes in a lesion-specific manner (**Fig. 1**). The critical role of DDR factors is underscored by the fact that mutations in these genes can lead to a large variety of diseases and cancer-predisposition syndromes (Ciccia

& Elledge, 2010). Conversely, targeting specific DDR factors in tumors has set the basis for synthetic-lethal treatment strategies (Bryant et al., 2005; Farmer et al., 2005).

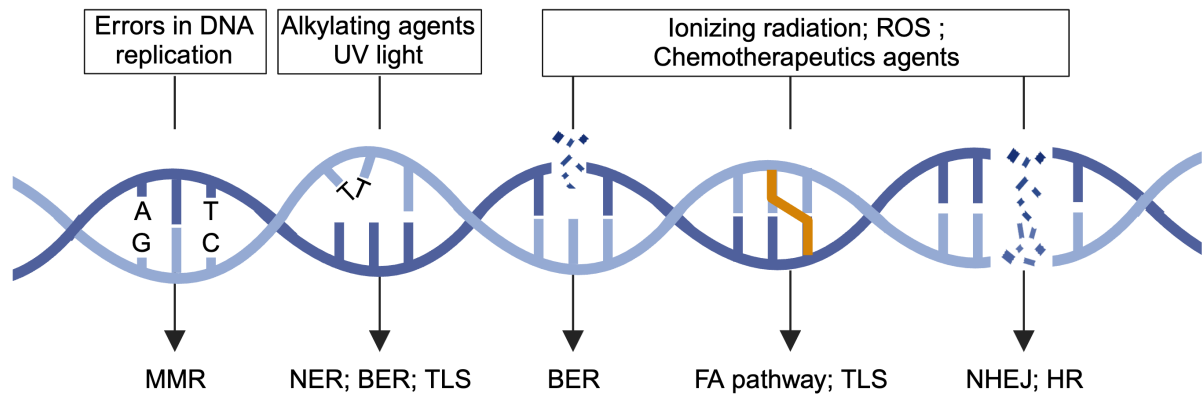


Figure 1. Sources of DNA damage, related lesions, and their main repair pathways.

Common sources of DNA damage, both exogenous and endogenous, are presented in the top boxes, with corresponding lesions illustrated on the double helix. The repair pathways specific to each type of lesion are indicated by the arrows at the bottom. Created with BioRender.com.

1.1.1. Sources of DNA damage

Spontaneous DNA damage can arise from various cellular processes. For example, hydrolysis reactions can create abasic sites and trigger deamination, a highly mutagenic process responsible for C > T and A > G transitions (Greenberg, 2014). Moreover, DNA replication itself contributes to DNA damage as the replicative polymerase can occasionally incorporate the wrong nucleotide into the growing strand. If left uncorrected, these errors become permanent mutations passed on to daughter cells. Additionally, reactive metabolites like reactive oxygen species (ROS) generated by mitochondria and peroxisomes can cause extensive genome damage, including base oxidation and DNA single-strand breaks (Cadet & Davies, 2017). DNA can also undergo damage from environmental and physical agents, such as cigarette smoke, ultraviolet (UV) radiation from sunlight, and ionizing radiation (IR). UV rays cause covalent bonds to form between two adjacent pyrimidines on a single DNA strand, creating photodimers. On the other hand, IR can induce base modifications, single and DNA double-strand breaks (DSBs) either through direct ionization or the generation of ROS. Additionally, exogenous DNA

damage can result from chemical agents employed in cancer chemotherapy, including alkylating and crosslinking agents like mitomycin C (MMC) or cisplatin (Ciccia & Elledge, 2010).

1.1.2. Repair of ssDNA damage

Damage to a single strand of the DNA double helix often arises from spontaneous chemical reactions within cells, such as hydrolysis and oxidation. Furthermore, single strand DNA (ssDNA) damage can be induced by alkylating agents, highly reactive chemicals capable of transferring alkyl-carbon groups onto DNA, resulting in various covalent adducts. These reactions can harm individual bases or entire nucleotides, potentially leading to alterations in DNA sequence and disrupting crucial cellular processes like DNA replication and gene expression. Therefore, alkylating agents are employed in chemotherapy (Fu et al., 2012). In the cell, the repair of ssDNA damage is crucial and primarily occurs through three pathways, all utilizing the other intact DNA strand as a template for restoration.

1.1.2.1. Mismatch repair

DNA replication, despite the proof-reading activity of the replicative DNA polymerases ϵ and δ , can still introduce base substitution errors, with rates ranging from 10^{-6} to 10^{-8} during eukaryotic DNA synthesis (Bębenek & Ziuzia-Graczyk, 2018). Moreover, replication of regions containing repetitive sequences, like microsatellites (MS), can be highly mutagenic due to incorrect reannealing of the polymerase (slippage) (Schlötterer & Tautz, 1992). Fortunately, these lesions are recognized and corrected in a post-replicative manner by mismatch mediated repair (MMR) (Kunkel & Erie, 2005), a highly conserved pathway that contributes to increase replication fidelity by at least 100-fold (Liu et al., 2017). Notably, MMR pathway defects result in microsatellite instability (MSI), characterized by an accumulation of insertion or deletion errors at these regions often observed in cancer cells (Ionov et al., 1993).

In the initial step of MMR, the MutS α heterodimer (MSH2/MSH6) recognizes the mismatch, forming a clamp on the lesion. Following an ATP-dependent conformational

change, MutS α recruits and binds the MutL α heterodimer (PMS2–MLH1) to form a tetrameric complex. Upon activation of its endonuclease activity by the Proliferating Cell Nuclear Antigen (PCNA), MutL α induces a break at the 5' of the mismatch. Subsequently, exonuclease 1 (EXO1) catalyze the 5'-3' excision of DNA segment containing the error. The gap is then filled in and repaired using a combination of Pol δ and Pol ϵ , followed by sealing by DNA ligase 1 (LIG1) (Kunkel & Erie, 2015; Liu et al., 2017) (**Fig. 2**).

1.1.2.2. Base Excision Repair

Base Excision Repair (BER) targets base modifications due to alkylation or oxidative damage (Barnes & Lindahl, 2004). It begins with a DNA glycosylase (Wallace, 2014), recognizing and cleaving the N-glycosyl bond between the damaged base and the sugar, forming an apurinic/apyrimidinic (AP) intermediate. Subsequently, the AP endonuclease (APE1) locates the AP site and cleaves the DNA backbone, creating a gap with an exposed 3'-OH and a 5'-deoxyribose phosphate (dRP). This process continues with either short-patch repair for a single-nucleotide gap or long-patch BER for a 2-20 nucleotide gap.

In short-patch repair, the resulting 3'-OH serves as a substrate for Pol β , which fills in the gap and cleaves the 5'-dRP (Matsumoto & Kim, 1995). Finally, the gap is subsequently sealed by LIG3 (Dianov & Lindahl, 1994; Robertson et al., 2009).

In contrast, long-patch repair, prevalent in proliferating cells, involves replication proteins like PCNA, which facilitates Pol β in synthesizing a long DNA segment. This mechanism generates a flap that is subsequently excised by flap structure-specific endonuclease 1 (FEN1) before ligation by LIG3 (**Fig. 2**). Notably, the endonucleases involved in BER generate single-strand breaks which are sensed and repaired by factors shared with the single-strand break repair (SSBR) pathway (Chaudhuri & Nussenzweig, 2017) (see section 1.1.3).



Figure 2. Mismatch Repair (MMR) and Base Excision Repair (BER) pathways. (Left) Errors that occur during DNA replication are identified and repaired through the Mismatch Repair (MMR) pathway. (Right) Adducts on the DNA bases are repaired by the Base Excision Repair (BER) pathway, which can involve either short-patch or long-patch repair depending on the extent of the lesion. Details of each step are described in section 1.1.2.1 and 1.1.2.2., respectively. Created with BioRender.com.

1.1.2.3. Nucleotide Excision Repair

Complex DNA lesions that result in structural distortions of the DNA molecule, such as UV-induced pyrimidine dimers, are repaired through the nucleotide excision repair (NER) pathway (Marteijn et al., 2014). NER involves the removal of an approximately 30 bp oligonucleotide containing the damaged bases, followed by gap filling (Marteijn et al., 2014). Mutations in this pathway give rise to Xeroderma Pigmentosum (XP), a syndrome predisposing to skin cancer and Cockayne Syndrome (CS) (Cleaver, 2005). NER is divided into global genome NER (GG-NER) and transcription-coupled NER (TC-NER) (**Fig. 3**).

In GG-NER, which primarily operates in non-transcribed regions, the complex formed by XPC, hRAD23B, and Centrin 2 (CETN2) identifies and binds to the lesion causing helix distortion (Min & Pavletich, 2007). In case of UV-induced lesions, the DNA-damage binding proteins (DDB1/2) further enhance lesion recognition by XPC complex. The XPC-bound DNA then serves as a substrate for the transcription initiation factor IIH (TFIIH). On the other hand, TC-NER comes into play when DNA damage leads to the stalling of the RNA polymerase (RNAP) II. This is sensed by Cockayne Syndrome group B (CSB), which strongly binds to RNAP II and forms a complex with Cockayne Syndrome group A (CSA). This complex facilitates the recruitment of TFIIH by removing the RNAP II (Spivak, 2015). Next, both in GG-NER and TC-NER, XPB and XPD, part of the TFIIH complex, unwind the DNA to create a 20–30-nucleotide repair bubble, which is rapidly bound by the replication protein A (RPA). Subsequently, after the detection of the damage by XPA, the endonucleases XPF-Excision Repair Cross-Complementing Polypeptide 1 (ERCC1) incise the damaged strand at the 5' end, followed by 3' cleavage by XPG (Fagbemi et al., 2011). Finally, the following steps of gap-filling and sealing are mediated by Pol δ , Pol ϵ and LIG1 (**Fig. 3**).

1.1.3. Single-strand break repair (SSBR)

Single-strand breaks (SSBs) represent one of the most abundant type of lesions, accounting for approximately 75% of all DNA damage events (Tubbs & Nussenzweig, 2017). They can arise as intermediates in the BER pathway or directly from oxidative damage, leading to deoxyribose oxidation (Xu et al., 1998). SSBs can also arise due to the activity of the DNA topoisomerase 1 (TOP1) enzyme, which creates temporary nicks to alleviate conformational stress during replication and transcription (Pommier, Sun, et al., 2016). Notably, certain chemotherapeutic drugs like camptothecin act by trapping the TOP1-DNA cleavage complex (TOP1cc), preventing the resealing step. Typically, TOP1-associated DNA damage is excised by enzymes like the tyrosyl-DNA phosphodiesterase (TDP1) (Pouliot et al., 1999).

All the above-mentioned sources expose either a 5'-dRP or 3'-OH damage ends, initially recognized by the enzyme PARP1 (Wang, 2002). Upon activation, PARP1 undergoes auto-modification through poly-ADP ribosylation (D'Amours et al., 1999). The scaffolding protein XRCC1 recognizes and binds PAR chains through its BRCT domain and creates a complex with other components of SSBR, such as Polynucleotide Kinase 3'-Phosphatase (PNKP), aprataxin (APTX) and Pol β (Caldecott, 2019). Upon PARP1 dissociation, DNA undergoes end processing. For free DNA ends, such as those in BER intermediates, processing is conducted by Pol β and LIG3, as previously discussed. In contrast, direct SSBs are processed by PNKP, restoring proper 5'-dRP and 3'-OH ends compatible for subsequent ligation (Caldecott, 2022) (**Fig. 3**). When intermediates with a 5' adenylate (AMP) resulting from abortive DNA ligation are encountered, APTX resolves them, facilitating the resumption of BER in short or long patches (Çağlayan et al., 2014). Notably, mutations in APTX and TDP1 lead to neurological disorders like spinocerebellar ataxia with axonal neuropathy 1 (SCAN1) and ataxia oculomotor apraxia 1 (AOA1), underscoring the role of unrepaired SSBs in progressive neurological dysfunction.

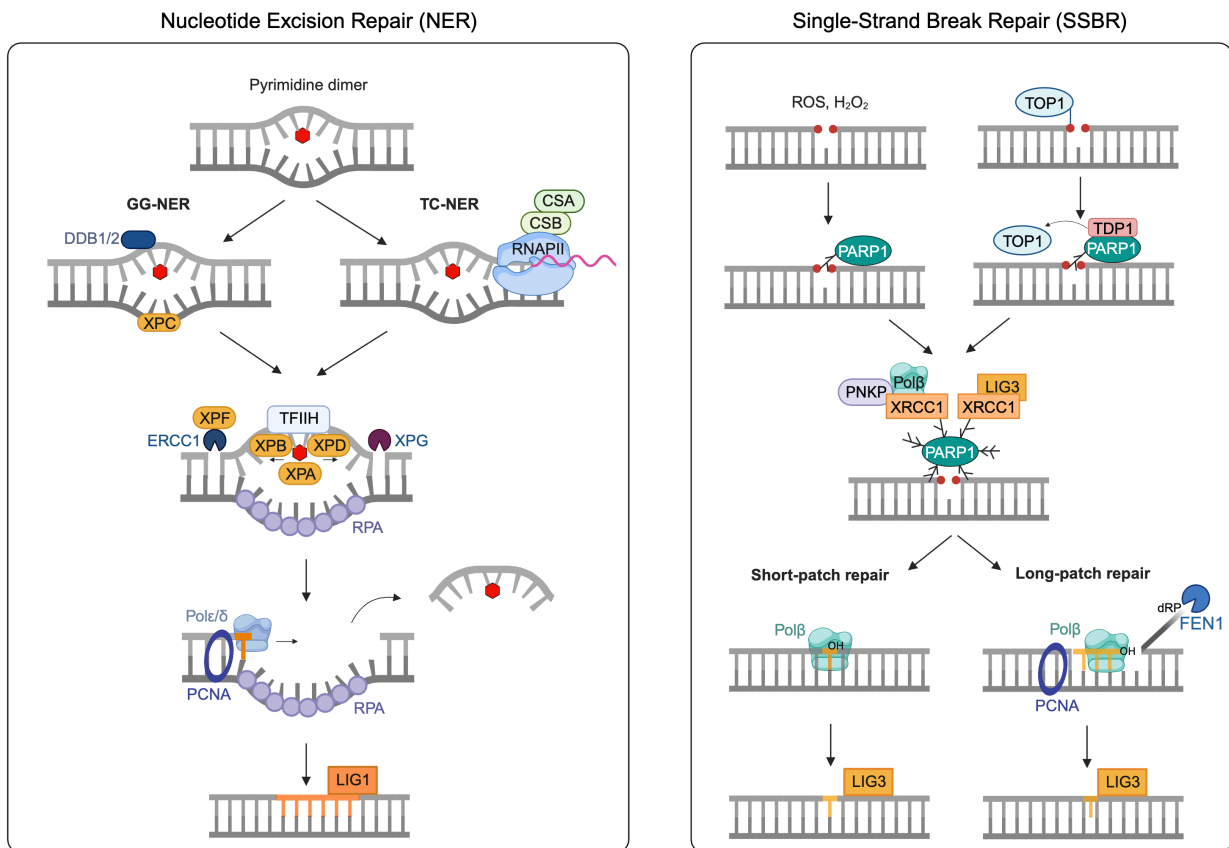


Figure 3. Nucleotide Excision Repair (NER) and Single-Strand Break Repair (SSBR) pathways. (Left) Lesions that induce helix distortions are repaired through Nucleotide Excision Repair (NER). NER is further divided into GG-NER, which repairs damage in non-transcribed regions, and TC-NER, which specifically deals with damage associated with transcription. (Right) SSBs can result from oxidative damage or the removal of the TOP1 cleavage complex. PARP1 serves as a scaffold to recruit the SSBR core complex, and DNA is subsequently ligated following the BER pathway. Details of each step are described in section 1.1.2.3 and 1.1.3., respectively. Created with BioRender.com.

1.1.4. Double-Strand Break (DSB) repair

In eukaryotic cells, DNA double-strand breaks (DSBs) are a common occurrence, with an estimated rate of 10–50 events per cell, daily (Hoeijmakers, 2009). These breaks involve the simultaneous disruption of the phosphate backbones in the two complementary DNA strands. DSBs can originate from both external sources like anticancer chemotherapeutic drugs, irradiation as well as internal cellular processes including DNA replication and transcription. While programmed DSBs take place in physiological conditions in the immune system (e.g., V(D)J recombination and class-switch recombination) (Chaudhuri et al., 2007; Fugmann et al., 2000) or in meiosis, other DSBs are pathological. In fact,

improper DSB repair can threaten genomic integrity, resulting in chromosome rearrangements, amplification or loss of genetic material, and translocations that disrupt gene structure and function (Agarwal et al., 2006).

Efficient repair of DSBs involves the detection of these lesions by cellular sensors, followed by precise activation of cell cycle checkpoints and coordinated repair through canonical non-homologous end-joining (c-NHEJ), which directly reconnects the broken ends, or homologous recombination (HR), a more precise method using template DNA for repair. More recently, alternative DSB repair mechanisms have emerged, including alternative end-joining (Alt-EJ) and single-strand annealing (SSA). These mutagenic pathways are activated when classical repair mechanisms are unavailable, often resulting in genomic changes that contribute to cancer development.

1.1.4.1. Sensing and signaling DSBs

The detection of DSBs is orchestrated by three different protein complexes (**Fig. 4**). The MRE11-RAD50-NBS1 (MRN) complex recognizes the DSB and through the C-terminal domain of NBS1 interact with the apical kinase ataxia-telangiectasia mutated (ATM) (You et al., 2005), resulting in its activation (Lee & Paull, 2005). Activated ATM initiates a wave of phosphorylation events on different targets, including the histone variant H2AX at Serine 139 (γ H2AX), which is a docking site for other factors such as the mediator of DNA damage checkpoint protein (MDC1). This latter recognizes and interacts with γ H2AX via its BRCT domains. Following recruitment, ATM phosphorylates MDC1, leading to its dimerization and the recruitment of the MRN complex through a direct interaction with NBS1. This results in further recruitment of ATM, coupled with additional γ H2AX formation, which rapidly spreads across a large chromatin domain, amplifying the DDR signaling (Rogakou et al., 1999). Subsequently, a cascade of ubiquitination events promoted by RNF186 near DSBs results in the modification of the histone variant H2A. Ubiquitinated-H2A can be recognized by 53BP1 and BRCA1, proteins involved in mutually exclusive DSB repair pathways (as discussed in section 1.1.4.5).

Interestingly, H2AX can also be phosphorylated by the ataxia telangiectasia mutated and Rad3 related kinase (ATR). ATR senses single strand DNA (ssDNA) coated by replication protein A (RPA), present during replicative stress or stalled replication fork (Abraham, 2001) (section 1.2.3.1) (**Fig. 4**). Nevertheless, despite differing at mechanism of activation and substrate preference, ATM and ATR pathways are interconnected (Maréchal & Zou, 2013). In fact, the target effector checkpoint kinase 1 (CHK1), phosphorylated by ATR (Shieh et al., 1997), and CHK2 and p53, phosphorylated by ATM (Matsuoka et al., 2000), could induce a variety of responses including cell cycle checkpoint activation, DNA repair or apoptosis/senescence depending on the extent of damage (section 1.1.4.2).

PARP1 and Ku70/Ku80 are additional DSB-sensing protein complexes. PARP1 detects both SSBs and DSBs through its zinc-binding (Zn) domains (Ikejima et al., 1990). This results in a conformational change that enables it to use Nicotinamide Adenine Dinucleotide (NAD⁺) as a substrate to poly-ADP(ribosyl)ate itself and various target proteins (Beck et al., 2014). One of these is the Ku70/Ku80 heterodimer, which recognizes and binds DNA blunt ends (Mimori & Hardin, 1986) (**Fig. 4**). Ku70 contains a PAR binding motif, suggesting that PARP1 is involved in recruiting it to DSB sites. Moreover, PAR-dependent chromatin relaxation enhances the recruitment of ZNF384, which interacts with Ku70/Ku80, promoting their assembly at DSB sites (Singh et al., 2021). However, a recent study showed that PARP1 and Ku70/Ku80 compete for binding at free DSBs, with PARP1 primarily binding during S phase (Yang et al., 2018). Once bound to DNA, Ku70/80 recruits and activates the DNA-dependent protein kinase (DNA-PKcs) (Gottlieb & Jackson, 1993; Lees-Miller et al., 1990) which initiates a series of phosphorylation events on downstream targets that are involved in DSB DNA blunt-ends processing (section 1.1.4.3.1).

DSB sensing, signalling and consequences

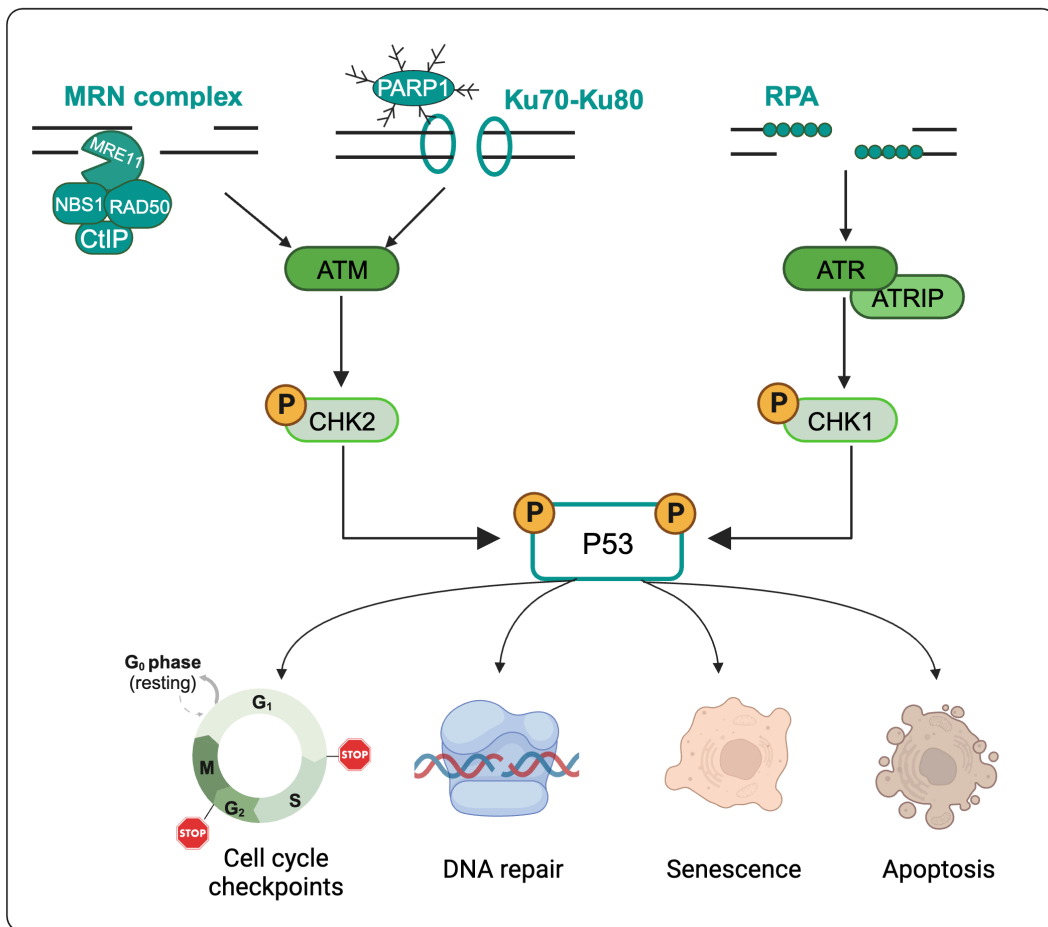


Figure 4. Detection, signaling, and consequences of DNA double-strand breaks (DSBs). (Top left) DSBs are detected by the MRN complex or PARP1, which recruits the Ku70-Ku80 heterodimer. (Top right) During replicative stress, ssDNA is protected by replication protein A (RPA) and sensed by ATR and its interactor ATRIP. (Middle) Activation of ATM and ATR initiates a phosphorylation cascade targeting the effectors CHK1/2. These effectors, in turn, activate p53. (Bottom) p53 functions to pause the cell cycle, allowing time for DNA repair. In cases of extensive damage, p53 may induce senescence or apoptosis. Details of each step are described in sections 1.1.4.1, 1.1.4.2 and 1.2.3.1. Created with BioRender.com.

1.1.4.2. Consequences of the DNA damage at the cellular level

DNA replication occurs within the context of the cell cycle, which is divided into two main phases: interphase and mitosis. Interphase constitutes most of the cell cycle and consists of three distinct stages (Vermeulen et al., 2003). In the G₁ phase, cells prepare for division by accumulating essential nutrients and assessing the cellular environment for potential challenges or damage that could hinder replication. During the S phase, the

entire genome undergoes duplication, ensuring that each daughter cell inherits an identical set of genetic instructions. In the G2 phase, organelles and cellular components are duplicated, providing the necessary resources for the upcoming division. The final phase, mitosis (M), is where the actual separation of the duplicated genetic material occurs.

Progression from one phase to the next in the cell cycle is monitored by different checkpoints, a cascade of signaling events that puts replication on hold when the cell encounters an obstacle. The G1-S checkpoint monitors the availability of nutrients and growth factors, primarily checking for DNA damage before its duplication. If cells are not ready, they can enter to a reversible quiescent state, called G0. In contrast, the G2-M mitosis checkpoint assesses cell size and whether DNA replication is complete, allowing entry into mitosis. Upon DNA damage, ATM and ATR activate the effectors P53 and CHK1/2 phosphorylate the Cell Division Cycle 25A (CDC25A) leading to cell cycle arrest at the G1 phase. This pause allows time for DNA repair mechanisms to fix the damage before DNA replication proceeds. Moreover, the effectors activate the G2/M checkpoint by phosphorylating Cell Division Cycle 25C (CDC25C) protein expression and activity, preventing the entry of damaged DNA into mitosis (Donzelli & Draetta, 2003). If DNA repair is successful, the cell cycle can resume (**Fig. 4**).

In certain scenarios where DNA damage is extensive and complete repair is unattainable, the activation of ATM and ATR pathways can trigger cellular senescence preventing damaged cells from further proliferation. Moreover, ATM and ATR have a direct impact on apoptosis, a programmed cell death pathway. ATM, for instance, phosphorylates and activates p53, a key player in the regulation of apoptosis (Shiloh & Ziv, 2013). When activated, p53 can induce the expression of pro-apoptotic proteins, ultimately leading to cell death if DNA damage cannot be adequately repaired (**Fig. 4**).

1.1.4.3. Classical DSB repair pathways

1.1.4.3.1. Resection independent repair: Canonical non-homologous end-joining

Canonical non-homologous end-joining (c-NHEJ) is the primary pathway for repairing DSBs in mammalian cells, responsible for approximately 80% of these events (Löbrich & Jeggo, 2017). c-NHEJ is mediated by the inhibition of DNA termini resection, a process regulated by 53BP1 (Callen et al., 2013) (section 1.1.4.5). Subsequently, the Ku70/Ku80 heterodimer binds to exposed DNA ends, safeguarding them from degradation and serving as a platform to recruit the repair machinery (Walker et al., 2001). Downstream, the kinase DNA-PKcs undergoes autophosphorylation, a critical step for initiating repair. Ultimately, DNA ends are sealed by the LIG4/ XRCC4/XLF complex (Graham et al., 2016) **(Fig. 5)**.

Numerous accessory factors favor c-NHEJ repair. Alongside PARP1 (as mentioned earlier), PARP3 promotes APLF recruitment, facilitating XRCC4/LIG4 complex retention within chromatin (Fenton et al., 2013). This allows c-NHEJ to efficiently join DNA termini without sequence homology. However, when the ends do not align correctly, the endonuclease Artemis processes them, creating small homologous regions filled by DNA polymerases Pol λ and Pol μ (Ma et al., 2002; Watanabe & Lieber, 2022). While this process facilitates end joining, it can lead to minor nucleotide losses or additions at the break site. Nonetheless, its rapid kinetics help safeguard genome integrity, especially by effectively tethering the two DNA ends of the DSB together (Bétermier et al., 2014). Moreover, c-NHEJ can operate on various substrates, including physiological DSBs arising during immune system development. Consequently, mutations in Artemis, XRCC4, and DNA-PKcs are associated with immunodeficiency disorders (Woodbine et al., 2014).

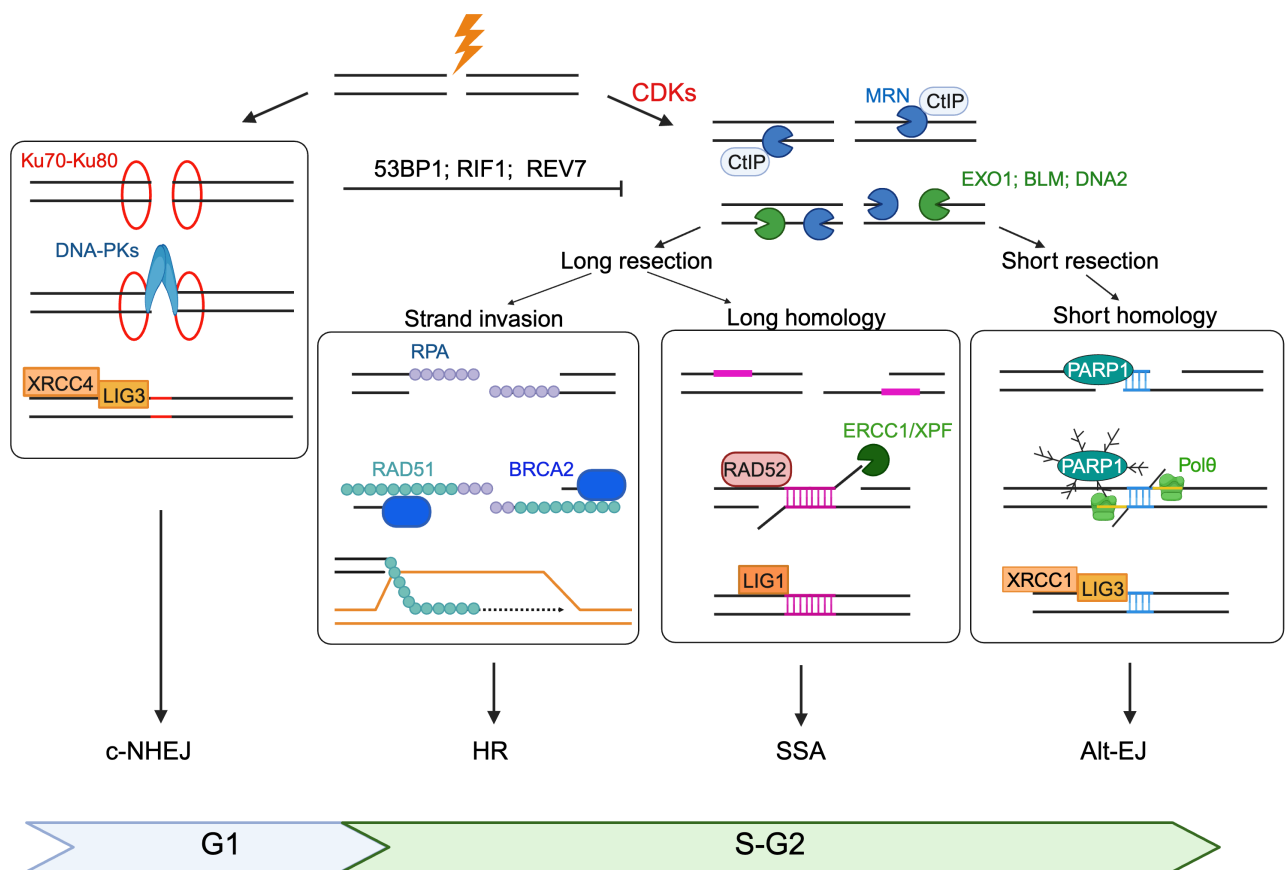


Figure 5. Overview of the DSB repair pathways. From the left to the right: Inhibition of resection by factors like 53BP1, RIF1, or REV7 favors classical non-homologous end-joining (c-NHEJ). When factors like CDK promote resection-dependent pathways, c-NHEJ is no longer available. Additional factors, such as the extent of resection or unavailability of certain mechanisms, influence DSB repair via HR, SSA, or Alt-EJ. Details in sections 1.1.4.3. to 1.1.4.5. Created with BioRender.com.

1.1.4.3.2. Resection and recombination-dependent repair: Homologous Recombination

DSBs are subject to repair via homologous recombination (HR), a highly accurate pathway reliant on an identical sequence, often from the sister chromatid, as a repair template. HR predominantly operates in cycling cells during the S or G2 phases, following DNA replication (Spies et al., 2021). Critical players in HR are the BRCA1/BRCA2 proteins, consequently mutations in these proteins heighten cancer susceptibility, classifying them as tumor suppressors (Scully & Livingston, 2000) (see section 2 of the Introduction).

The initial step in the HR pathway involves a short-range resection by the nucleases CtIP and MRE11, a member of the MRN complex as mentioned above. Importantly,

BRCA1-associated RING domain protein (BARD1) antagonize 53BP1 in favor of CtIP and the MRN-mediated resection in a 3'–5' direction (**Fig. 5**). This serves as an entry point for nucleases such as DNA2, EXO1, and the helicase Bloom Syndrome protein (BLM), which perform a long-range 5'–3' resection to generate 3' overhangs (Nimonkar et al., 2011). This event marks the cell commitment to the recombination repair process as Ku proteins cannot bind this substrate. Consequently, extensive regions of ssDNA are formed and promptly coated by the RPA protein, protecting DNA termini from nucleolytic degradation. Once loaded in the chromatin, RPA undergoes a series of post-translational modification (PTMs), including phosphorylation and ubiquitylation, favoring its displacement and the loading of the recombinase RAD51 (Maréchal et al., 2014). The binding of BRCA2 to the dsDNA-ssDNA junction promotes RAD51 nucleofilament formation on ssDNA (Carreira et al., 2009; Shivji et al., 2009). The physical occupancy of RAD51 on ssDNA prevents the repair by other alternative resection-dependent repair mechanisms (So et al., 2022). Then, the partner and localizer of BRCA2 (PALB2) acts as a scaffold between RAD51-bound BRCA2 and BRCA1 (Zhang et al., 2009). This latter promotes presynaptic complex formation during strand invasion. Subsequently, RAD51 filament begins the search for a homologous sequence. Once identified, the presynaptic filament invades the duplex DNA, displaces the original strand, and binds its complementary sequence forming a displacement loop (D-loop). This structure allows DNA synthesis to begin. The invading ssDNA strand serves as a primer for the DNA polymerases Pol δ to synthesize a new DNA strand complementary to the homologous template. This results in the restoration of the broken DNA sequence.

When the repair is completed, the D-loop can be resolved in several ways, depending on the specific context of the repair and the mechanism involved (Wright et al., 2018). Two such mechanisms are: synthesis-dependent strand annealing (SDSA) and the double Holliday junction resolution (dHJ) (**Fig. 6**). In SDSA, the newly synthesized DNA strand disconnects from its donor template and then pairs with the opposite end of the DSB. In contrast, the dHJ pathway involves capturing the opposite end of the DNA break with the

D-loop, leading to the formation of a double Holliday junction. Depending on how this junction is resolved, it can result in either crossover or non-crossover outcomes.

The third mechanism to resolve a D-loop involves the break-induced replication (BIR). This pathway mainly acts on single-ended DSBs, arising for example when replication fork encounters an obstacle. In BIR, where only one end of the DSB has a homologous template, the D-loop can be resolved by migrating the D-loop structure along the template and extending the synthesis process until the entire damaged strand is repaired (**Fig. 6**). Although it is essential to deal with the frequently occurring one-ended lesions, BIR is associated with a high frequency of mutations and gross chromosomal rearrangements and can lead to loss of heterozygosity (LOH).

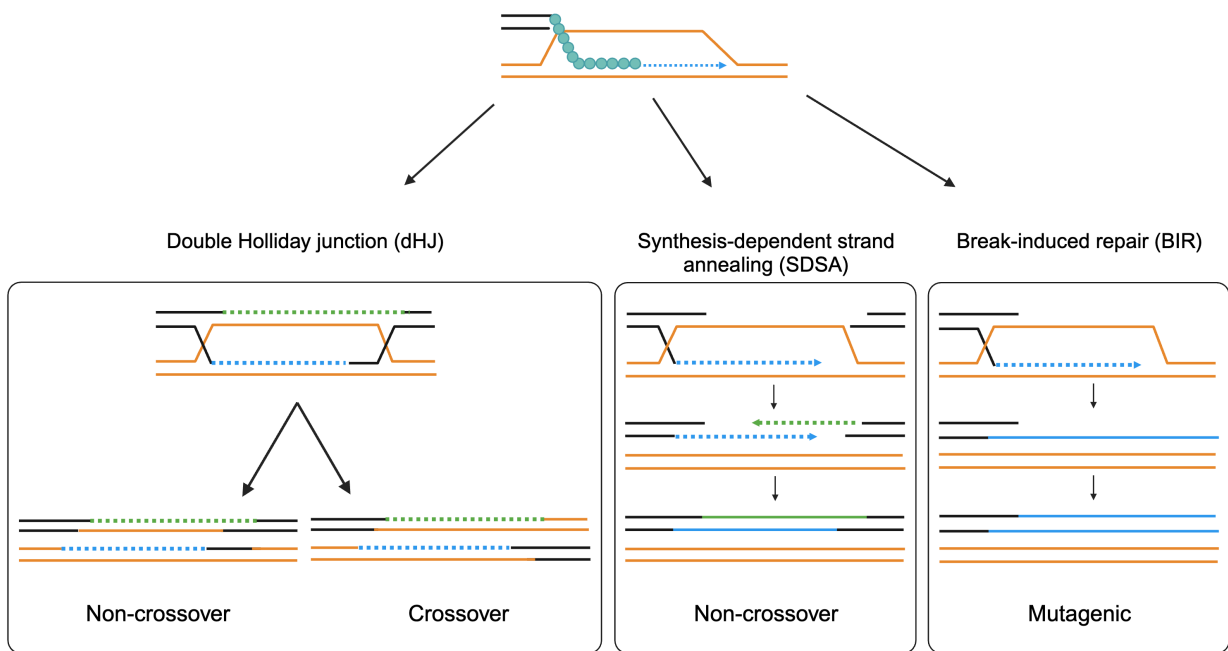


Figure 6. Sub-pathways of homologous recombination. Once HR repair pathway is committed, and the RAD51 nucleoprotein filament is formed, the next steps involve the search for homology, DNA invasion and formation of a D-loop structure. Resolution of the D-loop can follow different pathways, each leading to distinct outcomes in terms of gene conversion and fidelity. From left to right, formation of double Holliday junction (dHJ), synthesis-dependent strand annealing (SDSA) and break-induced replication (BIR). Details in section 1.1.4.3.2. Created with BioRender.com.

1.1.4.4. Alternative DSB repair pathways

1.1.4.4.1. Single strand annealing

Like HR, the initial step in single-strand annealing (SSA) involves resection mediated by CtIP and MRE11, however, this form of repair operates in sequence repeats within the same duplex DNA. When the resection reveals extended homologous regions, like tandem repeats, RAD52, the central mediator of SSA, facilitates the annealing of these ssDNA regions once coated by RPA (Bhargava et al., 2016) (**Fig. 5**). This process generates 3' flaps, which are subsequently cleaved by the ERCC1/XPF nucleases, followed by ligation. Consequently, SSA has the potential to result in the loss of genetic material, rendering it mutagenic.

1.1.4.4.2. Alternative End-Joining

Alternative end-joining (Alt-EJ) is an error-prone repair pathway operating when the predominant repair pathways, HR and c-NHEJ, are compromised (Iliakis et al., 2015). Remarkably, Alt-EJ combines features from both c-NHEJ and HR. Like HR and SSA, Alt-EJ initiates with a short-range resection, mediated by the nucleases CtIP and MRE11 (Truong et al., 2013). On the other hand, Alt-EJ can be considered a subset of c-NHEJ, as it fuses short regions of microhomology, typically ranging from 2 to 20 nucleotides, exposed by the resected ssDNA. Hence, Alt-EJ is often referred to as Microhomology-Mediated End Joining (MMEJ). However, Alt-EJ diverges significantly from the canonical NHEJ pathway. The key distinction lies in the requirement for PARP at the damaged ends in Alt-EJ, while classical NHEJ relies on the activity of the Ku heterodimer. Intriguingly, these two factors "compete" for binding to the DNA ends at the damage site (Wang et al., 2006). After an extensive resection, the involvement of PARP1 activity becomes pivotal for the recruitment of Alt-EJ factors, including Pol θ , a translesion synthesis (TLS) polymerase encoded by *POLQ* (**Fig. 5**). Pol θ assumes a critical role in stabilizing the annealed DNA ends (Yousefzadeh et al., 2014), thereby preventing excessive resection, a distinct feature of SSA. This process culminates in the formation of a stable intermediate (Chang et al., 2017). Upon recruitment, Pol θ initiates an error-prone gap-filling mechanism, ultimately sealing the ends with the assistance of LIG3.

Recent findings suggest that Pol θ , recruited by HR proteins in S phase, may operate on HR intermediates, while also playing a role in maintaining genomic stability during mitosis by promoting mitotic DSB repair (Gelot et al., 2023).

1.1.4.5. DNA repair pathway choice

The engagement of one or other DSB repair pathway depends mainly on the cell cycle phase, with c-NHEJ being favored in G1 and HR in S/G2, as well as the extent of DNA end resection (**Fig. 5**).

53BP1 functions as a barrier against extensive DNA end resection, a role highlighted in Brca1-knockout mice where the absence of 53BP1 partly restored HR (Bouwman et al., 2010). This finding suggested an antagonistic relationship between 53BP1 and BRCA1 at DSBs. In G1 phase, ATM-dependent phosphorylation of 53BP1 triggers the recruitment of its effectors, including RIF1, PTIP, and REV7 (MAD2L2) (Munoz et al., 2007; G. Xu et al., 2015; Zimmermann et al., 2013). RIF1 serves to counteract the accumulation of BRCA1/BARD1 at damage sites, inhibiting 5'–3' end resection (Chapman et al., 2013). Furthermore, REV7, a component of the translesion DNA polymerase Pol ζ , interacts with the Shieldin complex, reinforcing the inhibition of resection (Noordermeer et al., 2018). In contrast, during S/G2 phases of the cell cycle, ATM and cyclin-dependent kinase (CDK) phosphorylates CtIP, promoting its interaction with NBS1, and short-range resection. Phosphorylated CtIP also recruits BRCA1, which in turn is phosphorylated and activated by ATM.

Interestingly, chromatin modifications also play a role in pathway choice. Both BRCA1 and 53BP1 are recruited through the ATM-H2AX-NBS1-MDC1-RNF8-RNF168 signaling pathway (as discussed in section 1.1.4.1). Moreover, 53BP1 binds to the histone modification H4K20me2 via its Tudor domain (Botuyan et al., 2006). As cells progress through S phase, a decrease in H4K20me2 levels contributes to the reduction of 53BP1 foci in post-replicative chromatin. In parallel, BRCA1 interacts with H4K20me0 via its partner BARD1, leading to its recruitment to post-replicative chromatin (Nakamura et al., 2019). Also in S phase, ATM phosphorylates SPOP, a E3 ubiquitin ligase, which binds and

polyubiquitinates 53BP1 promoting its eviction from chromatin thus suppressing c-NHEJ (Wang et al., 2021).

1.2. Replication stress

1.2.1. The eukaryotic DNA replication process

As mentioned in previous sections, DNA replication is a fundamental and indispensable process for life, playing a crucial role in development, tissue growth and regeneration.

The first step of the process takes place in G1 where replication origins are recognized by the origin recognition complex (ORC), which binds to Cdt1 and Cdc6 favoring the recruitment the ring-shaped helicase MCM2-7 to form the pre-recognition complex (pre-RC) (Remus & Diffley, 2009). This step is also known as *origin licensing* and ensures that each origin is fired only once per cell cycle (Méchali, 2010). Additional factors like Cdc45 and GINS are required for the formation of the active helicase complex, named the CMG (Cdc45-MCM2-7-GINS) complex. Interestingly, recently the DOMSON protein has been identified as a key component favoring the loading of Cdc45 and GINS (Kingsley et al., 2023). This step is also known as *origin firing* and is tightly regulated: once an origin is fired, DNA synthesis begins. The CMG complex unwinds the DNA double helix, creating single-stranded DNA templates for DNA polymerases to synthesize new DNA strands.

This leads to the second phase, the elongation, where replisomal proteins, such as PCNA and RPA allow bidirectional progression of the fork throughout the genome until every region is duplicated (Masai et al., 2010). There are three main replicative DNA polymerases. The first, Pol α , generates a short RNA/DNA primer to initiate DNA synthesis. Pol α is then replaced by Pol ϵ which synthesizes the leading strand continuously in the 5'-3' direction, while Pol δ synthesizes the lagging strand discontinuously in short Okazaki fragments (Yuzhakov et al., 1996); these latter need to be further processed and ligated by FEN1 and LIG1, respectively (Burgers & Kunkel, 2016). PCNA, enhances polymerase association, increasing processivity.

Finally, the last stage, termination, occurs when two replication forks converge. It involves the completion of DNA synthesis, decatenation of daughter molecules by Topoisomerase II, and replisome disassembly (Fig. 7).

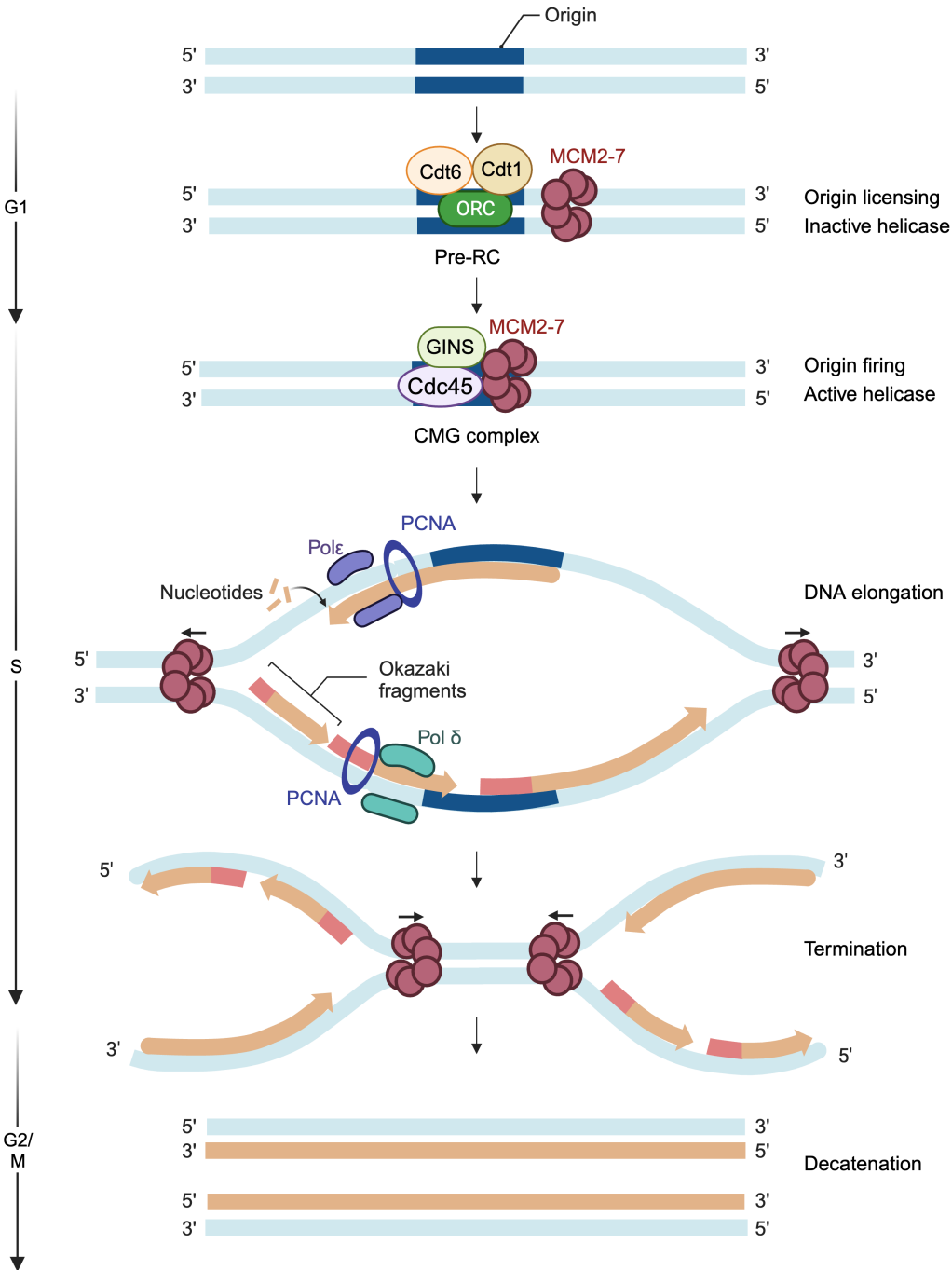


Figure 7. Overview of the eukaryotic DNA replication. Following origin recognition, the helicase complex is loaded (origin licensing) and subsequently activated (origin firing). The replication bubble advances bidirectionally to synthesize the leading strand continuously while forming the lagging strand with Okazaki fragments. Replication concludes when two replication forks converge. The left arrow indicated the cell cycle phase. Details in sections 1.2.1. Created with BioRender.com.

1.2.2. Source of replication stress

Replication stress indicates the deceleration or halting of replication fork advancement during DNA synthesis (Zeman & Cimprich, 2014). Besides DNA adducts, lesions and breaks whose mechanism or resolution has been described in section 1.1.2., a wide range of physical obstacles can induce replication forks stalling (**Fig. 8**). I will briefly describe these obstacles below.

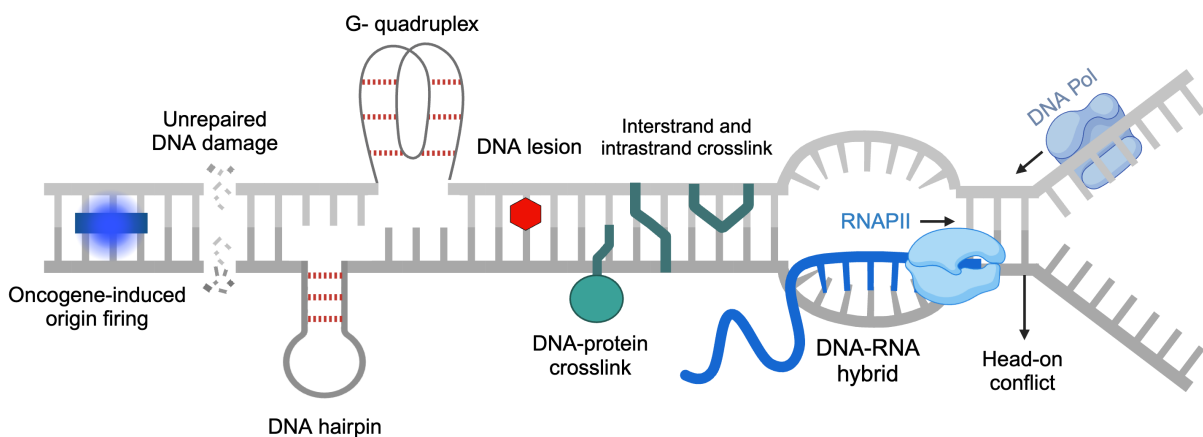


Figure 8. Sources of replication stress. Various impediments, such as increased origin firing, DNA secondary structures, DNA:RNA hybrids, intra and inter-strand crosslinks, and DNA-protein crosslinks induced by chemotherapeutics or arising from byproducts of cell metabolism, hinder the replication fork advancement. Further repair details for each obstacle are provided in sections 1.2.2.1 to 1.2.2.6. Created with BioRender.com.

1.2.2.1. TRCs and R-loops

Transcription-replication conflicts (TRC) refers to the collision between the two machineries. These conflicts are categorized based on the direction of movement: co-directional conflicts arise when replication forks and RNA polymerases travel in the same direction, while head-on collisions occur when they move in opposite directions. Head-on collisions promote the formation of R-loops (Costantino & Koshland, 2018), complex nucleic acid structures where an RNA molecule hybridizes with one DNA strand, leaving the other DNA strand of the duplex DNA unpaired (**Fig. 8**).

R-loops can be problematic as they hinder replication forks and are susceptible to cleavage by specific nucleases, leading to potential DNA damage. To counteract these effects cells have developed several mechanisms. Specifically, TOP1 plays a pivotal role in preventing replication fork collisions with R-loops, particularly at transcription termination sites, by alleviating the topological stress induced by DNA supercoiling (Promonet et al., 2020). On the other hand, upon R-loops formation, RNase H enzymes and DNA-RNA helicases are capable of unwinding and removing the RNA strand from the DNA-RNA hybrid (Skourti-Stathaki et al., 2011). Moreover, nucleases such as XPG and XPF, have the capacity to excise R-loops (Sollier et al., 2014). Remarkably, it has been discovered that both the BRCA1 and BRCA2 proteins are involved in the resolution of R-loops, a topic that will be explored in the following chapter.

1.2.2.2. DNA-protein crosslinks

DNA-protein crosslinks (DPCs) involve proteins covalently bound to DNA (**Fig. 8**) and they can be categorized as enzymatic or non-enzymatic. Enzymatic DPCs form when a DNA-binding enzyme becomes covalently attached to the DNA. This mechanism is exploited by some chemotherapeutic drugs, such as TOP1 and PARP1 inhibitors. Non-enzymatic DPCs result from the covalent crosslinking of any nearby protein with DNA. During replication, DPCs can undergo polyubiquitination, leading to their degradation by the proteasome (Sun et al., 2020). Alternatively, if the DNA polymerase extends the nascent DNA close to the lesion, SPRTN-mediated DPC proteolysis is activated (Stingele et al., 2017). This process effectively breaks down both modified and unmodified DPCs, leaving a peptide-DNA adduct that can be managed by specialized translesion synthesis (TLS) polymerases.

1.2.2.3. Inter-strand crosslinks

Inter-strand crosslinks (ICLs) occur due to covalent bonds between bases on different DNA strands. Endogenous sources like aldehyde metabolites or exogenous such as anti-cancer agents MMC and cisplatin induce this damage. In addition, these drugs cause intra-strand crosslinks, where the bonds form within the same DNA strand.

ICLs pose physical barriers to replication and transcription processes, necessitating efficient processing to prevent chromosome rearrangements or breakage. While non-replicating cells primarily utilize NER for ICL repair (Zhang & Walter, 2014), the dominant post-replicative repair mechanism involves the Fanconi anemia (FA) pathway (**Fig. 9**). In fact, biallelic mutations in any of the 22 identified FA genes result in Fanconi anemia, a rare autosomal disease characterized by congenital growth abnormalities, bone marrow failure, and elevated cancer predisposition (Kennedy & D'Andrea, 2005).

In the repair process, the recognition of stalling replication forks encountering ICLs is initiated by the FANCM–FAAP24–MHF1–MHF2 complex. Following the eviction of the stalled replicative helicase CMG by p97 (Fullbright et al., 2016), this complex recruits the FA core E3 ubiquitin ligase complex. Moreover, FANCM promotes ATR phosphorylation, which in turn phosphorylates and activates multiple FA proteins. The activated FA core complex recruits and monoubiquitinates the FANCI–FANCD2 heterodimer, the second group of FA repair proteins (Knipscheer et al., 2009). Monoubiquitinated FANCI–FANCD2 (ubD2–I) is recruited to the damaged chromatin where it undergoes conformational change, creating a clamp that encloses dsDNA (Alcón et al., 2020). Additionally, ubD2–I recruits the third group of FA repair proteins, including the endonuclease ERCC1 (NER) that incises the ICL, generating a DSB on one strand and a ssDNA gap on the other (Ceccaldi, Sarangi, et al., 2016). This latter is bypassed by translesion synthesis (TLS) polymerases such as REV1 or DNA polymerase ζ (REV3–REV7). The restored DNA duplex serves as template for the DSB repair which is preferentially mediated by HR. Complementation studies in ICL-sensitive cells provided evidence that many HR factors act in the FA pathway, namely RAD51 (FANCR), PALB2 (FANCN), BRCA1 (FANCS), BRCA2 (FANCD1) (Howlett et al., 2002; Zhang & Walter, 2014). Furthermore, RAD51–FANCR is also necessary to protect stalled forks from aberrant degradation at an ICL lesion (Wang et al., 2015) suggesting that RAD51 and BRCA2 are involved in several steps of the FA-pathway.

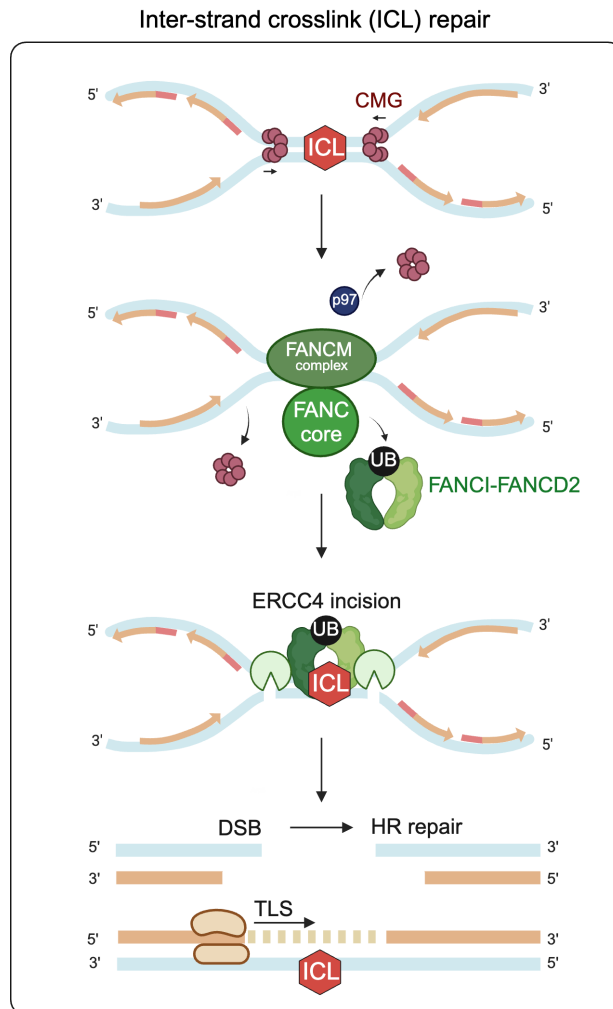


Figure 9. Inter-strand crosslink (ICL) repair pathway. Upon encountering an interstrand crosslink (ICL), the replicative helicases are displaced to create space for the Fanconi anemia (FA) pathway proteins, which recognize and cleave the crosslink. This cleavage allows for subsequent repair through translesion synthesis or homologous recombination (HR) mechanisms. Created with BioRender.com.

1.2.2.4. Secondary structures (hairpin, G quadruplex)

Besides the canonical double-helix structure, DNA can adopt various secondary structures. One of them include the hairpin, characterized by a single strand of DNA or RNA folding back on itself, creating a double-stranded stem with a loop (**Fig. 8**). This configuration occurs when complementary base pairs on the same strand bind together. On the other hand, when inverted repeats within a DNA molecule align, the DNA folds back upon itself, creating a structure resembling a cross or cruciform.

Finally, G-quadruplex (G4) structure form in regions of DNA rich in guanine. In this configuration, stacks of guanine bases are held together by hydrogen bonding, forming a stable, four-stranded arrangement (**Fig. 8**). When the replication machinery encounters such a structure, the DEAH-box helicase 36 (DHX36) facilitates the bypass of the CMG helicase past the G4 (Chen et al., 2015). Subsequently, the Fanconi anemia complementation group J helicase (FANCI) unwinds this structure, thereby enabling DNA synthesis (Sato et al., 2021).

1.2.2.5. Oncogene-induced replication stress

Aberrant replication origin firing is an additional cause of replication stress. This can be caused by mutations in genes that promote cell growth and cell division, such as proto-oncogenes. Once these genes are mutated, they can become oncogenes, promoting oncogenic transformation. An example of such a gene is MYC, which drives this transition by activating the transcription of genes encoding proteins involved in DNA synthesis and replication, including DNA polymerases and components of the pre-RC complex (Stine et al., 2015). Similarly, Cyclin E is a regulatory protein that controls the progression of the cell cycle from the G1 phase to the S phase. When Cyclin E is overexpressed, it can lead to an accelerated entry into the S phase (Ekholm-Reed et al., 2004). This increased speed of DNA replication can result in replication stress, characterized by stalled or slowed replication forks, DNA damage, and genomic instability.

1.2.2.6. Drugs and chemotherapeutics

In addition to PARP inhibitors, as mentioned earlier, various drugs used in cancer treatment induce replication stress through distinct mechanisms. Some compounds directly create bulky lesions and interstrand crosslinks in DNA. Notable examples include the alkylating agent Methyl Methanesulfonate (MMS), and drugs like Mitomycin C (MMC) and platinum-based agents such as Cisplatin, which induce interstrand crosslinks (ICLs) in the DNA structure. On a different note, Hydroxyurea (HU), employed in the treatment of chronic myeloid leukemia (CML), generates replication stress by disrupting the metabolism of deoxyribonucleotide triphosphates (dNTPs), essential for DNA synthesis.

Aphidicolin serves as a potent inhibitor of eukaryotic nuclear DNA replication, resulting in the arrest of the cell cycle during the early S phase. Conversely, camptothecin, etoposide, and doxorubicin disrupt the activities of topoisomerase 1 and 2, leading to significant topological stress within the DNA strands.

1.2.3. Mechanisms of resolution of replication stress

1.2.3.1. DNA replication checkpoint

Replicative stress or stalled replication fork result in the presence of RPA-coated ssDNA, sensed by ATR (Cimprich & Cortez 2008). Subsequently, the interaction between ATR with the ATR-interacting protein (ATRIP) is a prerequisite for the localization of activated ATR-TRIP complex at RPA-coated DNA damage site (Zou & Elledge, 2003).

ATR plays a multifaceted role in preserving the integrity of the replication process. For instance, it contributes to temporarily halting fork progression by phosphorylating multiple subunits of MCM2-7. This event inhibits the further unwinding activity of the CMG complex, effectively pausing the replication process to allow for necessary repairs. Among its downstream targets, activated ATR also phosphorylates CHK1 at specific sites, such as Serine 317 and 345 (Liu et al., 2000). As discussed in section 1.1.4.1., the ATR-mediated CHK1 pathway contributes to prevent cells from entering mitosis with unreplicated or damaged DNA by inducing the degradation CDKs (Bartek et al., 2004).

Once the checkpoint is activated, the restoration of the replication fork progression takes place through different mechanisms depending on the source of replication stress.

1.2.3.2. Replication stress tolerance mechanisms

When a replication fork encounters an obstacle, it can cause the uncoupling of the replicative polymerase and the helicase. As a result, replicative DNA polymerases halt their activity, while the helicase continues to unwind the DNA, creating single-stranded DNA (ssDNA) gaps, which can be repaired by the DNA damage tolerance pathways (DDT), which include translesion synthesis (TLS) or template switching (TS). Additionally, cells can restart DNA synthesis by repriming ahead of the fork, leaving a ssDNA gap that needs to

be repaired post-replicatively. Moreover, stalled forks may undergo reversal as a mean to prevent the degradation of the nascent strands and reduce the risk of fork collapse.

1.2.3.2.1. Translesion synthesis and template switching

In spite of the presence of specific DNA repair mechanisms to fix different DNA lesions, some of them persist during S-phase, hindering DNA replication. In response, the cell employs translesion synthesis (TLS) polymerases like Pol ζ or η to replace replicative polymerases, enabling DNA replication past these lesions (**Fig. 10**). However, TLS polymerases lack proofreading ability, increasing the likelihood of incorrect nucleotide insertion and mutations. Due to their mutagenic activity, TLS polymerases are tightly regulated by PCNA. In fact, this latter binds to TLS polymerases with lower affinity than to replicative polymerases. However, during replication stress PCNA is mono-ubiquitinated by RAD18, a modification recognized by TLS but not by replicative polymerases (Khatib et al., 2023). This mechanism ensures that TLS are employed exclusively in exceptional circumstances during DNA replication.

On the other hand, PCNA poly-ubiquitination mediated by yeast Rad5 or its human orthologue HLTF in humans, promotes template switching (TS) (Branzei, 2011). In this pathway, the stalled nascent strand switches its template and invades the newly synthesized, undamaged sister strand, which serves as the template for filling the gap. Then, the newly synthesized strand reunites with the original DNA strand, leading to an error-free repair of the DNA molecule.

1.2.3.2.2. Repriming

Repriming is the process by which DNA replication restarts ahead of an obstacle in the template strand (**Fig. 10**). This repriming event is mediated by PRIMPOL, which exhibits both primase and polymerase activities (Mourón et al., 2013). As a primase, PRIMPOL synthesizes short RNA primers on the ssDNA gaps. Then, it extends these RNA primers by adding DNA nucleotides, allowing replicative polymerases to resume DNA synthesis. The ssDNA gap left behind is then filled by TLS or TS (Berti et al., 2020). Remarkably, BRCA2 has been recently shown to operate in concert with MCM10, an integral member of the

replisome machinery, to impede PRIMPOL-dependent repriming (Kang et al., 2021). This inhibition effectively prevents gap formation and ensures the robust containment of the replication fork.

1.2.3.2.3. Fork reversal

One of the mechanisms used to alleviate replisome stalling is fork reversal (FR) (**Fig. 10**). FR leads to the formation of a four-strand DNA structure, also referred to as chicken-foot, characterized by the backtracking and annealing of the newly synthesized DNA strands in the opposite direction from the advancing replication fork (Neelsen & Lopes, 2015). It allows the replisome to temporarily retreat from the site of damage or stress to bypass the lesion through template switching once the fork restarts. This structure is promoted by the DNA translocase SMARCAL1, chromatin remodelers HLTF or ZRANB3 and RAD51. In contrast, BRCA1, BRCA2 are dispensable for fork reversal but necessary to protect reversed forks from excessive nucleolytic degradation (Qiu et al., 2021) (see section 2 of the Introduction).

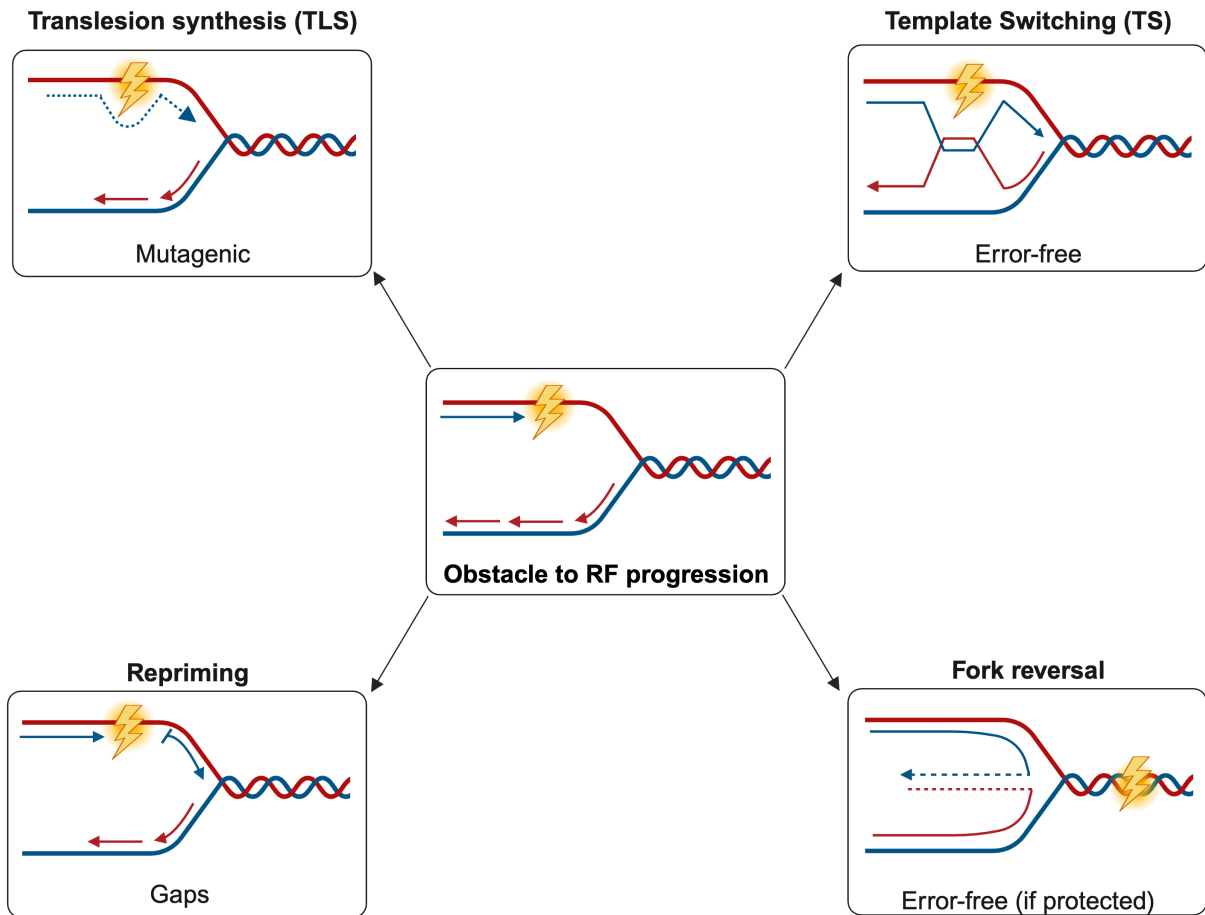


Figure 10. DNA damage tolerance (DDT) mechanisms at replication forks. Replication hurdles (depicted as lightning bolts) can be bypassed by translesion synthesis (TLS) or repaired by template switching using the newly synthesized strand as a template (TS) (top). These collectively form DNA damage tolerance pathways (DDT), enabling rapid replication resumption. TLS is mutagenic, while TS is error-free HR-mediated repair. Alternatively, repriming can restart DNA synthesis downstream of a stalled polymerase, leaving gaps behind the fork that need to be filled in post-replicatively (bottom left). Fork remodelers can promote fork reversal (bottom right), temporarily halting replication for lesion repair by TS; the process is error-free when the fork is protected. Details for each mechanism are provided in sections 1.2.3.2.1 to 1.2.3.2.3. Created with BioRender.com.

2. BRCA2, the custodian of genome integrity

2.1. The tumor suppressor BRCA2

Breast cancer associated gene 2 (BRCA2) was identified in 1995 through genetic linkage analysis in families with early-onset breast and ovarian cancers (Wooster et al., 1995). Mono-allelic mutations in *BRCA2* substantially increase the risk, with up to a 70% chance of breast cancer and a 17% risk of ovarian cancer by age 80 (Kuchenbaecker et al., 2017). Moreover, bi-allelic mutations in *BRCA2* are linked to Fanconi anemia subtype D1 (FA-D1) (Howlett et al., 2002). In such cases, one mutation is deleterious, while the other is hypomorphic (Biswas et al., 2011; Thirthagiri et al., 2016), as complete loss of BRCA2 function leads to embryonic lethality in mice (Evers & Jonkers, 2006). This body of evidence led to the classification of BRCA2 as a tumor suppressor (TS). Interestingly, early investigation in mice unveiled the co-localization and physical interaction observed between the well-established DNA repair factor Rad51 and Brca2, providing compelling evidence of its participation in DNA repair (Chen et al., 1998; Sharan et al., 1997).

Furthermore, the deficiency of the *Brca2* gene in cultured murine cells resulted in the formation of abnormal chromosomal structures and micronuclei, underscoring its crucial role in preserving genomic stability (Patel et al., 1998; Tutt et al., 1999). In the human pancreatic cancer cell line CAPAN-1, known for its HR repair deficiency (Moynahan & Jasin, 1997), the transient expression of BRCA2 effectively restored HR (Xia et al., 2001). This robustly supported BRCA2 central role in this DNA repair pathway.

Later, biochemical and structural studies showed that purified Brh2 (BRCA2 homologue from the fungus *Ustilago maydis*) facilitated Rad51 nucleation on RPA coated ssDNA and RAD51-mediated DNA strand exchange (Pellegrini et al., 2002; Yang et al., 2005). These results were later extended and confirmed with fragments and the full-length protein human BRCA2 (Carreira et al., 2009; Filippa et al., 2006; Jensen et al., 2010).

2.2. BRCA2 structure, functional domains and interactors

BRCA2 is a protein consisting of 3,418 amino acids (aa) with a molecular weight of approximately 390 kDa. Since its first identification, many domains and interaction sites or regions have been described (Fig. 12). Nevertheless, the lack of substantial sequence similarity with other human proteins, the presence of intrinsically disordered regions and its limited conservation throughout mammalian evolution (Connor, Smith, et al., 1997), except for regions like the BRC repeats (Bignell et al., 1997), has hampered the complete understanding of its functions.

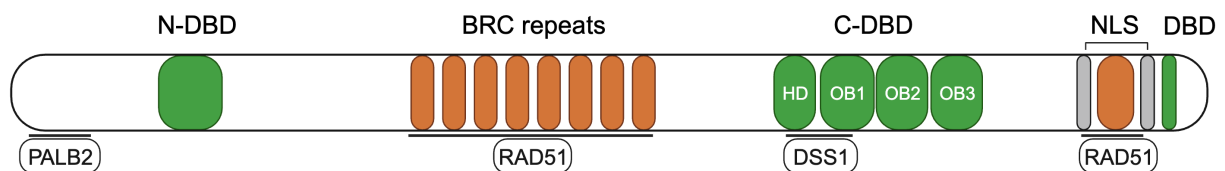


Figure 11. BRCA2 functional domains and main interacting partners. green boxes denote DNA-binding domains, while the orange boxes represent RAD51 binding domains. Abbreviations: N-DBD, N-terminal DNA binding domain; C-DBD, C-terminal DNA binding domain; NLS, nuclear localization signal. The main interacting partners are indicated below the scheme of BRCA2.

The BRC repeats- RAD51 binding

The BRC repeats constitute consecutive interspersed motifs of about 35 aa in length located in the central region of the primary sequence, corresponding to exon 11 of BRCA2 (**Fig. 11**). The BRC repeats promote BRCA2 interaction and loading of RAD51 onto RPA-coated ssDNA in HR pathway (Chen et al., 1999; Pellegrini et al., 2002). The role of the BRC repeats in HR will be described in detail in section 2.3.1. Pathogenic variants within these BRC motifs disrupt the interaction with RAD51 and are linked to familial early-onset cancer. In addition to RAD51, the BRC repeats interact with the meiotic recombinase DMC1, a paralogue of RAD51, and stimulate its binding to ssDNA (Martinez et al., 2016). These findings identified BRCA2 as a mediator of HR in meiotic cells.

The C-terminal DNA binding domain (C-DBD) – DSS1

The C-terminal DNA binding domain (C-DBD) represents the most conserved part of the BRCA2 protein, and it comprises four sub-domains: one helical domain (HD) and three oligonucleotide/oligosaccharide binding folds (OB folds) (**Fig. 11**). The C-DBD together with BRC3-4 are sufficient to promote the assembly of RAD51 onto ssDNA in vitro suggesting that a DNA binding unit and a RAD51 interaction domain is the minimal functional unit to load RAD51 (Filippo et al., 2006). The C-DBD binds DSS1 (Yang et al., 2002), a conserved acidic 70 aa disordered protein which has been shown promote the BRCA2 loading activity of RAD51 (Liu et al., 2010) and its stability (Li et al., 2006). In fact, DSS1 in combination with the C-DBD promote BRCA2-dependent HR by reducing the affinity of RPA for ssDNA, favoring RPA displacement for RAD51 binding to this substrate (Zhao et al., 2015). In addition, BRCA2 can form oligomers, a process counteracted by DSS1 and ssDNA (Le et al., 2020; Reuter et al., 2015; Shahid et al., 2014). This conformational change may play a role in controlling BRCA2 functions at DSBs or replication forks. In addition, the interaction of BRCA2 with DSS1 masks a nuclear export signal in BRCA2 and thereby controls both BRCA2 and RAD51 nuclear localization (Jeyasekharan et al., 2013): consequently, deleterious variants in this domain cause mislocalization of BRCA2 in the cytoplasm.

The C-terminal region: NLS, RAD51 and DNA binding domain

The extreme C-terminal region of BRCA2, corresponding to exon 27, harbors two nuclear localization signals (NLS) and a second RAD51 binding domain (**Fig. 11**). This latter has been involved in protecting replication forks from nucleolytic degradation (described in section 2.4.1) (Feng & Jasin, 2017; Lomonosov et al., 2003; Schlacher et al., 2012). This interaction is cell-cycle regulated by BRCA2 phosphorylation (Esashi et al., 2005). Interestingly, a recent study has revealed the presence of a third ss- and dsDNA binding domain close to the RAD51 binding site which, together with the canonical C-DBD, plays a role in enhancing the assembly of RAD51 presynaptic filaments (Kwon et al., 2023) (**Fig. 11**).

N-terminal domain (NTD)

Unlike the C-DBD, the N-terminal domain (NTD) of BRCA2 is particularly poorly conserved and highly disordered (Julien et al., 2020). Disordered regions can undergo different post-translational modifications, allowing change of conformations and binding of multiple proteins. One of the most-well characterized is the Partner and Localizer of BRCA2 (PALB2) (**Fig. 11**). PALB2 serves a dual function: first, it facilitates the recruitment of BRCA2 to DNA damage sites (Sy et al., 2009; Xia et al., 2006), and second, it acts as a molecular scaffold, bridging BRCA1 and BRCA2 during HR (Sy et al., 2009) (**Fig. 12**). Moreover, PALB2 exhibits DNA-binding capabilities and promote RAD51 strand invasion (Buisson et al., 2010). Like BRCA1/2, PALB2 is recognized as a tumor suppressor gene. Mono-allelic mutations in PALB2 predispose individuals to breast cancer (Antoniou et al., 2014; Rahman et al., 2007), while bi-allelic mutations are associated with the development of Fanconi Anemia (FANC-N) (Xia et al., 2007).

N-terminal DNA binding domain (N-DBD)

Our lab revealed and characterized an additional DBD in the NTD (N-DBD) in the region from 250-500 aa (**Fig. 11**). The N-DBD binds both ssDNA and dsDNA as well as ssDNA gap substrates in vitro. Interestingly, this N-DBD by itself can stimulate RAD51-mediated recombination in the presence of RPA, thus promoting HR (Nicolai et al., 2016). Moreover, N-DBD is required to prevent and repair HU-induced replication-associated ssDNA gaps by HR (Vugic et al., 2023) (**Fig. 12**).

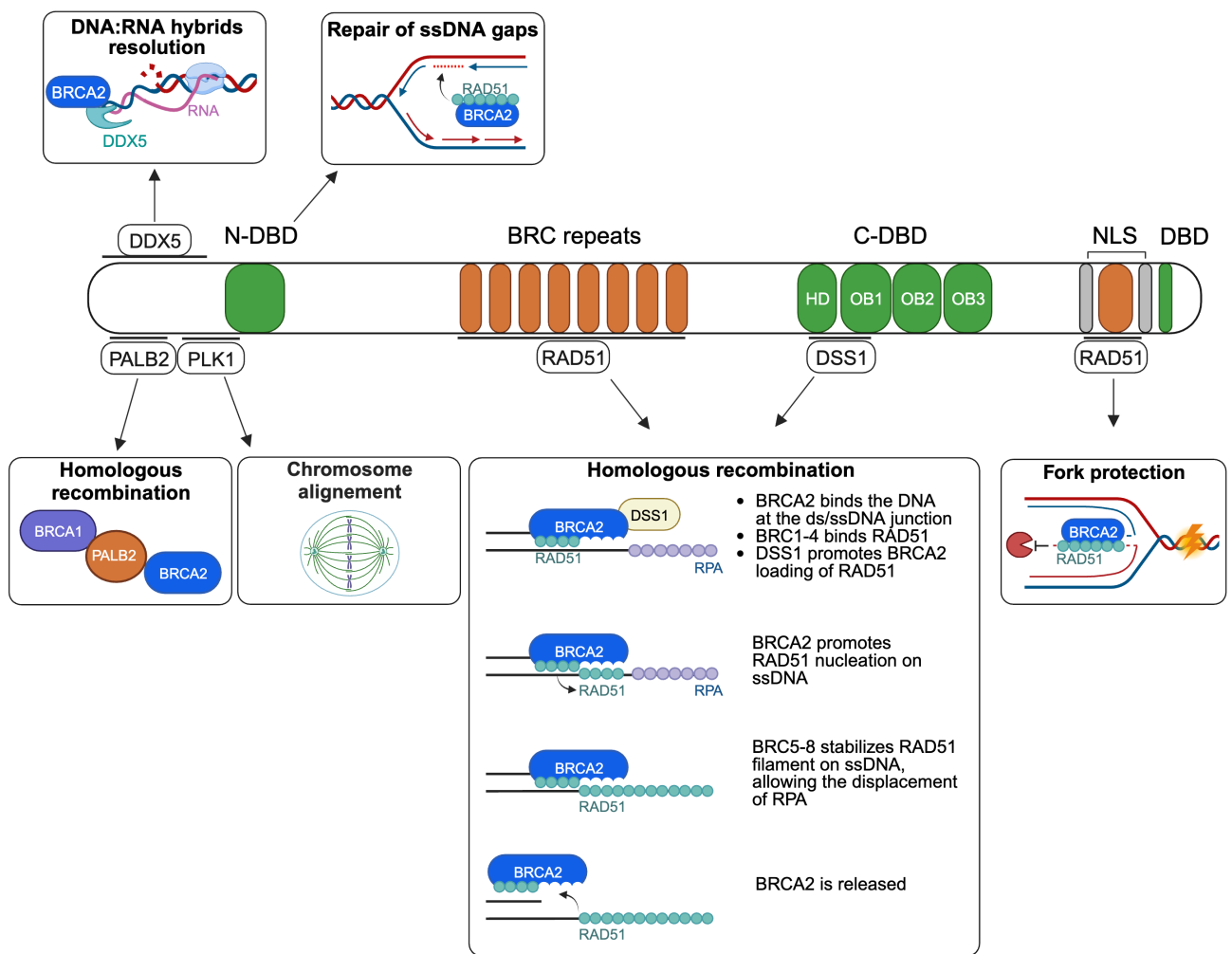


Figure 12. Overview of BRCA2 HR-dependent and non-canonical functions (below). Each arrow indicates the function of BRCA2 and its interacting partner, illustrated in each square. Details of interacting proteins and functions are described in section 2.2 and 2.3. Created with BioRender.com.

2.3. BRCA2 functions

2.3.1. HR-dependent functions

DSBs

As discussed in section 1.1.4.3.2., during HR, BRCA2 facilitates RAD51 strand-exchange activity through a series of coordinated steps. Initially, BRCA2 interaction with DSS1 triggers the displacement of RPA from ssDNA. Following this, the BRC repeats play a crucial role in promoting RAD51 nucleation on ssDNA (**Fig. 12**) (Zhao et al., 2015). Notably, the BRCs exhibit distinct functions (Carreira et al., 2009; Carreira & Kowalczykowski, 2011):

BRC1-4 bind with high affinity free RAD51 and preventing its assembly on dsDNA while facilitating its nucleation onto ssDNA. Subsequently, BRC5-8 bind to the RAD51 nucleoprotein filament, stabilizing it. These activities ultimately promote the strand exchange activity of RAD51 (Carreira & Kowalczykowski, 2011).

Fork protection (FP)

As previously discussed in 1.2.3.2.3., the replication fork (RF) can undergo reversal as a mechanism to cope with replicative stress (Zellweger et al., 2015). While this prevents the progression of DNA synthesis across lesions, it also exposes DNA ends to nucleolytic action. In this context, BRCA2 is a crucial mediator of the fork protection (FP) (**Fig.12**). Its C-terminal region interacts with RAD51, enabling RAD51 nucleation on nascent DNA, thus shielding it from uncontrolled degradation (Schlacher et al., 2011). Notably, mutants with a disrupted C-terminal interaction between BRCA2 and RAD51 are FP-deficient but HR-proficient, indicating that these two functions of BRCA2 are genetically distinct (Schlacher et al., 2011). Intriguingly, different from HR, the recruitment of PALB2-BRCA2 at the fork occurs independently of BRCA1 and may involve factors such as RPA, ATR and RNF168 (Tye et al., 2021). On the other hand, BRCA1 and FANCD2 are required to promote stabilization of the RAD51 filament (Daza-Martin et al., 2019; Schlacher et al., 2012).

Besides FP, RAD51 catalyzes fork reversal independently of BRCA2 (Zellweger et al., 2015). Intriguingly, while the complete silencing of RAD51 inhibits fork reversal (Mijic et al., 2017), partial depletion promotes it but does not ensure fork protection. This suggests that low levels of RAD51 are adequate for fork reversal but insufficient for full fork protection (Tye et al., 2021). Finally, a recent study illustrates how BRCA2 and RAD51 switch between HR and FP pathways. During G2, the kinase Nek1 phosphorylates RAD54, promoting RAD51 filament disassembly to complete the HR process (Spies et al., 2016). Conversely, during the S phase, RAD54 phosphorylation is inhibited to prevent the removal of RAD51 from stalled replication forks (Spies et al., 2016).

Gaps suppression (GS)

Replicative gaps frequently occur during the synthesis of the discontinuous Okazaki strand or when replicative stress leads to the uncoupling of the replication machinery and the helicase in the leading strand. Repriming helps resuming DNA synthesis beyond these lesions but leaves gaps behind. In humans, these gaps are subsequently filled in post-replication, primarily by the primase-polymerase, PRIMPOL, TS, and TLS (**Fig. 10**). Notably, BRCA proteins have been implicated in promoting gap processing and filling during the S and G2 phases (Tirman et al., 2021). Furthermore, recent research from our lab has revealed that BRCA2 N-DBD is sufficient for suppressing HU-induced ssDNA gaps; revealing that PARPi-induced ssDNA gaps and nucleotide depletion-induced ssDNA gaps elicit different gap suppression mechanisms and different domains of BRCA2 (Vugic et al., 2023) (**Fig. 12**).

2.3.2. Non-canonical functions

R-loops metabolism

The accumulation of R-loops in BRCA2-depleted cells initially hinted a role of BRCA2 in R-loop metabolism (Bhatia et al., 2014). BRCA2 interacts with TREX-2, a complex involved in mRNA processing and export. This association promotes BRCA2 recruitment and binding to R-loops at transcribed regions. Interestingly, our lab uncovered that the DEAD-box RNA helicase DDX5 unwinds DNA-RNA hybrids and that BRCA2 enhances this activity *in vitro*. Moreover, they found that both proteins are recruited near DSBs at highly transcribed regions promoting DNA-RNA hybrid resolution and the downstream HR process (Sessa et al., 2021) (**Fig. 12**). In addition, at DSBs, BRCA2 interacts with RNaseH2 as a mean to counteract RNA-DNA hybrids (D'Alessandro et al., 2018). Finally, BRCA2 was shown to promote active transcription elongation (Shivji et al., 2018). These findings suggest a multifunctional role for the BRCA2 repair protein in regulating R-loops.

Mitosis

Although it has been a controversial topic, BRCA2 seems to be involved in cytokinesis (Daniels et al., 2004; Mondal et al., 2012). It was shown that BRCA2 plays a scaffolding role

as a platform for binding for many proteins involved in abscission at the midbody. Its localization to the midbody is regulated by phosphorylation. In particular, the phosphorylation of BRCA2-T77 by CDK1 promotes BRCA2 phosphorylation at S193 by the cell cycle master regulator Polo-like kinase 1 (PLK1), resulting in BRCA2 localization to the midbody (Mondal et al., 2012; Takaoka et al., 2014).

Interestingly, recent work from our group unveiled BRCA2-T207 as a conserved mitotic phospho-site and docking site for PLK1 (Ehlén et al., 2020). This phosphorylation enhances a tetrameric complex composed of BRCA2, PLK1, PP2A, and BUBR1, that is crucial to ensure stable kinetochore-microtubule attachments (**Fig. 12**). Mutations disrupting this phosphorylation causes unstable kinetochore-microtubule interactions, leading to chromosome misalignment, segregation errors and aneuploidy.

2.4. HR, FP, and GS in cancer therapy

Due to deficiencies in HR, BRCA1/2-deficient cells exhibit high sensitivity to genotoxic agents such as ionizing radiation but especially to alkylating agents like MMC and cisplatin. These cells and tumors are also exquisitely sensitive to PARPi due to its synthetic lethal interaction with BRCA1/2 (Bryant et al., 2005; Farmer et al., 2005). Originally, the prevailing notion was that these inhibitors worked by impeding PARP1 repair of SSBs, which, upon replication, would be converted into DSBs (Ashworth, 2008; Ceccaldi, Rondinelli, et al., 2016; Pommier et al., 2016). Recent findings however suggest that instead of fork stalling, PARPi accelerate replication (Maya-Mendoza et al., 2018), which leads to the accumulation of replication-associated gaps behind the fork. Notably, BRCA-deficient cells tend to accumulate such lesions following exposure to PARPi, replicative stress induced by HU or multiple rounds of cisplatin (Cong et al., 2021; Panzarino et al., 2021; Quinet et al., 2021; Vugic et al., 2023). These discoveries strongly suggest that DNA gaps play a pivotal role as an underlying mechanism contributing to the toxicity associated with these drugs.

Intriguingly, the Cantor lab has shown that restricting replication or increasing TLS-mediated gap filling promotes chemoresistance (Guillemette et al., 2015), while restoring

HR or FP does not (Panzarino et al., 2021), although this notion is still under debate (Lim et al., 2023). Moreover, the lab of Keith Caldecott has demonstrated that PARP1 has a role in sensing and repairing unprocessed Okazaki fragments which may contribute to the toxicity of PARPi (Cong & Cantor, 2022; Hanzlikova et al., 2018).

Despite their initial effectiveness, around 40% of tumors treated with PARPi eventually develop resistance, which can be attributed to various mechanisms. In the case of BRCA2-associated tumors, this includes drug efflux systems (Vaidyanathan et al., 2016) and the restoration of HR via secondary BRCA2 gene mutations that repair the open-reading frame (ORF) of the gene (Lord & Ashworth, 2013). Another mechanism of PARPi resistance involves depleting PARP1 negative regulator, namely PARG (Gogola et al., 2018). One more example is the restoration of fork protection (FP): this is achieved by depleting PTIP, a member of the MLL3/4 complex that promote the recruitment of MRE11 nuclease to stalled replication forks (Chaudhuri et al., 2016). Loss of fork remodelers like ZRANB3, SMARCAL1 and HLF (Kolinjivadi et al., 2017; Tagliatela et al., 2017) and the remodeling factor CHD4 (Guillemette et al., 2015) can also restore FP in BRCA2-deficient cells. Despite these findings, in breast epithelial cells, HR and not FP seems to be required to restore cell viability (Feng et al 2017).

2.5. BRCA2 variants and cancer predisposition

Breast cancer is the predominant malignancy and the primary cause of cancer-related deaths among women worldwide (Sung et al., 2021). Breast cancer can be evaluated based on various parameters: firstly, tumor grade, which reflects the abnormality of cells and correlates with tumor aggressiveness. Secondly, hormonal status is based on the expression of the progesterone receptor (PR), estrogen receptor (ER), or amplification of the Her2 receptor. This is important because some treatment options vary based on the receptor expression in the tumor, with Her2-positive tumors being targeted by antibody-based therapy, and ER and PR-positive tumors benefiting from hormonal therapy. Tumors lacking the expression of all these hormonal receptors are referred to as triple-negative breast cancers (TNBC), which tend to be more aggressive and challenging to treat.

BRCA2-associated familial breast tumors are generally hormone-receptor positive and medium to high-grade (Roy et al., 2012). This can be explained by lineage tracing analysis revealing that *BRCA2* mutation mainly affects the L2 hormone-responsive luminal breast cell population (Palacios et al., 2005). In addition to breast and ovarian cancer, *BRCA2* mutations confer an increased risk of developing male breast, pancreatic, and prostate cancer (Asperen et al., 2005; Breast Cancer Consortium, 1999; Couch et al., 1996; Goggins et al., 1996).

Since the discovery of *BRCA2*, numerous variants have arisen, with founder mutations being common in specific populations like Ashkenazi Jewish and Icelandic. Among the 14,914 *BRCA2* variants reported in the ClinVar database, missense mutations are most prevalent (7,156), followed by frameshift (3,756), and nonsense mutations (1,040) (data of September 2023).

The majority of pathogenic variants are frameshift and nonsense mutations, creating premature stop codons that truncate the encoded protein and potentially reduce its expression through mRNA decay (Anczuków et al., 2008). In contrast, only a few missense variants, resulting in stable mutant proteins have been classified as pathogenic (Couch et al., 2014; Venkitaraman, 2019). However, up to 80% of missense variants are "variants of unknown clinical significance" (VUS), complicating genetic counseling due to uncertain impact on protein function and on cancer risk (Caputo et al., 2021). International initiatives like the Evidence-based Network for the Interpretation of Germline Mutant Alleles (ENIGMA) collect clinical and functional data to improve VUS classification (Spurdle et al., 2012). This consortium provides criteria for assessing variant significance based on multifactorial likelihood models, including family history, clinical assessments, bioinformatics predictions, co-segregation with the disease, and functional characterizations (Goldgar et al., 2008; Parsons et al., 2019). Data from ENIGMA are integrated into the global BRCA Exchange database, along with information from other databases (e.g., ClinVar, LOVD, GnomAD), providing updated variant interpretation reports (Cline et al., 2018). Nevertheless, for rare VUS, the functional evaluation such as

HR and sensitivity to PARPi and MMC becomes key to predict pathogenicity (Farrugia et al., 2008; Guidugli et al., 2013, 2014; Shimelis et al., 2017; Wu et al., 2005).

As mentioned above, germline pathogenic variant affecting a single copy of BRCA2 significantly increase the risk of breast and ovarian cancer. Accumulating evidence suggests that depending on the localization of *BRCA2* mutation in the sequence, their incidence in cancer and which cancer they predispose to may change (Rebbeck et al., 2015) (**Fig. 13**), although the reasons for these differences are still uncertain.

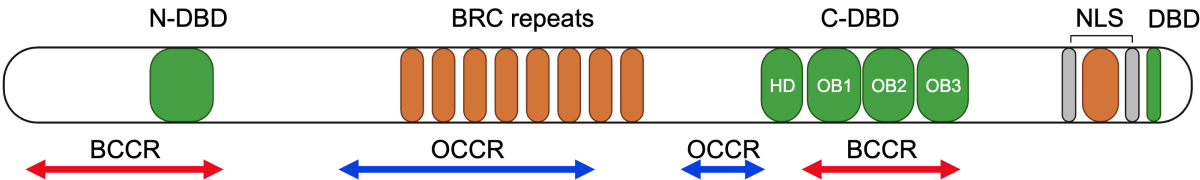


Figure 13. Schematic of cancer risk depending on BRCA2 mutation location. Red arrows indicate regions whose mutations are associated with breast (BCCR, red) or ovarian (OCCR, blue). Figure adapted from Rebbeck et al., 2015. Created with BioRender.com.

3. BRCA2 haploinsufficiency

As mentioned above, germline mutations affecting a single copy of BRCA2 significantly increase the risk of breast and ovarian cancer. However, the precise mechanism underlying tumor formation in this context is not fully understood. Contrary to the long-standing belief that the loss of the second WT allele is necessary for tumor development, a growing body of evidence suggests that tumorigenesis can occur despite the presence of a single functional allele. This entails that heterozygosity in BRCA2 confers haploinsufficiency, where a single copy of the gene is not sufficient to fully suppress tumor formation.

Here I will provide an overview of the findings, evidence and the ongoing debate regarding BRCA2 haploinsufficiency. Elements of this chapter are drawn from our recent Perspective article "BRCA1/2 haploinsufficiency: exploring the impact of losing one allele," *Journal of Molecular Biology*, Minello & Carreira, 2023 (see Appendix).

3.1. The two-hit model and the BRCA paradox

The initial paradigm for tumor formation in TS genes emerged from the 'two-hit' model (Knudson, 1971) proposing that individuals with a mono-allelic germline mutation acquired a second mutation (second hit) in the same gene, somatically. This hypothesis was formulated for the Retinoblastoma gene (RB)-related tumors and later extended to *BRCA1* and *BRCA2* to explain hereditary cancer susceptibility (Collins et al., 1995; Gudmundsson et al., 1995; Neuhausen & Marshall, 1994; Smith et al., 1992). However, the two-hit hypothesis was later refined to a continuous model to accommodate the fact that, in some cases, partial loss of a tumor suppressor was sufficient to promote tumorigenesis (Berger et al., 2011).

According to this theory, individuals with a mono-allelic germline mutation would acquire a second somatic mutation, the 'second hit', that inactivates the remaining functional allele, rendering the protein non-functional. This event is referred to as Loss of Heterozygosity (LOH). In the case of *BRCA1/2*, the mechanism of LOH is thought to arise

through allelic recombination (Moynahan & Jasin, 1997), genetic rearrangements, physical deletions, somatic mitotic recombination (Osorio et al., 2002; Thiagalingam et al., 2002) or promoter hypermethylation (BRCA1 only) (Dworkin et al., 2009). Interestingly, BRCA genes have recently been identified as common fragile sites (CFS) in the genome (Deshpande et al., 2022). These sites are prone to replication challenges and DNA breakage due to long repeated sequences. Replication fork stalling and subsequent error-prone repair can result in mutations or large deletions, leading to functional inactivation of the WT BRCA gene constituting another mechanism of LOH.

The mechanism of BRCA loss has been enigmatic: on the one hand, *BRCA* deficiency results in cell lethality in embryos and cell cycle arrest in cultured cells and, on the other, in tumors, *BRCA* loss promotes aberrant DNA replication and unrestricted proliferation, leading to the accumulation of genetic alterations that fuel malignancy. This so called “BRCA paradox” has been partly explained by the observation that in murine cells, the silencing of *Brca1* or *Brca2* leads to cell death unless combined with a knockout of *Tp53* (Hakem et al., 1996; Ludwig et al., 1997). Later studies revealed that *TP53* loss is a common characteristic of *BRCA*-related tumorigenesis, although it is not the sole factor (Crook et al., 1998; Rhei et al., 1998). Besides *TP53* loss, other mechanisms such as the loss of the tumor suppressor genes *RB1* or *PTEN* contribute to generating a premalignant environment in this context (Martins et al., 2012).

3.2. Evidence of locus-specific LOH from BRCA-mutated tumors

The initial studies on LOH at *BRCA1/2* loci in breast tumor samples from *BRCA*-mutation carriers revealed diverse LOH patterns within and among invasive lesions; these included cases where the loss predominantly affected the mutant allele rather than the WT allele (King et al., 2007). These observations suggested that LOH could play a role in the early stages of cancer development but may not be indispensable for tumor progression and maintenance. Supporting this notion, microarray-based analysis of normal breast tissue obtained from *BRCA*-mutation carriers undergoing prophylactic

mastectomy showed an increased prevalence of genetic abnormalities, despite the presence of the WT allele (Rennstam et al., 2010).

In recent years, the BRCA haploinsufficiency hypothesis has gained momentum with the increase of genetic testing thanks to the advances in next-generation sequencing (NGS). These technologies have led to the identification of distinguishable patterns of substitutions or genomic signatures for the different types of tumors (Alexandrov et al., 2013; Nik-Zainal et al., 2016) including those associated with *BRCA1/2* pathogenic variants. Inactivation of *BRCA1* or *BRCA2* results in a specific substitution pattern that is commonly known as homologous recombination deficient (HRD) signature (Alexandrov et al., 2013). This include single base substitution 3 (SBS3) and indel signature 6 (ID6), which are attributed to the error-prone DNA repair by alt-EJ (Alexandrov et al., 2020; Stok et al., 2021). Nevertheless, the use of SBS3 is insufficient for distinguishing between HR-proficient and HR-deficient tumors. Hence, an ensemble of substitution, indel, and rearrangement signatures as well as the presence of deletions with microhomology identified in *BRCA1/2* germline tumors has been integrated within the predictive tool known as HRDetect (Davies et al., 2017).

Interestingly, NGS analysis have revealed significant disparities between *BRCA1* and *BRCA2*-associated tumors in terms of LOH frequency. For example, in a cohort of 35 *BRCA2*-mutated familial breast cancers, LOH was found in 50% of cases, while in 41 *BRCA1*-mutated tumors, LOH prevalence was 90% (Maxwell et al., 2017). Similarly, an analysis of LOH in hereditary ovarian cancer *BRCA1*-associated cases exhibited a 100% LOH prevalence compared to the 76% observed in *BRCA2*-related cases (Kanchi et al., 2014). These differences suggest potential variations in the mechanisms of tumor formation due to *BRCA1*- or *BRCA2* mutations, which could underlie the distinct molecular features of these cancers (see section 3.3.). In addition, the retention of the WT allele has been observed in non-gynecological BRCA-associated tumors in mouse models. For instance, LOH was detected in only 37% of cell lines and xenografts derived from *BRCA2*-mutated pancreatic carcinoma (Goggins et al., 1996). Similarly, in a murine model of familial pancreatic cancer, three out of four tumors with germline heterozygosity for a

pathogenic *Brca2* mutation did not exhibit LOH at the mutation site (Skoulidis et al., 2010). These observations have fueled research in the quest for evidence of haploinsufficiency conferred by heterozygosity of *BRCA1/2*.

3.3. Molecular evidence and mechanisms of BRCA2 haploinsufficiency

BRCA2 haploinsufficiency has been investigated using diverse model systems. Notably, one study found that BRCA2-heterozygote lymphoblastoid cell lines (LCLs) demonstrated elevated levels of DNA damage, even in untreated conditions, which escalated upon treatment with DNA-alkylating agents such as MMC (Arnold et al., 2006). In the same study, BRCA2-mutated lymphocytes increased the rate of spontaneous sister chromatid exchanges (SCEs), a readout of ongoing genomic instability. Similarly, the lymphoblast chicken cell line DT-40 bearing a mono-allelic BRCA2 variant, which produced a truncated product, revealed decreased RAD51 foci formation after irradiation, as well as reduced proliferation, increased cell death, and heightened sensitivity to DNA-damaging agents (Warren et al., 2003). In stark contrast, a study using human HT-29 colon cancer cells reported that the presence of a single functional BRCA2 allele did not hinder RAD51 foci formation or compromised DNA repair capacity after irradiation (Tannenbaum et al., 2007). These discrepancies may be in part attributed to the presence of a truncated BRCA2 protein observed in the first study, acting as dominant negative, or, to differences related to the cell-line model system used.

Mouse cells expressing a homozygous deletion of exon 27 *Brca2*^{Δ27/Δ27} that comprises the C-terminal Rad51 binding site exhibited impaired HR repair and replication fork protection and accumulated ssDNA gaps (Kass et al., 2016; Lim et al., 2023; Schlacher et al., 2011). Interestingly, *Brca2*^{+/Δ27} cells showed intact HR but displayed defects in replication fork protection and ssDNA gap suppression (Lim et al., 2023). Nevertheless, it is important to note that BRCA-heterozygous mice are not prone to developing breast cancer (Berton et al., 2003; Sedic & Kuperwasser, 2016), while homozygous pathogenic variants often result in embryonic lethality or the development of blood tumors (Connor, Bertwistle, et al., 1997; Evers & Jonkers, 2006; Friedman et al., 1998). Therefore, despite

the enormous advances in the understanding of BRCA1/2 function and tumor progression they have provided (Jonkers et al., 2001; Ludwig et al., 2001), results from these models may not be easily extrapolated to mimic early stages of tumor formation linked to human *BRCA1/2* mutations. A way to partially circumvent this issue came from the generation of conditional mouse models, where the concurrent tissue-specific inactivation of *Brca1* or *Brca2* and *Tp53* led to the development of breast tumors (Jonkers et al., 2001; X. Liu et al., 2007). Nevertheless, some *BRCA1/2*-mutated tumors do not present *TP53* mutation raising the question of whether this is an early or necessary step in tumor development in humans (Greenblatt et al., 2001). Thus, the efforts to fully recapitulate the early steps of BRCA-related tumorigenesis in human model systems are still ongoing.

One approach to recapitulate precancerous steps involves the use of primary breast epithelial cells derived from *BRCA2*-mutation carriers. Interestingly, when compared to cells from non-carriers, several genes were found to be deregulated (Bellacosa et al., 2010). In a different report using also patient derived epithelial cells from *BRCA2*-mutation carriers the authors found impaired replication fork protection and induced chromosomal aberrations. These were attributed to selective proteasomal degradation of *BRCA2* driven by the accumulation of aldehydes, natural by-products of cellular metabolic processes (Tan et al., 2017). Using the same model, Karaayvaz-Yildirim and colleagues found that heterozygous *BRCA2* mutated cells display a weakened response to replication stress manifested in an increased DNA damage after hydroxyurea (HU) treatment and impaired replication checkpoint response (Karaayvaz-Yildirim et al., 2020).

Collectively, despite variations arising from diverse mutations or system models, these studies appear to support the hypothesis of *BRCA2* haploinsufficiency (**Fig. 14**).

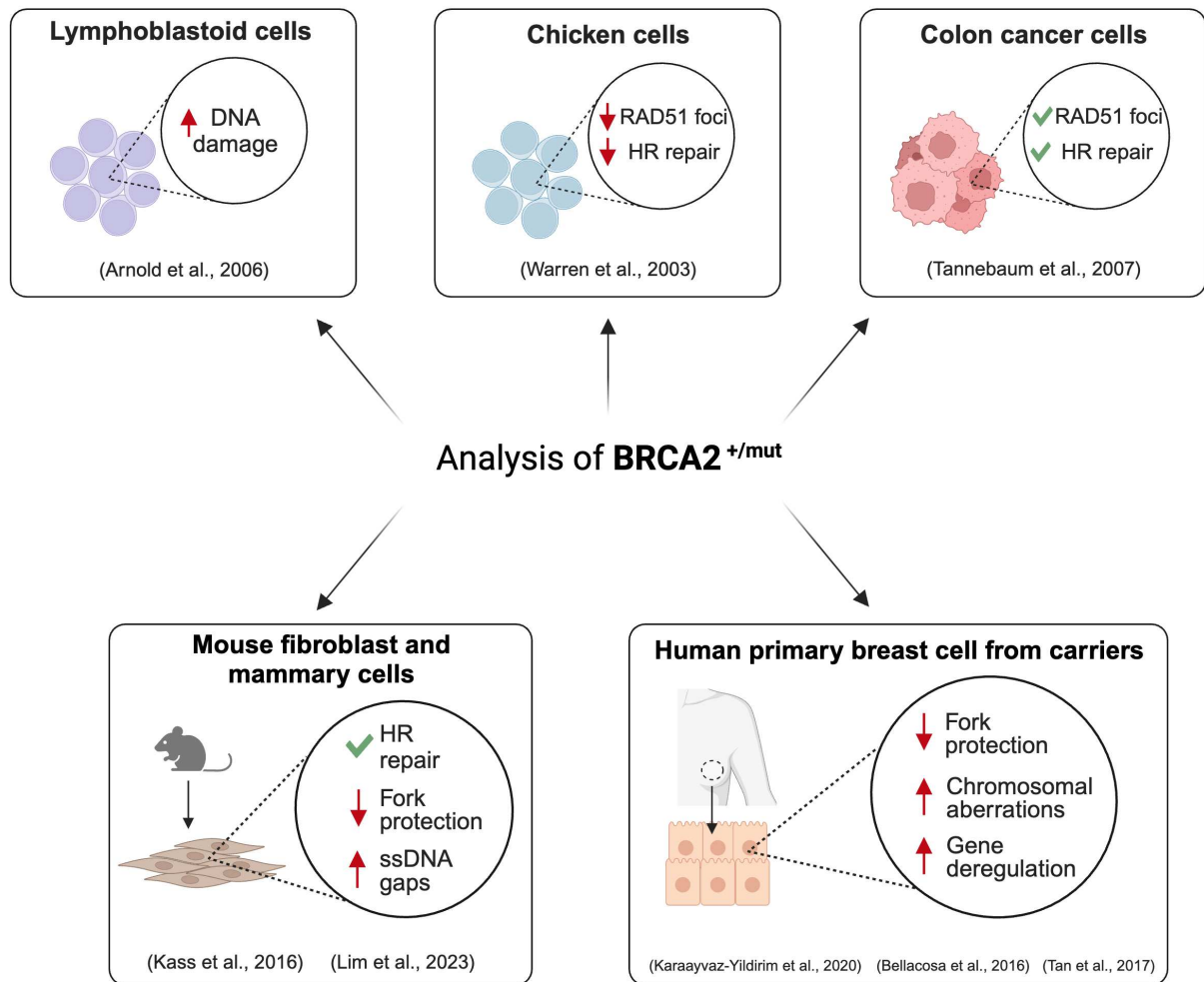


Figure 14. Overview of key findings supporting the $BRCA2$ haploinsufficiency hypothesis. Each box illustrates the system model used along with the primary characterized phenotypes. For details see section 3.3. Created with BioRender.com.

Chapter 2 – Objectives and Results

1. Hypothesis

As mentioned above in the Introduction, inherited mono-allelic pathogenic variants in the tumor suppressor gene BRCA2 confer predisposition to breast and ovarian cancer (King et al., 2007; Melchor & Benítez, 2013; Narod & Foulkes, 2004). Although the deleterious effect of the BRCA2 deficiency is well-established, what drives tumor formation in BRCA2 mutation carriers has not been completely elucidated. According to the two-hit model (Knudson, 1971), the essential step for carcinogenesis in BRCA2-mutated cells seems to be the somatic inactivation of the BRCA2 WT allele, also referred to as loss of heterozygosity (LOH). However, this model has been revisited as a fraction of cancers retain an intact second allele (Goggins et al., 1996; Kanchi et al., 2014; Maxwell et al., 2017; Skoulidis et al., 2010). This emerging evidence suggest that cells bearing a BRCA2 mono-allelic variant could display *per se* a distinct genome instability signature that could mimic a pre-cancerous lesion, thus entailing BRCA2 haploinsufficiency. This PhD project aims to test this hypothesis and determine whether different BRCA2 pathogenic variants underlie distinct mechanisms of tumor formation.

2. Preliminary data

Two different mono-allelic BRCA2 truncating pathogenic variants result in distinct transcriptomic profiles

To investigate our hypothesis, we focused on two common truncating pathogenic variants of BRCA2 (**Fig. 1A**). The first, the c.771-775del, also known as 999del5 (del5), is an Icelandic founder mutation. The 5 base-pairs deletion in exon 9 leads to a premature stop codon (Mikaelsdottir et al., 2004). The corresponding truncated protein, predicted to be of 256 amino acids, is unstable, undetected and is considered null. The second variant, the c.5946del (delT), is prevalent in individuals with Ashkenazi Jewish ancestry (Oddoux et al., 1996). The one-nucleotide deletion in exon 11 induces a frameshift, resulting in a premature stop codon leading to a truncated protein ending at aa 1982, within the BRC repeats motif (**Fig. 1A**). Due to the loss of the C-terminal domain, which includes the

nuclear localization signals (NLS), the truncated protein is miss-localized in the cytoplasm (Spain et al., 1999).

Before my arrival in the lab, the variants were introduced into one allele of the gene in MCF10A, a non-transformed human mammary epithelial cell line with a relatively stable genome (Soule et al., 1990) using gene-editing techniques. Specifically, the BRCA2+/delT clone was generated using site-specific transcription-activator like effector nuclease (TALEN) while CRISPR-Cas9 nickase was utilized for the BRCA2+/del5 clone. Each nuclease was co-transfected with a plasmid containing homologous flanking regions to the target sequence and the desired deletion (**Fig. 1B**). The generation of the +/delT clone resulted in a deletion in the following nucleotide, leading to +/5947delG. Nevertheless, as both mutations lead to the same premature stop codon, this clone was selected for further studies. A clone that tested negative for the mutation was chosen as control for the analysis, in addition to the parental cell line.

Subsequently, the impact of the two different BRCA2 mono-allelic variants on the transcriptome was explored by profiling 3 technical replicates of each cell line at early passage using RNA-sequencing (RNAseq). The identification of differentially expressed genes (DEGs) was performed by Nicolas Servant and Marc Deloger from the Bioinformatic platform of Institut Curie, applying a log₂ fold change > 1.5 for each BRCA2-mutated clone compared to the parental control. The results were visualized in a principal component analysis (PCA) plot, illustrating the transcriptomic differences between samples along the axis (**Fig. 1C**). Notably, the horizontal axis explained ~60% of the variance, distinguishing the parental and +/del5 cell lines from the +/delT clone. Specifically, the +/del5 cell line showed minimal variations in gene expression, with only ~400 deregulated genes (**Fig.1D, top**). On the other hand, the +/delT mutated clone showed significant differences, affecting the expression of ~1400 genes (**Fig. 1D, bottom**). To confirm these findings in a different cell system, the mono-allelic delT variant was introduced by CRISPR-Cas9 into a different cell system, specifically the MDA-MB-231 triple-negative breast cancer (TNBC) cell line (kind gift from Prof. Krogan, QBI, UCSF). RNAseq analysis was performed using the same bioinformatic pipeline on three technical

replicates for both the control and +/delT mutated clone. Similarly to MCF10A analysis, the resulting PCA plot (**Fig. 1E**) exhibited a ~50% variance along the horizontal axis, clearly separating the control from the +/delT cell line, consistent with the previous observations in MCF10A cells.

Collectively, these analyses indicated that the mono-allelic BRCA2 delT variant shows a stronger impact on the gene expression profile of cells compared to the del5.

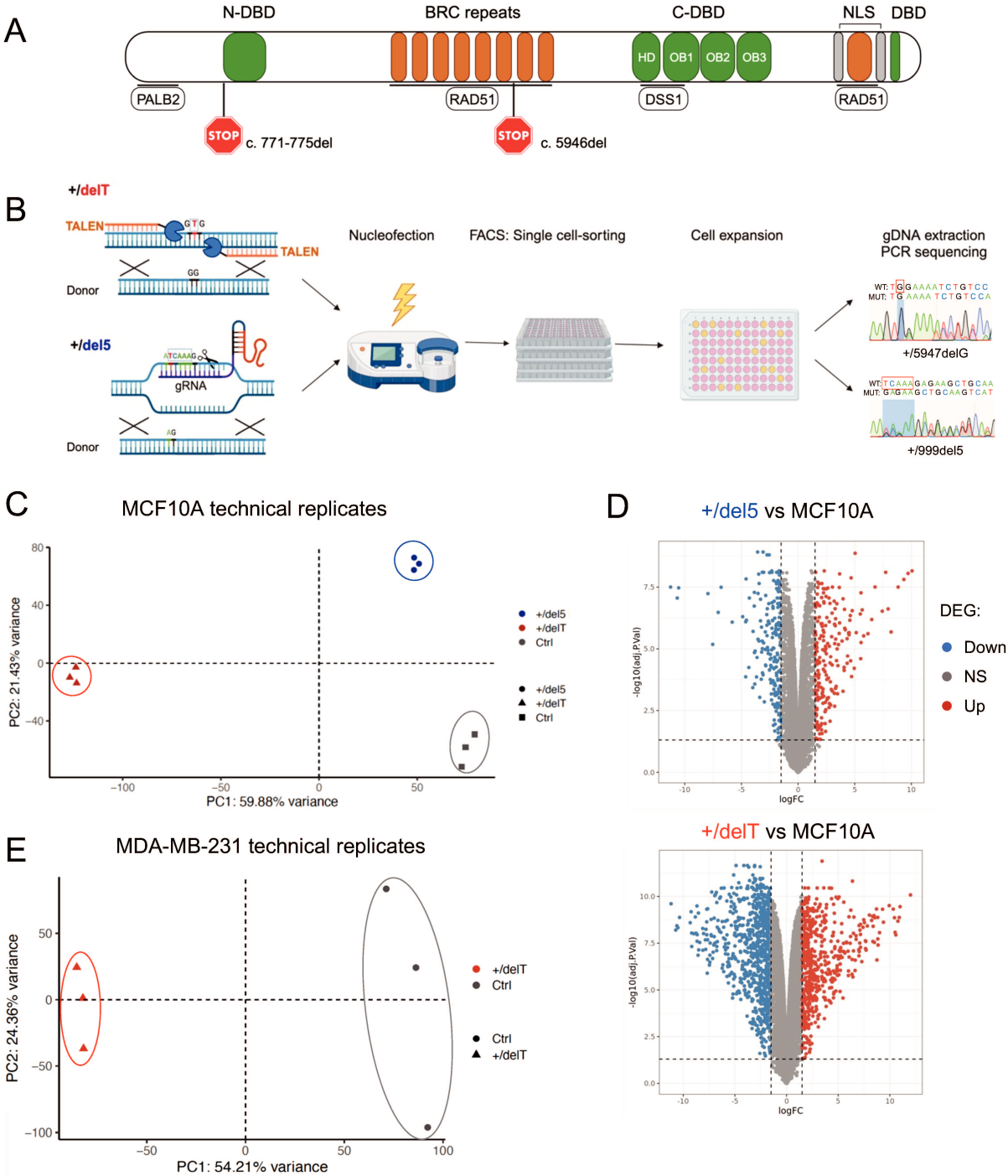


Figure 1. Two different mono-allelic BRCA2 truncating pathogenic variants resulted in distinct transcriptomic profile. **A.** BRCA2 schematic structure including functional domains (above), the two pathogenic variants object of the study (stop) and interactants (below). DNA and RAD51 binding domains are represented in red and blue, respectively. Abbreviations: NTD, N-terminal domain; CTD, C-terminal domain; HD, helical domain; OB folds, oligonucleotide/oligosaccharide binding-fold; NLS, nuclear localization signal. **B.** Creation of stable heterozygote cell lines in MCF10A cells. (Top) Generation of the +/delT cell line via transfection of TALEN endonucleases (orange) and a donor plasmid with homologous flanking regions lacking the T nucleotide (c.5946del). (Bottom) Generation of the +/del5 cell line using CRISPR-Cas9 nickase (scissors), a guide RNA (violet), and a homologous donor plasmid lacking the 5 nucleotides (c.999del5). After transfection and single-cell sorting, clones were expanded for genomic DNA extraction and Sanger sequencing to confirm the mono-allelic BRCA2 mutation. Created with BioRender.com. **C.** Principal component analysis (PCA) plot showing the gene expression profile of 3 technical replicates of the MCF10A control (grey), +/del5 (blue) and +/delT (red). **D.** Volcano plots representing the differentially expressed genes (DEGs) between (top) MCF10A control and +/del5 (~400) and (bottom) +/delT (~1400). Grey dots represent not significantly deregulated genes. **E.** PCA plot showing the gene expression profile of 3 technical replicates of the MDA-MB-231 control (grey) and +/delT (red). **C-F.** DEGs were obtained applying a log₂ fold change > 1.5 and an adjusted p-value of 0.05.

3. Objectives

OBJECTIVE 1: Explore the impact of two different mono-allelic pathogenic variants of BRCA2 on the transcriptome of breast epithelial cells

To achieve this, I performed an extended RNAseq analysis, incorporating two additional biological replicates for each mutated clone coming from the same screen. Then, in collaboration with Elodie Girard and Nicolas Servant (bioinformatic platform of I. Curie) we also analyzed the transcriptome of breast primary tumors bearing the same germline pathogenic variants. Since cancers accumulate genetic aberrations, when possible, we used the matched non-neoplastic surrounding tissue as control, sharing the same BRCA2 variant in heterozygosity and microenvironment as the tumor. The transcriptome of the tumor pairs expressing the same variant was analyzed to get a consensus list of common DEGs to identify potential cancer drivers.

OBJECTIVE 2: Functional characterization of BRCA2 +/-del5 and +/-delT breast epithelial cell lines

Given the function of BRCA2 in genome integrity, we hypothesize that due to a dosage effect, BRCA2 heterozygous cell lines may display distinct genome instability phenotypes that could mimic pre-cancerous lesions. Hence, the second objective involves performing several functional assays to assess defects related to BRCA2-deficiency, like the cell-based homologous recombination assay already set up in the lab (Vugic et al., 2020) and measure the sensitivity to drugs such as MMC and PARPi. Unless otherwise indicated, all experiments were conducted in clone #1 for each BRCA2-mutated clones and clones #2 and #3 for the MCF10A control. To further confirm that the alterations observed were specifically induced by the BRCA2 variant, I employed the CRISPR-Cas9 system in one of the mutated biological replicates to create two cell lines in which the BRCA2 +/-delT and +/-del5 variants were corrected, restoring the WT sequence (hereafter +/-revdelT and +/-revdel5).

OBJECTIVE 3: Reveal the genomic changes induced by two different truncating variants in BRCA2-mutated tumors

In recent years, Whole Genome Sequencing (WGS) has been extensively used to characterize the genome of different cancer types. Those analysis have revealed different patterns of mutations, also referred to as mutational signatures. A specific pattern is observed in *BRCA1/2* deficient tumors. Thus, the third objective of my PhD project was to characterize by WGS two small cohorts of breast tumors to assess whether they display different mutational patterns. Like for the transcriptomic analysis, when possible, the tumor samples were compared to their non-cancerous surrounding tissue. gDNA was extracted and quantified by our collaborators at the University of Iceland and Institut Curie. Subsequently, I assessed its purity and concentration before sending it for WGS at the sequencing platform of Institut Curie. Subsequently WGS data analysis was conducted by our collaborator, Prof. Nik-Zainal (University of Cambridge, UK). With this approach, we aimed to uncover novel mechanisms of tumor formation in BRCA2-associated tumors.

4. Results

OBJECTIVE 1: Explore the impact of two different mono-allelic pathogenic variants of BRCA2 on the transcriptome of breast epithelial cells

The mono-allelic BRCA2 delT pathogenic variant induces deregulation of cell migration-related pathways in MCF10A cells

To validate the initial RNAseq findings and exclude potential off-target effects, we included two more biological replicates from the same screen of parental and +/-delT cell lines. For the +/-del5 variant, only one clone was generated; however, in the same gene-editing screening, we obtained two more clones that deleted 2 and 4 nucleotides adjacent to the same residue. In the first case, the resulting truncated protein is identical to that of del5, whereas in the second causes a frameshift and a premature stop codon 40 aa downstream of the mutation. However, as they are both predicted to result in a truncated product that is not expressed, we incorporated both clones into our analysis.

The PCA plot (**Fig. 2A**) revealed variations within the biological replicates of control and +/-del5 clones. Due to these variances and their strong similarity, the analysis did not identify any significantly deregulated genes in the +/-del5 clones when compared to the control MCF10A. In contrast, the +/-delT clones formed a tight cluster. In this case, the horizontal axis of the PCA plot exhibited a distinct separation from both the control and +/-del5 clones. Consequently, the differential analysis revealed a total of 677 DEGs, comprising 259 up-regulated and 418 down-regulated genes (**Fig. 2B**).

We then conducted a Gene Ontology (GO) enrichment analysis on these DEGs (see Material and Methods), which prominently revealed deregulation in the biological process associated with cell migration (**Fig. 2C**).

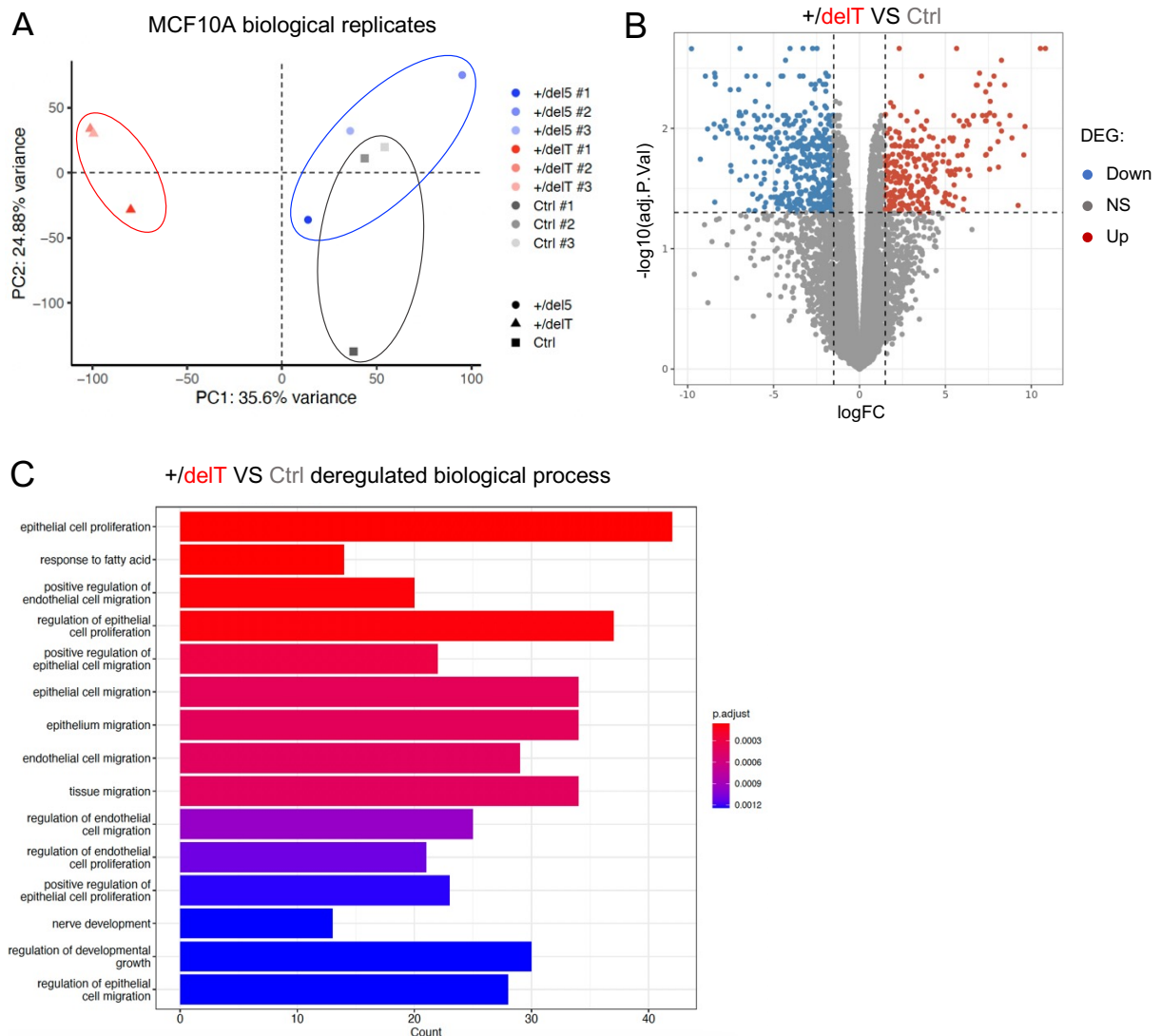


Figure 2. The mono-allelic BRCA2 delT pathogenic variant induces deregulation of cell migration-related pathways in MCF10A cells. **A.** PCA plot showing the gene expression profile of three biological replicates of the MCF10A control (grey), +/del5 (blue) and +/delT clones (red). **B.** Volcano plot representing the differentially up-regulated (red) and down-regulated genes (blue) of +/delT clones when compared to MCF10A control. Grey dots represent not significantly deregulated genes. **C.** Bar charts showing the top 15 Gene Ontology terms for biological process in +/delT biological replicates, ranked by adjusted p-value (red to blue: higher to lower significance) using clusterProfiler (v4.4.4). **B-C.** DEGs were obtained applying a log₂ fold change > 1.5 and an adjusted p-value of 0.05.

Breast epithelial cells and familial breast tumors bearing the BRCA2 delT pathogenic variant down-regulate cell adhesion pathways

After examining the transcriptome of our cell model system, we extended our study to primary breast tumors carrying the same pathogenic BRCA2 variants as the MCF10A clones, using the same bioinformatic approach. Since the genotype of each individual influences the mutational burden of the tumor, we used the non-neoplastic surrounding tissue as control which bears the same BRCA2 pathogenic variant in heterozygosis and shares the same micro-environment. In collaboration with Dominique Stoppa-Lyonnet and the CRB of the Institut Curie Hospital, we obtained RNA sample from 9 tumor pairs with the delT variant and 1 carrying the del5 variant. We also received 5 RNA tumor samples from our collaborator Stefán Sigurdsson (University of Iceland); however, due to the absence of healthy controls for these samples, we restricted RNAseq analysis to the delT tumors only.

The cohort predominantly comprised female participants, with only one male participant. Dr. Anne Vincent-Salomon and her team at the CRB (I. Curie) provided the information on the histology of the tumors: adenocarcinoma and carcinoma of moderate to high grade, consistently demonstrating positivity for estrogen (ER) and progesterone receptors (PR), while the expression of the human epidermal growth factor receptor 2 (HER2) was absent in all samples (**Fig. 3A, extended information on Table 12**).

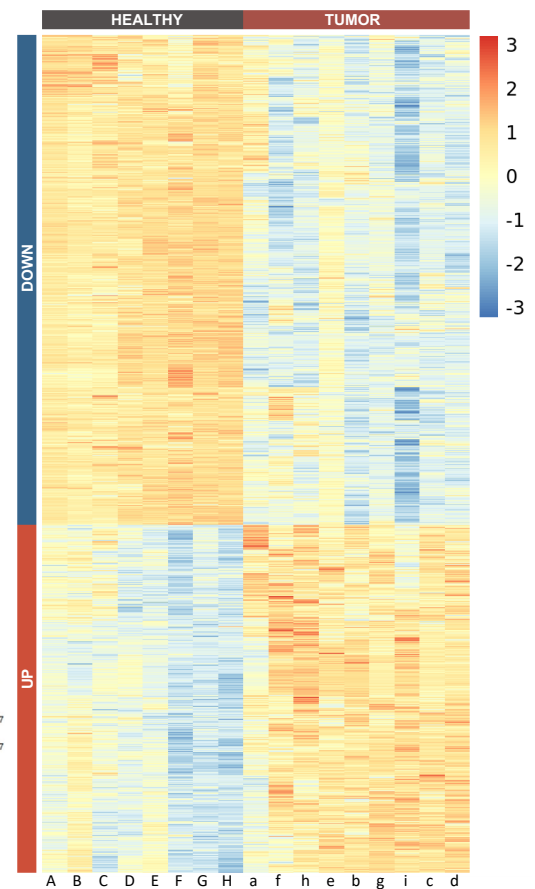
The RNAseq analysis of the 9 tumor pairs with the delT variant exhibited an enrichment of 868 up-regulated and 1363 down-regulated genes, compared to the corresponding non-tumoral controls (**Fig. 3B**). Notably, one control (sample I) was excluded due to its clustering with the tumors and is therefore not represented in the graph. Importantly, the GO analysis revealed deregulations in biological processes associated with extracellular organization including actin filament and cell junction assembly (**Fig. 3C**), similarly to what observed in +/-delT cells (**Fig. 2C**). Additionally, the GO analysis indicated alterations in biological processes linked to cell division and chromosome segregation, suggesting aberrant mitosis, a hallmark of cancer.

A

Sex	8 women, 1 man
Histological type	Carcinoma, adenocarcinoma
Grade	Moderated - elevated
ER	+
PR	+
HER2	-

B

DelT tumors Differentially Expressed Genes (DEGs):



C

DelT tumors deregulated biological process (BP):

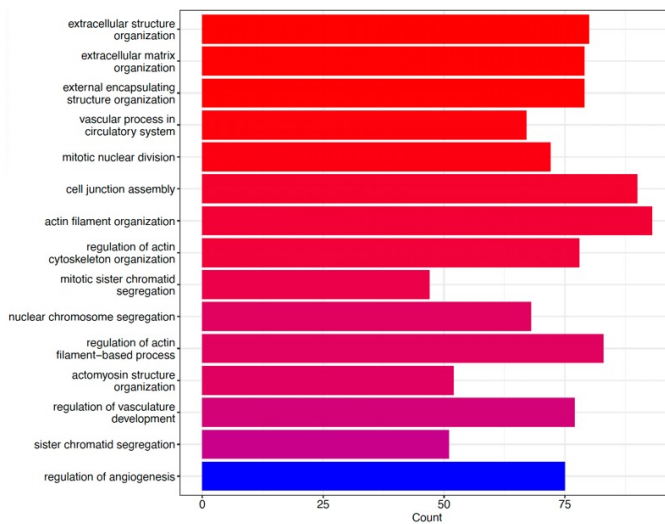


Figure 3. Transcriptomic analysis of familial breast tumors bearing the BRCA2 delT pathogenic variant. A. Summary table of the main clinical characteristics of BRCA2-delT tumor cohort. ER: estrogen receptor; PR: progesterone receptor; PR: progesterone receptor; HER2: human epidermal growth factor receptor 2. **B.** Heatmap of differentially expressed genes in 9 BRCA2-delT mutated tumors (dark red) versus 8 matching non-tumoral tissue (grey); Blue and red bars on the side indicate downregulation upregulation in tumors. Below: uppercase letter corresponds to each healthy control, and the corresponding tumor tissue is indicated in lowercase. DEGs were obtained applying a log2 fold change > 1.5 and an adjusted p-value of 0.05. **C.** Bar charts showing the top GO terms for biological process in BRCA2 delT tumors compared to their non-tumoral surrounding, ranked by adjusted p-value (red to blue: higher to lower significance) using clusterProfiler (v4.4.4).

OBJECTIVE 2: Functional characterization of BRCA2 +/-del5 and +/-delT breast epithelial cell lines

+/-delT cells display enhanced colony formation ability in 2D and 3D settings

After identifying deregulated cell adhesion processes in the transcriptome analysis, we hypothesized that the +/-delT cell line might exhibit structural alterations indicative of potential invasiveness. Intriguingly, actin filament staining (performed by Jesus Gomez, a post-doc in our lab) demonstrated that both parental and +/-del5 cells exhibited a cuboidal shape, characteristic of epithelial cell lines (**Fig. 4A**). In contrast, the +/-delT cells displayed an elongated shape and less well-defined cell boundaries, with a fibroblast-like morphology. Evaluation of the circularity of the cells confirmed these results (**Fig. 4B**).

Next, I conducted a clonogenic survival assay to assess the colony formation capacity of these cell lines, cells transfected with BRCA2-siRNA was used as negative control. As expected, BRCA2 depletion led to a reduction in colony formation compared to the parental and siCTRL controls (**Fig. 4C**). Interestingly, while in the +/-del5 clone the number of colonies decreased, the +/-delT clone displayed a slightly enhanced colony-forming ability.

Considering these results, I performed a soft agar assay to quantify the ability of the cells to form colonies in an anchorage-independent manner, a hallmark of tumoral cells. I included breast tumoral cell line MCF7 as positive control, already known to form colonies under these conditions (Manni et al., 1991). MCF7 cells formed colonies with a median area of 2000 μ^2 (**Fig. 4E**). Notably, the +/-delT colonies were significantly larger, measuring about 1250 μ^2 , in contrast to both the parental and +/-del5 clones, which had colonies of approximately 500 μ^2 each.

To confirm that the observed phenotype was attributed to the BRCA2 pathogenic variant, I employed the CRISPR-Cas9 system to revert the BRCA2-delT variant (**Fig. 4D**). Remarkably, correcting the delT variant was sufficient to rescue the invasive phenotype, restoring colony size to that of the MCF10A control (**Fig. 4E**).

We also assessed the potential invasive capability of the +/delT clone in a 3D setting. For this, Jesus Gomez in our lab generated an isogenic organoid system with MCF10A parental and BRCA2-mutated cells. The results indicated that +/delT organoids exhibited an increased colony formation capacity in 3D, and this phenotype was restored in the +/revdelT clone (**Fig. 4F**), consistent with the results in **Fig 4E**.

To rule out the possibility that the disparities in colony-forming ability could be attributed to an enhanced proliferation rate of +/delT cells, I evaluated their growth rate over 7 days using the IncuCyte cell system (**Fig. 4G**). Interestingly, the +/delT clone exhibited a significant slower rather than faster proliferation rate compared to the control cells whereas +/del5 did not. These results are in line with the previous RNAseq analysis, showing downregulated proliferation genes in the +/delT clone (**Fig. 2C**).

Finally, to determine a possible difference due to changes in the cell cycle distribution I conducted cell cycle analysis by flow cytometry. A slight accumulation in S phase was observed for the +/delT clones, although this change did not achieve statistical significance (**Fig. 4H**).

Collectively, these findings suggest that despite its lower proliferation rate, the +/delT clone exhibits an elevated capacity for colony formation including in an anchorage-independent conditions in both 2D and 3D settings.

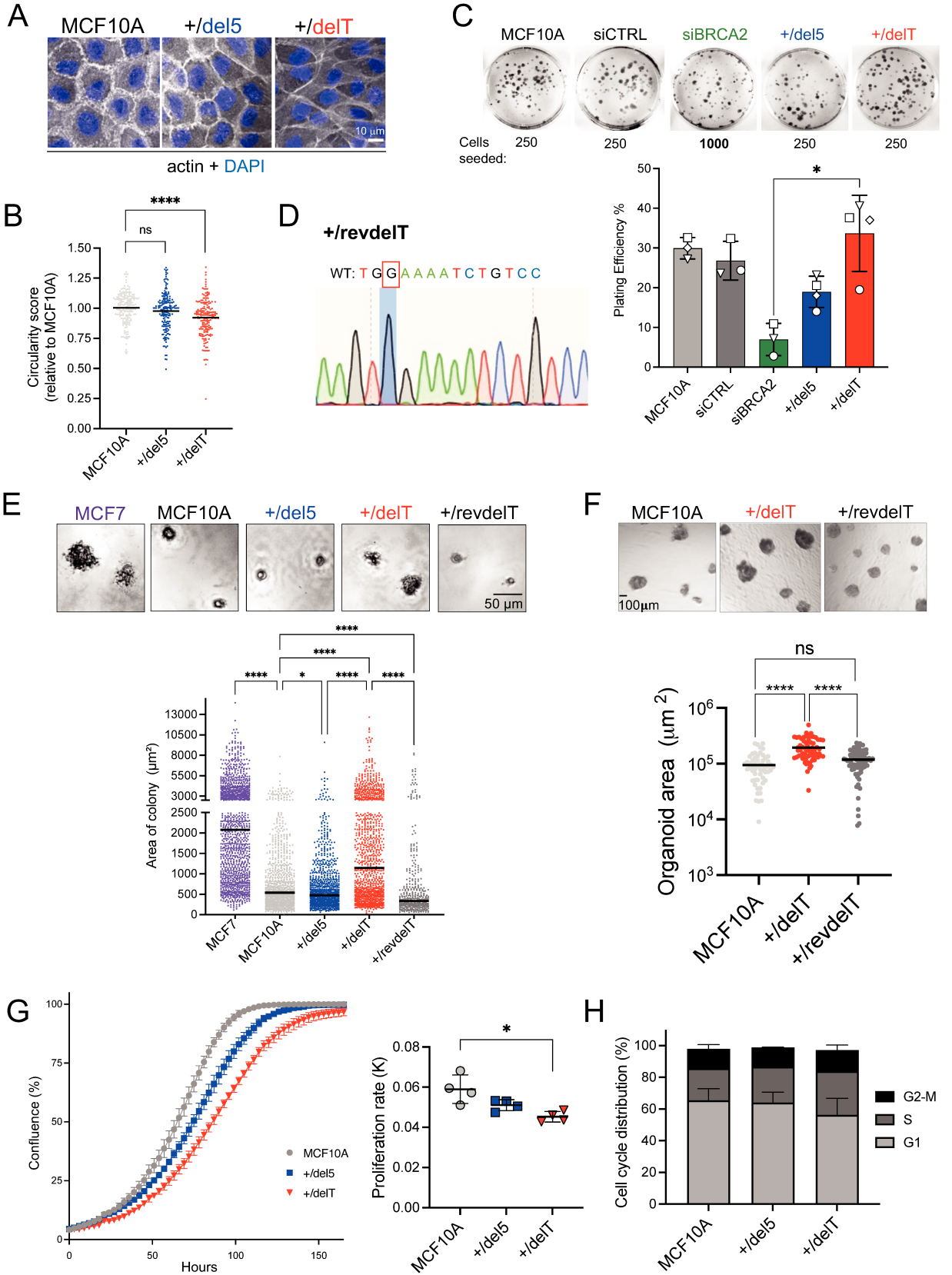


Figure 4. The BRCA2 +/-delT clone show increased cell invasion ability. A. Representative immunofluorescence images of MCF10A cells stained for actin (white); nuclei were counterstained with DAPI (blue). **B.** Quantification of the circularity score based on the actin staining at the junctions and calculated using "cell shape" descriptor in ImageJ software. Each dot represents a cell from four independent experiments and normalized to MCF10A control. Statistical difference was determined with Kruskal-Wallis test with Dunn's multiple comparisons test: ****, $p < 0.0001$. **C.** (Top) Representative plates of plating efficiency. Cells were seeded according to the number below each image in three technical replicates. (Bottom) Quantification of plating efficiency. Values represent the mean +SD of three biological replicates for MCF10A, siCTRL and siBRCA2 and four replicates for +/-del5 and +/-delT (different experiments are represented in different shapes). Statistical difference was determined by a Kruskal-Wallis test with Dunnett's multiple comparisons tests. *, $p = 0.0287$. **D.** Sanger Sequencing chromatogram confirming the correction of the BRCA2 delT mutation. **E.** (Top) Representative images of anchorage-independent growth of the MCF10A clones measured by soft agar assay as compared to MCF7 breast tumoral cells. (Bottom) Quantification of colony size measured using the ImageJ software. The values are the median of six replicates except for the +/-revdelT ($n=3$). Statistical difference was determined with Kruskal-Wallis test with Dunnett's multiple comparisons test (the p-values show the significant differences compared MCF10A): *, $p = 0.0375$; **, $p = 0.0046$; ****, $p < 0.0001$. **F.** Quantification of MCF10A organoids area from 3 independent experiments. Statistical difference was determined with Kruskal-Wallis test with Dunn's multiple comparisons test (the p-values show the significant differences among all): ****, $p < 0.0001$. **G.** (Left) Representative graph illustrating the mean + SEM of the confluence over time of three technical replicates of the MCF10A clones. (Right) Proliferation rates were calculated from the interpolation of logistic growth curve obtained in four independent experiments. Statistical difference was determined by a Kruskal-Wallis test with Dunnett's multiple comparisons tests. *, $p = 0.0134$. **H.** Histogram showing the percentage of cells in each phase of the cell cycle obtained after FACS analysis. Each experiment was repeated three times and values are the mean + SD. Statistical difference was determined by a two-way ANOVA test with Dunnett's multiple comparisons tests. **C, F, G.** Only significant p-values are shown.

The +/-delT clone shows normal BRCA2 protein levels

To further characterize the two cell lines expressing distinct heterozygous truncating variants, I examined BRCA2 protein levels (**Fig. 5A**). We observed a 50% reduction in BRCA2 full-length protein levels in +/-del5 clone compared to the control, in line with previous findings (Tan et al., 2017) (**Fig. 5B, left**). However, in the +/-delT cell line, the levels of full-length BRCA2 protein were nearly as abundant as in the parental cells, suggesting an up-regulation of the BRCA2 WT allele expression in this cell line.

BRCA2 modulates the RAD51 recombinase DNA binding activity to mediate repair by HR (see Introduction, section 1.1.4.3.2.). Thus, we next investigated whether the differences observed in BRCA2 protein abundance could impact the levels of RAD51. Interestingly, RAD51 protein levels were reduced in the del5 clone but not in the +/-delT (**Fig. 5A, 5B right**).

The Western Blot analysis on other biological clones seemed to indicate increased BRCA2 and RAD51 levels within the +/-delT cells (**Fig. 5C**). However, due to the notably low BRCA2 levels in the parental control when compared to Fig. 5A or 5D, we cannot draw a definitive conclusion and we are currently replicating this experiment. In contrast, the +/-del5 cells consistently exhibited reduced expression of these protein, although an increased level of RAD51 was observed in the +/-del5 clone #3 (**Fig. 5D**). As expected, both reverted clones, including +/-revdel5, exhibited protein levels returning to WT conditions (**Fig. 5C, 5D**).

Finally, the RNAseq analysis did not reveal any significant difference in BRCA2 and RAD51 expression between the parental clone and mutated cell lines (**Fig. 5E**). In fact, also in the case of +/-del5 clone #2, the levels of BRCA2 and RAD51 were similarly reduced as in Ctrl #2.

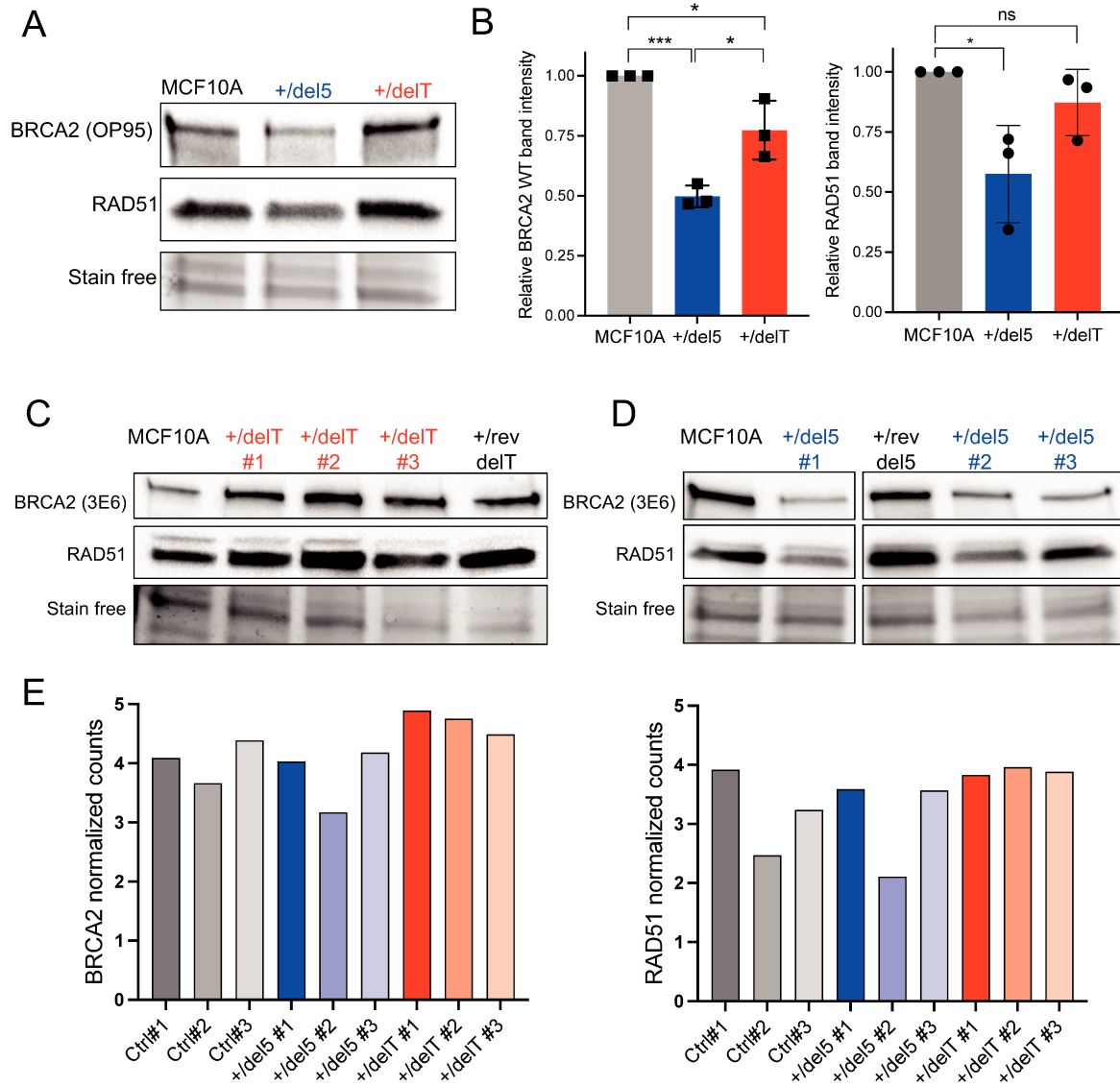


Figure 5. The +/delT clone shows increased BRCA2 WT protein levels. **A.** (Left) Representative Western Blot analysis of BRCA2 and RAD51 in clone #1 of MCF10A cells. **B.** Western Blot quantification of (left) BRCA2 and (right) RAD51 levels. Bands were normalized on the stain free (loading control) and to BRCA2 or RAD51 levels of the control cell line. The error bars represent the mean \pm SD of three independent experiments, each represent with a different shape. Statistical difference was determined by one-way ANOVA test followed by Tuckey's multiple comparison test. *, $p = 0.0239$ (MCF10A vs +/delT), $p = 0.0101$ (+/del5 vs +/delT), ***, $p = 0.0004$. Representative Western Blot analysis of BRCA2 and RAD51 in **(C)** +/delT and **(D)** +/del5 clones together with the two BRCA2-corrected clones. **E.** Normalized counts of BRCA2 (left) and RAD51 mRNA levels (right) in control, +/del5 and +/delT cell lines.

The +/-del5 clone shows increased sensitivity to PARPi and MMC treatment

The reduced levels of BRCA2 in the +/-del5 led us to hypothesize potential defects for this clone in HR repair. To investigate this, I performed cell survival assays under different genotoxic conditions.

Initially, I monitored cell viability using MTT assays during a 6-day treatment with Olaparib (0-2.5-5-10 μ M), a PARP inhibitor (PARPi) known to selectively kill HR-deficient cells (Bryant et al., 2005). This synthetic lethal association provides a fundamental basis for the clinical use of Olaparib in the treatment of BRCA2-mutated tumors (Farmer et al., 2005). As expected, BRCA2 depleted cells exhibited a marked reduction in survival, showing only 20% relative viability at the highest drug concentration, whereas the parental and siCTRL transfected cells maintained a viability of 75% at the same concentration (**Fig. 6A**). Intriguingly, the +/-delT clone displayed higher drug resistance, resulting in 90% viability. In contrast, +/-del5 exhibited increased sensitivity to PARPi, with relative viability reaching only 40% at the maximum dose, indicating potential defects in the HR repair pathway. As an additional control, we included another biological replicate for each BRCA2-mutated cell line, which produced similar results (**Fig 6A**). Importantly, correcting the BRCA2-del5 variant by CRISPR-Cas9, +/-rev del5, (**Fig. 6B**) restored the sensitivity phenotype, with a viability reaching 70%, similar to that of the parental control (**Fig. 6A**).

As a member of the Fanconi anemia (FA) pathway, BRCA2 (FANCD1) plays a crucial role in repairing inter-strand crosslinks (ICLs) (Howlett et al., 2002). Notably, BRCA2-deficient cells exhibit hypersensitivity to ICL-inducing agents like cisplatin and Mitomycin C (MMC). Thus, I aimed to evaluate the sensitivity of MCF10A cells to MMC using the MTT assay. The experimental setup involved one-hour exposure to MMC (0-1-2-4 μ M), followed by a recovery period of one day; cell viability was evaluated six days later. Our observations mirrored the results from MTT assays with PARPi (**Fig.6C**): at the highest concentration of MMC, only 20% of BRCA2-depleted cells retained viability, while 70% of the MCF10A

control remained viable. Notably, the +/delT clone exhibited increased viability compared to the parental control, suggesting resistance, while the +/del5 clone displayed hypersensitivity especially at the higher dose, implying potential defects in ICL repair.

Both PARPi and MMC induce replication stress and BRCA2 plays a pivotal role in preserving replication fork stability (Kolinjivadi et al., 2017). A more specific source of replication stress is nucleotide depletion induced by Hydroxyurea (HU), a drug that inhibits the enzyme ribonucleotide reductase (RNR) precluding nucleotide incorporation (Krakoff et al., 1968). BRCA2 deficient cells are sensitive to HU, we therefore treated our cells with HU for 24 hours (0-2.5-5 mM), and analyzed their survival after 6 days. Notably, the presence of the BRCA2 mono-allelic variants did not lead to acute sensitivity to HU; in fact, both +/del5 and +/delT clones exhibited similar viability compared to the MCF10A control reaching 30-40% at the highest concentration of HU tested (**Fig. 6D**).

In the HR pathway, BRCA2 plays a critical role in binding and modulating the DNA binding activity of the RAD51 recombinase for repair (Carreira et al., 2009; Jensen et al., 2010; Yang et al., 2005). We aimed to uncover whether the increased sensitivity of +/del5 to PARPi and MMC arose from diminished levels of BRCA2, impacting the recruitment of RAD51 to DNA damage sites. In collaboration with Prof. Matthias Altmeyer (University of Zurich, CH), we employed quantitative image-based cytometry (QIBC), a high-throughput microscopy technique enabling precise quantification of DNA damage foci in a cell cycle-resolved manner (Forment & Jackson, 2015). Following a 24h treatment either with 3 μ M MMC or 10 μ M Olaparib, we evaluated the number of DNA damage foci using the DNA-damage marker γ H2AX and RAD51 as HR marker (**Fig. 6E**). Under these conditions, PARPi treatment did not induce elevated levels of DNA damage as indicated by the small increase in γ H2AX intensity compared to the untreated condition whereas it clearly increased after MMC treatment (**Fig. 6E, top**). Intriguingly, among the 3 clones, +/delT displayed a small reduction in γ H2AX and RAD51 intensity compared to the parental control suggesting overall reduced DNA damage or faster recovery. The +/del5 clone exhibited decreased RAD51 foci levels after MMC treatment (**Fig. 6E, bottom**), consistent with the MMC sensitivity observed for this clone. In summary, +/del5 cells show increased

sensitivity to PARPi and MMC, while +/-delT displayed increased resistance to both treatments. The number of RAD51 foci was reduced in both clones only in MMC conditions.

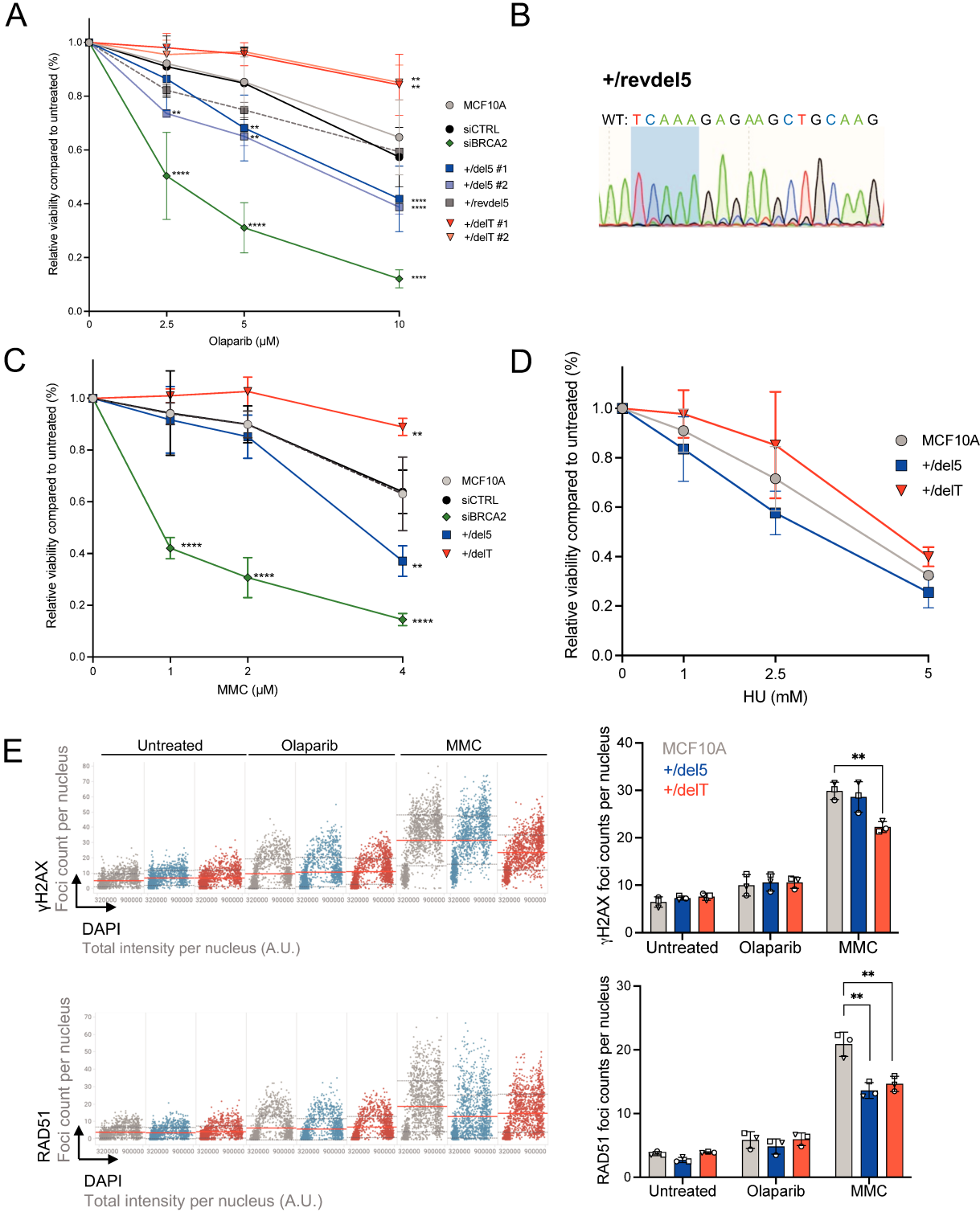


Figure 6. The +/-del5 clone shows increased sensitivity to PARPi and MMC treatment.

A: Quantification of the relative cell viability of MCF10A, +/-del5 and +/-delT biological replicates monitored by MTT assay upon treatment with increasing doses of the PARP inhibitor Olaparib over 6 days. The data represent the mean \pm SD of the following number of independent experiments: siCTRL and +/-del5 n=6, MCF10A: n=5, +/-delT#1 and +/-del5 #2: n=4, siBRCA2, +/-delT#2 and +/-revdel5: n=3. **B.** Sanger Sequencing chromatogram confirming the correction of the BRCA2 del5 variant. **C.** Quantification of the relative cell viability monitored by MTT assay upon one-hour treatment with increasing doses of MMC as indicated, followed by one day release. After seeding, viability was monitored for 6 days. The data represent the mean \pm SD of three independent experiments. **D.** Quantification of the relative cell viability monitored by MTT assay upon 24 hours treatment with increasing doses of HU as indicated. Viability was monitored after 6 days. The data represent the mean \pm SD of two independent experiments. Statistical difference in **A, C-D** was determined by a two-way ANOVA test with Dunnett's multiple comparisons test. The p-values show significant differences compared to the MCF10A clone. ** p < 0.01, **** p < 0.00001. **E.** (Left) Representative QIBC experiment to monitor γ H2AX (top) and RAD51 foci (bottom) over DAPI intensity in MCF10A clones treated for 24 h with 10 μ M of Olaparib or 3 μ M of MMC. (Right) Quantification of γ H2AX (top) and RAD51 foci (bottom). Each experiment was repeated three times and values are the mean + SD. Statistical difference was determined by unpaired t-test. The p-values show significant differences compared to the MCF10A clone: ** p = 0.036 (+/delT, γ H2AX), p= 0.053 (+/del5, RAD51), p=0.087 (+/delT, RAD51). Only significant p-values are shown.

+/-del5 cells show HR defects and accumulate PARPi-induced single stranded DNA (ssDNA) gaps

Considering the PARPi sensitivity observed in the +/-del5 clone and the fact that HR deficient cells are sensitive to PARPi, we next assessed the HR capacity of these cells using a modified version of the cell-based HR assay previously established in our laboratory (Vugic et al., 2020). The experiment, performed by Jesus Gomez in our lab, consisted in introducing a single DSB at the genomic AAVS1 locus within the PPP1R2C gene using a site-specific guide RNA (gRNA) and CRISPR-Cas9 nicking. Co-transfection of a GFP version of the nuclease, a plasmid containing the gRNA and a promoterless mCherry donor plasmid that contains a region of homology with the targeted sequence allowed us to measure HR-mediated integration of the mCherry plasmid, as it results in the expression of mCherry and can be detected by flow cytometry. To account for nonspecific mCherry integration, a control condition lacking the gRNA was included for each cell line. Only

GFP+ cells (transfected with the Cas9 plasmid) were counted. MCF10A cells exhibited an average of 1.5% of mCherry positive cells. In contrast, +/del5 cells showed only 0.7% of mCherry expressing cells, indicating defective HR (**Fig. 7A**). On the other hand, the +/delT clone showed no significant difference compared to the control, with an average of 1.2% of cells being mCherry positive.

PARPi has been shown to generate ssDNA gaps and these are exacerbated in BRCA2-deficient cells (Cong et al., 2021; Nagaraju & Scully, 2007; Panzarino et al., 2021; Vugic et al., 2023). Given the sensitivity to PARPi observed in +/del5 cells, I investigated the presence of PARPi-induced ssDNA gaps in the same cells by DNA combing (Meroni et al., 2023). Cells were initially subjected to a 20 min. pulse of the thymidine analog IdU, followed by a 2h labelling with the second analog CldU during simultaneous treatment with 30 μ M Olaparib. Once released from the pulse, cells were either left untreated or incubated for 30 min with S1 nuclease, an enzyme that nicks ssDNA resulting in the shortening of the CldU track length at regions where ssDNA gaps accumulate (**Fig. 7B, top**). A reduction of CldU/IdU ratio upon S1 treatment would be indicative of the presence of ssDNA gaps. MCF10A displayed no difference in the CldU/IdU ratio in S1-treated compared to the untreated cells. The same result was obtained for +/delT cells. Remarkably, a significant reduction in the CldU/IdU ratio was observed in S1-treated +/del5 cells. These results suggested an accumulation of ssDNA gaps in the +/del5 clone, in agreement with the sensitivity to PARPi observed in this cell line (**Fig. 6A**).

Finally, we hypothesized that the accumulation of ssDNA gaps would result in an increased chromosomal instability. To explore this idea, Jesus Gomez in our lab conducted an analysis of chromosomal aberrations in metaphase spreads of cells following a 24h treatment with 10 μ M Olaparib (**Fig. 7C**). While no notable differences were observed in untreated conditions among the different cell lines, Olaparib treatment induced a significant increase in the occurrences of small breaks or gaps in +/del5 cells. In contrast, the levels of chromosomal aberrations in the parental control and the +/delT remained unaffected by PARPi treatment (**Fig. 7C**).

In summary, only +/del5 cells displayed defective HR capacity and accumulate PARPi-induced ssDNA gaps detected by S1 sensitivity and DNA combing and manifested as well in metaphase spreads.

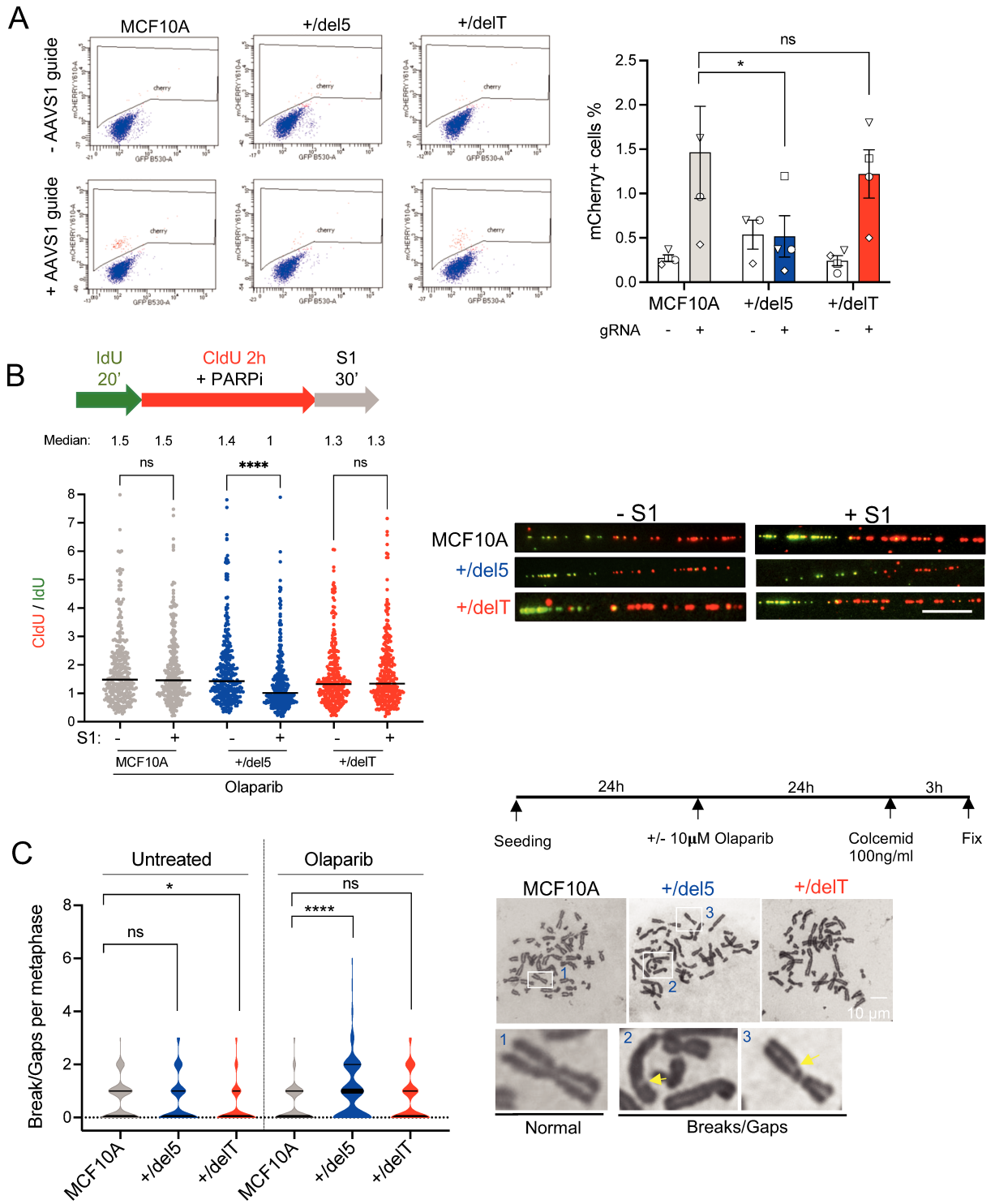


Figure 7. +/-del5 cells show HR defects and accumulate PARPi-induced ssDNA gaps.

A. Example of the flow cytometry gating and analysis of mCherry positive cells as a readout from the HR assay at eight days post-transfection in MCF10A control and BRCA2-mutated cells. Right: Quantification of the frequency of mCherry positive cells in control conditions (empty bars) or with the AAVS1 gRNA (filled bars). The error bars represent the mean \pm SEM of three independent experiments, each experiment is represented with a different symbol shape. Statistical difference was determined by two-way ANOVA test followed by Dunn's multiple comparison test. ns, not significant, * $p = 0.0447$. **B.** Top: (left) Labeling scheme and (right) representative images of the replication tracks labeled as indicated from MCF10A control and BRCA2-mutated cells, in 30 μ M Olaparib treated condition followed by 30 min of S1 nuclease (or S1 buffer only) treatment, as indicated. The scale bar indicates 15 μ m. (Bottom) Quantification of CldU/IdU ratio in cells. Data represent the median of three independent experiments with 100 fibers analyzed for each. Statistical difference was determined by the Kruskal–Wallis test followed by Dunn's multiple comparison test. ns, not significant, **** $p < 0.0001$. **C.** (Left) Quantification, (right) experimental setup and representative images of chromatid breaks/gaps from the same cells either left untreated or upon treatment with Olaparib (10 μ M for 24 h) as indicated. Scale bar indicates 10 μ m. Statistical difference was determined by the two-way ANOVA test followed by Dunn's multiple comparison test. ns, not significant, * $p=0.037$, **** $p < 0.0001$. $n=3$ independent experiments with at least 40 metaphases analyzed per condition.

OBJECTIVE 3: Reveal the genomic changes induced by two different truncating variants in BRCA2-mutated tumors

Whole genome profiling uncovers similar mutational patterns in primary breast tumors bearing two different BRCA2 truncating variants

In recent years, Whole Genome Sequencing (WGS) has been widely employed to analyze the genomes of human cancers, revealing diverse mutation patterns known as mutational signatures. Currently, over 100 of these signatures have been identified according to the type of nucleotide substitution in a defined nucleotide context, which reflects a specific mutagenesis process. Previous work on the mutational landscape of breast cancers showed that the somatic or germline abrogation of the BRCA2 gene gives rise to at least five different mutational signatures, including HR deficiency, mismatch repair deficiency and APOBEC-related mutagenesis (Alexandrov et al., 2013; Nik-Zainal et al., 2016). Thus, we aimed to characterize the mutational landscape of two small cohorts of BRCA2-mutated bearing the BRCA2 del5 (c.771-775del) and delT (c.5946del)

pathogenic variants. This approach could uncover novel cancer drivers and illuminate mechanisms underlying tumorigenesis linked to BRCA2.

We obtained the DNA of seven pairs of tumors with the delT variant from the same cohort used in the transcriptome analysis (see **Fig. 3A**) and one pair with the del5 variant from I. Curie. Moreover, in collaboration with Stefán Sigurdsson group (University of Iceland), we obtained two more del5 tumor samples and matched blood DNA samples. To complement our analysis, we incorporated published WGS data from eight del5 tumors, processed using our established bioinformatic pipeline (see Material and Methods section).

The WGS analysis of both tumor cohorts unveiled a comparable spectrum of substitutions, insertions, and deletions (**Fig. 8A**). According to the COSMIC-Catalogue of Somatic Mutations in Cancer, Sanger, UK- the analysis performed by our collaborator Serena Nik-Zainal group (University of Cambridge) revealed six distinct single base substitution (SBS) signatures consistently present across all tumor samples (**Fig. 8B**). Notably, in both cohorts, the most predominant signatures were SBS3 and SBS8, corresponding to defective HR repair and strongly associated with germline BRCA1/BRCA2 null cancers (Alexandrov et al., 2013; Nik-Zainal et al., 2012). Additionally, we identified signatures SBS2 and SBS13, associated with APOBEC-related mutagenesis, as well as SBS1, linked to cytosine deamination, and SBS5, of unknown origin. Interestingly, some of the delT samples also exhibited additional signatures, including SBS17 and SBS125, with unknown etiology, and SBS18, associated with reactive oxygen species (ROS).

We then evaluated tumor HR deficiency using HRDetect (Davies et al., 2017), a quantitative model that examines six parameters linked to HR deficiency: microhomology-mediated indels, reflecting alternative and mutagenic DNA repair processes, HRD index, comprising of HRD-LOH score, HRD-telomeric allelic imbalance score (TAI), and HRD-large-scale state transition score (LST), HRD-associated SBS3 and SBS8, and rearrangement signatures (RS) 3 and 5. These RSs consider structural variations involving

large chromosomal segments and potentially resulting in deletion, duplication, or reassembly. RS3 is primarily associated with small tandem duplications under 10 kb, while RS5 is linked to non-clustered deletions under 100 kb. A classification threshold of 0.7 was applied to the HRDetect score; according to this criterion, all BRCA2-mutated tumors in both cohorts were categorized as HR deficient (HRD) (**Fig. 8C**).

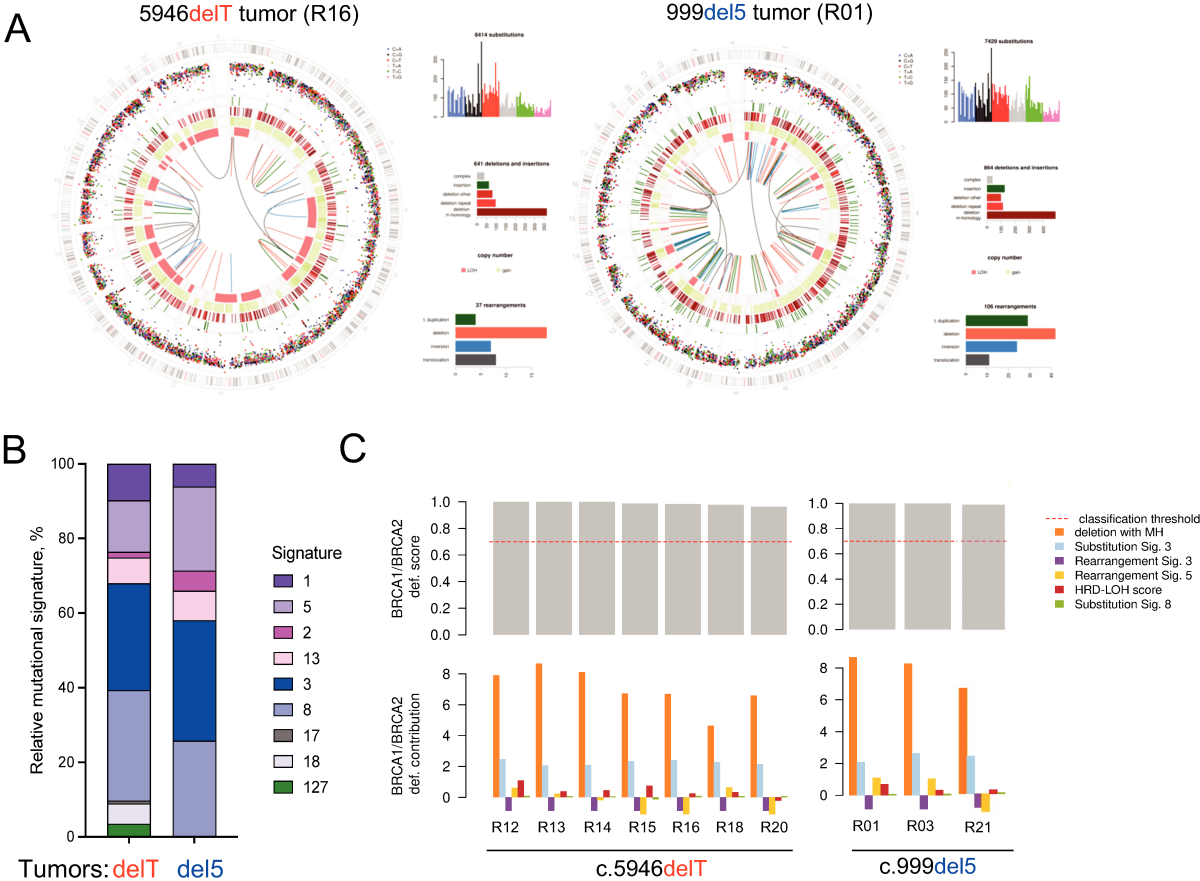


Figure 8. Breast tumors bearing the BRCA2 delT or del5 variant show HRD mutational signature. **A.** Examples of genome plots are shown for a BRCA2 delT tumor (left) and a del5 tumor (right). The features depicted in the circo plots from the outermost rings moving inwards are (I) the karyotypic ideogram; (II) base substitutions; dot color: blue, C>A; black, C>G; red, C>T; gray, T>A; green, T>C; pink, T>G); (III) insertions shown as short green lines; (IV) deletions shown as short red lines; (V) major (green blocks, gain) and minor (red blocks, loss); and (VI) rearrangements shown as central lines (green, duplications; red, deletions; blue, inversions; grey, translocation). Next each circo plot are histograms showing the: (top) number of mutations contributing to each substitution signature; (middle) deletion and insertion; (bottom) the number of rearrangements contributing to each rearrangement signature. **B.** Proportion of base substitution mutations contributing to each signature (legend on the right) in 7 primary tumors bearing the BRCA2delT variant and 11 with the BRCA2 del5 variant. The error bars indicate the

mean \pm SEM of mutation count per signature within tumors. **C.** (Top) Bar plot of HRDetect scores for each sample. The threshold is fixed at 70% (red dotted line). (Bottom) Quantification of the contribution of each mutation signature per sample explaining the total HRD score (legend on the right).

Breast tumors bearing the germline BRCA2 del5 or delT variant show different LOH frequency

Despite the differences in the functional analysis of cell lines bearing the two variants shown in Objective 2, the WGS analysis of tumors bearing the same variants revealed remarkable similarities in the mutational patterns in our two tumor cohorts.

This discrepancy raised the question of whether the delT and del5 mutation carriers would show different frequency of BRCA2 WT LOH allele during the tumorigenic transformation; thus, we set out to test the locus-specific BRCA2 LOH (see Material and Methods section) in our small cohorts and in previously published data (Aradottir et al., 2015; Maxwell et al., 2017) for each tumor type. Although the number of tumors for each variant we could recover is so far uneven, the LOH frequency was 60% for delT breast tumors (n=15) (**Fig. 9**), and 53% for breast del5 tumors (n=55).

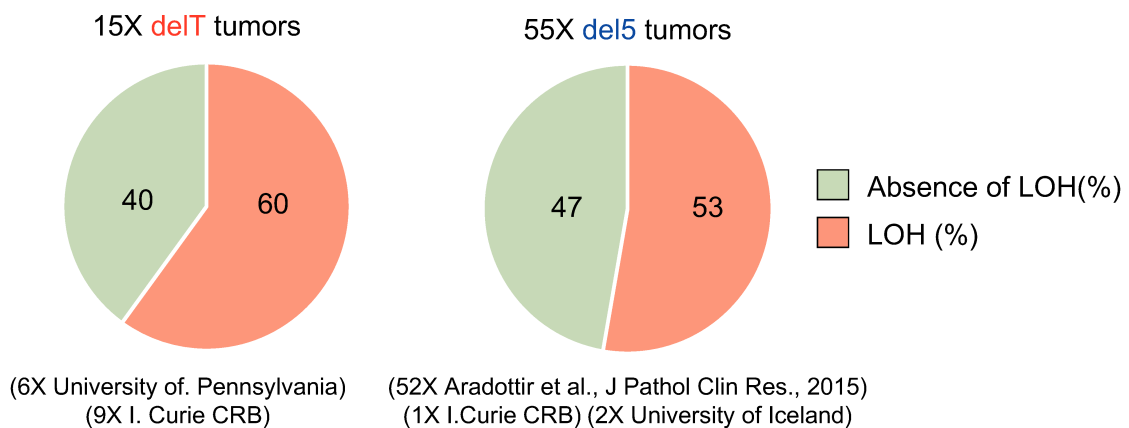


Figure 9. Breast tumors bearing the BRCA2 delT variant show increased frequency of locus-specific LOH. Pie charts representing the frequency of LOH (red) or no LOH (green) at BRCA2 genomic locus in the delT and del5 tumors cohorts. The number of tumors analyzed as well as their origin are indicated in the figure.

Chapter 3 – Discussion

Recent evidence underscores that a functional BRCA2 allele alone may not fully prevent tumorigenesis, suggesting haploinsufficiency. Several reports have suggested that BRCA2 heterozygosity can lead to deficiencies in the HR DNA repair pathway (Arnold et al., 2006; Warren et al., 2003) while in some others, replication stress-related defects emerged (Karaayvaz-Yildirim et al., 2020; Lim et al., 2023; Tan et al., 2017). To investigate this further, we established two stable human breast epithelial cell lines, each carrying a mono-allelic common BRCA2 pathogenic truncating variant, c.5946del (delT) and c.771-775del (del5). We then assessed their impact on both the transcriptomic profile and phenotype.

Our study revealed distinct outcomes of genomic instability resulting from these two BRCA2 variants in heterozygosity. Specifically, the +/del5 mutant displayed increased sensitivity to both MMC and PARPi while the +/delT mutant displayed hyper-resistance to these treatments (**Fig. 6A, 6C**).

The divergent sensitivities observed among the mutated clones may be due to variations in BRCA2 protein levels. Notably, the +/del5 clone exhibited reduced BRCA2 protein levels, which align with the presence of only one functional allele (**Fig. 5A**). Unexpectedly, there was also a marked decrease in RAD51 protein levels in the same clone (**Fig. 5A**). Importantly, this reduction was present in different biological +/del5 clones and was rescued by reverting the BRCA2-del5 variant (**Fig. 5D**), ruling out the possibility of an off-target effect due to gene-editing. Notably, in CAPAN-1, a pancreatic adenocarcinoma cellular model expressing only the BRCA2 delT mutant (-/delT) following LOH, the transfection with BRCA2 cDNA was sufficient to increase the protein levels of RAD51 (Brown & Holt, 2009) in agreement with the correlation of BRCA2 and RAD51 protein levels we observed in +/del5 cells (Brown & Holt, 2009).

Intriguingly, we observed a reduction in BRCA2 and RAD51 levels in +/del5 clones but not in +/delT clones. Consequently, RAD51 protein levels in +/delT clones were comparable to those in the MCF10A cell line (**Fig. 5A**). However, these findings appear to contradict a previous report where cells carrying the same BRCA2-delT mono-allelic

variant showed a 50% reduction in BRCA2 protein levels (Tan et al., 2017); conversely, they found 50% reduction in cells showing del5 variant in heterozygosis as we do. We are not certain for the reason of these discrepancies, but they may arise from the use of different cellular systems.

Based on our results, we postulate that the normal levels of WT BRCA2 protein in the +/delT cells underlies their full HR proficiency (**Fig. 7A**) which subsequently contributes to their resistance to PARPi and MMC (**Fig. 6A, 6C**). Interestingly, upon MMC treatment, both +/del5 and +/delT cells displayed a reduction in RAD51 foci, in the case of +/delT this may be linked to the overall reduced DNA damage observed in these cells, as indicated by a decreased in γ H2AX foci (**Fig. 6E**). However, further investigation is needed to understand the factors contributing to the increased drug resistance observed in the +/delT clone compared to the control.

Interestingly, BRCA2 +/delT cell line formed colonies in an anchorage-independent context (**Fig. 4E, 4F**). Reverting the BRCA2-delT variant rescued this phenotype hinting that this deregulation is specifically linked to this variant. Therefore, we suggest that the BRCA2 delT variant may confer a potential invasive capacity. Interestingly, a study analyzing PARP1-resistant (-/delT) CAPAN-1 cells reported an upregulation of genes associated with epithelial-to-mesenchymal transition (EMT), such as ZEB1 and TWIST (Guo et al., 2022). However, in the RNAseq analysis our +/delT cells these genes were downregulated including those associated with cell-cell and basal membrane adhesion (**Fig. 2C**). Nonetheless, the specific mechanism responsible for gene down-regulation induced by the BRCA2 delT mutant, as well as whether this effect is direct or indirect, necessitates further investigation (see Perspectives). Intriguingly, the analysis of breast tumors bearing the delT variant also indicated a deregulation in cell-cell junction and actin organization (**Fig. 3C**), reinforcing the hypothesis that this phenotype is specific to the delT mutant. To confirm this, we will analyze the transcriptome of del5 tumors.

In contrast to +/delT cells, the +/del5 variant, while resulting in minimal alterations in the gene expression profile compared to the parental clone (**Fig. 2B**), led to significant

genomic instability. This was notably demonstrated by its increased sensitivity to PARPi and the accumulation of ssDNA gaps and chromatid breaks under these conditions (**Fig. 7C**); in contrast, neither cell line displayed sensitivity to HU (**Fig. 6D**). These results further underscore the connection between PARPi-induced ssDNA gaps and the heightened sensitivity to this drug (Cong et al., 2021).

Our results are consistent with a recent report from our lab where we found that the impaired PARPi-induced replication stress is distinct and requires a different domain in BRCA2 than HU-induced replication stress (Vugic et al., 2023). In agreement with this, recent findings indicate that Brca2 heterozygous mouse and human cells bearing an exon 27 deletion that impairs RAD51 filament stability exhibit compromised fork protection and accumulate gaps upon HU treatment, yet they retained an intact HR repair (Lim et al., 2023). Those findings suggest that the ssDNA gap suppression and FP functions of BRCA2 (induced by HU) are particularly sensitive to gene-dosage whereas HR is not (Lim et al., 2023). In contrast, our results with the +/del5 clone reveal a gene-dosage effect on both ssDNA gaps (induced by PARPi) and HR repair. These discrepancies might be linked to the use of distinct BRCA2 pathogenic variants in heterozygosis, which affect the truncated product differently. In their study, the $\Delta 27$ mutant expresses the BRC repeats and the C-DBD, crucial for efficient HR (Lim et al., 2023; Schlacher et al., 2011, 2012) whereas the del5 product is not expressed.

Another study reported that primary BRCA2 heterozygous cells from healthy tissues of carriers show a compromised replication stress response as observed with an increased DNA damage upon HU treatment (Karaayvaz-Yildirim et al., 2020). Although we could not find differences in HU sensitivity for +/del5 neither by colony formation assay nor MTT, the sensitivity of these tests might not be sufficient to detect small changes in DNA damage levels as the ones they observed using comet assays.

Despite the differences observed in our two cell lines, the genomic analysis of BRCA2 delT and del5 breast primary tumors uncovered a shared mutational signature associated to defective HR repair along with elevated HRD scores (Davies et al., 2017) (**Fig. 8B, 8C**).

Conversely, the analysis of BRCA2 locus-specific LOH indicated a higher percentage in the delT cohort compared to the del5 cohort (**Fig. 9**). Although the numbers of tumors are still small and uneven, this difference in LOH may explain why HR-proficient heterozygous cells (+/delT) develop HR-deficient tumors. Absence of LOH has been associated with decrease overall survival in ovarian cancer BRCA-mutated patients treated with cisplatin chemotherapy consistent with an increase resistance to treatment (Maxwell et al., 2017). Thus, the difference in LOH frequency we observe might have clinical implications. However, an increase in statistical power by gathering more LOH information on tumors is required to confirm these differences.

According to our findings, we propose a model (**Fig. 10**) in which cells carrying the mono-allelic BRCA2 delT variant exhibit highly deregulated genes, an enhanced invasive phenotype while reduced genome instability. We hypothesize that the decreased genome instability protects them from transformation and therefore increases the need to undergo early LOH for tumorigenesis. Conversely, cells bearing the +/del5 variant exhibit HR deficiency and increased sensitivity to MMC and PARPi. This treatment results in the accumulation of ssDNA gaps and chromatid breaks, which we attribute to decreased levels of BRCA2 and RAD51 proteins. Given the ongoing genome instability, it is plausible that the loss of the WT allele is not necessary for tumorigenesis, potentially occurring less frequently or at a later stage in tumor progression.

In summary, our study confirms the haploinsufficiency conferred by BRCA2 heterozygosity but implies that different BRCA2 variants may confer different forms of haploinsufficiency. In the case of del5, it appears to be a dosage-related issue, while in +/delT, there may be a dominant effect exerted by the mutated allele (see Perspectives).

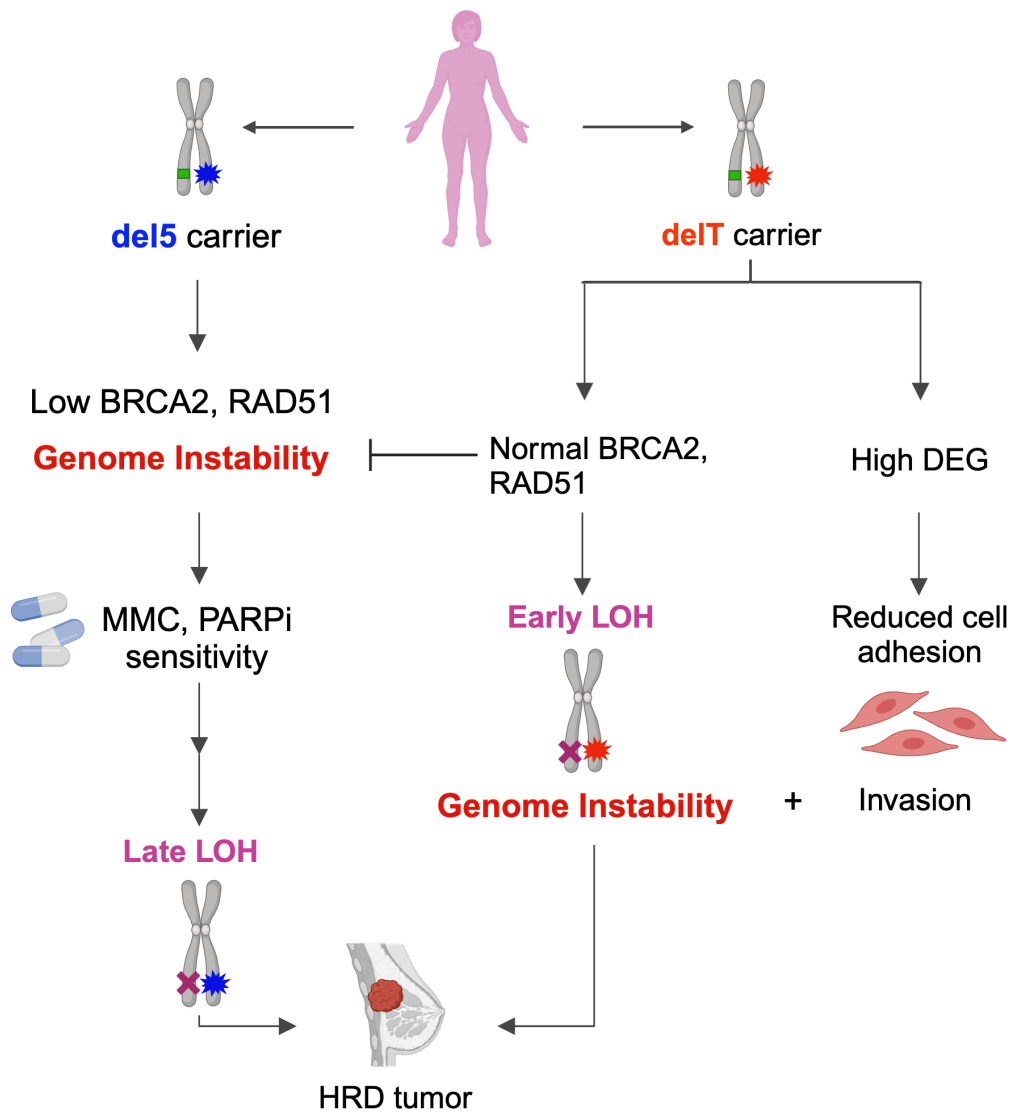


Figure 10. Proposed model of tumorigenesis for distinct BRCA2 germline pathogenic variants. (Left branch) Reduced BRCA2 and RAD51 levels in +/del5 carriers lead to increased sensitivity to genotoxic agents, initiating genomic instability before LOH, which might occur late or be absent. (Right branch) BRCA2 +/delT carriers, while displaying alterations in invasion pathways, exhibit normal BRCA2 and RAD51 levels that suppress genomic instability. Consequently, an early LOH becomes a necessary event for tumor formation. Created with BioRender.com.

Perspectives

One of the questions arising from this study is why +/delT cells display such an increased number of deregulated genes. A previous study reported the expression of the cDNA bearing the same variant in the cytoplasm (Spain et al., 1999). However, we performed a fractionation experiment and found that the endogenous truncated product of c.5946delT was present in both the nucleus and cytoplasm in our +/delT MCF10A cells (**Fig. 11A, top**). To have a better resolution of the BRCA2 truncated band, the technical controls for the fractionation were migrated in a separate gel (**Fig. 11A, bottom**). Although preliminary, the localization in the nucleus could therefore interfere with the BRCA2 WT and may be associated with the substantial gene deregulation observed in this clone. It is worth noting that the N-terminal region of BRCA2, included in the product of delT, contains a transactivation domain (Milner et al., 1997). Interestingly, this domain is also the site of interaction of the co-transcriptional activator and histone acetyltransferase (HAT) PCAF (Fuks et al., 1998).

We hypothesize that BRCA2 delT truncated product may interfere with PCAF activity which, in turn, might result in an altered transcription of a subset of genes.

Interestingly, a previous report has shown that BRCA2 directly binds to the transcription start site (TSS) of genes related to the NF- κ B pathway, which leads to chromatin remodeling through acetylation of Histone H4, and this effect leads to increased survival in EGF-free media upon transient depletion of BRCA2 (Gruber et al., 2019). Given that PCAF acetylates H4, we will determine the possible effect of the BRCA2 delT mutant in H4 acetylation. A preliminary Western Blot analysis indicates reduced acetylation of H4 in +/delT and not in +/del5 compared to the parental control (**Fig. 11B**). If confirmed, we plan to perform BRCA2 chromatin immunoprecipitation (ChIP) followed by RT-PCR of the commonly deregulated genes in +/delT cells and in delT tumors, as they both show similar deregulated pathways. This strategy will help us answer whether the downregulated genes in +/delT cells correlate with a reduced BRCA2 binding at the same loci and whether these are potential changes required for tumor formation.

Another question we would like to answer is whether the PARPi-induced ssDNA gaps observed in +/del5 cells are generated by PRIMPOL repriming as it has been shown in BRCA2 deficient cells (Lim et al., 2023; Quinet et al., 2021; Tirman et al., 2021) (Introduction, section 1.2.3.2.2.). We are currently performing these experiments.

Finally, we would like to address whether the differences we observed in this study are applicable to other variants and whether the LOH status follows the model we proposed (**Fig. 10**). In a follow-up study, we plan to broaden our investigation to include other BRCA2 pathogenic variants to assess this possibility. If our hypothesis is validated, it could potentially impact the clinical management of BRCA2-mutated tumors, leading to more individualized, variant-specific treatment strategies.

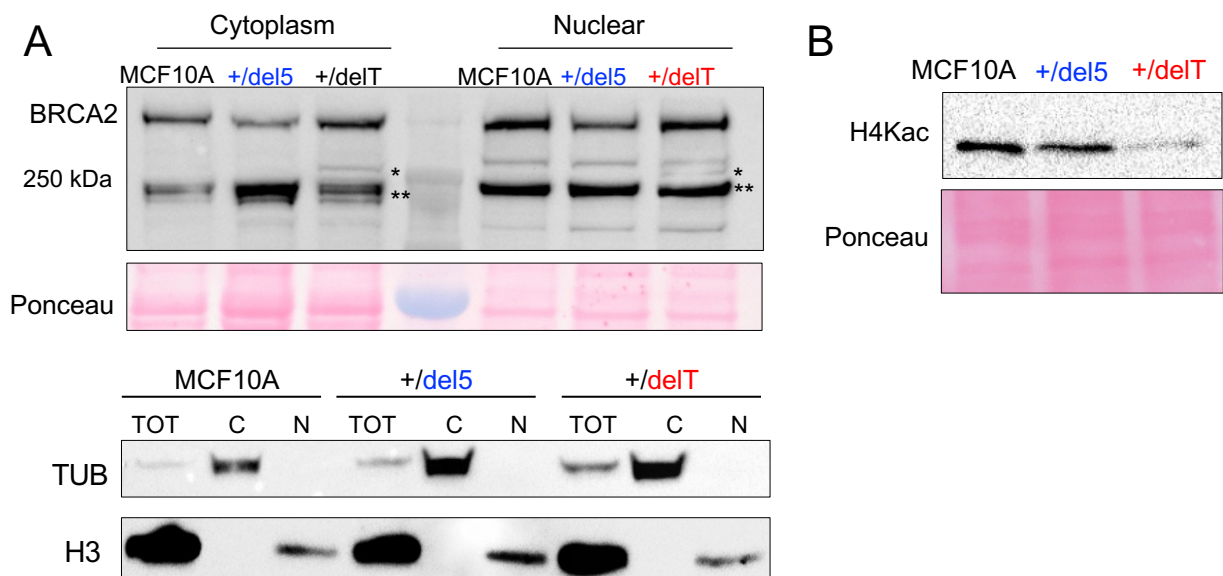


Figure 11. A. (Top) Sub-cellular fractionation to determine the levels of BRCA2 in the cytoplasm and nucleus. * denotes a band with the size (predicted for the truncated BRCA2-delT product 250kDa); ** indicate a non-specific band. The antibody used for BRCA2 recognizes an epitope in the N-terminal region (house-made). (Bottom). Western blot analysis of total (tot), cytoplasmic (C), and nuclear (N) fractions showing tubulin (tub) and Histone3 (H3) as controls for the fractionation. **B.** Western Blot analysis of acetylated lysines (K5, K8, K12, K16) on histone 4 (H4Kac). (n = 1 for all experiments).

References

1. Abraham, R. T. (2001). Cell cycle checkpoint signaling through the ATM and ATR kinases. *Genes & Development*, 15(17), 2177–2196. <https://doi.org/10.1101/gad.914401>
2. Agarwal, S., Tafel, A. A., & Kanaar, R. (2006). DNA double-strand break repair and chromosome translocations. *DNA Repair*, 5(9–10), 1075–1081. <https://doi.org/10.1016/j.dnarep.2006.05.029>
3. Alcón, P., Shakeel, S., Chen, Z. A., Rappsilber, J., Patel, K. J., & Passmore, L. A. (2020). FANCD2–FANCI is a clamp stabilized on DNA by monoubiquitination of FANCD2 during DNA repair. *Nature Structural & Molecular Biology*, 27(3), 240–248. <https://doi.org/10.1038/s41594-020-0380-1>
4. Alexandrov, L. B., Kim, J., Haradhvala, N. J., Huang, M. N., Ng, A. W. T., Wu, Y., Boot, A., Covington, K. R., Gordenin, D. A., Bergstrom, E. N., Islam, S. M. A., Lopez-Bigas, N., Klimczak, L. J., McPherson, J. R., Morganella, S., Sabarinathan, R., Wheeler, D. A., Mustonen, V., Alexandrov, L. B., ... Mering, C. von. (2020). The repertoire of mutational signatures in human cancer. *Nature*, 578(7793), 94–101. <https://doi.org/10.1038/s41586-020-1943-3>
5. Alexandrov, L. B., Nik-Zainal, S., Wedge, D. C., Aparicio, S. A. J. R., Behjati, S., Biankin, A. V., Bignell, G. R., Bolli, N., Borg, A., Børresen-Dale, A.-L., Boyault, S., Burkhardt, B., Butler, A. P., Caldas, C., Davies, H. R., Desmedt, C., Eils, R., Eyfjörd, J. E., Foekens, J. A., ... Stratton, M. R. (2013). Signatures of mutational processes in human cancer. *Nature*, 500(7463), 415–421. <https://doi.org/10.1038/nature12477>
6. Anczuków, O., Ware, M. D., Buisson, M., Zetoune, A. B., Stoppa-Lyonnet, D., Sinilnikova, O. M., & Mazoyer, S. (2008). Does the nonsense-mediated mRNA decay mechanism prevent the synthesis of truncated BRCA1, CHK2, and p53 proteins? *Human Mutation*, 29(1), 65–73. <https://doi.org/10.1002/humu.20590>
7. Antonis, A., Silvia, C., Tuomas, H., Daniel, B., Katri, P., Jonathan, R., Andrew, L., Deepak, S., Kim, D. L., Florentia, F., Eva, T., L., N. S., L., T. Z., Sofia, K., Kristiina, A., S., M. J., Clare, T., Sheila, S., Arto, M., ... Marc, T. (2014). Breast-Cancer Risk in Families with Mutations in PALB2. *New England Journal of Medicine*, 371(6), 497–506. <https://doi.org/10.1056/nejmoa1400382>
8. Aradottir, M., Reynisdottir, S. T., Stefansson, O. A., Jonasson, J. G., Sverrisdottir, A., Tryggvadottir, L., Eyfjörd, J. E., & Bodvarsdottir, S. K. (2015). Aurora A is a prognostic marker for breast cancer arising in BRCA2 mutation carriers. *The Journal of Pathology: Clinical Research*, 1(1), 33–40. <https://doi.org/10.1002/cjp2.6>
9. Arnold, K., Kim, M.-K., Frerk, K., Edler, L., Savelyeva, L., Schmezer, P., & Wiedemeyer, R. (2006). Lower level of BRCA2 protein in heterozygous mutation carriers is correlated with an increase in DNA double strand breaks and an impaired DSB repair. *Cancer Letters*, 243(1), 90–100. <https://doi.org/10.1016/j.canlet.2005.11.041>
10. Ashworth, A. (2008). A Synthetic Lethal Therapeutic Approach: Poly(ADP) Ribose Polymerase Inhibitors for the Treatment of Cancers Deficient in DNA Double-Strand Break Repair. *Journal of Clinical Oncology*, 26(22), 3785–3790. <https://doi.org/10.1200/jco.2008.16.0812>
11. Asperen, C. J. van, Brohet, R. M., Meijers-Heijboer, E. J., Hoogerbrugge, N., Verhoef, S., Vasen, H. F. A., Ausems, M. G. E. M., Menko, F. H., Garcia, E. B. G., Klijn, J. G. M., Hogervorst, F. B. L.,

- Houwelingen, J. C. van, Veer, L. J. van't, Rookus, M. A., Leeuwen, F. E. van, & (HEBON), N. C. G. on H. B. C. (2005). Cancer risks in BRCA2 families: estimates for sites other than breast and ovary. *Journal of Medical Genetics*, 42(9), 711. <https://doi.org/10.1136/jmg.2004.028829>
12. Barnes, D. E., & Lindahl, T. (2004). Repair and genetic consequences of endogenous DNA base damage in mammalian cells. *Annual Review of Genetics*, 38(1), 445–476. <https://doi.org/10.1146/annurev.genet.38.072902.092448>
 13. Bartek, J., Lukas, C., & Lukas, J. (2004). Checking on DNA damage in S phase. *Nature Reviews Molecular Cell Biology*, 5(10), 792–804. <https://doi.org/10.1038/nrm1493>
 14. Bębenek, A., & Ziuzia-Graczyk, I. (2018). Fidelity of DNA replication—a matter of proofreading. *Current Genetics*, 64(5), 985–996. <https://doi.org/10.1007/s00294-018-0820-1>
 15. Beck, C., Robert, I., Reina-San-Martin, B., Schreiber, V., & Dantzer, F. (2014). Poly(ADP-ribose) polymerases in double-strand break repair: Focus on PARP1, PARP2 and PARP3. *Experimental Cell Research*, 329(1), 18–25. <https://doi.org/10.1016/j.yexcr.2014.07.003>
 16. Bellacosa, A., Godwin, A. K., Peri, S., Devarajan, K., Caretti, E., Vanderveer, L., Bove, B., Slater, C., Zhou, Y., Daly, M., Howard, S., Campbell, K. S., Nicolas, E., Yeung, A. T., Clapper, M. L., Crowell, J. A., Lynch, H. T., Ross, E., Kopelovich, L., & Knudson, A. G. (2010). Altered Gene Expression in Morphologically Normal Epithelial Cells from Heterozygous Carriers of BRCA1 or BRCA2 Mutations. *Cancer Prevention Research*, 3(1), 48–61. <https://doi.org/10.1158/1940-6207.capr-09-0078>
 17. Berger, A. H., Knudson, A. G., & Pandolfi, P. P. (2011). A continuum model for tumour suppression. *Nature*, 476(7359), 163–169. <https://doi.org/10.1038/nature10275>
 18. Berti, M., Cortez, D., & Lopes, M. (2020). The plasticity of DNA replication forks in response to clinically relevant genotoxic stress. *Nature Reviews Molecular Cell Biology*, 21(10), 633–651. <https://doi.org/10.1038/s41580-020-0257-5>
 19. Berton, T. R., Matsumoto, T., Page, A., Conti, C. J., Deng, C.-X., Jorcano, J. L., & Johnson, D. G. (2003). Tumor formation in mice with conditional inactivation of Brca1 in epithelial tissues. *Oncogene*, 22(35), 5415–5426. <https://doi.org/10.1038/sj.onc.1206825>
 20. Bhargava, R., Onyango, D. O., & Stark, J. M. (2016). Regulation of Single-Strand Annealing and its Role in Genome Maintenance. *Trends in Genetics*, 32(9), 566–575. <https://doi.org/10.1016/j.tig.2016.06.007>
 21. Bhatia, V., Barroso, S. I., García-Rubio, M. L., Tumini, E., Herrera-Moyano, E., & Aguilera, A. (2014). BRCA2 prevents R-loop accumulation and associates with TREX-2 mRNA export factor PCID2. *Nature*, 511(7509), 362–365. <https://doi.org/10.1038/nature13374>
 22. Bignell, G., Micklem, G., Stratton, M. R., Ashworth, A., & Wooster, R. (1997). The BRC Repeats are Conserved in Mammalian BRCA2 Proteins. *Human Molecular Genetics*, 6(1), 53–58. <https://doi.org/10.1093/hmg/6.1.53>
 23. Biswas, K., Das, R., Alter, B. P., Kuznetsov, S. G., Stauffer, S., North, S. L., Burkett, S., Brody, L. C., Meyer, S., Byrd, R. A., & Sharan, S. K. (2011). A comprehensive functional characterization of BRCA2 variants associated with Fanconi anemia using mouse ES cell-based assay. *Blood*, 118(9), 2430–2442. <https://doi.org/10.1182/blood-2010-12-324541>

24. Botuyan, M. V., Lee, J., Ward, I. M., Kim, J.-E., Thompson, J. R., Chen, J., & Mer, G. (2006). Structural Basis for the Methylation State-Specific Recognition of Histone H4-K20 by 53BP1 and Crb2 in DNA Repair. *Cell*, 127(7), 1361–1373. <https://doi.org/10.1016/j.cell.2006.10.043>
25. Bouwman, P., Aly, A., Escandell, J. M., Pieterse, M., Bartkova, J., Gulden, H. van der, Hiddingh, S., Thanasoula, M., Kulkarni, A., Yang, Q., Haffty, B. G., Tommiska, J., Blomqvist, C., Drapkin, R., Adams, D. J., Nevanlinna, H., Bartek, J., Tarsounas, M., Ganesan, S., & Jonkers, J. (2010). 53BP1 loss rescues BRCA1 deficiency and is associated with triple-negative and BRCA-mutated breast cancers. *Nature Structural & Molecular Biology*, 17(6), 688–695. <https://doi.org/10.1038/nsmb.1831>
26. Branzei, D. (2011). Ubiquitin family modifications and template switching. *FEBS Letters*, 585(18), 2810–2817. <https://doi.org/10.1016/j.febslet.2011.04.053>
27. Brown, E. T., & Holt, J. T. (2009). Rad51 overexpression rescues radiation resistance in BRCA2-defective cancer cells. *Molecular Carcinogenesis*, 48(2), 105–109. <https://doi.org/10.1002/mc.20463>
28. Bryant, H. E., Schultz, N., Thomas, H. D., Parker, K. M., Flower, D., Lopez, E., Kyle, S., Meuth, M., Curtin, N. J., & Helleday, T. (2005). Specific killing of BRCA2-deficient tumours with inhibitors of poly(ADP-ribose) polymerase. *Nature*, 434(7035), 913–917. <https://doi.org/10.1038/nature03443>
29. Buisson, R., Dion-Côté, A.-M., Coulombe, Y., Launay, H., Cai, H., Stasiak, A. Z., Stasiak, A., Xia, B., & Masson, J.-Y. (2010). Cooperation of breast cancer proteins PALB2 and piccolo BRCA2 in stimulating homologous recombination. *Nature Structural & Molecular Biology*, 17(10), 1247–1254. <https://doi.org/10.1038/nsmb.1915>
30. Burgers, P. M. J., & Kunkel, T. A. (2016). Eukaryotic DNA Replication Fork. *Annual Review of Biochemistry*, 86(1), 1–22. <https://doi.org/10.1146/annurev-biochem-061516-044709>
31. Cadet, J., & Davies, K. J. A. (2017). Oxidative DNA damage & repair: An introduction. *Free Radical Biology and Medicine*, 107, 2–12. <https://doi.org/10.1016/j.freeradbiomed.2017.03.030>
32. Çağlayan, M., Batra, V. K., Sassa, A., Prasad, R., & Wilson, S. H. (2014). Role of polymerase β in complementing aprataxin deficiency during abasic-site base excision repair. *Nature Structural & Molecular Biology*, 21(5), 497–499. <https://doi.org/10.1038/nsmb.2818>
33. Caldecott, K. W. (2019). XRCC1 protein; Form and function. *DNA Repair*, 81, 102664. <https://doi.org/10.1016/j.dnarep.2019.102664>
34. Caldecott, K. W. (2022). DNA single-strand break repair and human genetic disease. *Trends in Cell Biology*, 32(9), 733–745. <https://doi.org/10.1016/j.tcb.2022.04.010>
35. Callen, E., Di Virgilio, M., Kruhlak, M. J., Nieto-Soler, M., Wong, N., Chen, H.-T., Faryabi, R. B., Polato, F., Santos, M., Starnes, L. M., Wesemann, D. R., Lee, J.-E., Tubbs, A., Sleckman, B. P., Daniel, J. A., Ge, K., Alt, F. W., Fernandez-Capetillo, O., Nussenzweig, M. C., & Nussenzweig, A. (2013). 53BP1 Mediates Productive and Mutagenic DNA Repair through Distinct Phosphoprotein Interactions. *Cell*, 153(6), 1266–1280. <https://doi.org/10.1016/j.cell.2013.05.023>
36. Caputo, S. M., Golmard, L., Léone, M., Damiola, F., Guillaud-Bataille, M., Revillion, F., Rouleau, E., Derive, N., Buisson, A., Basset, N., Schwartz, M., Vilquin, P., Garrec, C., Privat, M., Gay-Bellile, M., Abadie, C., Abidallah, K., Airaud, F., Allary, A.-S., ... Stoppa-Lyonnet, D. (2021). Classification of 101 BRCA1 and BRCA2 variants of uncertain significance by cosegregation study: A powerful

- approach. *The American Journal of Human Genetics*, 108(10), 1907–1923. <https://doi.org/10.1016/j.ajhg.2021.09.003>
37. Carreira, A., Hilario, J., Amitani, I., Baskin, R. J., Shivji, M. K. K., Venkitaraman, A. R., & Kowalczykowski, S. C. (2009). The BRC Repeats of BRCA2 Modulate the DNA-Binding Selectivity of RAD51. *Cell*, 136(6), 1032–1043. <https://doi.org/10.1016/j.cell.2009.02.019>
 38. Carreira, A., & Kowalczykowski, S. C. (2011). Two classes of BRC repeats in BRCA2 promote RAD51 nucleoprotein filament function by distinct mechanisms. *Proceedings of the National Academy of Sciences*, 108(26), 10448–10453. <https://doi.org/10.1073/pnas.1106971108>
 39. Ceccaldi, R., Rondinelli, B., & D'Andrea, A. D. (2016). Repair Pathway Choices and Consequences at the Double-Strand Break. *Trends in Cell Biology*, 26(1), 52–64. <https://doi.org/10.1016/j.tcb.2015.07.009>
 40. Ceccaldi, R., Sarangi, P., & D'Andrea, A. D. (2016). The Fanconi anaemia pathway: new players and new functions. *Nature Reviews Molecular Cell Biology*, 17(6), 337–349. <https://doi.org/10.1038/nrm.2016.48>
 41. Chang, H. H. Y., Pannunzio, N. R., Adachi, N., & Lieber, M. R. (2017). Non-homologous DNA end joining and alternative pathways to double-strand break repair. *Nature Reviews Molecular Cell Biology*, 18(8), 495–506. <https://doi.org/10.1038/nrm.2017.48>
 42. Chapman, J. R., Barral, P., Vannier, J.-B., Borel, V., Steger, M., Tomas-Loba, A., Sartori, A. A., Adams, I. R., Batista, F. D., & Boulton, S. J. (2013). RIF1 Is Essential for 53BP1-Dependent Nonhomologous End Joining and Suppression of DNA Double-Strand Break Resection. *Molecular Cell*, 49(5), 858–871. <https://doi.org/10.1016/j.molcel.2013.01.002>
 43. Chaudhuri, A. R., Callen, E., Ding, X., Gogola, E., Duarte, A. A., Lee, J.-E., Wong, N., Lafarga, V., Calvo, J. A., Panzarino, N. J., John, S., Day, A., Crespo, A. V., Shen, B., Starnes, L. M., Ruitter, J. R. de, Daniel, J. A., Konstantinopoulos, P. A., Cortez, D., ... Nussenzweig, A. (2016). Replication fork stability confers chemoresistance in BRCA-deficient cells. *Nature*, 535(7612), 382–387. <https://doi.org/10.1038/nature18325>
 44. Chaudhuri, A. R., & Nussenzweig, A. (2017). The multifaceted roles of PARP1 in DNA repair and chromatin remodelling. *Nature Reviews Molecular Cell Biology*, 18(10), 610–621. <https://doi.org/10.1038/nrm.2017.53>
 45. Chaudhuri, J., Basu, U., Zarrin, A., Yan, C., Franco, S., Perlot, T., Vuong, B., Wang, J., Phan, R. T., Datta, A., Manis, J., & Alt, F. W. (2007). Evolution of the Immunoglobulin Heavy Chain Class Switch Recombination Mechanism. *Advances in Immunology*, 94(J. Biol. Chem.2822007), 157–214. [https://doi.org/10.1016/s0065-2776\(06\)94006-1](https://doi.org/10.1016/s0065-2776(06)94006-1)
 46. Chen, C.-F., Chen, P.-L., Zhong, Q., Sharp, Z. D., & Lee, W.-H. (1999). Expression of BRC Repeats in Breast Cancer Cells Disrupts the BRCA2-Rad51 Complex and Leads to Radiation Hypersensitivity and Loss of G2/M Checkpoint Control*. *Journal of Biological Chemistry*, 274(46), 32931–32935. <https://doi.org/10.1074/jbc.274.46.32931>
 47. Chen, J., Silver, D. P., Walpita, D., Cantor, S. B., Gazdar, A. F., Tomlinson, G., Couch, F. J., Weber, B. L., Ashley, T., Livingston, D. M., & Scully, R. (1998). Stable Interaction between the Products of the BRCA1 and BRCA2 Tumor Suppressor Genes in Mitotic and Meiotic Cells. *Molecular Cell*, 2(3), 317–328. [https://doi.org/10.1016/s1097-2765\(00\)80276-2](https://doi.org/10.1016/s1097-2765(00)80276-2)

48. Chen, M. C., Murat, P., Abecassis, K., Ferré-D'Amaré, A. R., & Balasubramanian, S. (2015). Insights into the mechanism of a G-quadruplex-unwinding DEAH-box helicase. *Nucleic Acids Research*, 43(4), 2223–2231. <https://doi.org/10.1093/nar/gkv051>
49. Ciccia, A., & Elledge, S. J. (2010). The DNA Damage Response: Making It Safe to Play with Knives. *Molecular Cell*, 40(2), 179–204. <https://doi.org/10.1016/j.molcel.2010.09.019>
50. Cleaver, J. E. (2005). Cancer in xeroderma pigmentosum and related disorders of DNA repair. *Nature Reviews Cancer*, 5(7), 564–573. <https://doi.org/10.1038/nrc1652>
51. Cline, M. S., Liao, R. G., Parsons, M. T., Paten, B., Alquaddoomi, F., Antoniou, A., Baxter, S., Brody, L., Cook-Deegan, R., Coffin, A., Couch, F. J., Craft, B., Currie, R., Dlott, C. C., Dolman, L., Dunnen, J. T. den, Dyke, S. O. M., Domchek, S. M., Easton, D., ... Spurdle, A. B. (2018). BRCA Challenge: BRCA Exchange as a global resource for variants in BRCA1 and BRCA2. *PLoS Genetics*, 14(12), e1007752. <https://doi.org/10.1371/journal.pgen.1007752>
52. Collins, N., McManus, R., Wooster, R., Mangion, J., Seal, S., Lakhani, S. R., Ormiston, W., Daly, P. A., Ford, D., & Easton, D. F. (1995). Consistent loss of the wild type allele in breast cancers from a family linked to the BRCA2 gene on chromosome 13q12-13. *Oncogene*, 10(8), 1673–1675.
53. Cong, K., & Cantor, S. B. (2022). Exploiting replication gaps for cancer therapy. *Molecular Cell*, 82(13), 2363–2369. <https://doi.org/10.1016/j.molcel.2022.04.023>
54. Cong, K., Peng, M., Kousholt, A. N., Lee, W. T. C., Lee, S., Nayak, S., Kraus, J., VanderVere-Carozza, P. S., Pawelczak, K. S., Calvo, J., Panzarino, N. J., Turchi, J. J., Johnson, N., Jonkers, J., Rothenberg, E., & Cantor, S. B. (2021). Replication gaps are a key determinant of PARP inhibitor synthetic lethality with BRCA deficiency. *Molecular Cell*, 81(15), 3128–3144.e7. <https://doi.org/10.1016/j.molcel.2021.06.011>
55. Connor, F., Bertwistle, D., Mee, P. J., Ross, G. M., Swift, S., Grigorieva, E., Tybulewicz, V. L., & Ashworth, A. (1997). Tumorigenesis and a DNA repair defect in mice with a truncating Brca2 mutation. *Nature Genetics*, 17(4), 423–430. <https://doi.org/10.1038/ng1297-423>
56. Connor, F., Smith, A., Wooster, R., Stratton, M., Dixon, A., Campbell, E., Tait, T.-M., Freeman, T., & Ashworth, A. (1997). Cloning, Chromosomal Mapping and Expression Pattern of the Mouse Brca2 Gene. *Human Molecular Genetics*, 6(2), 291–300. <https://doi.org/10.1093/hmg/6.2.291>
57. Consortium, T. B. C. L. (1999). Cancer Risks in BRCA2 Mutation Carriers. *JNCI: Journal of the National Cancer Institute*, 91(15), 1310–1316. <https://doi.org/10.1093/jnci/91.15.1310>
58. Costantino, L., & Koshland, D. (2018). Genome-wide Map of R-Loop-Induced Damage Reveals How a Subset of R-Loops Contributes to Genomic Instability. *Molecular Cell*, 71(4), 487–497.e3. <https://doi.org/10.1016/j.molcel.2018.06.037>
59. Couch, F. J., Farid, L. M., DeShano, M. L., Tavtigian, S. V., Calzone, K., Campeau, L., Peng, Y., Bogden, B., Chen, Q., Neuhausen, S., Shattuck-Eidens, D., Godwin, A. K., Daly, M., Radford, D. M., Sedlacek, S., Rommens, J., Simard, J., Garber, J., Merajver, S., & Weber, B. L. (1996). BRCA2 germline mutations in male breast cancer cases and breast cancer families. *Nature Genetics*, 13(1), 123–125. <https://doi.org/10.1038/ng0596-123>

60. Couch, F. J., Nathanson, K. L., & Offit, K. (2014). Two Decades After BRCA: Setting Paradigms in Personalized Cancer Care and Prevention. *Science*, *343*(6178), 1466–1470. <https://doi.org/10.1126/science.1251827>
61. Crook, T., Brooks, L. A., Crossland, S., Osin, P., Barker, K. T., Waller, J., Philp, E., Smith, P. D., Yulug, I., Peto, J., Parker, G., Allday, M. J., Crompton, M. R., & Gusterson, B. A. (1998). p53 mutation with frequent novel codons but not a mutator phenotype in BRCA1- and BRCA2-associated breast tumours. *Oncogene*, *17*(13), 1681–1689. <https://doi.org/10.1038/sj.onc.1202106>
62. D'Alessandro, G., Whelan, D. R., Howard, S. M., Vitelli, V., Renaudin, X., Adamowicz, M., Iannelli, F., Jones-Weinert, C. W., Lee, M., Matti, V., Lee, W. T. C., Morten, M. J., Venkitaraman, A. R., Cejka, P., Rothenberg, E., & Fagagna, F. d'Adda di. (2018). BRCA2 controls DNA:RNA hybrid level at DSBs by mediating RNase H2 recruitment. *Nature Communications*, *9*(1), 5376. <https://doi.org/10.1038/s41467-018-07799-2>
63. D'Amours, D., Desnoyers, S., D'Silva, I., & Poirier, G. G. (1999). Poly(ADP-ribosyl)ation reactions in the regulation of nuclear functions. *The Biochemical Journal*, *342* (Pt 2), 249–268.
64. Daniels, M. J., Wang, Y., Lee, M., & Venkitaraman, A. R. (2004). Abnormal Cytokinesis in Cells Deficient in the Breast Cancer Susceptibility Protein BRCA2. *Science*, *306*(5697), 876–879. <https://doi.org/10.1126/science.1102574>
65. Davies, H., Glodzik, D., Morganella, S., Yates, L. R., Staaf, J., Zou, X., Ramakrishna, M., Martin, S., Boyault, S., Sieuwerts, A. M., Simpson, P. T., King, T. A., Raine, K., Eyfjord, J. E., Kong, G., Borg, Å., Birney, E., Stunnenberg, H. G., Vijver, M. J. van de, ... Nik-Zainal, S. (2017). HRDetect is a predictor of BRCA1 and BRCA2 deficiency based on mutational signatures. *Nature Medicine*, *23*(4), 517–525. <https://doi.org/10.1038/nm.4292>
66. Daza-Martin, M., Starowicz, K., Jamshad, M., Tye, S., Ronson, G. E., MacKay, H. L., Chauhan, A. S., Walker, A. K., Stone, H. R., Beesley, J. F. J., Coles, J. L., Garvin, A. J., Stewart, G. S., McCorvie, T. J., Zhang, X., Densham, R. M., & Morris, J. R. (2019). Isomerization of BRCA1–BARD1 promotes replication fork protection. *Nature*, *571*(7766), 521–527. <https://doi.org/10.1038/s41586-019-1363-4>
67. Deshpande, M., Paniza, T., Jalloul, N., Nanjangud, G., Twarowski, J., Koren, A., Zaninovic, N., Zhan, Q., Chadalavada, K., Malkova, A., Khiabani, H., Madireddy, A., Rosenwaks, Z., & Gerhardt, J. (2022). Error-prone repair of stalled replication forks drives mutagenesis and loss of heterozygosity in haploinsufficient BRCA1 cells. *Molecular Cell*. <https://doi.org/10.1016/j.molcel.2022.08.017>
68. Dianov, G., & Lindahl, T. (1994). Reconstitution of the DNA base excision—repair pathway. *Current Biology*, *4*(12), 1069–1076. [https://doi.org/10.1016/s0960-9822\(00\)00245-1](https://doi.org/10.1016/s0960-9822(00)00245-1)
69. Donzelli, M., & Draetta, G. F. (2003). Regulating mammalian checkpoints through Cdc25 inactivation. *EMBO Reports*, *4*(7), 671–677. <https://doi.org/10.1038/sj.embor.embor887>
70. Dworkin, A. M., Spearman, A. D., Tseng, S. Y., Sweet, K., & Toland, A. E. (2009). Methylation not a frequent “second hit” in tumors with germline BRCA mutations. *Familial Cancer*, *8*(4), 339–346. <https://doi.org/10.1007/s10689-009-9240-1>
71. Ehlén, Å., Martin, C., Miron, S., Julien, M., Theillet, F.-X., Ropars, V., Sessa, G., Beaurepere, R., Boucherit, V., Duchambon, P., Marjou, A. E., Zinn-Justin, S., & Carreira, A. (2020). Proper

- chromosome alignment depends on BRCA2 phosphorylation by PLK1. *Nature Communications*, 11(1), 1819. <https://doi.org/10.1038/s41467-020-15689-9>
72. Ekholm-Reed, S., Méndez, J., Tedesco, D., Zetterberg, A., Stillman, B., & Reed, S. I. (2004). Deregulation of cyclin E in human cells interferes with prereplication complex assembly. *The Journal of Cell Biology*, 165(6), 789–800. <https://doi.org/10.1083/jcb.200404092>
 73. Esashi, F., Christ, N., Gannon, J., Liu, Y., Hunt, T., Jasin, M., & West, S. C. (2005). CDK-dependent phosphorylation of BRCA2 as a regulatory mechanism for recombinational repair. *Nature*, 434(7033), 598–604. <https://doi.org/10.1038/nature03404>
 74. Evers, B., & Jonkers, J. (2006). Mouse models of BRCA1 and BRCA2 deficiency: past lessons, current understanding and future prospects. *Oncogene*, 25(43), 5885–5897. <https://doi.org/10.1038/sj.onc.1209871>
 75. Fagbemi, A. F., Orelli, B., & Schäerer, O. D. (2011). Regulation of endonuclease activity in human nucleotide excision repair. *DNA Repair*, 10(7), 722–729. <https://doi.org/10.1016/j.dnarep.2011.04.022>
 76. Farmer, H., McCabe, N., Lord, C. J., Tutt, A. N. J., Johnson, D. A., Richardson, T. B., Santarosa, M., Dillon, K. J., Hickson, I., Knights, C., Martin, N. M. B., Jackson, S. P., Smith, G. C. M., & Ashworth, A. (2005). Targeting the DNA repair defect in BRCA mutant cells as a therapeutic strategy. *Nature*, 434(7035), 917–921. <https://doi.org/10.1038/nature03445>
 77. Farrugia, D. J., Agarwal, M. K., Pankratz, V. S., Deffenbaugh, A. M., Pruss, D., Frye, C., Wadum, L., Johnson, K., Mentlick, J., Tavtigian, S. V., Goldgar, D. E., & Couch, F. J. (2008). Functional Assays for Classification of BRCA2 Variants of Uncertain Significance. *Cancer Research*, 68(9), 3523–3531. <https://doi.org/10.1158/0008-5472.can-07-1587>
 78. Feng, W., & Jasin, M. (2017). BRCA2 suppresses replication stress-induced mitotic and G1 abnormalities through homologous recombination. *Nature Communications*, 8(1), 525. <https://doi.org/10.1038/s41467-017-00634-0>
 79. Fenton, A. L., Shirodkar, P., Macrae, C. J., Meng, L., & Koch, C. A. (2013). The PARP3- and ATM-dependent phosphorylation of APLF facilitates DNA double-strand break repair. *Nucleic Acids Research*, 41(7), 4080–4092. <https://doi.org/10.1093/nar/gkt134>
 80. Filippo, J. S., Chi, P., Sehorn, M. G., Echin, J., Krejci, L., & Sung, P. (2006). Recombination Mediator and Rad51 Targeting Activities of a Human BRCA2 Polypeptide*. *Journal of Biological Chemistry*, 281(17), 11649–11657. <https://doi.org/10.1074/jbc.m601249200>
 81. Forment, J. V., & Jackson, S. P. (2015). A flow cytometry–based method to simplify the analysis and quantification of protein association to chromatin in mammalian cells. *Nature Protocols*, 10(9), 1297–1307. <https://doi.org/10.1038/nprot.2015.066>
 82. Friedman, L. S., Thistlethwaite, F. C., Patel, K. J., Yu, V. P., Lee, H., Venkitaraman, A. R., Abel, K. J., Carlton, M. B., Hunter, S. M., Colledge, W. H., Evans, M. J., & Ponder, B. A. (1998). Thymic lymphomas in mice with a truncating mutation in Brca2. *Cancer Research*, 58(7), 1338–1343.
 83. Fu, D., Calvo, J. A., & Samson, L. D. (2012). Balancing repair and tolerance of DNA damage caused by alkylating agents. *Nature Reviews Cancer*, 12(2), 104–120. <https://doi.org/10.1038/nrc3185>

84. Fugmann, S. D., Lee, A. I., Shockett, P. E., Villey, I. J., & Schatz, D. G. (2000). The RAG Proteins and V(D)J Recombination: Complexes, Ends, and Transposition. *Annual Review of Immunology*, 18(1), 495–527. <https://doi.org/10.1146/annurev.immunol.18.1.495>
85. Fuks, F., Milner, J., & Kouzarides, T. (1998). BRCA2 associates with acetyltransferase activity when bound to P/CAF. *Oncogene*, 17(19), 2531–2534. <https://doi.org/10.1038/sj.onc.1202475>
86. Fullbright, G., Rycenga, H. B., Gruber, J. D., & Long, D. T. (2016). p97 Promotes a Conserved Mechanism of Helicase Unloading during DNA Cross-Link Repair. *Molecular and Cellular Biology*, 36(23), 2983–2994. <https://doi.org/10.1128/mcb.00434-16>
87. Gelot, C., Kovacs, M. T., Miron, S., Mylne, E., Haan, A., Boeffard-Dosierre, L., Ghouil, R., Popova, T., Dingli, F., Loew, D., Guirouilh-Barbat, J., Nery, E. D., Zinn-Justin, S., & Ceccaldi, R. (2023). Polθ is phosphorylated by PLK1 to repair double-strand breaks in mitosis. *Nature*, 621(7978), 415–422. <https://doi.org/10.1038/s41586-023-06506-6>
88. Goggins, M., Schutte, M., Lu, J., Moskaluk, C. A., Weinstein, C. L., Petersen, G. M., Yeo, C. J., Jackson, C. E., Lynch, H. T., Hruban, R. H., & Kern, S. E. (1996). Germline BRCA2 gene mutations in patients with apparently sporadic pancreatic carcinomas. *Cancer Research*, 56(23), 5360–5364.
89. Gogola, E., Duarte, A. A., Ruitter, J. R. de, Wiegant, W. W., Schmid, J. A., Bruijn, R. de, James, D. I., Llobet, S. G., Vis, D. J., Annunziato, S., Broek, B. van den, Barazas, M., Kersbergen, A., Ven, M. van de, Tarsounas, M., Ogilvie, D. J., Vugt, M. van, Wessels, L. F. A., Bartkova, J., ... Rottenberg, S. (2018). Selective Loss of PARG Restores PARylation and Counteracts PARP Inhibitor-Mediated Synthetic Lethality. *Cancer Cell*, 33(6), 1078–1093.e12. <https://doi.org/10.1016/j.ccell.2018.05.008>
90. Goldgar, D. E., Easton, D. F., Byrnes, G. B., Spurdle, A. B., Iversen, E. S., Greenblatt, M. S., & Group, for the I. U. G. V. W. (2008). Genetic evidence and integration of various data sources for classifying uncertain variants into a single model. *Human Mutation*, 29(11), 1265–1272. <https://doi.org/10.1002/humu.20897>
91. Gottlieb, T. M., & Jackson, S. P. (1993). The DNA-dependent protein kinase: Requirement for DNA ends and association with Ku antigen. *Cell*, 72(1), 131–142. [https://doi.org/10.1016/0092-8674\(93\)90057-w](https://doi.org/10.1016/0092-8674(93)90057-w)
92. Graham, T. G. W., Walter, J. C., & Loparo, J. J. (2016). Two-Stage Synapsis of DNA Ends during Non-homologous End Joining. *Molecular Cell*, 61(6), 850–858. <https://doi.org/10.1016/j.molcel.2016.02.010>
93. Greenberg, M. M. (2014). Abasic and Oxidized Abasic Site Reactivity in DNA: Enzyme Inhibition, Cross-Linking, and Nucleosome Catalyzed Reactions. *Accounts of Chemical Research*, 47(2), 646–655. <https://doi.org/10.1021/ar400229d>
94. Greenblatt, M. S., Chappuis, P. O., Bond, J. P., Hamel, N., & Foulkes, W. D. (2001). TP53 mutations in breast cancer associated with BRCA1 or BRCA2 germ-line mutations: distinctive spectrum and structural distribution. *Cancer Research*, 61(10), 4092–4097.
95. Gruber, J. J., Chen, J., Geller, B., Jäger, N., Lipchik, A. M., Wang, G., Kurian, A. W., Ford, J. M., & Snyder, M. P. (2019). Chromatin Remodeling in Response to BRCA2-Crisis. *Cell Reports*, 28(8), 2182–2193.e6. <https://doi.org/10.1016/j.celrep.2019.07.057>

96. Gudmundsson, J., Johannesdottir, G., Bergthorsson, J. T., Arason, A., Ingvarsson, S., Egilsson, V., & Barkardottir, R. B. (1995). Different tumor types from BRCA2 carriers show wild-type chromosome deletions on 13q12-q13. *Cancer Research*, *55*(21), 4830–4832.
97. Guidugli, L., Carreira, A., Caputo, S. M., Ehlen, A., Galli, A., Monteiro, A. N. A., Neuhausen, S. L., Hansen, T. V. O., Couch, F. J., Vreeswijk, M. P. G., & consortium, on behalf of the E. (2014). Functional Assays for Analysis of Variants of Uncertain Significance in BRCA2. *Human Mutation*, *35*(2), 151–164. <https://doi.org/10.1002/humu.22478>
98. Guidugli, L., Pankratz, V. S., Singh, N., Thompson, J., Erding, C. A., Engel, C., Schmutzler, R., Domchek, S., Nathanson, K., Radice, P., Singer, C., Tonin, P. N., Lindor, N. M., Goldgar, D. E., & Couch, F. J. (2013). A Classification Model for BRCA2 DNA Binding Domain Missense Variants Based on Homology-Directed Repair Activity. *Cancer Research*, *73*(1), 265–275. <https://doi.org/10.1158/0008-5472.can-12-2081>
99. Guillemette, S., Serra, R. W., Peng, M., Hayes, J. A., Konstantinopoulos, P. A., Green, M. R., & Cantor, S. B. (2015). Resistance to therapy in BRCA2 mutant cells due to loss of the nucleosome remodeling factor CHD4. *Genes & Development*, *29*(5), 489–494. <https://doi.org/10.1101/gad.256214.114>
100. Guo, N., Li, M.-Z., Wang, L.-M., Chen, H.-D., Song, S.-S., Miao, Z.-H., & He, J.-X. (2022). Repeated treatments of Capan-1 cells with PARP1 and Chk1 inhibitors promote drug resistance, migration and invasion. *Cancer Biology & Therapy*, *23*(1), 69–82. <https://doi.org/10.1080/15384047.2021.2024414>
101. Hakem, R., Pompa, J. L. de la, Sirard, C., Mo, R., Woo, M., Hakem, A., Wakeham, A., Potter, J., Reitmair, A., Billia, F., Firpo, E., Hui, C. C., Roberts, J., Rossant, J., & Mak, T. W. (1996). The Tumor Suppressor Gene Brca1 Is Required for Embryonic Cellular Proliferation in the Mouse. *Cell*, *85*(7), 1009–1023. [https://doi.org/10.1016/s0092-8674\(00\)81302-1](https://doi.org/10.1016/s0092-8674(00)81302-1)
102. Hanahan, D., & Weinberg, R. A. (2011). Hallmarks of Cancer: The Next Generation. *Cell*, *144*(5), 646–674. <https://doi.org/10.1016/j.cell.2011.02.013>
103. Hanzlikova, H., Kalasova, I., Demin, A. A., Pennicott, L. E., Cihlarova, Z., & Caldecott, K. W. (2018). The Importance of Poly(ADP-Ribose) Polymerase as a Sensor of Unligated Okazaki Fragments during DNA Replication. *Molecular Cell*, *71*(2), 319–331.e3. <https://doi.org/10.1016/j.molcel.2018.06.004>
104. Harper, J. W., & Elledge, S. J. (2007). The DNA Damage Response: Ten Years After. *Molecular Cell*, *28*(5), 739–745. <https://doi.org/10.1016/j.molcel.2007.11.015>
105. Hoeijmakers, J. H. J. (2009). DNA Damage, Aging, and Cancer. *The New England Journal of Medicine*, *361*(15), 1475–1485. <https://doi.org/10.1056/nejmra0804615>
106. Howlett, N. G., Taniguchi, T., Olson, S., Cox, B., Waisfisz, Q., Die-Smulders, C. de, Persky, N., Grompe, M., Joenje, H., Pals, G., Ikeda, H., Fox, E. A., & D'Andrea, A. D. (2002). Biallelic Inactivation of BRCA2 in Fanconi Anemia. *Science*, *297*(5581), 606–609. <https://doi.org/10.1126/science.1073834>
107. Ikejima, M., Noguchi, S., Yamashita, R., Ogura, T., Sugimura, T., Gill, D. M., & Miwa, M. (1990). The zinc fingers of human poly(ADP-ribose) polymerase are differentially required for the recognition of DNA breaks and nicks and the consequent enzyme activation. Other structures recognize intact

- DNA. *Journal of Biological Chemistry*, 265(35), 21907–21913. [https://doi.org/10.1016/s0021-9258\(18\)45824-3](https://doi.org/10.1016/s0021-9258(18)45824-3)
108. Iliakis, G., Murmann, T., & Soni, A. (2015). Alternative end-joining repair pathways are the ultimate backup for abrogated classical non-homologous end-joining and homologous recombination repair: Implications for the formation of chromosome translocations. *Mutation Research/Genetic Toxicology and Environmental Mutagenesis*, 793, 166–175. <https://doi.org/10.1016/j.mrgentox.2015.07.001>
109. Ionov, Y., Peinado, M. A., Malkhosyan, S., Shibata, D., & Perucho, M. (1993). Ubiquitous somatic mutations in simple repeated sequences reveal a new mechanism for colonic carcinogenesis. *Nature*, 363(6429), 558–561. <https://doi.org/10.1038/363558a0>
110. Jensen, R. B., Carreira, A., & Kowalczykowski, S. C. (2010). Purified human BRCA2 stimulates RAD51-mediated recombination. *Nature*, 467(7316), 678–683. <https://doi.org/10.1038/nature09399>
111. Jeyasekharan, A. D., Liu, Y., Hattori, H., Pisupati, V., Jonsdottir, A. B., Rajendra, E., Lee, M., Sundaramoorthy, E., Schlachter, S., Kaminski, C. F., Ofir-Rosenfeld, Y., Sato, K., Savill, J., Ayoub, N., & Venkitaraman, A. R. (2013). A cancer-associated BRCA2 mutation reveals masked nuclear export signals controlling localization. *Nature Structural & Molecular Biology*, 20(10), 1191–1198. <https://doi.org/10.1038/nsmb.2666>
112. Jonkers, J., Meuwissen, R., Gulden, H. van der, Peterse, H., Valk, M. van der, & Berns, A. (2001). Synergistic tumor suppressor activity of BRCA2 and p53 in a conditional mouse model for breast cancer. *Nature Genetics*, 29(4), 418–425. <https://doi.org/10.1038/ng747>
113. Julien, M., Miron, S., Carreira, A., Theillet, F.-X., & Zinn-Justin, S. (2020). 1H, 13C and 15N backbone resonance assignment of the human BRCA2 N-terminal region. *Biomolecular NMR Assignments*, 14(1), 79–85. <https://doi.org/10.1007/s12104-019-09924-8>
114. Kanchi, K. L., Johnson, K. J., Lu, C., McLellan, M. D., Leiserson, M. D. M., Wendl, M. C., Zhang, Q., Koboldt, D. C., Xie, M., Kandoth, C., McMichael, J. F., Wyczalkowski, M. A., Larson, D. E., Schmidt, H. K., Miller, C. A., Fulton, R. S., Spellman, P. T., Mardis, E. R., Druley, T. E., ... Ding, L. (2014). Integrated analysis of germline and somatic variants in ovarian cancer. *Nature Communications*, 5(1), 3156. <https://doi.org/10.1038/ncomms4156>
115. Kang, Z., Fu, P., Alcivar, A. L., Fu, H., Redon, C., Foo, T. K., Zuo, Y., Ye, C., Baxley, R., Madireddy, A., Buisson, R., Bielinsky, A.-K., Zou, L., Shen, Z., Aladjem, M. I., & Xia, B. (2021). BRCA2 associates with MCM10 to suppress PRIMPOL-mediated repriming and single-stranded gap formation after DNA damage. *Nature Communications*, 12(1), 5966. <https://doi.org/10.1038/s41467-021-26227-6>
116. Karaayvaz-Yildirim, M., Silberman, R. E., Langenbucher, A., Saladi, S. V., Ross, K. N., Zarcaro, E., Desmond, A., Yildirim, M., Vivekanandan, V., Ravichandran, H., Mylavagnanam, R., Specht, M. C., Ramaswamy, S., Lawrence, M., Amon, A., & Ellisen, L. W. (2020). Aneuploidy and a deregulated DNA damage response suggest haploinsufficiency in breast tissues of BRCA2 mutation carriers. *Science Advances*, 6(5), eaay2611. <https://doi.org/10.1126/sciadv.aay2611>
117. Kass, E. M., Lim, P. X., Helgadottir, H. R., Moynahan, M. E., & Jasin, M. (2016). Robust homology-directed repair within mouse mammary tissue is not specifically affected by Brca2 mutation. *Nature Communications*, 7(1), 13241. <https://doi.org/10.1038/ncomms13241>

118. Kennedy, R. D., & D'Andrea, A. D. (2005). The Fanconi Anemia/BRCA pathway: new faces in the crowd. *Genes & Development*, 19(24), 2925–2940. <https://doi.org/10.1101/gad.1370505>
119. Khatib, J. B., Nicolae, C. M., & Moldovan, G.-L. (2023). Role of Translesion DNA Synthesis in the metabolism of replication-associated nascent strand gaps. *Journal of Molecular Biology*, 168275. <https://doi.org/10.1016/j.jmb.2023.168275>
120. King, T. A., Li, W., Brogi, E., Yee, C. J., Gemignani, M. L., Olvera, N., Levine, D. A., Norton, L., Robson, M. E., Offit, K., Borgen, P. I., & Boyd, J. (2007). Heterogenic Loss of the Wild-Type BRCA Allele in Human Breast Tumorigenesis. *Annals of Surgical Oncology*, 14(9), 2510–2518. <https://doi.org/10.1245/s10434-007-9372-1>
121. Kingsley, G., Skagia, A., Passaretti, P., Fernandez-Cuesta, C., Reynolds-Winczura, A., Koscielniak, K., & Gambus, A. (2023). DONSON facilitates Cdc45 and GINS chromatin association and is essential for DNA replication initiation. *Nucleic Acids Research*, 51(18), 9748–9763. <https://doi.org/10.1093/nar/gkad694>
122. Knipscheer, P., Räschle, M., Smogorzewska, A., Enoiu, M., Ho, T. V., Schärer, O. D., Elledge, S. J., & Walter, J. C. (2009). The Fanconi Anemia Pathway Promotes Replication-Dependent DNA Interstrand Cross-Link Repair. *Science*, 326(5960), 1698–1701. <https://doi.org/10.1126/science.1182372>
123. Knudson, A. G. (1971). Mutation and Cancer: Statistical Study of Retinoblastoma. *Proceedings of the National Academy of Sciences*, 68(4), 820–823. <https://doi.org/10.1073/pnas.68.4.820>
124. Kolinjivadi, A. M., Sannino, V., Antoni, A. D., Zadorozhny, K., Kilkenny, M., Técher, H., Baldi, G., Shen, R., Ciccia, A., Pellegrini, L., Krejci, L., & Costanzo, V. (2017). Smarcal1-Mediated Fork Reversal Triggers Mre11-Dependent Degradation of Nascent DNA in the Absence of Brca2 and Stable Rad51 Nucleofilaments. *Molecular Cell*, 67(5), 867–881.e7. <https://doi.org/10.1016/j.molcel.2017.07.001>
125. Krakoff, I. H., Brown, N. C., & Reichard, P. (1968). Inhibition of ribonucleoside diphosphate reductase by hydroxyurea. *Cancer Research*, 28(8), 1559–1565.
126. Kuchenbaecker, K. B., Hopper, J. L., Barnes, D. R., Phillips, K.-A., Mooij, T. M., Roos-Blom, M.-J., Jervis, S., Leeuwen, F. E. van, Milne, R. L., Andrieu, N., Goldgar, D. E., Terry, M. B., Rookus, M. A., Easton, D. F., Antoniou, A. C., Consortium, B. and B. C., McGuffog, L., Evans, D. G., Barrowdale, D., ... Olsson, H. (2017). Risks of Breast, Ovarian, and Contralateral Breast Cancer for BRCA1 and BRCA2 Mutation Carriers. *JAMA*, 317(23), 2402–2416. <https://doi.org/10.1001/jama.2017.7112>
127. Kunkel, T. A., & Erie, D. A. (2005). DNA MISMATCH REPAIR*. *Annual Review of Biochemistry*, 74(1), 681–710. <https://doi.org/10.1146/annurev.biochem.74.082803.133243>
128. Kunkel, T. A., & Erie, D. A. (2015). Eukaryotic Mismatch Repair in Relation to DNA Replication. *Annual Review of Genetics*, 49(1), 1–23. <https://doi.org/10.1146/annurev-genet-112414-054722>
129. Kwon, Y., Rösner, H., Zhao, W., Selemenakis, P., He, Z., Kawale, A. S., Katz, J. N., Rogers, C. M., Neal, F. E., Shabestari, A. B., Petrosius, V., Singh, A. K., Joel, M. Z., Lu, L., Holloway, S. P., Burma, S., Mukherjee, B., Hromas, R., Mazin, A., ... Sung, P. (2023). DNA binding and RAD51 engagement by the BRCA2 C-terminus orchestrate DNA repair and replication fork preservation. *Nature Communications*, 14(1), 432. <https://doi.org/10.1038/s41467-023-36211-x>

130. Le, H. P., Ma, X., Vaquero, J., Brinkmeyer, M., Guo, F., Heyer, W.-D., & Liu, J. (2020). DSS1 and ssDNA regulate oligomerization of BRCA2. *Nucleic Acids Research*, 48(14), gkaa555-. <https://doi.org/10.1093/nar/gkaa555>
131. Lee, J.-H., & Paull, T. T. (2005). ATM Activation by DNA Double-Strand Breaks Through the Mre11-Rad50-Nbs1 Complex. *Science*, 308(5721), 551–554. <https://doi.org/10.1126/science.1108297>
132. Lees-Miller, S. P., Chen, Y.-R., & Anderson, C. W. (1990). Human Cells Contain a DNA-Activated Protein Kinase that Phosphorylates Simian Virus 40 T Antigen, Mouse p53, and the Human Ku Autoantigen. *Molecular and Cellular Biology*, 10(12), 6472–6481. <https://doi.org/10.1128/mcb.10.12.6472-6481.1990>
133. Li, J., Zou, C., Bai, Y., Wazer, D. E., Band, V., & Gao, Q. (2006). DSS1 is required for the stability of BRCA2. *Oncogene*, 25(8), 1186–1194. <https://doi.org/10.1038/sj.onc.1209153>
134. Lim, P. X., Zaman, M., & Jasin, M. (2023). *BRCA2 promotes genomic integrity and therapy resistance primarily through its role in homology-directed repair*. <https://doi.org/10.1101/2023.04.11.536470>
135. Liu, D., Keijzers, G., & Rasmussen, L. J. (2017). DNA mismatch repair and its many roles in eukaryotic cells. *Mutation Research/Reviews in Mutation Research*, 773, 174–187. <https://doi.org/10.1016/j.mrrev.2017.07.001>
136. Liu, J., Doty, T., Gibson, B., & Heyer, W.-D. (2010). Human BRCA2 protein promotes RAD51 filament formation on RPA-covered single-stranded DNA. *Nature Structural & Molecular Biology*, 17(10), 1260–1262. <https://doi.org/10.1038/nsmb.1904>
137. Liu, Q., Guntuku, S., Cui, X. S., Matsuoka, S., Cortez, D., Tamai, K., Luo, G., Carattini-Rivera, S., DeMayo, F., Bradley, A., Donehower, L. A., & Elledge, S. J. (2000). Chk1 is an essential kinase that is regulated by Atr and required for the G(2)/M DNA damage checkpoint. *Genes & Development*, 14(12), 1448–1459.
138. Liu, X., Holstege, H., Gulden, H. van der, Treur-Mulder, M., Zevenhoven, J., Velds, A., Kerkhoven, R. M., Vliet, M. H. van, Wessels, L. F. A., Peterse, J. L., Berns, A., & Jonkers, J. (2007). Somatic loss of BRCA1 and p53 in mice induces mammary tumors with features of human BRCA1-mutated basal-like breast cancer. *Proceedings of the National Academy of Sciences*, 104(29), 12111–12116. <https://doi.org/10.1073/pnas.0702969104>
139. Löbrich, M., & Jeggo, P. (2017). A Process of Resection-Dependent Nonhomologous End Joining Involving the Goddess Artemis. *Trends in Biochemical Sciences*, 42(9), 690–701. <https://doi.org/10.1016/j.tibs.2017.06.011>
140. Lomonosov, M., Anand, S., Sangrithi, M., Davies, R., & Venkitaraman, A. R. (2003). Stabilization of stalled DNA replication forks by the BRCA2 breast cancer susceptibility protein. *Genes & Development*, 17(24), 3017–3022. <https://doi.org/10.1101/gad.279003>
141. Lord, C. J., & Ashworth, A. (2013). Mechanisms of resistance to therapies targeting BRCA-mutant cancers. *Nature Medicine*, 19(11), 1381–1388. <https://doi.org/10.1038/nm.3369>
142. Ludwig, T., Chapman, D. L., Papaioannou, V. E., & Efstratiadis, A. (1997). Targeted mutations of breast cancer susceptibility gene homologs in mice: lethal phenotypes of Brca1, Brca2, Brca1/Brca2, Brca1/p53, and Brca2/p53 nullizygous embryos. *Genes & Development*, 11(10), 1226–1241. <https://doi.org/10.1101/gad.11.10.1226>

143. Ludwig, T., Fisher, P., Murty, V., & Efstratiadis, A. (2001). Development of mammary adenocarcinomas by tissue-specific knockout of Brca2 in mice. *Oncogene*, 20(30), 3937–3948. <https://doi.org/10.1038/sj.onc.1204512>
144. Ma, Y., Pannicke, U., Schwarz, K., & Lieber, M. R. (2002). Hairpin Opening and Overhang Processing by an Artemis/DNA-Dependent Protein Kinase Complex in Nonhomologous End Joining and V(D)J Recombination. *Cell*, 108(6), 781–794. [https://doi.org/10.1016/s0092-8674\(02\)00671-2](https://doi.org/10.1016/s0092-8674(02)00671-2)
145. Manni, A., Wright, C., & Buck, H. (1991). Growth factor involvement in the multihormonal regulation of MCF-7 breast cancer cell growth in soft agar. *Breast Cancer Research and Treatment*, 20(1), 43–52. <https://doi.org/10.1007/bf01833356>
146. Maréchal, A., Li, J.-M., Ji, X. Y., Wu, C.-S., Yazinski, S. A., Nguyen, H. D., Liu, S., Jiménez, A. E., Jin, J., & Zou, L. (2014). PRP19 Transforms into a Sensor of RPA-ssDNA after DNA Damage and Drives ATR Activation via a Ubiquitin-Mediated Circuitry. *Molecular Cell*, 53(2), 235–246. <https://doi.org/10.1016/j.molcel.2013.11.002>
147. Maréchal, A., & Zou, L. (2013). DNA Damage Sensing by the ATM and ATR Kinases. *Cold Spring Harbor Perspectives in Biology*, 5(9), a012716. <https://doi.org/10.1101/cshperspect.a012716>
148. Marteijn, J. A., Lans, H., Vermeulen, W., & Hoeijmakers, J. H. J. (2014). Understanding nucleotide excision repair and its roles in cancer and ageing. *Nature Reviews Molecular Cell Biology*, 15(7), 465–481. <https://doi.org/10.1038/nrm3822>
149. Martinez, J. S., Nicolai, C. von, Kim, T., Ehlén, Å., Mazin, A. V., Kowalczykowski, S. C., & Carreira, A. (2016). BRCA2 regulates DMC1-mediated recombination through the BRC repeats. *Proceedings of the National Academy of Sciences*, 113(13), 3515–3520. <https://doi.org/10.1073/pnas.1601691113>
150. Martins, F. C., De, S., Almendro, V., Gönen, M., Park, S. Y., Blum, J. L., Herlihy, W., Ethington, G., Schnitt, S. J., Tung, N., Garber, J. E., Fettes, K., Michor, F., & Polyak, K. (2012). Evolutionary Pathways in BRCA1-Associated Breast Tumors. *Cancer Discovery*, 2(6), 503–511. <https://doi.org/10.1158/2159-8290.cd-11-0325>
151. Masai, H., Matsumoto, S., You, Z., Yoshizawa-Sugata, N., & Oda, M. (2010). Eukaryotic Chromosome DNA Replication: Where, When, and How? *Annual Review of Biochemistry*, 79(1), 89–130. <https://doi.org/10.1146/annurev.biochem.052308.103205>
152. Matsumoto, Y., & Kim, K. (1995). Excision of Deoxyribose Phosphate Residues by DNA Polymerase β During DNA Repair. *Science*, 269(5224), 699–702. <https://doi.org/10.1126/science.7624801>
153. Matsuoka, S., Rotman, G., Ogawa, A., Shiloh, Y., Tamai, K., & Elledge, S. J. (2000). Ataxia telangiectasia-mutated phosphorylates Chk2 in vivo and in vitro. *Proceedings of the National Academy of Sciences*, 97(19), 10389–10394. <https://doi.org/10.1073/pnas.190030497>
154. Maxwell, K. N., Wubbenhorst, B., Wenz, B. M., Sloover, D. D., Pluta, J., Emery, L., Barrett, A., Kraya, A. A., Anastopoulos, I. N., Yu, S., Jiang, Y., Chen, H., Zhang, N. R., Hackman, N., D'Andrea, K., Daber, R., Morrissette, J. J. D., Mitra, N., Feldman, M., ... Nathanson, K. L. (2017). BRCA locus-specific loss of heterozygosity in germline BRCA1 and BRCA2 carriers. *Nature Communications*, 8(1), 319. <https://doi.org/10.1038/s41467-017-00388-9>

155. Maya-Mendoza, A., Moudry, P., Merchut-Maya, J. M., Lee, M., Strauss, R., & Bartek, J. (2018). High speed of fork progression induces DNA replication stress and genomic instability. *Nature*, 559(7713), 279–284. <https://doi.org/10.1038/s41586-018-0261-5>
156. Méchali, M. (2010). Eukaryotic DNA replication origins: many choices for appropriate answers. *Nature Reviews Molecular Cell Biology*, 11(10), 728–738. <https://doi.org/10.1038/nrm2976>
157. Melchor, L., & Benítez, J. (2013). The complex genetic landscape of familial breast cancer. *Human Genetics*, 132(8), 845–863. <https://doi.org/10.1007/s00439-013-1299-y>
158. Meroni, A., Wells, S. E., Fonseca, C., Chaudhuri, A. R., Caldecott, K. W., & Vindigni, A. (2023). DNA Combing versus DNA Spreading and the Separation of Sister Chromatids. *BioRxiv*, 2023.05.02.539129. <https://doi.org/10.1101/2023.05.02.539129>
159. Mijic, S., Zellweger, R., Chappidi, N., Berti, M., Jacobs, K., Mutreja, K., Ursich, S., Chaudhuri, A. R., Nussenzweig, A., Janscak, P., & Lopes, M. (2017). Replication fork reversal triggers fork degradation in BRCA2-defective cells. *Nature Communications*, 8(1), 859. <https://doi.org/10.1038/s41467-017-01164-5>
160. Mikaelssdottir, E. K., Valgeirsdottir, S., Eyfjord, J. E., & Rafnar, T. (2004). The Icelandic founder mutation BRCA2 999del5: analysis of expression. *Breast Cancer Research*, 6(4), R284. <https://doi.org/10.1186/bcr785>
161. Milner, J., Ponder, B., Hughes-Davies, L., Seltmann, M., & Kouzarides, T. (1997). Transcriptional activation functions in BRCA2. *Nature*, 386(6627), 772–773. <https://doi.org/10.1038/386772a0>
162. Mimori, T., & Hardin, J. A. (1986). Mechanism of interaction between Ku protein and DNA. *Journal of Biological Chemistry*, 261(22), 10375–10379. [https://doi.org/10.1016/s0021-9258\(18\)67534-9](https://doi.org/10.1016/s0021-9258(18)67534-9)
163. Min, J.-H., & Pavletich, N. P. (2007). Recognition of DNA damage by the Rad4 nucleotide excision repair protein. *Nature*, 449(7162), 570–575. <https://doi.org/10.1038/nature06155>
164. Mondal, G., Rowley, M., Guidugli, L., Wu, J., Pankratz, V. S., & Couch, F. J. (2012). BRCA2 Localization to the Midbody by Filamin A Regulates CEP55 Signaling and Completion of Cytokinesis. *Developmental Cell*, 23(1), 137–152. <https://doi.org/10.1016/j.devcel.2012.05.008>
165. Mourón, S., Rodríguez-Acebes, S., Martínez-Jiménez, M. I., García-Gómez, S., Chocrón, S., Blanco, L., & Méndez, J. (2013). Repriming of DNA synthesis at stalled replication forks by human PrimPol. *Nature Structural & Molecular Biology*, 20(12), 1383–1389. <https://doi.org/10.1038/nsmb.2719>
166. Moynahan, M. E., & Jasin, M. (1997). Loss of heterozygosity induced by a chromosomal double-strand break. *Proceedings of the National Academy of Sciences*, 94(17), 8988–8993. <https://doi.org/10.1073/pnas.94.17.8988>
167. Munoz, I. M., Jowsey, P. A., Toth, R., & Rouse, J. (2007). Phospho-epitope binding by the BRCT domains of hPTIP controls multiple aspects of the cellular response to DNA damage. *Nucleic Acids Research*, 35(16), 5312–5322. <https://doi.org/10.1093/nar/gkm493>
168. Nagaraju, G., & Scully, R. (2007). Minding the gap: The underground functions of BRCA1 and BRCA2 at stalled replication forks. *DNA Repair*, 6(7), 1018–1031. <https://doi.org/10.1016/j.dnarep.2007.02.020>

169. Nakamura, K., Saredi, G., Becker, J. R., Foster, B. M., Nguyen, N. V., Beyer, T. E., Cesa, L. C., Faull, P. A., Lukauskas, S., Frimurer, T., Chapman, J. R., Bartke, T., & Groth, A. (2019). H4K20me0 recognition by BRCA1–BARD1 directs homologous recombination to sister chromatids. *Nature Cell Biology*, 21(3), 311–318. <https://doi.org/10.1038/s41556-019-0282-9>
170. Narod, S. A., & Foulkes, W. D. (2004). BRCA1 and BRCA2: 1994 and beyond. *Nature Reviews Cancer*, 4(9), 665–676. <https://doi.org/10.1038/nrc1431>
171. Neelsen, K. J., & Lopes, M. (2015). Replication fork reversal in eukaryotes: from dead end to dynamic response. *Nature Reviews Molecular Cell Biology*, 16(4), 207–220. <https://doi.org/10.1038/nrm3935>
172. Neuhausen, S. L., & Marshall, C. J. (1994). Loss of heterozygosity in familial tumors from three BRCA1-linked kindreds. *Cancer Research*, 54(23), 6069–6072.
173. Nicolai, C. von, Ehlén, Å., Martin, C., Zhang, X., & Carreira, A. (2016). A second DNA binding site in human BRCA2 promotes homologous recombination. *Nature Communications*, 7(1), 12813. <https://doi.org/10.1038/ncomms12813>
174. Nik-Zainal, S., Alexandrov, L. B., Wedge, D. C., Loo, P. V., Greenman, C. D., Raine, K., Jones, D., Hinton, J., Marshall, J., Stebbings, L. A., Menzies, A., Martin, S., Leung, K., Chen, L., Leroy, C., Ramakrishna, M., Rance, R., Lau, K. W., Mudie, L. J., ... Consortium, the B. C. W. G. of the I. C. G. (2012). Mutational Processes Molding the Genomes of 21 Breast Cancers. *Cell*, 149(5), 979–993. <https://doi.org/10.1016/j.cell.2012.04.024>
175. Nik-Zainal, S., Davies, H., Staaf, J., Ramakrishna, M., Glodzik, D., Zou, X., Martincorena, I., Alexandrov, L. B., Martin, S., Wedge, D. C., Loo, P. V., Ju, Y. S., Smid, M., Brinkman, A. B., Morganello, S., Aure, M. R., Lingjærde, O. C., Langerød, A., Ringnér, M., ... Stratton, M. R. (2016). Landscape of somatic mutations in 560 breast cancer whole-genome sequences. *Nature*, 534(7605), 47–54. <https://doi.org/10.1038/nature17676>
176. Nimonkar, A. V., Genschel, J., Kinoshita, E., Polaczek, P., Campbell, J. L., Wyman, C., Modrich, P., & Kowalczykowski, S. C. (2011). BLM–DNA2–RPA–MRN and EXO1–BLM–RPA–MRN constitute two DNA end resection machineries for human DNA break repair. *Genes & Development*, 25(4), 350–362. <https://doi.org/10.1101/gad.2003811>
177. Noordermeer, S. M., Adam, S., Setiawati, D., Barazas, M., Pettitt, S. J., Ling, A. K., Olivieri, M., Álvarez-Quilón, A., Moatti, N., Zimmermann, M., Annunziato, S., Krastev, D. B., Song, F., Brandsma, I., Frankum, J., Brough, R., Sherker, A., Landry, S., Szilard, R. K., ... Durocher, D. (2018). The shieldin complex mediates 53BP1-dependent DNA repair. *Nature*, 560(7716), 117–121. <https://doi.org/10.1038/s41586-018-0340-7>
178. Oddoux, C., Struwing, J. P., Clayton, C. M., Neuhausen, S., Brody, L. C., Kaback, M., Haas, B., Norton, L., Borgen, P., Jhanwar, S., Goldgar, D., Ostrer, H., & Offit, K. (1996). The carrier frequency of the BRCA2 6174delT mutation among Ashkenazi Jewish individuals is approximately 1%. *Nature Genetics*, 14(2), 188–190. <https://doi.org/10.1038/ng1096-188>
179. Osorio, A., Hoya, M. de la, Rodríguez-López, R., Martínez-Ramírez, A., Cazorla, A., Granizo, J. J., Esteller, M., Rivas, C., Caldés, T., & Benítez, J. (2002). Loss of heterozygosity analysis at the BRCA loci in tumor samples from patients with familial breast cancer. *International Journal of Cancer*, 99(2), 305–309. <https://doi.org/10.1002/ijc.10337>

180. Palacios, J., Honrado, E., Osorio, A., Cazorla, A., Sarrió, D., Barroso, A., Rodríguez, S., Cigudosa, J. C., Diez, O., Alonso, C., Lerma, E., Dopazo, J., Rivas, C., & Benítez, J. (2005). Phenotypic characterization of BRCA1 and BRCA2 tumors based in a tissue microarray study with 37 immunohistochemical markers. *Breast Cancer Research and Treatment*, 90(1), 5–14. <https://doi.org/10.1007/s10549-004-1536-0>
181. Panzarino, N. J., Krais, J. J., Cong, K., Peng, M., Mosqueda, M., Nayak, S. U., Bond, S. M., Calvo, J. A., Doshi, M. B., Bere, M., Ou, J., Deng, B., Zhu, L. J., Johnson, N., & Cantor, S. B. (2021). Replication Gaps Underlie BRCA Deficiency and Therapy Response. *Cancer Research*, 81(5), 1388–1397. <https://doi.org/10.1158/0008-5472.can-20-1602>
182. Parsons, M. T., Tudini, E., Li, H., Hahnen, E., Wappenschmidt, B., Feliubadaló, L., Aalfs, C. M., Agata, S., Aittomäki, K., Alducci, E., Alonso-Cerezo, M. C., Arnold, N., Auber, B., Austin, R., Azzollini, J., Balmaña, J., Barbieri, E., Bartram, C. R., Blanco, A., ... Spurdle, A. B. (2019). Large scale multifactorial likelihood quantitative analysis of BRCA1 and BRCA2 variants: An ENIGMA resource to support clinical variant classification. *Human Mutation*, 40(9), 1557–1578. <https://doi.org/10.1002/humu.23818>
183. Patel, K. J., Yu, V. P. C. C., Lee, H., Corcoran, A., Thistlethwaite, F. C., Evans, M. J., Colledge, W. H., Friedman, L. S., Ponder, B. A. J., & Venkitaraman, A. R. (1998). Involvement of Brca2 in DNA Repair. *Molecular Cell*, 1(3), 347–357. [https://doi.org/10.1016/s1097-2765\(00\)80035-0](https://doi.org/10.1016/s1097-2765(00)80035-0)
184. Pellegrini, L., Yu, D. S., Lo, T., Anand, S., Lee, M., Blundell, T. L., & Venkitaraman, A. R. (2002). Insights into DNA recombination from the structure of a RAD51–BRCA2 complex. *Nature*, 420(6913), 287–293. <https://doi.org/10.1038/nature01230>
185. Pommier, Y., O'Connor, M. J., & Bono, J. de. (2016). Laying a trap to kill cancer cells: PARP inhibitors and their mechanisms of action. *Science Translational Medicine*, 8(362), 362ps17. <https://doi.org/10.1126/scitranslmed.aaf9246>
186. Pouliot, J. J., Yao, K. C., Robertson, C. A., & Nash, H. A. (1999). Yeast Gene for a Tyr-DNA Phosphodiesterase that Repairs Topoisomerase I Complexes. *Science*, 286(5439), 552–555. <https://doi.org/10.1126/science.286.5439.552>
187. Promonet, A., Padioleau, I., Liu, Y., Sanz, L., Biernacka, A., Schmitz, A.-L., Skrzypczak, M., Sarrazin, A., Mettling, C., Rowicka, M., Ginalski, K., Chedin, F., Chen, C.-L., Lin, Y.-L., & Pasero, P. (2020). Topoisomerase 1 prevents replication stress at R-loop-enriched transcription termination sites. *Nature Communications*, 11(1), 3940. <https://doi.org/10.1038/s41467-020-17858-2>
188. Qiu, S., Jiang, G., Cao, L., & Huang, J. (2021). Replication Fork Reversal and Protection. *Frontiers in Cell and Developmental Biology*, 9, 670392. <https://doi.org/10.3389/fcell.2021.670392>
189. Quinet, A., Tirman, S., Cybulla, E., Meroni, A., & Vindigni, A. (2021). To skip or not to skip: choosing repriming to tolerate DNA damage. *Molecular Cell*, 81(4), 649–658. <https://doi.org/10.1016/j.molcel.2021.01.012>
190. Rahman, N., (UK), T. B. C. S. C., Seal, S., Thompson, D., Kelly, P., Renwick, A., Elliott, A., Reid, S., Spanova, K., Barfoot, R., Chagtai, T., Jayatilake, H., McGuffog, L., Hanks, S., Evans, D. G., Eccles, D., Easton, D. F., & Stratton, M. R. (2007). PALB2, which encodes a BRCA2-interacting protein, is a breast cancer susceptibility gene. *Nature Genetics*, 39(2), 165–167. <https://doi.org/10.1038/ng1959>

191. Rebbeck, T. R., Mitra, N., Wan, F., Sinilnikova, O. M., Healey, S., McGuffog, L., Mazoyer, S., Chenevix-Trench, G., Easton, D. F., Antoniou, A. C., Nathanson, K. L., Consortium, C., Laitman, Y., Kushnir, A., Paluch-Shimon, S., Berger, R., Zidan, J., Friedman, E., Ehrencrona, H., ... Andrulis, I. (2015). Association of Type and Location of BRCA1 and BRCA2 Mutations With Risk of Breast and Ovarian Cancer. *JAMA*, *313*(13), 1347–1361. <https://doi.org/10.1001/jama.2014.5985>
192. Remus, D., & Diffley, J. F. (2009). Eukaryotic DNA replication control: Lock and load, then fire. *Current Opinion in Cell Biology*, *21*(6), 771–777. <https://doi.org/10.1016/j.ceb.2009.08.002>
193. Rennstam, K., Ringberg, A., Cunliffe, H. E., Olsson, H., Landberg, G., & Hedenfalk, I. (2010). Genomic alterations in histopathologically normal breast tissue from BRCA1 mutation carriers may be caused by BRCA1 haploinsufficiency. *Genes, Chromosomes and Cancer*, *49*(1), 78–90. <https://doi.org/10.1002/gcc.20723>
194. Reuter, M., Zelensky, A., Smal, I., Meijering, E., Cappellen, W. A. van, Gruiter, H. M. de, Belle, G. J. van, Royen, M. E. van, Houtsmuller, A. B., Essers, J., Kanaar, R., & Wyman, C. (2015). BRCA2 diffuses as oligomeric clusters with RAD51 and changes mobility after DNA damage in live cells. *Journal of Cell Biology*, *208*(6), 857–857. <https://doi.org/10.1083/jcb.20140501402182015c>
195. Rhei, E., Bogomolny, F., Federici, M. G., Maresco, D. L., Offit, K., Robson, M. E., Saigo, P. E., & Boyd, J. (1998). Molecular genetic characterization of BRCA1- and BRCA2-linked hereditary ovarian cancers. *Cancer Research*, *58*(15), 3193–3196.
196. Robertson, A. B., Klungland, A., Rognes, T., & Leiros, I. (2009). DNA Repair in Mammalian Cells. *Cellular and Molecular Life Sciences*, *66*(6), 981–993. <https://doi.org/10.1007/s00018-009-8736-z>
197. Roy, R., Chun, J., & Powell, S. N. (2012). BRCA1 and BRCA2: different roles in a common pathway of genome protection. *Nature Reviews Cancer*, *12*(1), 68–78. <https://doi.org/10.1038/nrc3181>
198. Sato, K., Martin-Pintado, N., Post, H., Altelaar, M., & Knipscheer, P. (2021). Multistep mechanism of G-quadruplex resolution during DNA replication. *Science Advances*, *7*(39), eabf8653. <https://doi.org/10.1126/sciadv.abf8653>
199. Schlacher, K., Christ, N., Siaud, N., Egashira, A., Wu, H., & Jasin, M. (2011). Double-Strand Break Repair-Independent Role for BRCA2 in Blocking Stalled Replication Fork Degradation by MRE11. *Cell*, *145*(4), 529–542. <https://doi.org/10.1016/j.cell.2011.03.041>
200. Schlacher, K., Wu, H., & Jasin, M. (2012). A Distinct Replication Fork Protection Pathway Connects Fanconi Anemia Tumor Suppressors to RAD51-BRCA1/2. *Cancer Cell*, *22*(1), 106–116. <https://doi.org/10.1016/j.ccr.2012.05.015>
201. Schlötterer, C., & Tautz, D. (1992). Slippage synthesis of simple sequence DNA. *Nucleic Acids Research*, *20*(2), 211–215. <https://doi.org/10.1093/nar/20.2.211>
202. Scully, R., & Livingston, D. M. (2000). In search of the tumour-suppressor functions of BRCA1 and BRCA2. *Nature*, *408*(6811), 429–432. <https://doi.org/10.1038/35044000>
203. Sedic, M., & Kuperwasser, C. (2016). BRCA1-haploinsufficiency: Unraveling the molecular and cellular basis for tissue-specific cancer. *Cell Cycle*, *15*(5), 621–627. <https://doi.org/10.1080/15384101.2016.1141841>

204. Sessa, G., Gómez-González, B., Silva, S., Pérez-Calero, C., Beaupere, R., Barroso, S., Martineau, S., Martin, C., Ehlén, Å., Martínez, J. S., Lombard, B., Loew, D., Vagner, S., Aguilera, A., & Carreira, A. (2021). BRCA2 promotes DNA-RNA hybrid resolution by DDX5 helicase at DNA breaks to facilitate their repair[‡]. *The EMBO Journal*, *40*(7), e106018. <https://doi.org/10.15252/embj.2020106018>
205. Shahid, T., Soroka, J., Kong, E. H., Malivert, L., McIlwraith, M. J., Pape, T., West, S. C., & Zhang, X. (2014). Structure and mechanism of action of the BRCA2 breast cancer tumor suppressor. *Nature Structural & Molecular Biology*, *21*(11), 962–968. <https://doi.org/10.1038/nsmb.2899>
206. Sharan, S. K., Morimatsu, M., Albrecht, U., Lim, D.-S., Regel, E., Dinh, C., Sands, A., Eichele, G., Hasty, P., & Bradley, A. (1997). Embryonic lethality and radiation hypersensitivity mediated by Rad51 in mice lacking Brca2. *Nature*, *386*(6627), 804–810. <https://doi.org/10.1038/386804a0>
207. Shieh, S.-Y., Ikeda, M., Taya, Y., & Prives, C. (1997). DNA Damage-Induced Phosphorylation of p53 Alleviates Inhibition by MDM2. *Cell*, *91*(3), 325–334. [https://doi.org/10.1016/s0092-8674\(00\)80416-x](https://doi.org/10.1016/s0092-8674(00)80416-x)
208. Shiloh, Y., & Ziv, Y. (2013). The ATM protein kinase: regulating the cellular response to genotoxic stress, and more. *Nature Reviews Molecular Cell Biology*, *14*(4), 197–210. <https://doi.org/10.1038/nrm3546>
209. Shimelis, H., Mesman, R. L. S., Nicolai, C. V., Ehlen, A., Guidugli, L., Martin, C., Calléja, F. M. G. R., Meeks, H., Hallberg, E., Hinton, J., Lilyquist, J., Hu, C., Aalfs, C. M., Aittomäki, K., Andrulis, I., Anton-Culver, H., Arndt, V., Beckmann, M. W., Benitez, J., ... Collaborators, for N. (2017). BRCA2 Hypomorphic Missense Variants Confer Moderate Risks of Breast Cancer. *Cancer Research*, *77*(11), 2789–2799. <https://doi.org/10.1158/0008-5472.can-16-2568>
210. Shivji, M. K. K., Mukund, S. R., Rajendra, E., Chen, S., Short, J. M., Savill, J., Klenerman, D., & Venkitaraman, A. R. (2009). The BRC repeats of human BRCA2 differentially regulate RAD51 binding on single- versus double-stranded DNA to stimulate strand exchange. *Proceedings of the National Academy of Sciences*, *106*(32), 13254–13259. <https://doi.org/10.1073/pnas.0906208106>
211. Shivji, M. K. K., Renaudin, X., Williams, Ç. H., & Venkitaraman, A. R. (2018). BRCA2 Regulates Transcription Elongation by RNA Polymerase II to Prevent R-Loop Accumulation. *Cell Reports*, *22*(4), 1031–1039. <https://doi.org/10.1016/j.celrep.2017.12.086>
212. Singh, J. K., Smith, R., Rother, M. B., Groot, A. J. L. de, Wiegant, W. W., Vreeken, K., D’Augustin, O., Kim, R. Q., Qian, H., Krawczyk, P. M., González-Prieto, R., Vertegaal, A. C. O., Lamers, M., Huet, S., & Attikum, H. van. (2021). Zinc finger protein ZNF384 is an adaptor of Ku to DNA during classical non-homologous end-joining. *Nature Communications*, *12*(1), 6560. <https://doi.org/10.1038/s41467-021-26691-0>
213. Skoulidis, F., Cassidy, L. D., Pisupati, V., Jonasson, J. G., Bjarnason, H., Eyfjord, J. E., Karreth, F. A., Lim, M., Barber, L. M., Clatworthy, S. A., Davies, S. E., Olive, K. P., Tuveson, D. A., & Venkitaraman, A. R. (2010). Germline Brca2 heterozygosity promotes Kras(G12D) -driven carcinogenesis in a murine model of familial pancreatic cancer. *Cancer Cell*, *18*(5), 499–509. <https://doi.org/10.1016/j.ccr.2010.10.015>
214. Skourti-Stathaki, K., Proudfoot, N. J., & Gromak, N. (2011). Human Senataxin Resolves RNA/DNA Hybrids Formed at Transcriptional Pause Sites to Promote Xrn2-Dependent Termination. *Molecular Cell*, *42*(6), 794–805. <https://doi.org/10.1016/j.molcel.2011.04.026>

215. Smith, S. A., Easton, D. F., Evans, D. G. R., & Ponder, B. A. J. (1992). Allele losses in the region 17q12–21 in familial breast and ovarian cancer involve the wild-type chromosome. *Nature Genetics*, 2(2), 128–131. <https://doi.org/10.1038/ng1092-128>
216. So, A., Dardillac, E., Muhammad, A., Chailleux, C., Sesma-Sanz, L., Ragu, S., Le Cam, E., Canitrot, Y., Masson, J. Y., Dupaigne, P., Lopez, B. S., & Guirouilh-Barbat, J. (2022). RAD51 protects against nonconservative DNA double-strand break repair through a nonenzymatic function. *Nucleic Acids Research*, 50(5), gkac073-. <https://doi.org/10.1093/nar/gkac073>
217. Sollier, J., Stork, C. T., García-Rubio, M. L., Paulsen, R. D., Aguilera, A., & Cimprich, K. A. (2014). Transcription-Coupled Nucleotide Excision Repair Factors Promote R-Loop-Induced Genome Instability. *Molecular Cell*, 56(6), 777–785. <https://doi.org/10.1016/j.molcel.2014.10.020>
218. Soule, H. D., Maloney, T. M., Wolman, S. R., Peterson, W. D., Brenz, R., McGrath, C. M., Russo, J., Pauley, R. J., Jones, R. F., & Brooks, S. C. (1990). Isolation and characterization of a spontaneously immortalized human breast epithelial cell line, MCF-10. *Cancer Research*, 50(18), 6075–6086.
219. Spain, B. H., Larson, C. J., Shihabuddin, L. S., Gage, F. H., & Verma, I. M. (1999). Truncated BRCA2 is cytoplasmic: Implications for cancer-linked mutations. *Proceedings of the National Academy of Sciences*, 96(24), 13920–13925. <https://doi.org/10.1073/pnas.96.24.13920>
220. Spies, J., Polasek-Sedlackova, H., Lukas, J., & Somyajit, K. (2021). Homologous Recombination as a Fundamental Genome Surveillance Mechanism during DNA Replication. *Genes*, 12(12), 1960. <https://doi.org/10.3390/genes12121960>
221. Spies, J., Waizenegger, A., Barton, O., Sürder, M., Wright, W. D., Heyer, W.-D., & Löbrich, M. (2016). Nek1 Regulates Rad54 to Orchestrate Homologous Recombination and Replication Fork Stability. *Molecular Cell*, 62(6), 903–917. <https://doi.org/10.1016/j.molcel.2016.04.032>
222. Spivak, G. (2015). Nucleotide excision repair in humans. *DNA Repair*, 36, 13–18. <https://doi.org/10.1016/j.dnarep.2015.09.003>
223. Spurdle, A. B., Healey, S., Devereau, A., Hogervorst, F. B. L., Monteiro, A. N. A., Nathanson, K. L., Radice, P., Stoppa-Lyonnet, D., Tavtigian, S., Wappenschmidt, B., Couch, F. J., Goldgar, D. E., & ENIGMA, on behalf of. (2012). ENIGMA—Evidence-based network for the interpretation of germline mutant alleles: An international initiative to evaluate risk and clinical significance associated with sequence variation in BRCA1 and BRCA2 genes. *Human Mutation*, 33(1), 2–7. <https://doi.org/10.1002/humu.21628>
224. Stine, Z. E., Walton, Z. E., Altman, B. J., Hsieh, A. L., & Dang, C. V. (2015). MYC, Metabolism, and Cancer. *Cancer Discovery*, 5(10), 1024–1039. <https://doi.org/10.1158/2159-8290.cd-15-0507>
225. Stingele, J., Bellelli, R., & Boulton, S. J. (2017). Mechanisms of DNA–protein crosslink repair. *Nature Reviews Molecular Cell Biology*, 18(9), 563–573. <https://doi.org/10.1038/nrm.2017.56>
226. Stok, C., Kok, Y. P., van den Tempel, N., & van Vugt, M. A. T. M. (2021). Shaping the BRCAness mutational landscape by alternative double-strand break repair, replication stress and mitotic aberrancies. *Nucleic Acids Research*, 49(8), gkab151. <https://doi.org/10.1093/nar/gkab151>
227. Sun, Y., Jenkins, L. M. M., Su, Y. P., Nitiss, K. C., Nitiss, J. L., & Pommier, Y. (2020). A conserved SUMO pathway repairs topoisomerase DNA–protein cross-links by engaging ubiquitin-mediated

- proteasomal degradation. *Science Advances*, 6(46), eaba6290. <https://doi.org/10.1126/sciadv.aba6290>
228. Sung, H., Ferlay, J., Siegel, R. L., Laversanne, M., Soerjomataram, I., Jemal, A., & Bray, F. (2021). Global Cancer Statistics 2020: GLOBOCAN Estimates of Incidence and Mortality Worldwide for 36 Cancers in 185 Countries. *CA: A Cancer Journal for Clinicians*, 71(3), 209–249. <https://doi.org/10.3322/caac.21660>
229. Sy, S. M. H., Huen, M. S. Y., & Chen, J. (2009). PALB2 is an integral component of the BRCA complex required for homologous recombination repair. *Proceedings of the National Academy of Sciences*, 106(17), 7155–7160. <https://doi.org/10.1073/pnas.0811159106>
230. Sy, S. M.-H., Huen, M. S. Y., Zhu, Y., & Chen, J. (2009). PALB2 Regulates Recombinational Repair through Chromatin Association and Oligomerization*. *Journal of Biological Chemistry*, 284(27), 18302–18310. <https://doi.org/10.1074/jbc.m109.016717>
231. Tagliatela, A., Alvarez, S., Leuzzi, G., Sannino, V., Ranjha, L., Huang, J.-W., Madubata, C., Anand, R., Levy, B., Rabadan, R., Cejka, P., Costanzo, V., & Ciccio, A. (2017). Restoration of Replication Fork Stability in BRCA1- and BRCA2-Deficient Cells by Inactivation of SNF2-Family Fork Remodelers. *Molecular Cell*, 68(2), 414–430.e8. <https://doi.org/10.1016/j.molcel.2017.09.036>
232. Takaoka, M., Saito, H., Takenaka, K., Miki, Y., & Nakanishi, A. (2014). BRCA2 Phosphorylated by PLK1 Moves to the Midbody to Regulate Cytokinesis Mediated by Nonmuscle Myosin IIC. *Cancer Research*, 74(5), 1518–1528. <https://doi.org/10.1158/0008-5472.can-13-0504>
233. Tan, S. L. W., Chadha, S., Liu, Y., Gabasova, E., Perera, D., Ahmed, K., Constantinou, S., Renaudin, X., Lee, M., Aebbersold, R., & Venkitaraman, A. R. (2017). A Class of Environmental and Endogenous Toxins Induces BRCA2 Haploinsufficiency and Genome Instability. *Cell*, 169(6), 1105–1118.e15. <https://doi.org/10.1016/j.cell.2017.05.010>
234. Tannenbaum, B., Mofunanya, T., & Schoenfeld, A. R. (2007). DNA damage repair is unaffected by mimicked heterozygous levels of BRCA2 in HT-29 cells. *International Journal of Biological Sciences*, 3(7), 402–407. <https://doi.org/10.7150/ijbs.3.402>
235. Thiagalingam, S., Foy, R. L., Cheng, K., Lee, H. J., Thiagalingam, A., & Ponte, J. F. (2002). Loss of heterozygosity as a predictor to map tumor suppressor genes in cancer: molecular basis of its occurrence. *Current Opinion in Oncology*, 14(1), 65–72. <https://doi.org/10.1097/00001622-200201000-00012>
236. Thirthagiri, E., Klarmann, K. D., Shukla, A. K., Southon, E., Biswas, K., Martin, B. K., North, S. L., Magidson, V., Burkett, S., Haines, D. C., Noer, K., Matthai, R., Tessarollo, L., Loncarek, J., Keller, J. R., & Sharan, S. K. (2016). BRCA2 minor transcript lacking exons 4–7 supports viability in mice and may account for survival of humans with a pathogenic biallelic mutation. *Human Molecular Genetics*, 25(10), 1934–1945. <https://doi.org/10.1093/hmg/ddw066>
237. Tirman, S., Quinet, A., Wood, M., Meroni, A., Cybulla, E., Jackson, J., Pegoraro, S., Simoneau, A., Zou, L., & Vindigni, A. (2021). Temporally distinct post-replicative repair mechanisms fill PRIMPOL-dependent ssDNA gaps in human cells. *Molecular Cell*, 81(19), 4026–4040.e8. <https://doi.org/10.1016/j.molcel.2021.09.013>
238. Truong, L. N., Li, Y., Shi, L. Z., Hwang, P. Y.-H., He, J., Wang, H., Razavian, N., Berns, M. W., & Wu, X. (2013). Microhomology-mediated End Joining and Homologous Recombination share the

- initial end resection step to repair DNA double-strand breaks in mammalian cells. *Proceedings of the National Academy of Sciences*, 110(19), 7720–7725. <https://doi.org/10.1073/pnas.1213431110>
239. Tubbs, A., & Nussenzweig, A. (2017). Endogenous DNA Damage as a Source of Genomic Instability in Cancer. *Cell*, 168(4), 644–656. <https://doi.org/10.1016/j.cell.2017.01.002>
240. Tutt, A., Gabriel, A., Bertwistle, D., Connor, F., Paterson, H., Peacock, J., Ross, G., & Ashworth, A. (1999). Absence of Brca2 causes genome instability by chromosome breakage and loss associated with centrosome amplification. *Current Biology*, 9(19), 1107–S1. [https://doi.org/10.1016/s0960-9822\(99\)80479-5](https://doi.org/10.1016/s0960-9822(99)80479-5)
241. Tye, S., Ronson, G. E., & Morris, J. R. (2021). A fork in the road: Where homologous recombination and stalled replication fork protection part ways. *Seminars in Cell & Developmental Biology*, 113, 14–26. <https://doi.org/10.1016/j.semcdb.2020.07.004>
242. Vaidyanathan, A., Sawers, L., Gannon, A.-L., Chakravarty, P., Scott, A. L., Bray, S. E., Ferguson, M. J., & Smith, G. (2016). ABCB1 (MDR1) induction defines a common resistance mechanism in paclitaxel- and olaparib-resistant ovarian cancer cells. *British Journal of Cancer*, 115(4), 431–441. <https://doi.org/10.1038/bjc.2016.203>
243. Venkitaraman, A. R. (2019). How do mutations affecting the breast cancer genes BRCA1 and BRCA2 cause cancer susceptibility? *DNA Repair*, 81, 102668. <https://doi.org/10.1016/j.dnarep.2019.102668>
244. Vermeulen, K., Bockstaele, D. R. V., & Berneman, Z. N. (2003). The cell cycle: a review of regulation, deregulation and therapeutic targets in cancer. *Cell Proliferation*, 36(3), 131–149. <https://doi.org/10.1046/j.1365-2184.2003.00266.x>
245. Vugic, D., Dumoulin, I., Martin, C., Minello, A., Alvaro-Aranda, L., Gomez-Escudero, J., Chaaban, R., Lebdy, R., Nicolai, C. von, Boucherit, V., Ribeyre, C., Constantinou, A., & Carreira, A. (2023). Replication gap suppression depends on the double-strand DNA binding activity of BRCA2. *Nature Communications*, 14(1), 446. <https://doi.org/10.1038/s41467-023-36149-0>
246. Vugic, D., Ehlén, Å., & Carreira, A. (2020). Homologous Recombination, Methods and Protocols. *Methods in Molecular Biology*, 2153, 115–126. https://doi.org/10.1007/978-1-0716-0644-5_9
247. Walker, J. R., Corpina, R. A., & Goldberg, J. (2001). Structure of the Ku heterodimer bound to DNA and its implications for double-strand break repair. *Nature*, 412(6847), 607–614. <https://doi.org/10.1038/35088000>
248. Wallace, S. S. (2014). Base excision repair: A critical player in many games. *DNA Repair*, 19, 14–26. <https://doi.org/10.1016/j.dnarep.2014.03.030>
249. Wang, A. T., Kim, T., Wagner, J. E., Conti, B. A., Lach, F. P., Huang, A. L., Molina, H., Sanborn, E. M., Zierhut, H., Cornes, B. K., Abhyankar, A., Sougnez, C., Gabriel, S. B., Auerbach, A. D., Kowalczykowski, S. C., & Smogorzewska, A. (2015). A Dominant Mutation in Human RAD51 Reveals Its Function in DNA Interstrand Crosslink Repair Independent of Homologous Recombination. *Molecular Cell*, 59(3), 478–490. <https://doi.org/10.1016/j.molcel.2015.07.009>
250. Wang, D., Ma, J., Botuyan, M. V., Cui, G., Yan, Y., Ding, D., Zhou, Y., Krueger, E. W., Pei, J., Wu, X., Wang, L., Pei, H., McNiven, M. A., Ye, D., Mer, G., & Huang, H. (2021). ATM-phosphorylated SPOP

- contributes to 53BP1 exclusion from chromatin during DNA replication. *Science Advances*, 7(25), eabd9208. <https://doi.org/10.1126/sciadv.abd9208>
251. Wang, J. C. (2002). Cellular roles of DNA topoisomerases: a molecular perspective. *Nature Reviews Molecular Cell Biology*, 3(6), 430–440. <https://doi.org/10.1038/nrm831>
252. Wang, M., Wu, W., Wu, W., Rosidi, B., Zhang, L., Wang, H., & Iliakis, G. (2006). PARP-1 and Ku compete for repair of DNA double strand breaks by distinct NHEJ pathways. *Nucleic Acids Research*, 34(21), 6170–6182. <https://doi.org/10.1093/nar/gkl840>
253. Warren, M., Lord, C. J., Masabanda, J., Griffin, D., & Ashworth, A. (2003). Phenotypic effects of heterozygosity for a BRCA2 mutation. *Human Molecular Genetics*, 12(20), 2645–2656. <https://doi.org/10.1093/hmg/ddg277>
254. Watanabe, G., & Lieber, M. R. (2022). Dynamics of the Artemis and DNA-PKcs Complex in the Repair of Double-Strand Breaks. *Journal of Molecular Biology*, 434(23), 167858. <https://doi.org/10.1016/j.jmb.2022.167858>
255. Woodbine, L., Gennery, A. R., & Jeggo, P. A. (2014). The clinical impact of deficiency in DNA non-homologous end-joining. *DNA Repair*, 16, 84–96. <https://doi.org/10.1016/j.dnarep.2014.02.011>
256. Wooster, R., Bignell, G., Lancaster, J., Swift, S., Seal, S., Mangion, J., Collins, N., Gregory, S., Gumbs, C., Micklem, G., Barfoot, R., Hamoudi, R., Patel, S., Rices, C., Biggs, P., Hashim, Y., Smith, A., Connor, F., Arason, A., ... Stratton, M. R. (1995). Identification of the breast cancer susceptibility gene BRCA2. *Nature*, 378(6559), 789–792. <https://doi.org/10.1038/378789a0>
257. Wright, W. D., Shah, S. S., & Heyer, W.-D. (2018). Homologous recombination and the repair of DNA double-strand breaks. *Journal of Biological Chemistry*, 293(27), 10524–10535. <https://doi.org/10.1074/jbc.tm118.000372>
258. Wu, K., Hinson, S. R., Ohashi, A., Farrugia, D., Wendt, P., Tavtigian, S. V., Deffenbaugh, A., Goldgar, D., & Couch, F. J. (2005). Functional evaluation and cancer risk assessment of BRCA2 unclassified variants. *Cancer Research*, 65(2), 417–426.
259. Xia, B., Dorsman, J. C., Ameziane, N., Vries, Y. de, Rooimans, M. A., Sheng, Q., Pals, G., Errami, A., Gluckman, E., Llera, J., Wang, W., Livingston, D. M., Joenje, H., & Winter, J. P. de. (2007). Fanconi anemia is associated with a defect in the BRCA2 partner PALB2. *Nature Genetics*, 39(2), 159–161. <https://doi.org/10.1038/ng1942>
260. Xia, B., Sheng, Q., Nakanishi, K., Ohashi, A., Wu, J., Christ, N., Liu, X., Jasin, M., Couch, F. J., & Livingston, D. M. (2006). Control of BRCA2 Cellular and Clinical Functions by a Nuclear Partner, PALB2. *Molecular Cell*, 22(6), 719–729. <https://doi.org/10.1016/j.molcel.2006.05.022>
261. Xia, F., Taghian, D. G., DeFrank, J. S., Zeng, Z.-C., Willers, H., Iliakis, G., & Powell, S. N. (2001). Deficiency of human BRCA2 leads to impaired homologous recombination but maintains normal nonhomologous end joining. *Proceedings of the National Academy of Sciences*, 98(15), 8644–8649. <https://doi.org/10.1073/pnas.151253498>
262. Xu, G., Chapman, J. R., Brandsma, I., Yuan, J., Mistrik, M., Bouwman, P., Bartkova, J., Gogola, E., Warmerdam, D., Barazas, M., Jaspers, J. E., Watanabe, K., Pieterse, M., Kersbergen, A., Sol, W., Celie, P. H. N., Schouten, P. C., Broek, B. van den, Salman, A., ... Rottenberg, S. (2015). REV7 counteracts

- DNA double-strand break resection and affects PARP inhibition. *Nature*, 521(7553), 541–544. <https://doi.org/10.1038/nature14328>
263. Xu, Y., Kim, E. Y., & Demple, B. (1998). Excision of C-4'-oxidized Deoxyribose Lesions from Double-stranded DNA by Human Apurinic/Apyrimidinic Endonuclease (Ape1 Protein) and DNA Polymerase β^* . *Journal of Biological Chemistry*, 273(44), 28837–28844. <https://doi.org/10.1074/jbc.273.44.28837>
264. Yang, G., Liu, C., Chen, S.-H., Kassab, M. A., Hoff, J. D., Walter, N. G., & Yu, X. (2018). Super-resolution imaging identifies PARP1 and the Ku complex acting as DNA double-strand break sensors. *Nucleic Acids Research*, 46(7), gky088-. <https://doi.org/10.1093/nar/gky088>
265. Yang, H., Jeffrey, P. D., Miller, J., Kinnucan, E., Sun, Y., Thomä, N. H., Zheng, N., Chen, P.-L., Lee, W.-H., & Pavletich, N. P. (2002). BRCA2 Function in DNA Binding and Recombination from a BRCA2-DSS1-ssDNA Structure. *Science*, 297(5588), 1837–1848. <https://doi.org/10.1126/science.297.5588.1837>
266. Yang, H., Li, Q., Fan, J., Holloman, W. K., & Pavletich, N. P. (2005). The BRCA2 homologue Brh2 nucleates RAD51 filament formation at a dsDNA–ssDNA junction. *Nature*, 433(7026), 653–657. <https://doi.org/10.1038/nature03234>
267. You, Z., Chahwan, C., Bailis, J., Hunter, T., & Russell, P. (2005). ATM Activation and Its Recruitment to Damaged DNA Require Binding to the C Terminus of Nbs1. *Molecular and Cellular Biology*, 25(13), 5363–5379. <https://doi.org/10.1128/mcb.25.13.5363-5379.2005>
268. Yousefzadeh, M. J., Wyatt, D. W., Takata, K., Mu, Y., Hensley, S. C., Tomida, J., Bylund, G. O., Doublé, S., Johansson, E., Ramsden, D. A., McBride, K. M., & Wood, R. D. (2014). Mechanism of Suppression of Chromosomal Instability by DNA Polymerase POLQ. *PLoS Genetics*, 10(10), e1004654. <https://doi.org/10.1371/journal.pgen.1004654>
269. Yuzhakov, A., Turner, J., & O'Donnell, M. (1996). Replisome Assembly Reveals the Basis for Asymmetric Function in Leading and Lagging Strand Replication. *Cell*, 86(6), 877–886. [https://doi.org/10.1016/s0092-8674\(00\)80163-4](https://doi.org/10.1016/s0092-8674(00)80163-4)
270. Zellweger, R., Dalcher, D., Mutreja, K., Berti, M., Schmid, J. A., Herrador, R., Vindigni, A., & Lopes, M. (2015). Rad51-mediated replication fork reversal is a global response to genotoxic treatments in human cells. *Journal of Cell Biology*, 208(5), 563–579. <https://doi.org/10.1083/jcb.201406099>
271. Zeman, M. K., & Cimprich, K. A. (2014). Causes and consequences of replication stress. *Nature Cell Biology*, 16(1), 2–9. <https://doi.org/10.1038/ncb2897>
272. Zhang, F., Fan, Q., Ren, K., & Andreassen, P. R. (2009). PALB2 Functionally Connects the Breast Cancer Susceptibility Proteins BRCA1 and BRCA2. *Molecular Cancer Research*, 7(7), 1110–1118. <https://doi.org/10.1158/1541-7786.mcr-09-0123>
273. Zhang, J., & Walter, J. C. (2014). Mechanism and regulation of incisions during DNA interstrand cross-link repair. *DNA Repair*, 19, 135–142. <https://doi.org/10.1016/j.dnarep.2014.03.018>
274. Zhao, W., Vaithiyalingam, S., San Filippo, J., Maranon, D. G., Jimenez-Sainz, J., Fontenay, G. V., Kwon, Y., Leung, S. G., Lu, L., Jensen, R. B., Chazin, W. J., Wiese, C., & Sung, P. (2015). Promotion of BRCA2-Dependent Homologous Recombination by DSS1 via RPA Targeting and DNA Mimicry. *Molecular Cell*, 59(2), 176–187. <https://doi.org/10.1016/j.molcel.2015.05.032>

275. Zimmermann, M., Lottersberger, F., Buonomo, S. B., Sfeir, A., & Lange, T. de. (2013). 53BP1 Regulates DSB Repair Using Rif1 to Control 5' End Resection. *Science*, 339(6120), 700–704. <https://doi.org/10.1126/science.1231573>
276. Zou, L., & Elledge, S. J. (2003). Sensing DNA Damage Through ATRIP Recognition of RPA-ssDNA Complexes. *Science*, 300(5625), 1542–1548. <https://doi.org/10.1126/science.1083430>

Material and Methods

Cell culture

MCF10A cells, obtained from Marie Dutreix Lab and tested negative for mycoplasma contamination, were grown in DMEM-HG/F-12 (Biowest) supplemented with 5% horse serum (Thermo Fisher Scientific), 20 ng ml⁻¹ human epidermal growth factor (Sigma-Aldrich), 0.5 mg ml⁻¹ hydrocortisone (Sigma-Aldrich), 100 ng ml⁻¹ cholera toxin (Sigma-Aldrich), 10 µg ml⁻¹ insulin (Sigma-Aldrich), and 1% penicillin–streptomycin (Thermo Fisher). MCF7 (kindly provided by Patricia Uguen) and MDA-MB-231 cells (kind gift from Prof. Krogan, QBI, UCSF) were cultured using DMEM-HG/F-12 high glucose (Biowest) supplemented with 10% FBS (EuroBio Abcys) and 1% of L-Glutamine (EuroBio Abcys).

Generation of BRCA2-mutated clones

+/~~5~~, +/~~revdel5~~, were obtained using CRISPR-Cas9-nickase editing. 2 µg for each of the following plasmids were used: Cas9-GFP (Addgene #44719), a guideRNA sequence cloned in the pBS U6 sgRNA plasmid (Addgene #43860, kind gift from C. Giovannangeli (M. Histoire Naturelle, FR)) expressing a mCherry reporter gene. We also transfected a single strand oligonucleotide (either forward or reverse) containing the mutation flanked by homology arms to the endogenous BRCA2 region where the mutated base is located and two LNA modifications in the middle of the sequence and purified by PAGE (Sigma-Aldrich).

+/~~revdelT~~ was obtained using CRISPR by transfecting 2 µg of the following plasmids: Cas9-GFP (Addgene #44719) and pU6-pegRNA-GG-acceptor (Addgene#132777), containing the target sequence and the homology sequence.

+/~~delT~~ was obtained using 5 µg of each TALEN encoding plasmids (TALEN-5' #V35620 and TALEN-3' #V35820, Life Technologies) and 1 µg of double-strand oligonucleotide comprising the delT mutation flanked with homology arms obtained by PCR from CAPAN-1 genomic DNA. The target sequences for gRNA or TALEN are listed in table 5, the oligonucleotides used in Table 6 and plasmids in Table 7.

Cells were transfected using AMAXA technology (Lonza) nucleofactor kit T (Cat. #VCA-1002) according to manufacturer instructions. The day after transfection the media was changed and 48 h post-transfection the cells were trypsinized. Individual GFP-mCherry double-positive cells were sorted using a BD FACSAria III (BD Bioscience) into 96 well-plates containing complete culture medium. Single cell derived colonies were gradually expanded and confirmed by Sanger sequencing of the region comprising the mutation.

RNA extraction, sequencing and analysis for RNAseq

2×10^6 cells were harvested and RNA isolated using the NucleoSpin Triprep kit (Macherey-Nagel). Before sequencing, RNA integrity and purity were verified through BioAnalyzer RNA 6000 Nano (Agilent). The barcodes associated to each RNAseq run are included in Table 11. Raw sequences were generated per sample using either the TruSeq Stranded mRNA kit on the Illumina HiSeq 2500 (run B255) or the Stranded mRNA prep Ligation-Illumina on the NovaSeq 6000 (runs D610, D1342 and D1471) by the NGS platform of the Institut Curie, resulting in the creation of 100bp paired-end fastq files.

Raw data were then processed using the Institut Curie RNAseq pipeline (10.5281/zenodo.7443721). The overall quality of the reads was first checked using FastQC (respectively v0.11.9 for the run D1471, v0.11.8 otherwise) and the sequencing orientation, also known as strandness, was assessed using RseQC (respectively v4.0.0 for the run D1471, v2.6.4 otherwise). For the quality control (QC), those reads were then aligned on both a ribosomal RNAs database using bowtie (respectively v1.3.0 for the run D1471, v1.2.3 otherwise) and subsequently on the human reference genome (hg19 assembly) using STAR (respectively v2.7.6a for the run D1471, v2.6.1a otherwise).

Raw counts were generated by the bioinformatics platform pipeline using Star gene quantification mode (`-quantMode GeneCounts`) on the Gencode v19 gene database. On the 58720 Ensembl genes available, only 18699 protein-coding genes on autosomal and X chromosomes were kept in further analysis. Raw counts were normalized using the TMM method using the R packages EdgeR (v3.38.2) and Limma's voom function (v3.52.2). Genes with almost null expression were filtered out ($n=13842$). Principal Component Analysis

(PCA) was performed on normalized data using the R package FactoMineR (v2.6). Heatmaps were generated using the R package pheatmap (v1.0.12).

A linear model considering the annotation (Ctrl, +/-del5, +/-delT) was fitted to the counts. An adjusted p-value of 0.05 and a log fold change of 1.5 were set to consider a gene differentially expressed (DEGs). The R package clusterProfiler v4.4.4 was used to perform gene set enrichment analysis for previous lists of DEGs.

The DNA and RNA from the delT tumors and adjacent tissue was obtained from the Center for Biological Resources (CRB) of Institut Curie following standard protocols, DNA was extracted by ethanol/chlorophorm after tissue dissociation whereas the RNA was extracted using Qiazol followed by myRNeasy kit (Qiagen). The RNAseq from the tumors were analysed using the same pipeline as mentioned for the cell clones.

The DNA from del5 tumors and corresponding adjacent tissue was obtained from either the CRB of Institut Curie (1) as above or from our collaborator S. Sigurdsson (University of Iceland) in which case blood DNA from the same patients was used as controls (2), and the DNA was extracted following the same protocol as the one described above.

Actin staining and circularity score

Confluent MCF10A cells seeded in coverslips inside of 24 well plates were fixed with Paraformaldehyde 4% (Electron Microscopy Science) for 15 min. After a wash with PBS, they were permeabilized with 0.1% TritonX-100 (Fisher Scientific) in PBS for 10 min, and then blocked in 2% BSA (Sigma-Aldrich) in PBS for 30 min. Primary antibodies were diluted into Blocking media and incubated overnight. Day after, coverslips were washed 3 times with PBS, and secondary antibody incubation was performed in a wet chamber at 37 °C for 1 hour. Then they were washed 3 times with PBS and mounted with glass FluoromontG mounting media (Thermo Fisher).

Images were acquired with a 63X objective in a LSM800 Inverted Confocal Microscope (Zeiss) and analyzed using ImageJ software. For intensity, ROIs were selected around cells or junctions of cells, and mean pixel intensity was measured. For circularity score, cell shape parameters were measured in ImageJ, using a ROI around each cell.

Gene silencing of BRCA2

siRNA transfections were performed in serum-containing medium with the transfection reagent JetPrime (Ozyme) following manufacturer's instructions. For BRCA2 depletion we transfected 20 nM of BRCA2 siRNA (Dharmacon D-003462-04, see Table 3). The non-targeting oligonucleotide (Dharmacon D-001810-04-20, 20 nM) was used as control (siCTRL) in the cells. Experiments were performed 48h after transfection.

Cell proliferation and clonogenic survival

For proliferation assays, 5×10^3 cells of MCF10A WT and BRCA2-mutated cells were seeded in triplicate in 24 well culture plates (Falcon/Corning). Cells were then incubated for 8 h at 37 °C in a humidified chamber to adhere to the culture plate. Cells growth was imaged each 3 hours over 7 days using the Incucyte System (Sartorius). The software calculates the % of confluence covered by cells at each time point. The proliferation rate was calculated from the interpolation of logistic growth curve obtained in four independent experiments using GraphPrism software (v. 9.0.0).

In the clonogenic survival assay, cells were serially diluted in complete growth media (Eurobio) and seeded in triplicates in 60 mm plates. A total of 250 cells were seeded for all conditions, except for the siBRCA2 condition, which was seeded at 1000 cells. The media was changed every third day, after 14 days in culture the plates were stained with crystal violet (Sigma-Aldrich), colonies were counted and the surviving fraction was determined for calculated as the ratio of the number of colonies formed to the total number of cells plated.

Colony formation by soft-agar

1×10^4 MCF10A cells were suspended in a top layer of DMEM-F12 supplemented media containing 0.30 % agar (Sigma) and plated on a bottom layer DMEM-F12 supplemented media containing 0.6 % agar in 35 mm plates. The cells were additionally supplied with complete medium every 3 days. After 3 weeks, colonies were stained and fixed with 0.01 % crystal violet and 10 % ethanol in H₂O. Colonies were imaged with a 10X objective in a DM6000B upright widefield Microscope (Leica). For each condition, 20 fields were

acquired. Images were quantified using ImageJ. The plugin extended depth of field was used to convert 3D acquisitions to 2D images; subsequently colony size and circularity were measured using ImageJ version 1.53t.

Cell cycle analysis

1×10^6 cells were harvested and washed twice with PBS. Cells were then fixed in ice-cold 70% ethanol overnight, before being pelleted, resuspended in ice-cold PBS, and then incubated in the dark in propidium iodide (PI) staining buffer (3.5 mM Tris HCl, pH 7.6, 50 μ g/ml PI, 50 μ g/ml RNase A, 0.1% NP-40, 10mM NaCl, ddH₂O) for 30 min at room temperature. Cell cycle distribution was analyzed by flow cytometry BD FACSAria III (BD Bioscience) using the FACSDiva software and data were analyzed with the FlowJo 10.5 software (Tree Star Inc.).

Western blot

Cellular pellet was lysed in lysis buffer (50mM Hepes pH 7.5, 250mM NaCl, 5mM EDTA, 1% NP-40, 1mM DTT, 1mM PMSF, 1X protease inhibitor cocktail (Roche)) and cells were incubated on ice for 60 min, vortexed every 10 minutes. Lysates were sonicated (3 times x 5 seconds) and then centrifuged at 18,000 x *g* for 30 minutes at 4°C. The supernatant was transferred to a prechilled Eppendorf tube and stored at -80°C. For protein electrophoresis, samples were heated in 1x SDS sample buffer for 5 min at 95°C, loaded on a stain-free 4-15% SDS gel (Bio-Rad), and migrated at 130 Volts for 90 minutes in running buffer (1x Tris-Glycine, 0.1% SDS). The stain-free gel was visualized using a ChemiDoc camera (Bio-Rad). For transfer, a nitrocellulose membrane (VWR) was pre-equilibrated in dH₂O and transfer buffer (1x Tris-Glycine, 0.025% SDS, 10% methanol). The proteins were transferred for 2 hours at 0.35 A at 4°C. The membrane was blocked in 5% milk in 1x TBS-T at room temperature for 45 minutes and then incubated with the respective antibody (see antibodies below) in 5% milk in 1x TBS-T overnight at 4°C. After extensive washes in TBS-T (3x 10 min), the membrane was incubated for 1h with the appropriate secondary HRP-antibody at room temperature on a shaker. After 3 more

washes in TBS-T, the membrane was developed using ECL prime western blotting detection reagent (VWR) and visualized using a ChemiDoc camera (Biorad).

Subcellular fractionation

1×10^7 cells were pelleted and incubated in ice for 20 minutes with 500 μ l of BAD buffer (10mM Hepes pH 7.9, 10mM KCl, 10% glycerol, 1.5mM $MgCl_2$, 0.34M Sucrose, 1mM DTT, 0.1mM PMSF, 1X protease inhibitor cocktail (Roche), 0.1mM Na_3VO_4) complemented with 0.1% of Triton X-100). After collecting 20 μ l of total lysate, then pellets were centrifuged at 1300 x *g* for 5 minutes at 4°C. The supernatant, containing the cytoplasmic fraction, was transferred to a prechilled Eppendorf tube. Pellets containing the nuclear fraction, were then washed twice with 1.5ml of BAD buffer, each time centrifugating at 1300 x *g* for 5 minutes at 4°C, and finally incubated in 500 μ l of lysis buffer (50mM Hepes pH 7.5, 250mM NaCl, 5mM EDTA, 1% NP-40, 1mM DTT, 1mM PMSF, 1X protease inhibitor cocktail (Roche)) for 40 minutes. Protein electrophoresis was performed as described above.

Antibodies used for Western Blot

mouse anti-BRCA2 (1:500, OP95, EMD Millipore), rabbit anti-BRCA2 (1:1000, 3E6, GenScript), rabbit anti-RAD51 (1:2000, Abcam), mouse anti-alpha Tubulin (1:5000, Euromedex, Recombinant Anti-Histone H4 (acetyl K5 + K8 + K12 + K16)(abcam, 1:5000), Horseradish peroxidase (HRP) conjugated secondary antibodies used: goat anti-mouse IgG-HRP (1:10,000, Cat.# 115-035-003, Jackson ImmunoResearch), goat anti-rabbit IgG-HRP (1:10,000, Cat.# 111-035-003, Jackson ImmunoResearch).

MTT assay

Cell viability was assessed in MCF10A WT cells, or in parental clones transfected either with siCTRL or siBRCA2, and in MCF10A BRCA2-mutated clones.

Olaparib (AZD2281, Selleck Chemicals): Cells were seeded in triplicate in 96 well-plates (TPP). The following day they were treated at increasing concentrations of the drug (0.5, 1.0, and 2.5 μ M) for 6 days. MMC (Sigma-Aldrich) and HU (Sigma-Aldrich): 3×10^5 cells were seeded in a 6 well-plate (TPP). For MMC, cells were treated for one hour the following concentration of drug: 0, 1.0, 2.0 and 4.0 μ M. For HU, cells were treated for 24h the

following concentration of drug: 0, 2.5, 5 mM. Subsequently cells were harvested and seeded in triplicate in 96 well-plate. On the 6th day, the media was removed and cells were washed with 1x PBS. Cell viability was assessed with 3-[4,5-Dimethylthiazol-2-yl]-2,5-diphenyltetrazolium bromide (MTT, Sigma Aldrich). The solution was removed and MTT crystals were dissolved in 100µl 100% DMSO (Sigma-Aldrich). The absorbance was obtained from the Tristar 3 microplate reader (Berthold Technologies) at 570 nm. The relative surviving cells was calculated by dividing the absorbance of the treated cells by the absorbance obtained in the untreated condition of the same clone.

γH2AX and RAD51 immunofluorescence staining

Cells were grown on 96 well plates (ibidi, 89626) and treated with DMSO as control, 10 µM PARPi Olaparib (AZD2281, Selleck Chemicals), or 3 µM MMC (Sigma-Aldrich) for 24h as indicated. Subsequently cells were fixed in 3% formaldehyde in PBS for 15 min. at room temperature, washed twice in PBS, permeabilized for 5 minutes at room temperature in 0.2% Triton X-100 (Sigma-Aldrich) in PBS, and washed twice in PBS. Primary and secondary antibodies were diluted in filtered DMEM containing 10% FBS and 0.02% sodium azide. Incubations in primary and secondary antibodies were performed at room temperature for 2 and 1h, respectively, with three washes in PBS in between. Cells were then washed once with PBS and incubated for 10 minutes at room temperature with PBS containing 4',6-diamidino-2-phenylindole dihydrochloride (DAPI, 0.5 µg/ml) to stain DNA. Cells were subsequently washed three times in PBS before imaging.

Quantitative image-based cytometry (QIBC)

Automated multichannel widefield microscopy for quantitative image-based cytometry (QIBC) was performed as described previously (REF PMID: 36894693, 29992957) on an Olympus ScanR Screening System (ScanR Image Acquisition 3.01) equipped with an inverted motorized Olympus IX83 microscope, a motorized stage, IR-laser hardware autofocus, a fast emission filter wheel with one set of bandpass filters for multi-wavelength acquisition (DAPI (ex BP 395/25, em BP 435/26), FITC (ex BP 470/24, em BP 511/23), TRITC (ex BP 550/15, em BP 595/40), Cy5 (ex BP 640/30, em BP 705/72)), and a

Hamamatsu ORCA-FLASH 4.0 V2 sCMOS camera (2048 × 2048 pixel, pixel size 6.5 × 6.5 μm) with a ×20 UPLSAPO (NA 0.75) air objective. For each condition, image information of large cohorts of cells (typically at least 1000 cells for the UPLSAPO 20x objective (NA 0.75)) was acquired under non-saturating conditions, and identical settings were applied to all samples within one experiment. Images were analyzed with the Olympus ScanR Image Analysis Software (version 3.3.0), a dynamic background correction was applied, and nuclei segmentation was performed using an integrated intensity-based object-detection module based on the DAPI signal. Nuclear foci segmentation was performed using an integrated spot-detection module. All downstream analyses were focused on properly detected interphase nuclei containing a 2N-4N DNA content as measured by total and mean DAPI intensities. Color-coded scatter plots of asynchronous cell populations were generated with Spotfire data visualization software (version 10.10.1.7, TIBCO). Within one experiment, similar cell numbers were compared for the different conditions. For visualization of discrete data in scatter plots, mild jittering (random displacement of data points along the discrete data axes) was applied to demerge overlapping data points. Representative scatter plots and quantifications of independent experiments are shown.

Homologous recombination assay

2.5×10^6 cells for control, 3×10^6 for BRCA2-mutated clones, were seeded in 10 cm plate. The following day, cells were detached and counted. 1×10^6 cells were mixed in a total amount of 400 μl of Optimem (Gibco) with 5 μg of each of these three plasmids: spCas9-GFP, AAVS1-gRNA, and the plasmid coding for the mCherry protein flanked with two regions of homology for the AAVS1 site (Vugic et al., 2020). For control cells, AAVS1-gRNA (gRNA) plasmid was excluded from the mix. Cells were electroporated in a 0.4 μm cuvette with Gene Pulser (BioRad) at 350V and 960 μF and seeded into a P6 well plate. 2 days after, cells were detached and GFP+ cells (expressing spCas9) were sorted using FACS-Aria Fusion Sorting Cytometer. The same number of GFP+ sorted cells were seeded for each condition. 6 days after (8 days from electroporation), the percentage of mCherry+ of cells was quantified using a FACS-Aria Fusion Cytometer.

DNA combing assay with Olaparib and S1 nuclease treatment

Cells were plated in 10 cm plate and allowed to adhere for 24 h (2×10^6 cells for control, 3.5×10^6 for BRCA2-mutated clones). The following day, DNA was labeled for 30 min with 100 μ M IdU (Sigma-Aldrich) and washed 2 \times with PBS followed simultaneous incubation for 2h with 100 μ M CldU (Sigma-Aldrich) and 30 μ M Olaparib (AZD2281, Selleck Chemicals). After labelling, cells were washed 2 \times with PBS and permeabilized with 5 ml CSK buffer in 10 cm plate (10 mM PIPES, pH 6.8, 0.1 M NaCl, 0.3 M sucrose, 3 mM MgCl₂, EDTA-free Protease Inhibitor Cocktail (Roche)) at room temperature for 10 min. Subsequently, cells were incubated with 1ml of S1 buffer (30 mM sodium acetate pH 4.6, 1 mM zinc sulfate, 50 mM NaCl) was added with or without S1 nuclease (20 U) (Thermo Fisher) for 30 min at 37 °C. Finally, cells were collected by scraping, pelleted, and resuspended in PBS (45 μ l per 400,000 cells).

500 μ l of cells were transferred to a new tube, briefly heated at 42 °C, and resuspended with 500 μ l melted 2% agarose type VII (SIGMA) to make the agarose plugs. Plugs were left to solidify for 20 min at 4 °C and were then digested with Proteinase K (400 mM EDTA pH 8, 10% Proteinase K, 1% Sarcosyl) in a waterbath at 42 °C overnight. The next day, plugs were washed trice with TE 1X buffer. TE solution was removed and a solution containing 50 mM MES pH 5.5, 100 mM NaCl was added to the plugs that were heated at 68 °C for 20 min. Agarose plugs were then dissolved by adding 2 μ l of β -agarase (NEB) and incubated at 42 °C overnight. The following day, dissolved agarose plugs were transferred to the combing machine (Genomic Vision) where DNA was combed onto silane-coated coverslips (Genomic Vision) following the manufacturer's specifications. Combed coverslips were baked overnight at 60 °C, denatured in denaturation buffer (25 mM NaOH, 200 mM NaCl in H₂O) for 15 min, washed trice with 1X PBS, and dehydrated by incubation with increasing concentrations of ethanol 70%, 90%, and 100% each for 5 min. For the IF staining, the coverslips were incubated with BlockAid (Thermo Fisher) for 15 min. Incubations in primary and secondary antibodies were performed at room temperature for 1 hour, with three washes in PBS in between.

Slides were air-dried for 5–10 min and were mounted with 7 μ l mounting media (80% Glycerol and 20% PBS) and sealed with clear nail polish. Track lengths were measured in Fiji and the ratio was calculated dividing the IdU (green) over CldU (red) signal.

Metaphase spreads

$1,25 \times 10^4$ MCF10A cells were seeded into glass coverslips in P24 well plate. The day after, cells were treated with 10 μ g of Olaparib for another 24 hours. Cell division was blocked with 100 ng/ml colcemid (Thermo Fisher) for 3h. Then, a hypotonic shock was performed with 1:7 FBS in distilled water for 40 minutes and cells were fixed adding 1 volume of a solution composed of Methanol-Acetic Acid 3:1. After an incubation of 15 min at RT, fixation media was changed for another 15 min. Finally, another fixation media change was done, and the coverslips were incubated for 30 min at 4 degrees. Coverslips were air-dried and stained with 2% Giemsa solution (Thermo Fisher) diluted in Gurr buffer (Thermo Fisher) for 10 min. The coverslips were rinsed in water and air-dried at RT, then mounted with Eukitt mounting media (Sigma-Aldrich). Images were acquired with a 100X objective with a CMOS camera (LEICA).

Organoids

1×10^3 MCF10A cells were seeded on top of 250 μ l of Cultrex Reduced Growth Factor Basement Membrane Gel (RyD) in P24 wells and feeded with DMEM/F12 media (Gibco) supplemented with L-Glutamine, 1X B27 (Gibco), 10 μ g/ml insulin (Merck), 20 μ g/ml hEGF (Sigma-Aldrich) and 1 μ g/ml Hydrocortisone (Sigma-Aldrich). Media was changed each 2-3 days, and images were taken along the experiment to monitor growth.

Whole-genome sequencing

DNA was extracted from both tumor and corresponding normal tissue and samples were subjected to whole-genome sequencing as described previously (Nik-Zainal et al., 2016). Resulting BAM files were aligned to the reference human genome (GRCh37) using Burrows–Wheeler aligner, BWA (v0.5.9). Mutation calling was performed as described previously (Nik-Zainal et al., 2016). Briefly, CaVEMan (Cancer Variants Through Expectation Maximization; <http://cancerit.github.io/CaVEMan/>) was used to call somatic substitutions.

Indels in the tumor and normal genomes were called using modified Pindel version 2.0 (<http://cancerit.github.io/cgpPindel/>) on the NCBI37 genome build44. Structural variants were discovered using a bespoke algorithm, BRASS (BReakpoint AnalySiS) (<https://github.com/cancerit/BRASS>) through discordantly mapping paired-end reads followed by de novo local assembly using Velvet45 to determine exact coordinates and features of breakpoint junction sequence.

Extraction of mutational signatures

Mutational signatures analysis was performed following a three-step process: (i) hierarchical de novo extraction based on somatic substitutions and their immediate sequence context, (ii) updating the set of consensus signatures using the mutational signatures extracted from breast cancer genomes, and (iii) evaluating the contributions of each of the updated consensus signatures in each of the breast cancer samples. The detailed steps are described in Nik-Zainal et al, 2016.

HRD score

The HRD score determination was conducted using the HRDetect predictor, considering the following genomic features, listed in their respective order of importance: deletions with microhomology, substitution signature 3, rearrangement signatures 3 and 5, HRD index, and substitution signature 8. For further details, see Davies et al., 2017.

Allele-specific LOH

BRCA2-del5 Icelandic cohort (n = 52) (Stefansson et al., 2011): The proportion of BRCA2 WT alleles was quantitatively measured relative to 999del5 BRCA2 mutated alleles in tumor DNA samples by quantitative PCR (7500 Realtime PCR system; Applied Biosystems) with a TaqMan method by using a single BRCA2-specific, minor groove-binding probe (MGB-probe) 5'-end-labeled with FAM and a nonfluorescent quencher (NFQ) at the 3' end, a single BRCA2-specific forward primer, and two allele-specific reverse primers. The BRCA2 WT- to mutant-allele ratios were quantified by measuring differences in fluorescence intensity of FAM performed in duplicate, and the Ct values (number of cycles

to reach intensity threshold) were averaged. Ct measures with standard deviation higher than 0.5 ($SD > 0.5$) were rejected and remeasured. The wild-type to mutant-allele ratios were calculated to wt/allele frequencies by the following equation: Frequency of allele1 = $1/(2\Delta Ct + 1)$ where $\Delta Ct = (Ct \text{ of allele1} - Ct \text{ of allele2})$.

BRCA2-delT Penn cohort (n = 4) (Maxwell et al., 2017): A combination of VarScan241, allele frequency comparisons, and allele-specific copy number calls were used to determine BRCA locus-specific LOH. Estimates of tumor purity (cellularity) were determined using Sequenza and inputted into VarScan2 variant calling. The sample was assigned a locus-specific LOH positive status if the VarScan2 somatic P-value was significant and a locus-specific LOH negative status if the VarScan2 germline P-value was significant. Allele-specific copy number calls of the genomic region containing the BRCA1 or BRCA2 mutation were determined by Sequenza. The copy number of the genomic region surrounding the germline BRCA1 or BRCA2 mutation (CN) and the number of mutant (m) alleles as per the output of the Sequenza program were used to assign two states of absent locus-specific LOH—heterozygous diploid (CN = 2; m = 1) or amplified with gain of non-mutant (wildtype) allele (CN > 2; m = 1)—and three states of locus-specific LOH—loss (CN = 1; m = 1), copy neutral LOH (CN = 2; m = 2), and amplified with LOH (CN > 2; m > 2). The genomic regions surrounding the germline BRCA1 and BRCA2 mutation ranged from less than one to over 100 Mb in length. In cases where the VarScan2 and ASCN calls differed (six of 100 TCGA tumors and four of 60 Penn tumors), the difference between cellularity corrected tumor allele frequency and blood allele frequency (ΔAF) was determined; the sample was assigned a locus-specific LOH positive status if $\Delta AF > 0.2028$. Finally, five of 100 TCGA tumors had a germline BRCA1 or BRCA2 mutation identified only by normal variant calling by Mutect; for these a combination of ASCN and ΔAF was used to determine locus-specific LOH.

Curie cohort (n = 12): Raw sequences were generated per sample using the PCR Free Roche KAPA Hyper Prep Library on the Illumina Novaseq 6000 (run D458) at the NGS platform of the Institut Curie, resulting in the creation of 150bp paired-end fastq files.

Raw data were then processed using the Institut Curie raw-qc pipeline (10.5281/zenodo.8340106). The overall quality of the reads was checked using FastQC (v0.11.8). Reads were then aligned on the hg19 reference genome using bwa mem (v0.7.15). Aligned data were processed using Facets (v0.5.1) that takes advantage of both the B-allele ratio (BAF) and the read depth to estimate the allele-specific copy number variants and the optimal ploidy and tumor cellularity, after a GC percentage correction. Total copy number (number of A and B in the genotype) and minor copy number (number of B in the genotype) were defined for each segment. Loss-Of-Heterozygosity was considered for segments with a minor copy number of 0.

Chemical, reagents, oligonucleotides, antibodies

Table 1. Cell lines	
Product	Source
MCF10A (human breast epithelial cells)	Kind gift from Marie Dutreix
MCF7 (human breast cancer cells)	Kind gift from Patricia Uguen
MDA-MB-231 (human breast cancer cells)	Kind gift form Prof. Krogan

Table 2. Chemicals, reagents, cell media		
Product	Source	Identifier
DMEM-F12	Biowest	Cat#L0092
DMEM High Glucose	Biowest	Cat# L0101
Cultrex Reduced Growth Factor Basement Membrane Gel (RyD)	R&D Systems	Cat#3533-010-02
Accutase	Biowest	Cat#L0950
Horse serum	Thermo Fisher	Cat#16050122
Human epidermal growth factor	Sigma-Aldrich	Cat#E9644
Hydrocortisone	Sigma-Aldrich	Cat#H-0888
Cholera toxin	Sigma-Aldrich	Cat#C8052
Insulin	Sigma-Aldrich	Cat#I9278
Penicillin–streptomycin	Thermo Fisher Scientific	Cat# CABPES01
L-Glutamine	Eurobio Abcys	Cat#CSTGLU00
L-Glutamine	Gibco	Cat# 25030081
jetPRIME®	Ozyme	Cat#POL114
Clontech Labs 3P PRIMESTAR GXL DNA POLYMERASE	Takara Bio	Cat# C9911-100R050A
Paraformaldehyde	Electron Microscopy Sciences	Cat# 15710
BSA	Sigma-Aldrich	Cat#A9647
Cristal violet	Sigma-Aldrich	Cat#C0775
Triton X-100	Thermo Fisher Scientific	Cat#10254583
cOmplete, EDTA-free Protease Inhibitor Cocktail	Sigma-Aldrich	Cat#000000011873580001
DL-Dithiothreitol (DTT) Sigma-Aldrich	Sigma-Aldrich	Cat#D9779
Mini-PROTEAN TGX Stain-Free gels	Bio Rad	Cat#456-8084
UltraPure™ 0.5M EDTA pH8.0	Thermo Fisher Scientific	Cat#15575020

Invitrogen novex NuPAGE 4 12%	Thermo Fisher Scientific	Cat#NP0321BOX
Invitrogen novex NuPAGE MES SDS Running Buffer (20X)	Millipore Sigma	Cat#8086100100
Tris-Glycine 10X	Biorad	Cat##1610771
Amersham Protran Nitrocellulose Blotting Membrane	GE Healthcare Life Science	Cat#10600008
Amersham ECL Prime Western Blotting Detection Reagent	GE Healthcare Life Science	Cat#RPN2236
Olaparib	Euromedex	Cat#S1060
MMC	Sigma-Aldrich	
HU	Sigma-Aldrich	Cat#H8627
S1 nuclease	Thermo Fisher Scientific	Cat#18001016
50-well plug molds	Biorad	Cat#1703713
Agarose Type VII	Sigma-Aldrich	Cat#A4018
IdU	Sigma-Aldrich	Cat#I7125
CldU	Sigma-Aldrich	Cat#C689
Silane-treated slides	Genomic Vision	Cat#COV-002-10
Sarcosyl (N-Lauroylsarcosine sodium salt solution)	Sigma-Aldrich	Cat#61747
TE 100X	EMD Millipore	Cat#574793
MES	Sigma-Aldrich	Cat#M3671
Sodium Acetate	Thermo Fisher Scientific	Cat#15693800
Zinc sulfate	Merck	Cat#83265
β -Agarase I	NEB	Cat#M0392S
Block aid	Life technologies	Cat# B10710
DAPI	Merk Millipore	Cat#28718-90-3
MTT	Sigma-Aldrich	Cat #M5655
FluoromontG	Thermo Fisher Scientific	Cat#00-4958-02
Colcemid	Thermo Fisher Scientific	Cat#15212012
Giemsa	Thermo Fisher Scientific	Cat#10092013
Gurr	Thermo Fisher Scientific	Cat#10-582-013
Eukitt mounting media	Sigma-Aldrich	Cat#03989

Table 3. SiRNA		
Target and sequence (5'-3')	Source	Identifier
BRCA2: GAAGAAUGCAGGUUUAUA	Dharmacon	Cat# D-003462-04
Non targeting oligonucleotide (siCTRL)	Dharmacon	Cat# D-001810-01

Table 4. Primers for BRCA2 genotyping			
Sequence (5'-3')	Mean	Source	Lab Identifier
GCTGACATTCAGAGTGAAGAAATTTACAAC	delT F	Eurofins MWG	oAC337
GCAGATGAATTTACCACATTATATGAAAAGCC	delT R	Eurofins MWG	oAC338
GGACAAAGGGATGATTCATGTCCCAAG	del5 F	Eurofins MWG	oAC525
GGTGAAATGCCATCTCTACTAAAAATACAATAGTT G	del5 R	Eurofins MWG	oAC517

Table 5. sgRNA target sequences	
Sequence (5'-3')	Mean
Talen 1: TGTGGGATTTTAGCACAG	BRCA2-delT mutation (TALEN)
Talen 2: TGAAGCATCTGATACCTG	
GACAGTGAAAACACAAATCA	BRCA2-del5 mutation (CRISPR)
GCACAGCAAGTGAAAATCTGTCC	correct BRCA2-delT mutation (CRISPR)
GACAGTGAAAACACAAAGAG	correct BRCA2-del5 mutation (CRISPR)
GGGGCCACTAGGGACAGGAT	generate a DSB in the AAVS locus (CRISPR)

Table 6. Oligonucleotides			
Sequence (5'-3')	Mean	Source	Lab Identifier
GTCCTGCAACTTGTTACACAAATCA GTCC	Forward to made homologous PCR from gDNA CAPAN-1 for TALEN BRCA2delT	Eurofins MWG	oAC350
CCCCAACTGACTACACAAAATG GCTG	Reverse to made homologous PCR from gDNA CAPAN-1 for TALEN BRCA2delT	Eurofins MWG	oAC378
ACACCGACAGTGAAAACACAAATC AG	Forward to clone gRNA for BRCA2del5	Eurofins MWG	oAC522
AAAACTGATTTGTGTTTTCACTGTC G	Reverse to clone gRNA for BRCA2del5	Eurofins MWG	oAC523
TTCAACTAAACAGAGGACTTACCAT GACTTGCAGCTTCTCTTTGTGTTTTC ACTGTCTGTCACAGAAGCGATAAAT CTAT	Homology oligo containing the BRCA2 999del5 mutation	Sigma-Aldrich	oAC513
CACCGCACAGCAAGTGAAAATCTG TCCGTTTTAGAGCTAGAAATAGCAA GTTAAAATAAGGCTAGTCCGTTATC AACTTGAAAAAGTGGCACCGAGTC GGTGCGGACAGATTTTCCACTTGCT GTGCTAA	Forward for cloning sgRNA to revert BRCA2 delT mutation	Eurofins MWG	oAC1002
AAAATTAGCACAGCAAGtGGAAAA TCTGTCCGCACCGACTCGGTGCCAC TTTTTCAAGTTGATAACGGACTAGC CTTATTTTAACTTGCTATTTCTAGCT CTAAAACGGACAGATTTTCACTTGC TGTGC	Reverse for cloning sgRNA to revert BRCA2 delT mutation	Eurofins MWG	oAC1003
ACACCGACAGTGAAAACACAAAG AGG	Forward to clone gRNA for correcting BRCA2del5	Eurofins MWG	oAC995
AAAACCTCTTTGTGTTTTCACTGTC G	Reverse to clone gRNA for correcting BRCA2del5	Eurofins MWG	oAC996

TTCAACTAAACAGAGGACTTAC CATGACTTGCAGCTTCTCTTTGA TTTGTGTTTTCACTGTCTGTCACA GAAGCGATAAATCTAT	Homology oligo to revert the BRCA2 999del5 mutation	Sigma- Aldrich	oAC994
---	---	-------------------	--------

Table 7. Plasmids		
Construct	Source	Identifier
TALEN BRCA2 delT fok F pcDNA6.2/N-EmGFP-DEST GW	Life technologies	#V35620
TALEN BRCA2delT fok R pcDNA6.2/N-YFP-DEST GW	Life technologies	#V35820
pCas9-GFP	Addgene	#44719
pBS U6 sgRNA CRISPR	Addgene (gift from Carine Giovannangeli)	#43860
pU6-pegRNA-GG-acceptor	Addgene	#132777

Table 8. Commercial kits		
Product	Source	Identifier
NucleoSpin Plasmid	Macherey-Nagel	Cat# 740588
Maxiprep	Qiagen	Cat#12162
AMAXA Cell Line Nucleofector® Kit T	Lonza	Cat#VCA-1002
NucleoSpin TriPrep	Macherey-Nagel	Cat#740966
Wizard® SV Gel and PCR Clean-Up System	Promega	Cat#A9285
Quick-DNA Universal Kit ZYMO	Ozyme	Cat#ZD4069
Bioanalyzer	Agilent	Cat#5067-1511
Qubit	Thermo Fisher Scientific	Cat#Q32851

SPECIES AND ANTIGEN	SOURCE	IDENTIFIER	DIL. + EXP
Mouse anti-BRCA2	EMD Millipore	OP95	1:500, WB
Rabbit anti-BRCA2	In-house	3E6	1:1000, WB
Rabbit anti-RAD51	abcam	ab63801	1:2000, WB
Rabbit Anti-Histone H4 (acetyl K5 + K8 + K12 + K16)	abcam	ab177790	1:1000, WB
Rat anti-BrdU (CldU)	abcam	ab6326	1:50, combing
Mouse anti-BrdU (IdU)	BD Bioscience	#347580	1:25, combing
Alexa Fluor™ 647 Phalloidin	Thermo Fisher Scientific	#A22287	1:250, IF
Mouse anti-H2AX Phospho S139	BioLegend	#613401	1:1000, IF
Rabbit anti-RAD51	BioAcademia	#70-002	1:1000, IF

SPECIES AND ANTIGEN	SOURCE	IDENTIFIER	DILUTION+EXP
HRP-conjugated goat antimouse	Jackson Immuno	#115-035-003	1:10 000, WB
HRP-conjugated goat antirabbit	Jackson Immuno	#111-035-003	1:10 000; WB
Alexa donkey anti-mouse 488	Thermo Fisher Scientific	#A-21202	1:50, combing
Alexa goat anti-rat 555	Thermo Fisher Scientific	#A-21434	1:50, combing
Alexa Goat Anti-Mouse 568	Thermo Fisher Scientific	#A11031	1:500, IF
Alexa Goat Anti-Rabbit 488	Thermo Fisher Scientific	#A11034	1:500, IF

ID	Barcode
Ctrl #1	B255T01
Ctrl #2	D610T170

Ctrl #3	D1471T148
+/del5 #1	D956T267
+/del5 #2	D956T268
+/del5 #3	D1342T008
+/delT #1	D956T269
+/delT #2	D610T171
+/delT #3	D610T172

Table 12. Tumors clinical pathology

Sample	Cohort	Mutation	Donor gender	Age	Specimen type	Histology	ER	PR	HER2	Subtype	Tumour grade	Tumour stage	Source of normal	Parity	Mitotic score
PD4872a	Nik-Zainal et al., 2016	c.771-775del p.N257fs*17	F	40	Primary	ductal carcinoma	+	+	-	NA	NA	T2	NA	GxPx	NA
PD4876a	Nik-Zainal et al., 2016	c.771-775del p.N257fs*17	F	30	Primary	ductal carcinoma	+	+	-	NA	NA	T3	NA	GxPx	NA
PD4951a	Nik-Zainal et al., 2016	c.771-775del p.N257fs*17	F	39	Primary	ductal carcinoma	+	+	-	LumA	II	Tx	blood	GxP3	high
PD4952a	Nik-Zainal et al., 2016	c.771-775del p.N257fs*17	F	44	Primary	ductal carcinoma	+	+	-	NA	III	Tx	blood	GxP1	high
PD4953a	Nik-Zainal et al., 2016	c.771-775del p.N257fs*17	F	67	Primary	ductal carcinoma	+	-	-	LumB	II	Tx	blood	GxP5	low
PD4954a	Nik-Zainal et al., 2016	c.771-775del p.N257fs*17	F	51	Primary	ductal carcinoma	+	+	-	NA	II	Tx	blood	GxP2	high
PD4957a	Nik-Zainal et al., 2016	c.771-775del p.N257fs*17	F	38	Primary	ductal carcinoma	+	+	-	LumA	II	Tx	blood	GxP2	NA
PD4958a	Nik-Zainal et al., 2016	c.771-775del p.N257fs*17	F	48	Primary	ductal carcinoma	+	+	-	LumB	II	Tx	blood	GxP2	high
371480H	I.Curie	c.771-775del p.N257fs*17	F	42	Primary	ductal carcinoma	-	-	NA	NA	III	T2	tissue	NA	NA
R01	Iceland Univ.	c.771-775del p.N257fs*17	F	NA	NA	NA	-	-	-	TNBC	NA	NA	blood	NA	NA
RO3	Iceland Univ.	c.771-775del p.N257fs*17	F	32	Primary	NA	+	+	-	LumB	NA	NA	blood	NA	NA
514207H	I.Curie	c.5946delT p.S1982fs	F	65	Primary	Invasive Ductal Carcinoma	+	-	-	Lum	III	NA	tissue	NA	high
462295H	I.Curie	c.5946delT p.S1982fs	F	47	Primary	Invasive Ductal Carcinoma	+	NA	-	NA	III	NA	tissue	NA	Moderate
631699H	I.Curie	c.5946delT p.S1982fs	F	49	Primary	invasive carcinoma	NA	+	-	NA	II	NA	tissue	NA	Moderate

Table 12. Tumors clinical pathology

Sample	Cohort	Mutation	Donor gender	Age	Specimen type	Histology	ER	PR	HER2	Subtype	Tumour grade	Tumour stage	Source of normal	Parity	Mitotic score
452087H	I.Curie	c.5946delT p.S1982fs	F	65	Primary	NA	NA	NA	NA	NA	NA	NA	tissue	NA	NA
619138H	I.Curie	c.5946delT p.S1982fs	F	33	Primary	Invasive Carcinoma	+	+	-	Lum B	III	NA	tissue	NA	high
H150105	I.Curie	c.5946delT p.S1982fs	F	49	Primary	Invasive Carcinoma	+	-	-	TNBC	III	NA	tissue	NA	high
638538H	I.Curie	c.5946delT p.S1982fs	F	79	Primary	Invasive Ductal Carcinoma	NA	NA	NA	NA	NA	NA	tissue	NA	NA
549025H	I.Curie	c.5946delT p.S1982fs	F	73	Metastasis	Invasive Ductal Carcinoma	+	+	-	Lum	NA	NA	tissue	NA	NA
H091731	I.Curie	c.5946delT p.S1982fs	F	76	Primary	Invasive adeno carcinoma	+	+	-	Lum A	II	NA	tissue	NA	NA
439267H	I.Curie	c.5946delT p.S1982fs				Invasive adeno carcinoma	+	NA	-		II				
514207H	I.Curie	c.5946delT p.S1982fs				Invasive adeno carcinoma	NA	NA	NA		III				
4756- Brca2Br1	Maxwell et al., 2017	c.5946delT p.S1982fs	F	70	Primary	Invasive Ductal Carcinoma	-	-	-	TNBC	III	T2	tissue	NA	NA
6013- Brca2Br4 9	Maxwell et al., 2017	c.5946delT p.S1982fs	F	62	Primary	Invasive Ductal Carcinoma	+	-	-	NA	I	T2	tissue	NA	NA
6035- Brca2Br1 0	Maxwell et al., 2017	c.5946delT p.S1982fs	F	43	Primary	Invasive Ductal Carcinoma	+	-	-	NA	III	T1	tissue	NA	NA
TCGA- AO-A03V	Maxwell et al., 2017	c.5946delT p.S1982fs	M	41	Primary	Invasive Ductal Carcinoma	+	-	-	NA	unknown	T1	tissue	NA	NA
6537	Penn Univ.	c.5946delT p.S1982fs	NA	NA	NA	NA	NA	NA	NA	NA	NA	NA	NA	NA	NA
7281	Penn Univ.	c.5946delT p.S1982fs	NA	NA	NA	NA	NA	NA	NA	NA	NA	NA	NA	NA	NA

Synthèse

L'intégrité du génome de la cellule eucaryote est constamment menacée par des lésions de l'ADN causées soit par des facteurs externes, soit par le métabolisme cellulaire. Ces dommages pouvant avoir des conséquences néfastes, les cellules disposent de divers mécanismes de réparation des dommages de l'ADN : parmi eux, la recombinaison homologue (HR) est l'un des plus importants, car elle effectue une réparation d'haute-fidélité des cassures double brin de l'ADN (DSB), des liaisons croisées inter-brins (ICL) ainsi que des lésions de l'ADN générées pendant la réplication en utilisant une séquence identique (la chromatide sœur) comme modèle.

BRCA2 est une protéine suppresseur de tumeurs essentielle au maintien de l'intégrité du génome grâce à son rôle clé dans la voie de la HR. De plus, BRCA2 est indispensable à la protection de la fourche de réplication ainsi qu'à la réparation et à la prévention de la formation de ponts d'ADN simple brin (ssDNA gaps). Par conséquent, les mutations mono-alléliques héréditaires de BRCA2 prédisposent au cancer du sein et de l'ovaire. Alors que les effets délétères de la déficience de BRCA2 sont connus, notamment les défauts de la HR, le stress réplicatif et l'accumulation ssDNA gaps, les mécanismes de formation des tumeurs chez les porteurs de mutations de BRCA2 restent mal définis. L'inactivation de l'allèle sauvage (perte d'hétérozygotie, LOH) semble être cruciale pour la carcinogenèse des cellules mutées de BRCA2. Cependant, certains cancers conservent le deuxième allèle intact, suggérant une haplo-insuffisance de BRCA2. Cette hypothèse a fait l'objet de nombreux débats, et différents résultats ont été obtenus selon le système modèle choisi. Pour répondre à cette question, nous avons édité génétiquement deux lignées cellulaires isogéniques épithéliales mammaires non tumorales, chacune portant un variant pathogène mono-allélique de BRCA2.

L'analyse par RNA-seq a révélé que le variant c.771-775del (del5) de BRCA2 avait un impact minimal sur l'expression génique tandis que le deuxième, le c.5946del (delT), entraînait des changements transcriptomiques substantiels, notamment la régulation négative de gènes liés à l'adhésion cellulaire. Les essais en soft-agar ont révélé que cette lignée avait une capacité accrue à former des colonies de manière indépendante de

l'ancrage, indiquant un phénotype invasif, en accord avec les changements d'expression génique observés. Ces mêmes résultats ont été confirmés en 3D dans un système isogénique d'organoides.

Les cellules portant le variant del5 présentait des niveaux protéiques réduits à la fois de BRCA2 et de son effecteur clé, RAD51. Cette réduction corrèle avec des déficiences dans la réparation médiée par la HR et avec une sensibilité accrue aux inhibiteurs de PARP (PARPi) et au traitement à la Mitomycine C (MMC). De plus, les cellules +/-del5 ont accumulé des ssDNA gaps en réponse au stress répliatif induit par le PARPi, suggérant une instabilité génomique persistante dans cette lignée, se manifestant par des cassures d'ADN sous le même traitement.

Ensuite, pour comparer les deux variants dans un contexte tumoral, nous avons analysé, par séquençage complet du génome (WGS), des échantillons d'ADN de tumeurs mammaires primaires et de tissus non néoplasiques adjacents. De manière surprenante, malgré les différences observées dans les cellules porteuses de mutations hétérozygotes de BRCA2, nous avons observé des profils génomiques similaires, indicatifs d'une déficience en recombinaison homologe (HRD) dans les deux cohortes de tumeurs. De plus, lorsque nous avons analysé la proportion de tumeurs ayant subi une LOH de BRCA2, nous avons trouvé des fréquences différentes entre les deux cohortes, suggérant une pression sélective différente pour cet événement dans les tumeurs.

En conclusion, notre travail suggère que différents variants pathogènes mono-alléliques de BRCA2 conduisent à des profils transcriptomiques et phénotypiques différents. Ces disparités pourraient potentiellement expliquer la fréquence variable de LOH dans les tumeurs, tandis que leur signature mutationnelle est principalement attribuée à une HRD. Ceci pourrait avoir des implications cliniques significatives, affectant la réponse des tumeurs associées à BRCA2 aux traitements chimiothérapeutiques comme les PARPi, qui se sont avérés plus efficaces dans les cellules subissant une LOH de BRCA2.

Appendix

During my PhD I contributed to the research article "Replication gap suppression depends on the double-strand DNA binding activity of BRCA2" (Vugic et al., *Nature Communications*, 2023) by performing DNA combing for Fig. 5C and supplementary Fig.5.

Additionally, in collaboration with my Ph.D. supervisor, I served as a first author for a review titled 'BRCA1/2 Haploinsufficiency: Exploring the Impact of Losing one Allele' available online in the *Journal of Molecular Biology* from September 2023.

I also contributed as co-first author to the meeting report entitled "At the Crossroads of RNA Biology, Genome Integrity, and Cancer," which was published in the *Bulletin de Cancer* in 2022.


I am currently in the process of preparing the manuscript to be submitted for publication containing the results from my PhD research project.

Replication gap suppression depends on the double-strand DNA binding activity of BRCA2

Received: 17 June 2022

Accepted: 17 January 2023

Published online: 27 January 2023

 Check for updates

Domagoj Vugic^{1,2,5}, Isaac Dumoulin^{1,2,5}, Charlotte Martin^{1,2,5}, Anna Minello^{1,2}, Lucia Alvaro-Aranda³, Jesus Gomez-Escudero³, Rady Chaaban^{1,2,3}, Rana Lebdy⁴, Catharina von Nicolai^{1,2}, Virginie Boucherit^{1,2}, Cyril Ribeyre⁴, Angelos Constantinou⁴ & Aura Carreira^{1,2,3} ✉

Replication stress (RS) is a major source of genomic instability and is intrinsic to cancer cells. RS is also the consequence of chemotherapeutic drugs for treating cancer. However, adaptation to RS is also a mechanism of resistance to chemotherapy. BRCA2 deficiency results in replication stress in human cells. BRCA2 protein's main functions include DNA repair by homologous recombination (HR) both at induced DNA double-strand breaks (DSB) and spontaneous replicative lesions. At stalled replication forks, BRCA2 protects the DNA from aberrant nucleolytic degradation and is thought to limit the appearance of ssDNA gaps by arresting replication and via post-replicative HR. However, whether and how BRCA2 acts to limit the formation of ssDNA gaps or mediate their repair, remains ill-defined. Here, we use breast cancer variants affecting different domains of BRCA2 to shed light on this function. We demonstrate that the N-terminal DNA binding domain (NTD), and specifically, its dsDNA binding activity, is required to prevent and repair/fill-in ssDNA gaps upon nucleotide depletion but not to limit PARPi-induced ssDNA gaps. Thus, these findings suggest that nucleotide depletion and PARPi trigger gaps via distinct mechanisms and that the NTD of BRCA2 prevents nucleotide depletion-induced ssDNA gaps.

Germline mono-allelic mutations in *BRCA2* predispose to breast and ovarian cancer with high penetrance¹; when biallelic, they result in Fanconi anemia (FA)².

BRCA2 tumor suppressor protein preserves genomic integrity through its mediator role in DNA repair by homologous recombination (HR)^{3–5}. On the one hand, BRCA2 loads and modulates the DNA binding activity of RAD51 preventing its non-productive association with double-stranded DNA (dsDNA) and promoting its nucleation onto the resected single-stranded DNA (ssDNA). On the other, it helps displace

RPA from ssDNA thus facilitating RAD51 nucleoprotein filament formation and strand invasion. Replication stress induces the formation of DNA lesions that block replication; under these conditions, RAD51 protects stalled replication forks from unscheduled nucleolytic degradation, a function that is promoted by BRCA2^{6–8}. In addition, RAD51 promotes replication fork reversal, a structure resulting from the annealing of the newly synthesized strands allowing to skip of a lesion^{9,10} and restart of replication; these functions seem to be independent of BRCA2.

¹Institut Curie, PSL Research University, CNRS, UMR3348, F-91405 Orsay, France. ²Paris-Saclay University CNRS, UMR3348, F-91405 Orsay, France. ³Genome Instability and Cancer Predisposition lab, Department of Genome Dynamics and Function, Centro de Biología Molecular Severo Ochoa (CBMSO, CSIC-UAM), Madrid 28049, Spain. ⁴Institut de Génétique Humaine, CNRS, Université de Montpellier, Montpellier, France. ⁵These authors contributed equally: Domagoj Vugic, Isaac Dumoulin, Charlotte Martin. ✉e-mail: acarreira@cbm.csic.es

Replication stress leads to the appearance of stretches of ssDNA or single-strand DNA gaps (ssDNA gaps). These gaps have been shown to accumulate in BRCA1/2-deficient cells, especially under replication-compromising conditions, such as nucleotide depletion induced by hydroxyurea, after multiple rounds of cisplatin treatments, or upon treatment with PARP inhibitors¹¹ suggesting the involvement of these factors in preventing replication-associated ssDNA gaps^{8,12–14}. The origin of ssDNA gaps is multiple varying from defects in Okazaki fragment processing to repriming by specialized polymerases¹⁵. Because they cannot be filled by conventional polymerases, several mechanisms need to act to “fill in” these ssDNA gaps left behind the forks. These include translesion synthesis (TLS), template switching (TS), and repriming by the primase-polymerase PRIMPOL (reviewed in refs. 15–17). RAD51-mediated homologous recombination (HR) through TS can repair ssDNA gaps in an error-free manner¹⁸ and has been shown to efficiently fill gaps opposite to bulky adducts in mammalian cells¹⁹. In the absence of a functional HR, such as in the BRCA1/2-deficient context, other mutagenic mechanisms take place to fill in the gaps including the TLS factors REV1-Pol ζ ^{20,21}.

The fate of ssDNA gaps in BRCA2-deficient cells and how BRCA2 is involved in their suppression/repair is still poorly understood. The ortholog of BRCA2 in *U. maydis*, Brh2, can load Rad51 onto gapped DNA *in vitro*²², an activity that requires a dsDNA/ssDNA junction²², and this requirement was also shown for the loading of RecA by the functional homolog of BRCA2 in bacteria, RecFOR²³. Although biochemical data is lacking, mammalian BRCA2 likely promotes ssDNA gap filled-in/ repair through an HR-dependent mechanism^{8,19,24,25}. Finally, if left unrepaired, ssDNA gaps may persist or lead to replication-associated DSBs both of which can be repaired via HR in an error-free manner^{21,26}. In the absence of a functional HR, these gaps or DSBs accumulate and manifest in chromatid gaps or breaks in metaphase spreads. The latter may be subjected to non-homologous end joining (NHEJ) repair that when ligated to different DSBs result in radial chromosomes both of which are observed in BRCA2-deficient cells²⁷.

Here, we investigate the role of BRCA2 at replication forks taking advantage of two variants in the N-terminal DNA binding domain (NTD) with either impaired dsDNA binding activity²⁷ or impaired ssDNA and dsDNA binding activities²⁸. We find that the NTD of BRCA2 and in particular, its dsDNA binding activity, is required for ssDNA gap suppression. ssDNA gaps form in cells expressing BRCA2-C315S despite a functional fork arrest and persist through mitosis as detected in metaphase spreads in the same cell cycle. Consistently, cells bearing the NTD variants show hypersensitivity to replication stress induced by hydroxyurea (HU). In contrast, these cells are resistant to PARP inhibitors (PARPi) and do not accumulate ssDNA gaps in these conditions. These findings suggest that nucleotide depletion and PARPi trigger gaps in a different manner and therefore require distinct functions for their repair. Moreover, using a gene-targeting cell-based assay, we show that cells bearing NTD variants are proficient in DSB repair, suggesting that the dsDNA binding activity of BRCA2, located at the NTD, is necessary for the repair of replication-associated gaps but dispensable for the repair of DSBs. Reconstituting ssDNA gap repair *in vitro*, we find that RAD51 can perform recombination from an ssDNA gap mimicking substrate without the requirement of an ssDNA 3'-end and that BRCA2_{NTD} can readily promote this reaction. Thus, the dsDNA binding activity of BRCA2 promotes ssDNA gap repair by HR.

Our findings establish BRCA2 dsDNA binding activity, unique to the NTD and impaired in the breast cancer variants C315S and S273L, as essential for the ssDNA gap suppression activity of BRCA2. These variants uncouple the function of BRCA2 in the recombinational repair of replication-associated gaps from the repair of DSBs.

Results

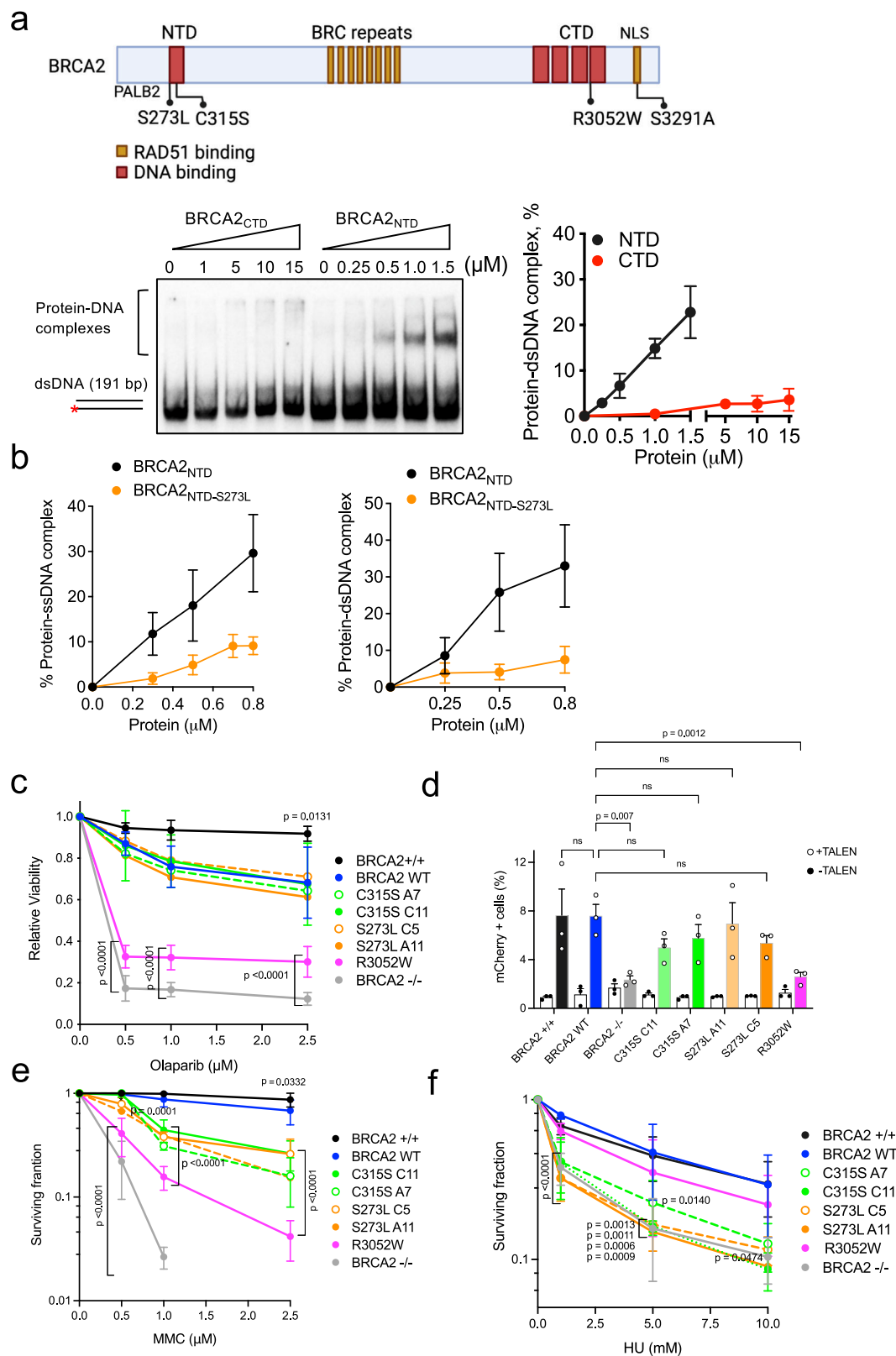
Breast cancer variants affecting the NTD or the CTD of BRCA2 confer different sensitivity to replication stress

In addition to the canonical C-terminus DNA binding domain (CTD), BRCA2 presents a second DNA binding site in the N-terminus (NTD)²⁸. Unlike the CTD, which binds ssDNA²⁹, the NTD can bind both ssDNA and dsDNA *in vitro*²⁸. The NTD can promote RAD51-dependent HR in isolation *in vitro*; however, the interdependencies between the NTD and the CTD in the context of the full-length BRCA2 and in cells have not been elucidated. Moreover, given the role of BRCA2 and HR in DSB repair and in the response to replication stress, we wondered which domains of BRCA2 were required for these different functions. To gain insight into these questions, we used breast cancer variants that impair the DNA binding ability of the NTD or the CTD. We focused on three variants, R3052W, a pathogenic variant that affects the ssDNA binding activity of the CTD and is therefore deficient in HR³⁰. C315S, a variant of unknown clinical significance (VUS) located in the NTD that impairs specifically the dsDNA binding activity of BRCA2 and cannot promote RAD51-mediated recombination at a resected-DNA mimicking substrate²⁸. Finally, we included a previously uncharacterized VUS located as well in the NTD region, S273L.

We have shown that the dsDNA binding activity of BRCA2 is located at the NTD and that the CTD is devoid of this activity²⁸; however, these experiments were performed with a short dsDNA substrate. As it has been suggested that the Tower domain of the CTD may interact with dsDNA²⁹ we first compared the dsDNA binding activity of recombinant CTD (aa 2474–3190) and NTD (aa 250–500) this time using a longer ³²P-labeled (191 bp) dsDNA substrate in electrophoretic mobility shift assays (EMSA) *in vitro*. Using this set-up, only the NTD showed dsDNA binding activity, confirming and extending our previous findings and indicating that the dsDNA binding activity of BRCA2 is unique to the NTD (Fig. 1a). We then purified the NTD bearing the VUS S273L and tested its DNA binding ability by EMSA with synthetic oligonucleotide substrates as previously performed for BRCA2_{NTD-C315S}²⁸. BRCA2_{NTD-S273L} impaired both ssDNA and dsDNA binding *in vitro* (Fig. 1b, Supplementary Fig. 1a, b).

We generated stable cell lines bearing the selected variants by transfecting the BRCA2 cDNA coding a GFP-MBP-tagged version of BRCA2 full-length protein (BRCA2 WT) or the variants C315S, S273L, or R3052W to complement DLD1 BRCA2 deficient human cells (hereafter BRCA2^{-/-}). In this cell line, both alleles of BRCA2 contain a deletion in exon 11 causing a premature stop codon after BRC5 and cytoplasmic localization of a truncated form of the protein³¹. When possible, we selected two stable clones of each variant to account for possible phenotypic differences observed due to the different protein levels among the clones compared to the wt clone (clone C1, hereafter BRCA2 WT) (Supplementary Fig. 2a). Next, we assessed the sensitivity of these cells to different genotoxic agents. We first tested their sensitivity to the poly (ADP-ribose) polymerase (PARP) inhibitor Olaparib. PARP1 is an enzyme required for the sensing of DNA single-strand breaks (SSBs) and double-strand breaks (DSBs) that becomes essential in the absence of a functional HR pathway^{32–34}. PARP1 inhibitors, in particular Olaparib, are currently used in the clinic to treat breast and ovarian cancer patients carrying germline mutations in BRCA1/2³⁵. In our settings, the relative viability of BRCA2^{-/-} cells was 12% upon a 6-days treatment with the highest Olaparib concentration used (2.5 μ M); in contrast, 70% of BRCA2 WT complemented cells remained viable. Similarly, cells expressing S273L or C315S survived the treatment to the same level as the cells expressing BRCA2 WT (Fig. 1c). Consistent with previous results³⁰, R3052W, the CTD variant that impairs HR activity, showed hypersensitivity to the treatment with only 30% of surviving cells at 2.5 μ M Olaparib (Fig. 1c).

To directly assess the capacity of these cells to repair DSBs by HR we performed a cell-based HR assay. Based on the classical



GFP-reporter assay³⁶, this test measures DSB-mediated gene targeting activity at a specific locus (AAVS1 site) within the endogenous PPP1R12C gene using a site-specific transcription-activator like effector nuclease (TALEN) and a promoter-less mCherry donor flanked by homology sequence to the targeted locus³⁷. DSB-mediated gene targeting results in mCherry expression from the endogenous PPP1R12C

promoter which can be measured by flow cytometry. Using this system, cells expressing the endogenous BRCA2 protein (BRCA2^{+/+}) or BRCA2 WT complemented cells showed ~7.5% of mCherry positive TALEN-transfected cells (mean of 7.6% for both BRCA2^{+/+} and BRCA2 WT) whereas BRCA2-deficient cells (BRCA2^{-/-}) showed only 2.3% of mCherry expressing cells, as expected (Fig. 1d, Supplementary Fig. 2b).

Fig. 1 | BRCA2 variants located in the NTD are sensitive to replication stress. **a** (Top) Schematic representation of BRCA2 structure indicating its DNA binding domains (in red) and RAD51 binding sites (in orange) with the variants/mutations located within them used in this study. The location of the PALB2 binding site and the nuclear localization signal (NLS) are also indicated. Figure created with BioRender.com. (Bottom) Representative EMSA and quantification comparing the binding of increasing concentrations of BRCA2_{NTD} and BRCA2_{CTD}, as indicated, to dsDNA (191 bp). The data represent the mean from three independent experiments. Error bars, SD. **b** Quantification of EMSA showing the binding of purified BRCA2_{NTD-S273L} or BRCA2_{NTD-S273L} at the indicated concentrations to ssDNA (dT₄₀) or dsDNA (42mer) ³²P-labeled substrates. The data represent the mean from three independent experiments. Error bars, SD. See also Supplementary Fig. 1. **c** Quantification of the relative cell viability monitored by MTT assay upon treatment with increasing doses of the PARP inhibitor Olaparib, as indicated. The data represent the mean \pm SD of four independent experiments. (ns, not significant). **d** Frequency of

mCherry positive cells in cells transfected with the promoter-less donor plasmid (AAVS1-2A-mCherry) without (-TALEN) (open circles) or with (+TALEN) nucleases (filled circles). The error bars represent the mean \pm SEM of three independent experiments. See also Supplementary Fig. 2b. **e** Quantification of the surviving fraction of BRCA2^{+/+} and BRCA2^{-/-} or BRCA2^{-/-} stable clones expressing BRCA2 WT or the variants C315S, S73L, R3052W, assessed by clonogenic survival upon exposure to MMC at the indicated concentrations. Data represent the mean \pm SD of three independent experiments. **f** Quantification of the surviving fraction of BRCA2^{+/+} and BRCA2^{-/-} or stable clones expressing BRCA2 WT or the variants C315S, S273L, R3052W, assessed by clonogenic survival upon exposure to HU at the indicated concentrations. Data represent the mean \pm SD of three independent experiments. See also Supplementary Fig. 3. Statistical difference in **c-f** was determined by a two-way ANOVA test with Dunnett's multiple comparisons tests. The *p*-values show significant differences compared to the BRCA2 WT clone. Only significant *p*-values are shown. Source data are provided as a Source Data file.

Table 1 | Main phenotypes observed in the different DLD1 BRCA2-mutated stable cell lines used in this study

Cell line	HR	FP	FA	GS HU	GS PARPi	PARPi response	HU response	MMC response
BRCA2 WT	+	+	+	+	+	Resistant	Resistant	Resistant
BRCA2 ^{-/-}	-	-	-	-	-	Sensitive	Sensitive	Sensitive
S273L	+	/	-	-	/	Resistant	Sensitive	mild sens.
C315S	+	+/-	+	-	+	Resistant	Sensitive	mild sens.
R3052W	-	+/-	+	+	-	Sensitive	Resistant	Sensitive
S3291A	/	+/-	+	+	/	/	/	/

HR homologous recombination, FP fork protection, FA fork arrest, GS gap suppression, *mild sens.* mild sensitivity.

In agreement with our previous report³⁰ cells expressing the CTD variant, R3052W, was HR deficient showing 2.6% of mCherry-expressing cells. Importantly, TALEN-transfected cells expressing BRCA2 variants S273L and C315S showed no significant difference with the BRCA2 WT complemented cells (means ranging from 5% to 7% depending on the clone) indicating a nearly normal or intact DSB repair activity by HR.

As a member of the Fanconi anemia pathway, BRCA2 (FANCD1)-deficient cells are extremely sensitive to crosslinking agents and platinum drugs such as cisplatin or mitomycin C (MMC)²; therefore, we next performed clonogenic survival assays to assess the sensitivity of cells bearing NTD variants and the CTD variant to increasing concentrations of MMC. As expected, BRCA2-deficient cells (BRCA2^{-/-}) showed hypersensitivity to MMC treatment already at 1 μ M MMC whereas BRCA2 WT cells complemented this phenotype almost to the same survival levels as the cells expressing the endogenous BRCA2 (BRCA2^{+/+}) (Fig. 1e, Supplementary Fig. 3). Cells bearing R3052W, the HR-deficient variant, displayed hypersensitivity to MMC. The stable clones expressing variants S273L and C315S also showed increased sensitivity to MMC although they resulted in an intermediate phenotype between the BRCA2 WT cells and cells expressing R3052W (Fig. 1e, Supplementary Fig. 3). Given that MMC treatment primarily generates inter-strand crosslinks which can inhibit transcription and replication in addition to prompting DNA breaks³⁸; we then tested whether the NTD or CTD variants rendered cells sensitive to other forms of replication stress. We exposed cells to hydroxyurea (HU), a drug that reduces the pool of dNTPs leading to stalled replication forks, and assessed their viability via clonogenic survival assay. DLD1 BRCA2-deficient cells were moderately sensitive to HU as compared to MMC treatment. Remarkably, the CTD variant R3052W restored the sensitivity to HU almost to BRCA2 WT levels. In contrast, BRCA2 NTD variants S273L and C315S displayed similar sensitivity to HU as the BRCA2-deficient cells (BRCA2^{-/-}) (Fig. 1f, Supplementary Fig. 3).

In conclusion, in the context of the full-length protein and in cells, the pathogenic mutation R3052W altering the DNA binding activity of

CTD renders cells sensitive to PARPi and MMC but not HU, whereas the VUS altering the DNA binding activity of the NTD (either dsDNA binding or both ssDNA and dsDNA binding) conferred moderate sensitivity to MMC and high sensitivity to HU, comparable to the BRCA2-deficient cells (Table 1).

BRCA2 co-localizes with nascent DNA and NTD, CTD variants and C-terminal mutant S3291A delay its recruitment to the fork

Given that the NTD variants confer HU sensitivity but their DSB repair activity appeared intact, we then tested whether BRCA2 was recruited to nascent DNA and whether or not the NTD variants altered this localization. To do so, we used a combination of click-chemistry with the thymidine analog EdU and in situ proximity ligation assay (PLA) to measure the association of proteins with nascent DNA³⁹. In this assay, the stable cell lines bearing BRCA2 WT or BRCA2 mutated forms are labeled with EdU, biotin is then conjugated to the EdU by click chemistry and PLA is used to detect BRCA2 in proximity to biotin-labeled nascent DNA. Consistent with previous results in *X. laevis*¹², we found that BRCA2 was in proximity to nascent DNA during unperturbed replication indicated by the presence of PLA foci (Fig. 2a). Upon a low dose of HU (0.2 mM) which is however sufficient to stall replication forks^{40,41}, the levels of BRCA2 WT associated with nascent DNA increased ~2-fold at 1 h treatment. To find out whether BRCA2 was specifically associated with nascent DNA we used thymidine chase experiments as previously described⁴¹ using the same set-up. As expected, the levels of PLA foci specific for histone H1-EdU were not altered at any time point following thymidine chase whereas the levels of PLA foci specific for PCNA-EdU, a protein that travels with the replication fork, were strongly reduced (Supplementary Fig. 4a). Thymidine chase strongly reduced the PLA signal of BRCA2-EdU in both unperturbed replication and replication stress conditions suggesting that at a large fraction of the BRCA2 pool is associated specifically with nascent DNA (Fig. 2b).

Similar to BRCA2 WT, BRCA2-R3052W was associated with nascent DNA in both conditions although the overall PLA signal was

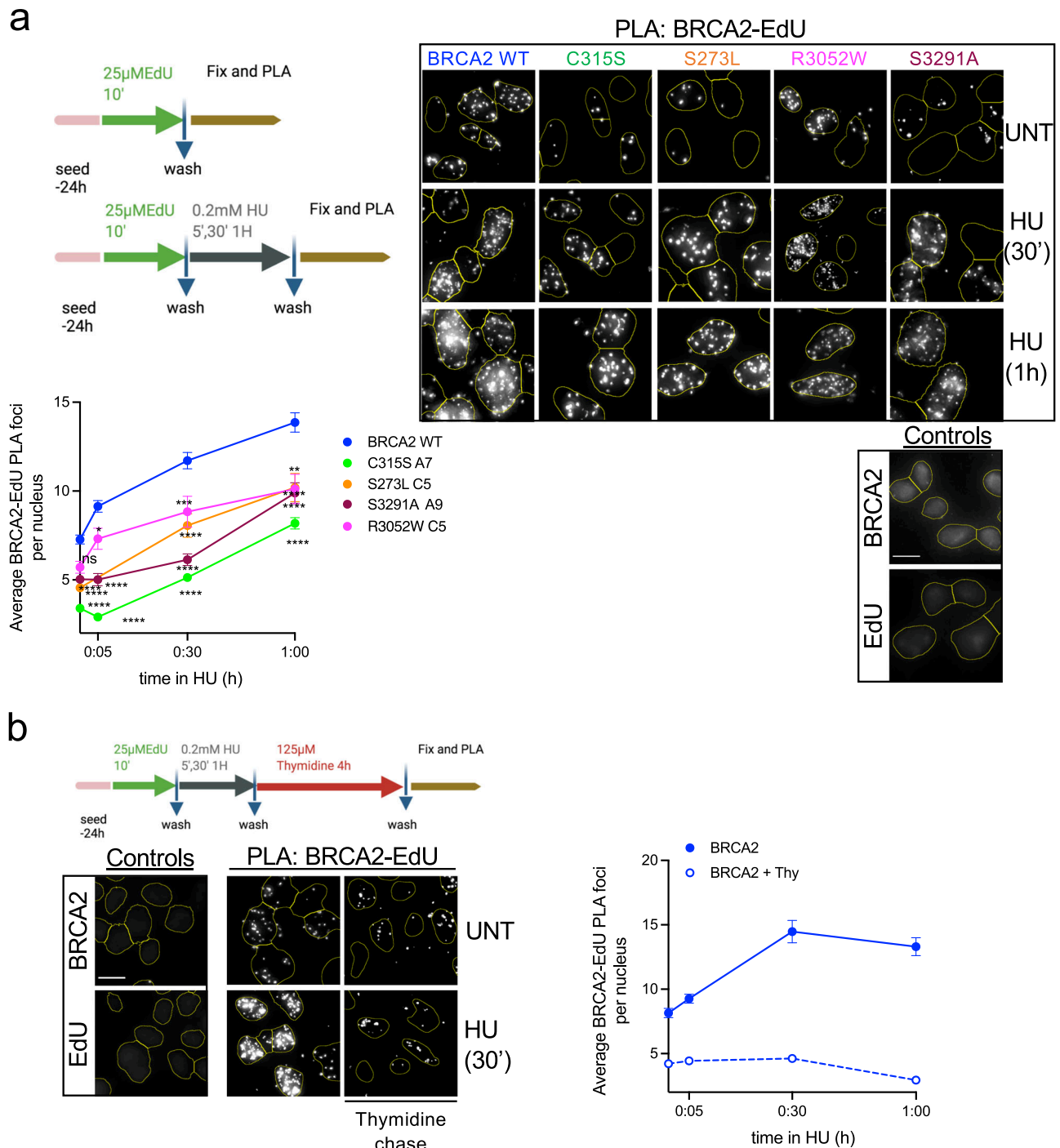
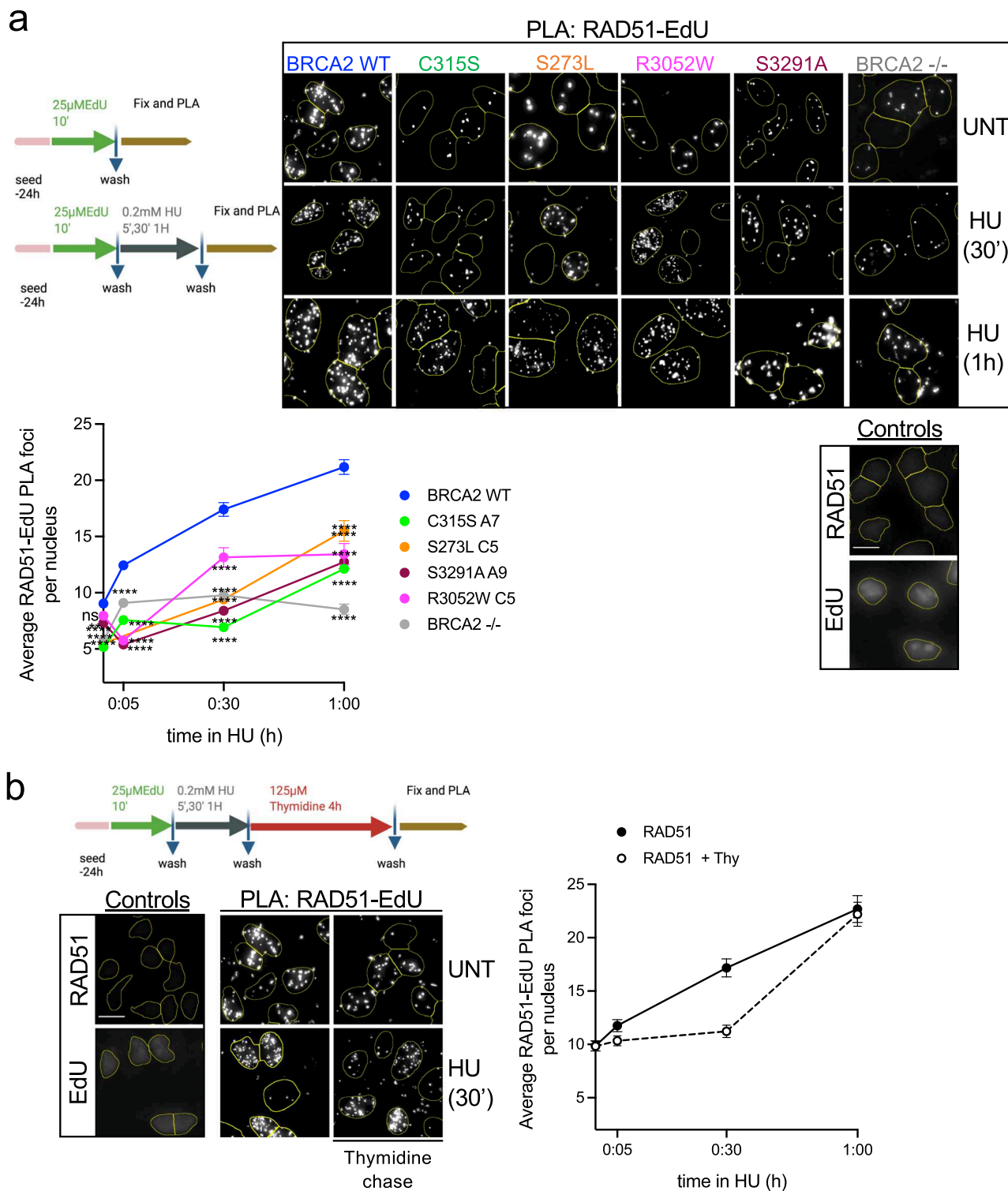


Fig. 2 | BRCA2 NTD and C-terminal domains contribute to BRCA2 location at nascent DNA. **a** (Top left) Scheme of the assay. (Top right): Representative images of in situ PLA on nascent DNA between biotinylated EdU detected with anti-biotin antibody and BRCA2-specific antibody in DLD1 BRCA2-deficient cells (BRCA2^{-/-}) stably expressing either BRCA2 WT or the variants C315S (A7), S273L (C5), R3052W, and S3291A mutant, as indicated. Cells left untreated (UNT) or treated with HU (30' or 1 h 0.2 mM) are shown. An individual signal is observed (focus) if the two probed proteins (BRCA2 and EdU-Biotin) are in close proximity (<40 nm). For all the experiments we carried out two single-antibody control (anti-BRCA2 and anti-biotin) to assess the specificity of the PLA signal. The scale bar indicates 10 µm. (Bottom) Quantification of the BRCA2 recruitment was measured as the number of PLA foci observed per nucleus. The data represent the mean + SEM with 200–300 cells analyzed in each experimental data set at each time point. The number of independent experiments performed was as follows: BRCA2 WT: (UNT *n* = 10; 5' *n* = 5; 30' *n* = 8; 1 h *n* = 7), C315S: (UNT *n* = 6; 5' *n* = 3; 30' *n* = 5; 1 h *n* = 5); S273L: (UNT *n* = 4; 30' *n* = 2; 1 h *n* = 2); S3291A: (UNT *n* = 3; 5' *n* = 2; 30' *n* = 2; 1 h *n* = 2); R3052W:

(UNT *n* = 6; 5' *n* = 3; 30' *n* = 3; 1 h *n* = 3). Statistical difference was determined by the Kruskal–Wallis test followed by Dunn's multiple comparison test. The *p*-values show significant differences compared to the BRCA2 WT clone. ns, not significant (*p* = 0.7539 in UNT BRCA2 WT vs. R3052W), **p* < 0.05 (*p* = 0.0136 at 5' BRCA2WT vs. R3052W), ***p* < 0.01 (*p* = 0.0042 at 1 h BRCA2WT vs. R3052W), ****p* < 0.001 (*p* = 0.0002 at 30' BRCA2WT vs. R3052W), *****p* < 0.0001). **b** (Left) Scheme of the assay and representative images of in situ PLA on nascent DNA between biotinylated EdU detected with anti-biotin antibody and BRCA2-specific antibody in DLD1 BRCA2 WT cells after 4 h Thymidine chase in cells left untreated or treated with HU (30' 0.2 mM). (Right) Quantification of the BRCA2 recruitment measured as the number of PLA foci observed per nucleus after 4 h Thymidine chase in BRCA2 WT cells at different time points. The data represent the mean + SEM of two independent experiments with 200–300 cells analyzed in each experimental data set at each time point. Schemes of the PLA assay created with BioRender.com. Source data are provided as a Source Data file.



reduced (Fig. 2a). Next, we generated cell lines expressing a mutant of BRCA2 located at the extreme C-terminus of BRCA2, S3291A (Supplementary Fig. 4b), which reduces RAD51 oligomer binding⁴² and was previously shown to impair replication fork protection⁷. Although present at the fork, the overall proximity of BRCA2-S3291A mutant to nascent DNA was considerably reduced (2-fold reduction after 30 min of HU treatment). A similar trend was observed for cells bearing BRCA2-S273L. Interestingly, cells expressing BRCA2-C315S showed an ever further reduction at all time points compared to the other cell lines (Fig. 2a).

The cell growth differences between the clones could have an impact on the levels of EdU incorporation; therefore, we controlled for the replication levels by performing biotin-biotin PLA⁴³. No significant difference was observed in the EdU PLA signal in cells expressing BRCA2 WT compared to C315S, S273L, R3052W, or S3291A (Supplementary Fig. 4c). Importantly, we performed this assay in stable clones that show similar or higher levels of BRCA2 protein than the WT cells (Supplementary Fig. 2a) discarding BRCA2 variants protein levels as a possible cause for the reduction of the PLA signal observed in these cells.

Fig. 3 | RAD51 efficient recruitment to nascent DNA requires BRCA2. **a** (Top) Scheme of the assay and representative images of in situ PLA on nascent DNA between biotinylated EdU detected with anti-biotin antibody and RAD51-specific antibody DLD1 BRCA2-deficient cells (BRCA2^{-/-}) or BRCA2^{-/-} stably expressing either BRCA2 WT or the variants C315S (A7), S273L (C5), R3052W, and S3291A mutant, as indicated. Cells left untreated (UNT) or treated with HU (30' or 1 h 0.2 mM) are shown. An individual signal is observed (focus) if the two probed proteins (RAD51 and EdU-Biotin) are in close proximity (<40 nm). For all the experiments we carried out two single-antibody control (anti-RAD51 and anti-biotin) to assess the specificity of the PLA signal. The scale bar indicates 10 μm. (Bottom) Quantification of RAD51 recruitment was measured as the number of PLA foci observed per nucleus. The data represent the mean + SEM with 200–300 cells analyzed in each experimental data set at each time point. The number of independent experiments performed was as follows: BRCA2 WT: (UNT $n = 9$, 30' $n = 4$, 30' $n = 8$, 1 h $n = 8$); C315S: (UNT $n = 7$, 30' $n = 2$, 30' $n = 4$, 1 h $n = 5$); S273L: (UNT $n = 3$, 30'

$n = 2$, 1 h $n = 2$); S3291A: (UNT $n = 4$, 30' $n = 3$, 30' $n = 2$, 1 h $n = 2$); R3052W: (UNT $n = 5$, 30' $n = 3$, 30' $n = 3$; 1 h $n = 3$); BRCA2^{-/-}: (UNT $n = 3$, 30' $n = 3$, 30' $n = 3$, 1 h $n = 3$). Statistical difference was determined by the Kruskal–Wallis test followed by Dunn's multiple comparison tests; the p -values show significant differences compared to the BRCA2 WT clone. ns not significant, ** $p < 0.01$ ($p = 0.0058$ at NT BRCA2 WT vs. S3291A), **** $p < 0.0001$. **b** (Left) Representative images of in situ PLA on nascent DNA between biotinylated EdU detected with anti-biotin antibody and RAD51-specific antibody in DLD1 BRCA2 WT cells after 4 h Thymidine chase in cells left untreated or treated with HU (30' 0.2 mM). (Right) Quantification of RAD51 recruitment measured as the number of PLA foci observed per nucleus after 4 h Thymidine chase in BRCA2 WT cells. The data represent the mean + SEM of two independent experiments with 200–300 cells analyzed in each experimental data set at each time point. Schemes of the PLA assay were created with BioRender.com. Source data are provided as a Source Data.

These results suggest that the NTD and the RAD51 binding site at the C-terminal region contribute to the recruitment of BRCA2 to nascent DNA.

RAD51 efficient recruitment to nascent DNA requires BRCA2

BRCA2 is a loader of RAD51 at DSBs^{3,22,44}. At stalled replication forks, BRCA2 protects the DNA from nucleolytic degradation, a function that is thought to be achieved by stabilizing RAD51 filaments through its C-terminal oligomeric-RAD51 binding site^{6,7}; whether and how RAD51 loading by BRCA2 takes place at stalled forks intermediates remains poorly defined. *Xenopus* Brca2 has been previously reported as being required for Rad51 recruitment at replicative chromatin¹². Because the mutated forms of BRCA2 affecting the different regions were less abundant than BRCA2 WT at active or stalled replication forks, we tested whether the recruitment of RAD51 was also altered in these cells. We monitored the RAD51-EdU PLA signal at different time points using the same conditions as for BRCA2-EdU PLA experiments (HU 0.2 mM). BRCA2-deficient cells showed 2-fold reduced recruitment of RAD51 to nascent DNA compared to BRCA2 WT cells (Fig. 3a). RAD51 recruitment to nascent DNA was delayed for cell lines bearing R3052W, S3291A, C315S, and S273L variants. RAD51 levels at nascent DNA also decreased in the thymidine chase experiment although to a lesser extent than BRCA2 indicating that RAD51 is bound to the chromatin as well as at the nascent DNA as previously shown^{8,41} (Fig. 3b).

Together, these results suggest that all three domains are important for the localization of RAD51 at active and HU-stalled replication forks. BRCA2-deficient cells did not completely abrogate the RAD51-EdU PLA signal suggesting there is some BRCA2-independent recruitment of RAD51 to the nascent DNA.

BRCA2 NTD, CTD, and the C-terminal RAD51 binding sites contribute to replication fork protection

BRCA2 stabilizes RAD51 filaments at stalled forks protecting them from nucleolytic degradation^{7,8}, defective protection results in stretches of ssDNA. Given the reduced recruitment to nascent DNA observed in cells expressing our variants, we next tested whether they were required for the protection of stalled forks using a DNA fiber assay. After two subsequent pulses of dNTP analogs IdU and CldU for 30 min to label nascent DNA as cells replicate, cells were treated with 5 mM HU for 4 h before fixation, a standard condition to reveal fork degradation/resection^{7,45}. Under these conditions, DLD1 BRCA2-deficient cells showed decreased CldU/IdU ratio compared to BRCA2 WT cells suggesting fork degradation as expected, however, the reduction in this cell system was much less pronounced than in other cell systems reported. Cells bearing R3052W, the CTD variant that impairs HR, S3291A, and C315S also reduced the CldU/IdU ratio although to a lesser extent than the BRCA2-deficient cells so that the differences with BRCA2 WT were not significant (Fig. 4a). Fork degradation may induce fork restart defects. To investigate this, we modified the labeling set up

to monitor fork restart under the same treatment conditions. We performed the first labeling with IdU for 20 min followed by HU treatment and then released the cells into CldU for 20 min and monitored fork restart using DNA combing. As the DNA fiber assay, this method allows the analysis of single DNA molecules aligned on a slide; however, in this case, the DNA stretching is performed at a constant speed⁴⁶. We found that ~50% of forks were able to restart upon release from HU in BRCA2 WT cells similar to previous reports^{7,47}. This was also the case for BRCA2-deficient cells and cells bearing the BRCA2 C315S variant (Fig. 4b).

Together, these results suggest that all three domains, NTD, CTD, and the C-terminal RAD51 binding site protect stalled replication forks from aberrant nucleolytic degradation. Under these conditions, neither BRCA2-deficient cells nor BRCA2 C315S cells displayed defects in replication fork restart.

BRCA2 contributes to the arrest of DNA replication under replication stress conditions

BRCA2-deficient cells challenged with mild doses of HU or multiple rounds of cisplatin fail to stall replication, which could be at the origin of ssDNA gap accumulation observed previously^{13,14}. Given the sensitivity to HU of cells expressing BRCA2-C315S, we monitored the replication track length in HU conditions using DNA combing. Following the first pulse with IdU, we added CldU in the presence or absence of 0.5 mM HU for 2 h, as previously described¹⁴. Under these conditions, replication forks were stalled in BRCA2 WT cells resulting in a 5-fold reduction of CldU track length compared to the non-treated conditions (median: 32 μm in UNT vs. 6 μm in HU) (Fig. 5a.i). DLD1 BRCA2-deficient cells showed already a reduced track length in the absence of HU compared to BRCA2 WT cells indicating an overall slower replication in these cells as previously reported⁴⁸. BRCA2-deficient cells also reduced the track length upon HU treatment although to a lesser extent (~2.5-fold) than BRCA2 WT cells (Fig. 5a.i) (median track length = 28 μm in UNT vs. 11 μm in HU). This defect was further revealed when representing the difference of the mean CldU track length between untreated and HU-treated conditions in the BRCA2-deficient cells compared to that in BRCA2 WT cells (26 in WT vs. 17 in BRCA2^{-/-}) (Fig. 5a.ii). All cells expressing BRCA2 C315S, R3052W, or S3291A also arrested the progression of the fork following HU treatment although there was a very mild defect in BRCA2-C315S bearing cells (3.4-fold reduction in track length compared to 5-fold reduction in BRCA2 WT cells). Interestingly, S273L cells showed 3.1-fold reduction in CldU track length, close to the levels of BRCA2-deficient cells suggesting a defective arrest.

These results suggest that in our isogenic cellular settings (DLD1 p53-mutated cell line), BRCA2 is partly required to arrest replication forks upon HU-induced replication stress. Moreover, neither the CTD nor the dsDNA binding activity of the NTD nor the C-terminal RAD51 binding site of BRCA2 seem specifically

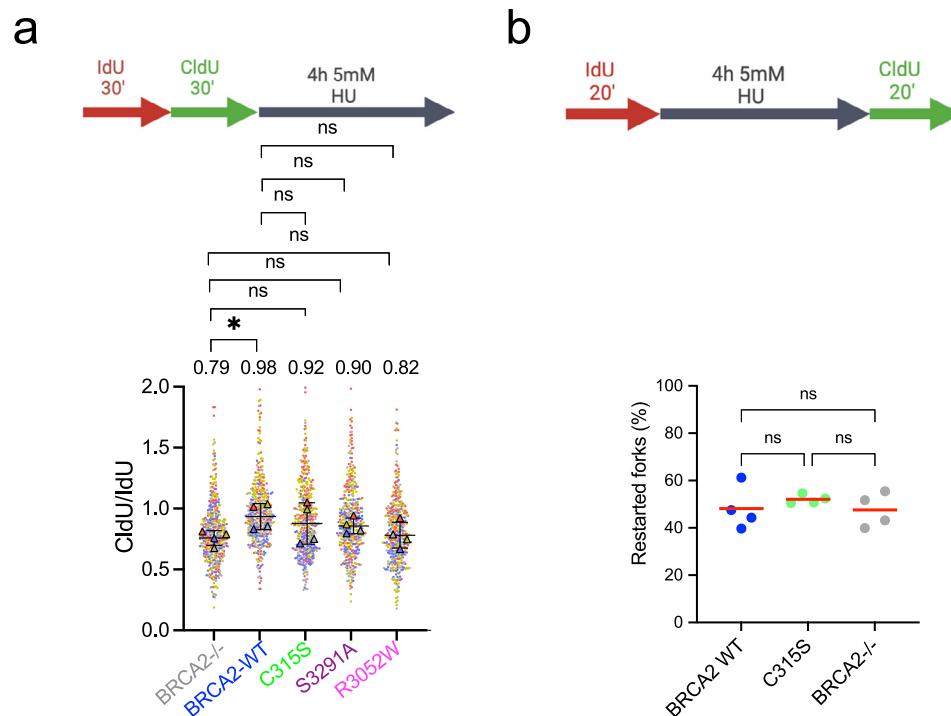


Fig. 4 | Different domains of BRCA2 contribute to replication fork protection. **a** Labeling scheme of thymidine analogs (IdU and CldU) followed by HU treatment. DLD1-BRCA2-deficient cells complemented with the BRCA2 WT and mutated forms of BRCA2 were labeled with IdU (30 min) and then with CldU (30 min) followed by 4 h treatment with 5 mM HU, as indicated, after which cells were processed for DNA fiber analysis. Quantification of the track length ratio of CldU vs. IdU. Individual experiments are represented as a scatter plot with a different color from 100 replication tracks per data set. The super plot representation superimposes the summary statistics from the four independent experiments on top of the data from all cells. Differences between experiments were calculated using one-way ANOVA

with Dunnett's multiple comparison tests on the mean of each experiment. ns, not significant, * $p < 0.05$ ($p = 0.0414$). **b** Schematic of the single-molecule DNA fiber tract analysis to detect fork restart after HU treatment. Quantification of restarted forks in BRCA2-deficient DLD1 cells, BRCA2 WT cells, or cells bearing the BRCA2 C315S variant, as indicated. Data are from four independent experiments; the percentage was calculated expressing the presence of CldU adjacent to IdU and was established on 200–500 tracks scored for each data set. The horizontal red line represents the mean. Statistics: Kruskal–Wallis test followed by Dunn's multiple comparison test. (ns, not significant). Labeling schemes created with BioRender.com. Source data are provided as a Source Data file.

required for this function whereas the ssDNA binding activity of the NTD might play a role.

BRCA2 dsDNA binding activity is required to limit HU-induced ssDNA gaps but not PARPi-induced ssDNA gaps

BRCA2-deficient cells show high levels of ssDNA gaps that are accentuated under mild replication stress conditions such as treatment with 0.5 mM HU^{12,14,16,20}. Given the HU sensitivity of cells expressing BRCA2-C315S and BRCA2-S273L, we wondered whether these cells accumulated ssDNA gaps under replicative stress. Hence, we subjected the cells to HU using previous conditions (Fig. 5a) now incorporating an extra step in the labeling scheme where we incubated the cells with S1 nuclease for 30 min (Fig. 5b top); this enzyme creates nicks in ssDNA regions without altering the dsDNA⁴⁷. As described in previous reports in different cell systems^{14,16,20}, DNA tracks in DLD1 BRCA2-deficient cells displayed high sensitivity to S1 nuclease as manifested by the shortening of the CldU track length, this was in contrast to the BRCA2 WT cells where the track length was only mildly reduced (Fig. 5b). Importantly, CldU-labeled nascent DNA tracks from cells bearing the BRCA2-C315S variant showed high sensitivity to S1 treatment suggesting that these cells accumulate ssDNA gaps after mild HU-induced replication stress. This was also the case for the other NTD variant S273L. In stark contrast, the CldU track length in cells bearing BRCA2 R3052W (CTD mutant) or BRCA2 S3291A (RAD51 C-terminal binding site) did not vary compared to the untreated conditions. We also performed this experiment in unchallenged conditions but in this case, only BRCA2-deficient cells displayed detectable ssDNA gaps (Supplementary Fig. 5). These

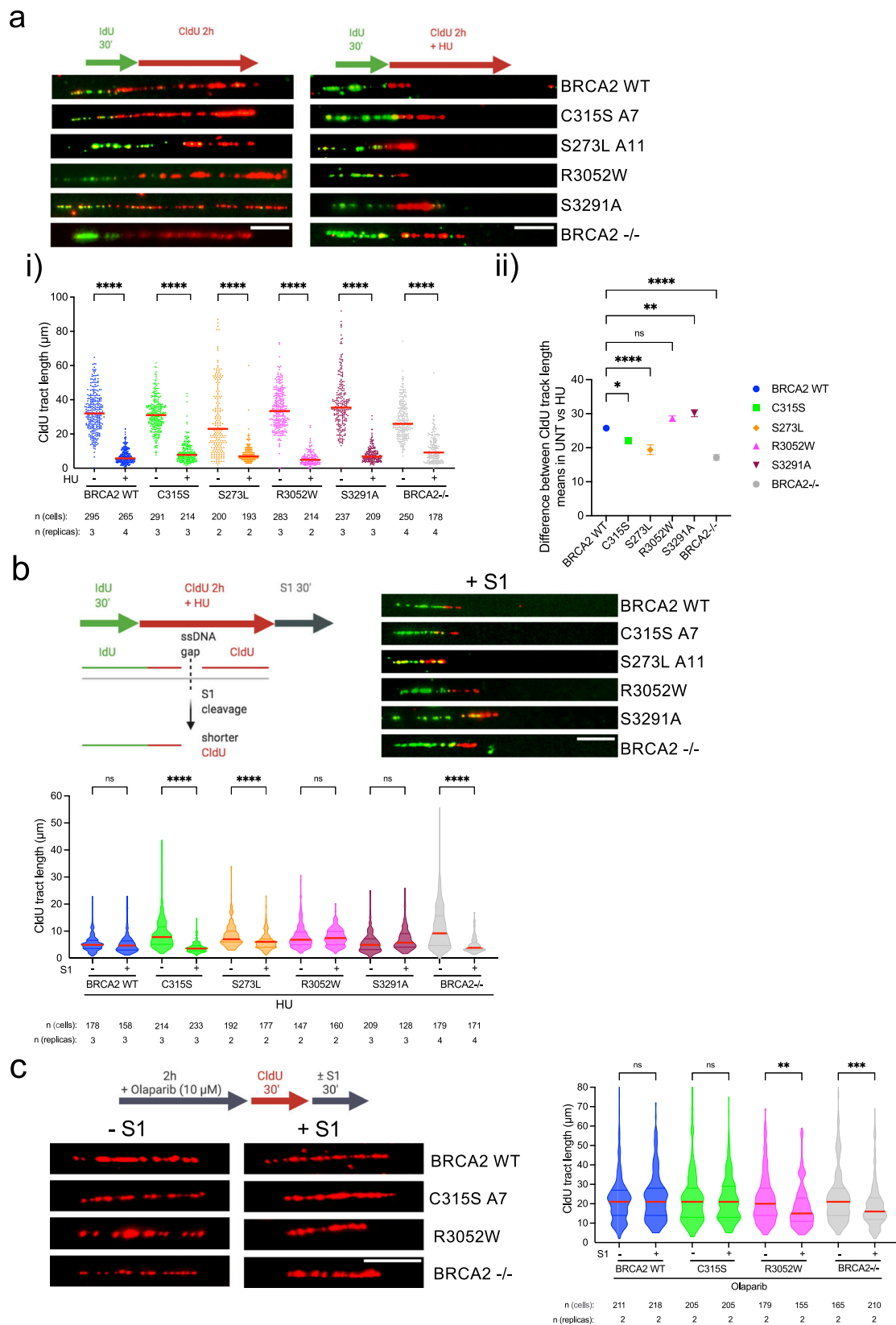
results suggest that the NTD and specifically its dsDNA binding activity, impaired in BRCA2 C315S, is required to prevent ssDNA gap formation upon mild HU-induced replication stress.

Given that PARPi has been shown to generate ssDNA gaps¹¹ and the fact that only cells bearing R3052W but not C315S are sensitive to PARPi, we then assessed the presence of ssDNA gaps upon PARPi treatment (2 h 10 μ M Olaparib) in these cells. As recently reported in a different cell system, BRCA2-deficient DLD1 cells showed high sensitivity to S1 treatment suggesting the accumulation of ssDNA gaps under these conditions. Similarly, cells bearing BRCA2-R3052W displayed ssDNA gaps. In stark contrast, the CldU track length of cells expressing BRCA2-C315S did not change, similarly to BRCA2 WT cells (Fig. 5c). These results perfectly correlate with the sensitivity of these cells to PARPi (Fig. 1c).

Together, cells expressing the NTD variants BRCA2-C315S and BRCA2-S273L display ssDNA gaps upon nucleotide depletion manifested by sensitivity to S1 nuclease that is not observed in cells bearing the R3052W CTD variant nor in cells expressing the C-terminus RAD51 binding mutant S3291A. In contrast, cells expressing R3052W CTD variant but not the NTD variants display PARPi-induced ssDNA gaps.

BRCA2-C315S activates ATR/CHK1 upon RS but is deficient in ssDNA gap repair via HR

ssDNA gaps in BRCA2-deficient cells challenged with replication stress may arise due to a defect in arresting fork progression^{14,49}. Fork arrest following a replication insult triggers the activation of the checkpoint kinase ATR/CHK1^{50,51}. We monitored the checkpoint activation in our cells under the replication stress conditions used to detect ssDNA gaps



(0.5 mM HU for 2 h). In our cell system (DLD1 cells, p53 mutated), BRCA2-deficient cells displayed only a small reduction in the activation of ATR/CHK1 compared to BRCA2 WT cells as detected by the levels in pS345-CHK1 (Fig. 6a). BRCA2-C315S showed increased levels of pCHK1 compared to BRCA2-WT cells, consistent with the increased number of ssDNA gaps in these cells (Fig. 5b). This effect was not due to a net

increase in S-phase cells (Fig. 6b, Supplementary Fig. 6a); these results agree with the functional fork arrest observed in BRCA2-C315S cells upon HU treatment (Fig. 5a).

ssDNA gaps may also persist as a consequence of a defect in their repair. We have previously shown that the dsDNA binding activity of the NTD is specifically required to stimulate the recombination activity

Fig. 5 | BRCA2 variants affecting dsDNA binding display ssDNA gaps despite being able to arrest replication upon HU treatment. **a** (Top) Labeling scheme of thymidine analogs (IdU and CldU) in the absence or presence of HU and representative images of the replication tracks labeled as indicated from DLD1 BRCA2-deficient cells (BRCA2^{-/-}) or BRCA2^{-/-} stably expressing either BRCA2 WT or the variants BRCA2-C315S (A7), BRCA2-S273L (A11), BRCA2-R3052W and BRCA2-S3291A mutant, as indicated, in unperturbed (left) or 0.5 mM HU-treated condition (right). The scale bar indicates 10 μ m. **i** Quantification of CldU track length in the cell lines in **(a)**. Data represent the median of two or more independent experiments per condition (details in the figure). Statistical difference was determined by the Kruskal–Wallis test followed by Dunn’s multiple comparison test (all **** $p < 0.0001$), (the p -values show the significant differences compared to the untreated conditions). **ii** Quantification of the difference of the mean CldU track length in –HU vs. +HU. One-way ANOVA with Tukey’s multiple comparison tests was performed on the difference between the means + SEM from an unpaired t -test calculated for each cell line separately. ns, not significant, * $p < 0.05$ ($p = 0.0310$), ** $p < 0.01$ ($p = 0.0064$), all **** $p < 0.0001$. **b** (Top left) Labeling scheme of thymidine analogs (IdU and CldU) in presence of HU followed by S1 nuclease treatment and schematic of the reduced CldU track length resulting from S1 cleavage at an ssDNA

region. (Top right) Representative images of the replication tracks labeled of the indicated cell lines in **(a)** in 0.5 mM HU treated condition followed by 30 min of S1 nuclease (or S1 buffer only) treatment, as indicated. The scale bar indicates 10 μ m. (Bottom) Quantification of CldU track length in cells from **(b top right)**. Data represent the median + 25% and 75% quartiles of two or more independent experiments per condition (details in the figure). Statistical difference was determined by the Kruskal–Wallis test followed by Dunn’s multiple comparison test (ns, not significant, all **** $p < 0.0001$). See also Supplementary Fig. 5. **c** (Left) Labeling scheme and representative images of the replication tracks labeled as indicated from BRCA2-deficient cells (BRCA2^{-/-}) alone or stably expressing either BRCA2-WT, BRCA2-C315S (A7), BRCA2-R3052W, in 10 μ M Olaparib treated condition followed by 30 min of S1 nuclease (or S1 buffer only) treatment, as indicated. The scale bar indicates 10 μ m. (Right) Quantification of CldU track length in cells from **(c left)**. Data represent the median + 25% and 75% quartiles of two independent experiments with the number of fibers analyzed detailed in the figure: Statistical difference was determined by the Kruskal–Wallis test followed by Dunn’s multiple comparison test. ns, not significant, ** $p < 0.01$ ($p = 0.0035$), *** $p < 0.001$ ($p = 0.0007$). Labeling schemes were created with BioRender.com. Source data are provided as a Source Data file.

of RAD51 in vitro at dsDNA/ssDNA containing DNA substrates and that this activity is defective in the NTD fragment mutated at C315S in vitro (BRCA2_{NTD-C315S}). Using an ssDNA substrate, BRCA2_{NTD-C315S} showed intact RAD51-mediated DNA strand exchange stimulation. These results suggested that BRCA2 dsDNA binding activity was required to stimulate recombination at dsDNA-containing substrates such as resected DNA or ssDNA gaps. We also showed that BRCA2_{NTD} could bind gapped DNA substrates in vitro²⁸. Given that the repair of ssDNA gaps by template switching is thought to involve BRCA2 and RAD51^{18,19,24,25,52} we wondered whether BRCA2-C315S cells were defective in the repair of ssDNA gaps. To test this hypothesis, we produced and purified BRCA2_{NTD} and BRCA2_{NTD-C315S} fragments from human cells, RAD51, and RPA from bacteria and used synthetic radio-labeled oligonucleotides that mimic an ssDNA gap to reconstitute an ssDNA gap recombination repair reaction in vitro. For comparison, we performed a 3'-tail reaction using the same donor dsDNA sequence to avoid sequence-dependent effects. To generate the ssDNA gap substrate, we used a set of three synthetic oligonucleotides that anneal at the two ends of a 167mer leaving an ssDNA stretch of 83 nucleotides (nt) (gap) in the middle. In this reaction, the ssDNA gap or the tailed substrate is first coated with RPA, and RAD51 is subsequently incubated with this complex in the presence or absence of BRCA2_{NTD} (or BRCA2_{NTD-C315S}) before adding the radiolabeled dsDNA donor. As expected, in the absence of RPA, RAD51 could perform DNA strand exchange on this synthetic-tailed substrate whereas when RPA was allowed to bind first, the reaction was strongly inhibited (Supplementary Fig. 6b). The same was true for the gapped DNA (Fig. 6c). As there is no 3'-overhang in this substrate and the dsDNA donor contains blunt ends, this result indicates that RAD51 can readily invade the template strand from an ssDNA gap without the need of an ssDNA 3'-end.

As previously shown for the tailed-substrate with a different dsDNA donor²⁸, BRCA2_{NTD} stimulated RAD51-driven strand exchange reaction overcoming RPA inhibition whereas BRCA2_{NTD-C315S} did not (Supplementary Fig. 6b). Importantly, BRCA2_{NTD} was also able to stimulate RAD51-mediated recombination at ssDNA gap mimicking substrates by 2-fold in a concentration-dependent manner whereas BRCA2_{NTD-C315S} could not stimulate the reaction even at the highest concentration tested (Fig. 6c). We previously showed that the CTD alone stimulates poorly RAD51-mediated DNA strand exchange in these experimental conditions²⁸ and therefore was not tested.

In conclusion, BRCA2-C315S expressing cells display functional ATR/CHK1 checkpoint activation. BRCA2_{NTD} stimulates RAD51-mediated ssDNA gap repair in vitro, a function that is impaired in BRCA2_{NTD-C315S}.

BRCA2-C315S cells display increased chromatid gaps in metaphase

ssDNA gaps near arrested replication forks may persist through mitosis or can be converted into DSBs^{15,53}. These lesions are expected to cause structural chromosomal aberrations such as chromatid breaks or complex chromosomal aberrations like radials and chromosome fusions which are well documented in HU-treated BRCA2-deficient cells^{6,48,54}. We thus analyzed metaphase chromosome spreads in our BRCA2-C315S-mutated cell lines either left untreated or treated with mild HU (0.5 mM 2 h) or acute HU (5 mM for 5 h) before releasing them into colcemid. As expected, DLD1 BRCA2-deficient cells displayed an increased number of chromosomal aberrations already in untreated conditions²⁷. This phenotype was mainly contributed by chromosome gaps, radial chromosomes, and fusions and it was exacerbated in the HU-treated cells (Fig. 7ai). In contrast, the levels of chromosomal aberrations in DLD1 BRCA2 WT cells were very limited (about 1 aberration per metaphase) in untreated conditions and the average number of aberrations did not change with HU although the counts per metaphase increased. Interestingly, cells bearing BRCA2-C315S showed an increased number of chromosomal aberrations in unchallenged conditions compared to BRCA2 WT cells and the difference was further accentuated in HU-treated cells (Fig. 7a i). Remarkably, the number of chromatid gaps per metaphase spread was as abundant in BRCA2-C315S cells as in BRCA2-deficient cells in unperturbed conditions or after treatment with mild replication stress (0.5 mM HU 2 h) or the acute dose of HU (5 mM 5 h), consistent with the presence of replication-associated gaps in these cells (Fig. 7a ii, Fig. 5b).

Finally, replication-associated gaps may result in regions of unreplicated DNA that could lead to chromatin bridges in anaphase. Therefore, we analyzed the presence of chromosome segregation errors by looking at anaphase bridges as previously shown in BRCA2-deficient cells^{54,55}. We found a slight increase in the number of cells with anaphase bridges in the BRCA2-C315S cell line compared to BRCA2 WT cells measured in unperturbed conditions which were accentuated in BRCA2-deficient cells (Fig. 7b). However, the levels of anaphase bridges did not increase upon mild HU treatment neither in the BRCA2-deficient cells nor in BRCA2-C315S cells suggesting that these structures may not be a direct consequence of ssDNA gaps (Supplementary Fig. 7).

Together, these results suggest that cells expressing the BRCA2-C315S variant accumulate replication-associated ssDNA gaps that persist through mitosis as manifested in metaphase spreads. The levels of ssDNA gaps that accumulate in cells expressing BRCA2-C315S in mitosis are comparable to those found in BRCA2-deficient cells.

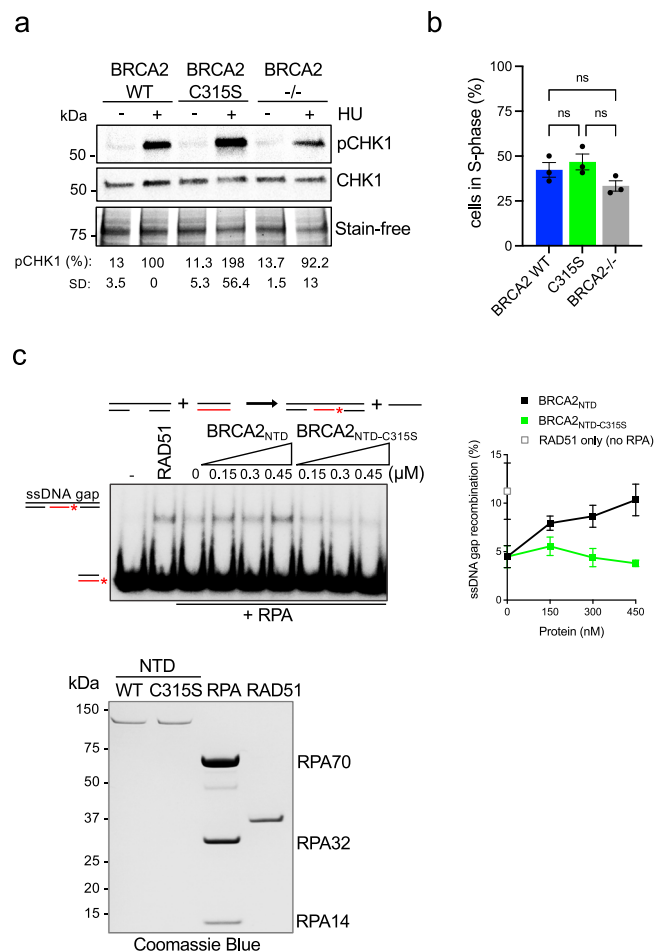


Fig. 6 | BRCA2-C315S cells show an active ATR checkpoint whereas NTD-C315S fragment shows reduced stimulation of RAD51-mediated ssDNA gap repair.

a (Left) Western blot showing the phosphorylation of CHK1 (pCHK1) after exposure to HU (0.5 mM, 2 h) as indicated in DLD1 BRCA2-deficient cells (BRCA2^{-/-}) or BRCA2^{-/-} cells stably expressing BRCA2 WT or the variant BRCA2-C315S. Stain-free cropped gel is used as the loading control. pCHK1 levels relative to the total CHK1 signal are shown below the blots, results are presented as a percentage of pCHK1/CHK1 compared to the BRCA2 WT clone treated with HU. The data represent the mean \pm SD of two independent experiments. **b** Frequency of S-phase cells in DLD1 BRCA2-deficient cells (BRCA2^{-/-}) or BRCA2^{-/-} cells stably expressing BRCA2 WT or the variant BRCA2-C315S. The data represent the mean \pm SEM of three independent experiments. Statistical difference was determined by the Kruskal–Wallis test followed by Dunn’s multiple comparison test (ns, not significant). See also Supplementary Fig. 6. **c** (Left) DNA strand exchange reaction using an ssDNA gap mimicking substrate (Table S1) in the presence or absence of RPA, RAD51, and increasing concentrations of BRCA2_{NTD-WT} or BRCA2_{NTD-C315S}, as indicated. (Right) Quantification of the reaction on the left. Data represent the mean from three independent experiments. Error bars SD. (Bottom) SDS-PAGE showing purified BRCA2_{NTD-WT} (1 μ g), BRCA2_{NTD-C315S} (1 μ g), RPA (3 μ g), and RAD51 (1.5 μ g) used in the DNA strand exchange reactions. Source data are provided as a Source Data file.

Discussion

Here we report that cells bearing a single amino acid variant of BRCA2, S273L, or C315S, that impair the DNA binding activity of BRCA2 at its N-terminal DNA binding domain (NTD)(Fig. 1b)²⁸, are highly sensitive to replication stress induced by HU. On the other hand, a pathogenic variant affecting the canonical DNA binding domain (CTD), R3052W³⁰, was resistant to HU treatment. Unlike R3052W, defective in DSB repair by HR and hypersensitive to PARP³⁰, variants at the NTD were resistant to PARPi and HR proficient based on a gene-targeting reporter assay³⁷ (Table 1).

Consistent with the sensitivity to HU, cells expressing the C315S and S273L variants reduced the localization of BRCA2 and RAD51 at both unperturbed or HU-challenged replication forks; this phenotype was also observed although to a different degree in the other variants/mutants analyzed. Cells expressing R3052W were highly sensitive to ICLs inducing agent MMC and resistant to HU as recently observed with another compound mutation at the CTD⁵⁶. However, unlike the compound mutation in the previous report, R3052W impaired HR. The strong effect of this pathogenic mutation might be due to the combined impact of R3052W on DNA binding and its predicted destabilization effect on the interface between oligonucleotide binding folds (OB) 2 and OB3 of the CTD^{29,57}. Indeed, cells bearing this variant also display a growth defect compared to the other cell lines used in this study.

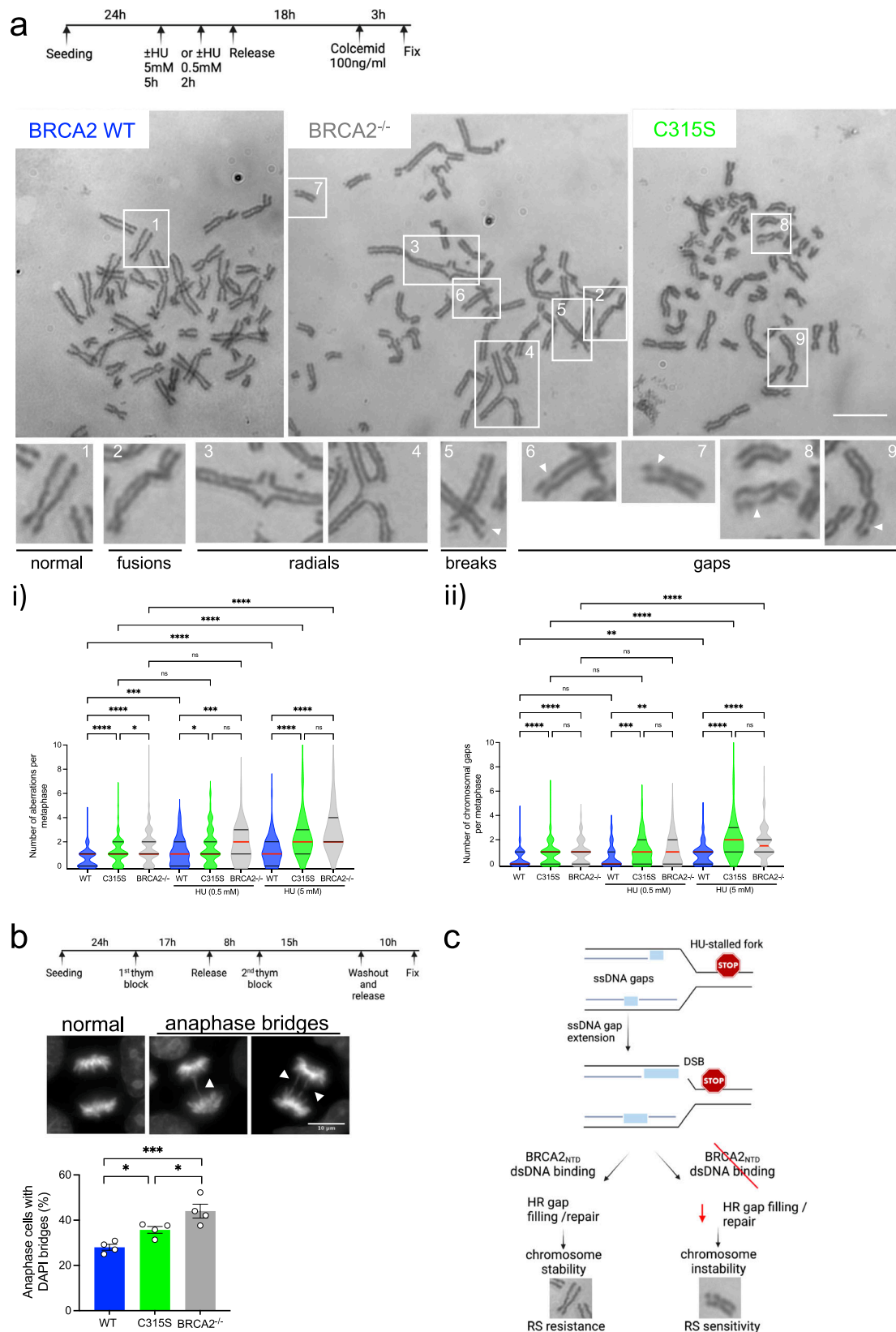
DLD1 BRCA2-deficient cells did not fully arrest replication forks upon mild replication stress (0.5 mM HU, 2 h) when assessed by DNA combing, although the effect was much more modest than the one reported¹⁴. This discrepancy may arise from the different cell systems utilized (DLD1 cells are p53 mutated and deficient in mismatch repair). However, it is important to note that the comparison between HU-treated cell lines might give rise to false interpretations as the basal replication fork track length among different cell lines might differ as we have observed. We, therefore, compared the difference of the mean between untreated and HU-treated conditions for each clone to compare the cell lines (Fig. 5a.ii). In doing so, we found that only one of the cell lines, the one expressing S273L, displayed a significant reduction in fork arrest capacity close to one observed in the BRCA2-deficient cells. These results suggest that BRCA2 contributes partially to fork arrest upon HU treatment and that the ssDNA binding activity of the NTD, impaired in cells bearing S273L, might be involved in this function.

Interestingly, despite the normal replication arrest and concomitant ATR activation, cells expressing BRCA2-C315S accumulated ssDNA gaps following replication stress as manifested by the sensitivity to S1 nuclease treatment and observed in metaphase spreads. The fact that BRCA2-C315S cells did not show a significant number of ssDNA gaps in unperturbed conditions whereas they were detected in similar numbers to those of the BRCA2 deficient cells in metaphase spreads suggests that the DNA combing and S1 nuclease may only detect a fraction of ssDNA gaps present in cells.

Overall, these findings are consistent with the recently proposed role of BRCA2 in gap suppression¹⁴ whereas it challenges the idea that fork arrest alone underlays gap suppression. Given that the NTD variant C315S is defective in dsDNA binding while preserving its ssDNA binding activity, these results strongly suggest that the dsDNA binding activity of BRCA2, unique to the NTD²⁸, is specifically required to suppress replication ssDNA gaps. Cells expressing S273L altering both ssDNA and dsDNA binding also presented ssDNA gaps reinforcing the idea that the NTD is involved in gap suppression. Moreover, the fact that all three variants tested showed similar defects in fork protection but neither cells expressing S3291A nor R3052W exhibited ssDNA gaps upon nucleotide depletion in this isogenic setting suggest that the fork protection function of BRCA2 can be uncoupled from its ssDNA gap suppression activity as recently proposed¹¹. These results are also consistent with a recent report in which the mutant S3291A in Chinese hamster cells was found devoid of ssDNA gaps¹⁴.

ssDNA gaps in BRCA2-deficient cells have been proposed to arise from PrimPol repriming^{13,21} or Okazaki fragment processing defects^{11,58}. The fact that we could not observe a substantial defect in replication fork arrest nor fork restart in cells bearing C315S is consistent with the latter however it requires future investigation.

ssDNA gaps are a substrate for repair by homologous recombination^{19,25,52}. Reconstitution of the ssDNA gap repair reaction in vitro indicated that RAD51 can perform strand invasion in this context without the need for a resected 3'-overhang, consistent with



the template switch model for repair¹⁸. Moreover, we found that in the presence of RPA-coated ssDNA, the NTD of BRCA2 could stimulate RAD51 recombination activity at ssDNA gaps. Interestingly, the capacity of BRCA2^{NTD-C315S} to promote recombination in ssDNA gaps-mimicking substrates in vitro was strongly reduced suggesting that the dsDNA binding activity of BRCA2 promotes ssDNA gap repair.

Interestingly, despite the HU-induced accumulation of ssDNA gaps, cells bearing the BRCA2-C315S variant showed resistance to PARPi, a chemotherapeutic drug that has been reported to accelerate replication⁵⁹ and cause ssDNA gaps in BRCA1/2-deficient cells¹¹. Importantly, analysis of the presence of ssDNA gaps in cells treated with PARPi indicated that cells expressing C315S do not accumulate

Fig. 7 | BRCA2-C315S cells accumulate gaps in metaphase chromosomes. **a** (Top) Schematic representation of the experiment timing and the dose of HU used to detect chromosomal aberrations. (Bottom) Representative images of metaphase spreads of DLD1 BRCA2-deficient cells (BRCA2^{-/-}) or BRCA2^{-/-} cells stably expressing BRCA2 WT or BRCA2-C315S (A7), as indicated, treated with 5 mM HU for 5 h. The type of chromosomal aberrations observed is indicated with numbers and magnified below. The scale bar indicated 10 μm. **i** Quantification of global chromosomal aberrations from the same cells either left untreated or upon treatment with HU (0.5 mM for 2 h or 5 mM for 5 h), as indicated. Statistical difference was determined by the Kruskal–Wallis test followed by Dunn’s multiple comparison test. ns, not significant, * $p < 0.05$ ($p = 0.0129$ in C315S vs. BRCA2^{-/-}, and $p = 0.044$ in WT 0.5 mM HU vs. C315S 0.5 mM HU), *** $p < 0.001$ ($p = 0.0002$ in WT vs. WT 0.5 mM HU, and $p = 0.0003$ in WT 0.5 mM HU vs. BRCA2^{-/-} 0.5 mM HU, **** $p < 0.0001$). **ii** Quantification of chromosomal gaps observed in the same cell lines. Data in (i) and (ii) represent the median and 25% and 75% quartiles of three independent experiments where 39–50 metaphase spreads were analyzed in each experimental data set. Only metaphases with at least 30 chromosomes were considered. Statistical difference was determined by the Kruskal–Wallis test followed by Dunn’s multiple comparison test. ns not significant, ** $p < 0.01$ ($p = 0.0011$ in WT 0.5 mM HU vs.

BRCA2^{-/-} 0.5 mM HU, and $p = 0.0019$ in WT vs. WT 5 mM HU), *** $p < 0.001$ ($p = 0.0002$), **** $p < 0.0001$). **b** (Top) Synchronization scheme and representative images of normal chromosome segregation stained with DAPI and type of aberrant chromosome segregation (DAPI bridges) that were observed in the DLD1 BRCA2 deficient cells (BRCA2^{-/-}) or BRCA2^{-/-} cells stably expressing BRCA2 WT or BRCA2-C315S (A7). The scale bar indicates 10 μm. (Bottom) Quantification of cells with aberrant chromosome segregation in BRCA2^{-/-} cells and in the BRCA2^{-/-} clones stably expressing BRCA2 WT, BRCA2-C315S, as indicated. Data represent the mean and SEM of four independent experiments: at least 150 anaphase cells were analyzed in each experimental data set. A two-way ANOVA test with Tukey’s multiple comparisons test was used to calculate the statistical significance of differences (normal vs cells with anaphase bridges, only cells with anaphase bridges are plotted in the graph). * $p < 0.05$ ($p = 0.048$ in WT vs. C315S, and $p = 0.0325$ in C315S vs. -/-), *** $p < 0.001$ ($p = 0.0001$). See also Supplementary Fig. 7. **c** Working model for the role of BRCA2 in the repair of replication-associated gaps following RS. Light blue rectangles represent ssDNA gaps. See text for details. Synchronization scheme and the model were created with BioRender.com. Source data are provided as a Source Data file.

PARPi-induced ssDNA gaps consistent with their resistance to PARPi. In contrast, cells expressing R3052W that were sensitive to PARPi displayed ssDNA gaps under these conditions. These findings reinforce the idea that PARPi-induced ssDNA gaps correlate with PARPi sensitivity as previously reported¹¹. Similarly, in our conditions, DSB repair capacity also correlates with PARPi resistance although in other works these two processes have been uncoupled. Along these lines, we show that HU-related gap suppression is separable from DSB repair capacity as cells expressing BRCA2-C315S or S273L are proficient in HR-mediated DSB repair but sensitive to HU. Moreover, ssDNA gaps do not necessarily result in DSBs as we mainly observe chromatid discontinuities without misalignment in metaphase spreads indicative of ssDNA gaps⁶⁰. Interestingly, as two different variants led to gaps in the presence of one agent but not the other, these results suggest that nucleotide depletion and PARPi induce different types of ssDNA gaps that in turn require distinct gap-filling mechanisms. These differences might be due to the nature of the DNA ends and/or the incorporation of ribonucleotides as has been described for the former⁶¹. Based on our results we propose that HU-induced ssDNA gaps are filled-in preferentially via HR/TS mechanisms.

Putting together our in vitro and cell-based results and our previous findings²⁸ in the context of the literature we propose a model (Fig. 7c) in which (a) BRCA2 localizes at unperturbed and stalled replication forks participating in the loading of RAD51 at these sites. (b) Upon nucleotide depletion-induced replication stress, BRCA2 protects replication forks from nucleolytic degradation, a function that is probably achieved through different domains including both DNA binding domains, CTD and NTD, and the C-terminal RAD51 binding site. (c) In contrast, BRCA2 gap suppression activity is particularly dependent on its dsDNA binding activity, located at the NTD which promotes the repair of the resulting replication-associated ssDNA gaps by RAD51. (d) Unrepaired replication-associated lesions in BRCA2-C315S cells lead to abundant chromatid discontinuities or gaps, especially in acute replication stress conditions, explaining their HU sensitivity.

Based on our results with BRCA2-C315S, BRCA2-S273L, and BRCA2-R3052W cells, we propose that the repair of DSBs requires the ssDNA binding activity via the canonical CTD of BRCA2 whereas the NTD is dispensable/redundant for this function.

Our data are consistent with C315S and S273L being separation of function variants defective in ssDNA gap suppression and replication-associated ssDNA gap repair/fill-in but not in the repair of DSBs.

Our findings may have clinical implications for the assessment of variants of unknown clinical significance (VUS) located at the NTD as defects in HR-repair of replicative lesions would not be picked up by

the current methods to assess HR proficiency^{30,57,62} as exemplified in the case of BRCA2-C315S or BRCA2-S273L, but may nonetheless be linked to cancer predisposition given the genome instability observed in cells bearing these variants.

Methods

Plasmids

Human 2XMBP-BRCA2_{250–500} and EGFP-MBP-BRCA2 subcloning in pHCMV1 expression vector were generated as described^{28,63}.

Site-directed mutagenesis

Point mutations (C315S, S273L, S3291A) were introduced in 2xMBP-BRCA2_{250–500}, EGFP-MBP-BRCA2 vector using QuikChange II and QuikChange XL site-directed mutagenesis kit (Agilent Technologies), respectively, as previously described^{28,30}.

Mutagenesis primers were designed using the QuickChange Primer Design program and purchased from MWG Eurofins. All mutations were verified by Sanger sequencing.

Cell lines, cell culture

The human cell lines HEK293-T cells (gift from Dr. Mounira Amor-Gueret) were cultured in DMEM (Eurobio Abcys, Courtaboeuf, France) media containing 25 mM sodium bicarbonate and 2 mM L-glutamine supplemented with 10% FBS (EuroBio Abcys). The BRCA2-deficient colorectal adenocarcinoma cell line DLD1 BRCA2^{-/-31} (HD 105-007) and the parental cell line DLD1 BRCA2^{+/+} (HD-PAR-008) were purchased from Horizon Discovery (Cambridge, England). The cells were cultured in RPMI media (EuroBio Abcys) containing 25 mM sodium bicarbonate and 2 mM L-glutamine (EuroBio Abcys) Supplemented with 10% FBS (EuroBio Abcys). The DLD1 BRCA2^{-/-} cells were maintained in growth media containing 0.1 mg/ml hygromycin B (Thermo Fisher Scientific). The stable cell lines of DLD1^{-/-} BRCA2-deficient cells expressing BRCA2 WT or variants of interest generated in this study were cultured in growth media containing 0.1 mg/ml hygromycin B (Thermo Fisher Scientific) and 1 mg/ml G418 (Sigma-Aldrich).

All cells were cultured at 37 °C with 5% CO₂ in a humidified incubator and all cell lines used in this study have been regularly tested for mycoplasma contamination (MycAlert, Lonza) and genotyped using GenePrint kit (Promega).

Stable cell line generation

To generate DLD1 BRCA2^{-/-} stable cell lines expressing human BRCA2 variants of interest we transfected one 100 mm plate of DLD1 BRCA2^{-/-} cells at 70% of confluence with 10 μg of a plasmid containing human EGFP-MBP-tagged BRCA2 cDNA (carrying mutation of interest) using

TurboFect (Thermo Fisher Scientific) according to manufacturer's instructions; 48 h post-transfection the cells were serially diluted and cultured in media containing 0.1 mg/ml hygromycin B (Thermo Fisher Scientific) and 1 mg/ml G418 (Sigma-Aldrich) for selection. Single-cell colonies were isolated and later expanded and their genomic DNA was extracted to verify the mutation by sequencing. BRCA2 protein levels were detected by Western Blot using BRCA2 antibody (1:1000, OP95, EMD Millipore).

Western blotting

Cellular pellet was lysed in lysis buffer (50 mM HEPES pH 7.5, 250 mM NaCl, 5 mM EDTA, 1% NP-40, 1 mM DTT, 1 mM PMSF, 1X protease inhibitor cocktail (Roche)) and cells were incubated on ice for 30 min, vortexed every 5 min. Lysates were centrifuged at $18,000 \times g$ for 1 h at 4 °C. The supernatant was transferred to a prechilled Eppendorf tube and stored at -80 °C. For protein electrophoresis, samples were heated in 1× SDS sample buffer for 5 min at 95 °C, loaded on a stain-free 4–15% SDS gel (Bio-Rad), and migrated at 130 V for 90 min in running buffer (1x Tris-Glycine, 0.1% SDS). The stain-free gel was visualized using a ChemiDoc camera (Bio-Rad). For transfer, a nitrocellulose membrane (VWR) was pre-equilibrated in dH₂O and transfer buffer (1x Tris-Glycine, 0.025% SDS, 10% methanol). The proteins were transferred for 2 h at 0.35 A at 4 °C. The membrane was blocked in 5% milk in 1× TBS-T at room temperature for 30 min and then incubated with the respective antibody (see antibodies below) in 5% milk in 1× TBS-T overnight at 4 °C. After extensive washes in TBS-T (3 × 10 min), the membrane was incubated for 1 h with the appropriate secondary HRP-antibody at room temperature on a shaker. After 3 more washes in TBS-T, the membrane was developed using ECL prime western blotting detection reagent (VWR) and visualized using a ChemiDoc camera (Biorad).

Antibodies used for western blotting

Mouse anti-MBP (1:5000, R29, Cat. #MA5-14122, Thermo Fisher Scientific), mouse anti-BRCA2 (1:1000, OP95, EMD Millipore), mouse anti-CHK1 (1:1000, Cat. #2360, Cell Signaling Technology), rabbit anti-pCHK1-S345 (1:500, Cat #2348, Cell Signaling Technology), Horse-radish peroxidase (HRP) conjugated secondary antibodies used: mouse-IgGk BP-HRP (IB: 1:5000, Cat. #sc-516102, Santa Cruz), HRP Goat anti-mouse IgG (1:10,000, Cat #115-035-003, Jackson Immuno), HRP Goat anti-rabbit IgG (1:10,000, Cat #111-035-003, Jackson Immuno).

Protein purification

Wild-type and mutant human 2×MBP-BRCA2_{NTD} fragment (BRCA2 aa 250–500) cDNAs were purified as described previously²⁸. Briefly, 10 × 15-cm plates of HEK293 cells were transiently transfected using TurboFect (Thermo Scientific) following the manufacturer's specifications and harvested 30 h post-transfection. Cell extracts were bound to amylose resin (NEB), and the protein was eluted with 10 mM maltose. The eluate was further purified by ion exchange using BioRex 70 resin (Bio-Rad) and step eluted at 250, 450, and 1 mM NaCl. Each fraction was tested for nuclease contamination. The CTD of BRCA2 and RAD51 were purified as described before²⁸. Only the nuclease-free fractions were used for EMSA or DNA strand exchange assays.

RPA was expressed from plasmid p11d-tRPA (kind gift from Marc Wold) in BL21(DE3) cells (Novagen) and purified as described⁶⁴.

Cell survival and viability assays

Clonogenic survival assay was assessed in DLD1 BRCA2^{+/+} expressing the endogenous BRCA2 protein, DLD1 BRCA2-deficient cells (BRCA2^{-/-}) or DLD1 BRCA2-deficient cells stably expressing either EGFP-MBP-BRCA2 WT or different clones expressing the variants (C315S, S273L, and R3052W). Cells seeded at 70% of confluence were treated either with MMC (Sigma-Aldrich) at concentrations: 0, 0.5, 1.0, and 2.5 μM or

with HU (Sigma-Aldrich) at concentrations 0, 1, 5, or 10 mM. After 1 h (MMC) or 24 h (HU) treatment, the cells were serially diluted in normal growth media/RPMI (Eurobio) and seeded at 100, 250, 500, 1000, or 10,000 cells in triplicates into six-well plates depending on the drug concentration. The media was changed every third day, after 10–12 days in culture the plates were stained with crystal violet (Sigma Aldrich) and colonies were counted. The surviving fraction was determined for each drug concentration as compared to the non-treated condition of the same clone.

MTT assay

Cell viability was assessed in DLD1 BRCA2^{+/+} expressing the endogenous BRCA2 protein, DLD1 BRCA2-deficient cells (BRCA2^{-/-}) or DLD1 BRCA2-deficient cells stably expressing either EGFP-MBP-BRCA2 WT or different clones expressing the variants (C315S, S273L, and R3052W). The cells were seeded at 2000–4000 cells per well depending on the clone and treated at increasing concentrations of Olaparib (AZD2281, Selleck Chemicals) 0.5, 1.0, and 2.5 μM for 6 days. On the 6th day, the media was removed and cells were washed with 1× PBS. Cell viability was assessed with 3-[4,5-dimethylthiazol-2-yl]-2,5-diphenyltetrazolium bromide (MTT, #M5655, Sigma Aldrich). The solution was removed and MTT crystals were dissolved in 100 μl 100% DMSO (Sigma-Aldrich). The absorbance was read in a microplate reader at 570 nm. The calculation was corrected for the absorbance of the blank (DMSO only) and the survival percentage was calculated by dividing the absorbance into the cells treated by the absorbance obtained in the untreated cells.

Proximity ligation assay on nascent DNA

500,000 cells were seeded on glass coverslips the day before the experiment to reach 70% confluence. The next day, cells were pulse-labeled with 25 μM EdU (Thermo Fisher) for 10 min. In the case of HU treatment, cells were washed once with 1× PBS and incubated with 0.2 mM HU at 5 min, 30 min, and 1 h time points. For thymidine chase experiments, cells were washed with 1× PBS 3 times and incubated in a medium supplemented with 125 μM thymidine (Sigma-Aldrich) for 4 h. After treatment and labeling cells were washed 3 times with 1× PBS and put on ice for another wash with cold PBS. Cells were then incubated and washed once with CSK buffer (10 mM PIPES, pH 6.8, 0.1 M NaCl, 0.3 M sucrose, 3 mM MgCl₂, EDTA-free Protease Inhibitor Cocktail (Roche)) followed by CSK-T (10 mM PIPES, pH 6.8, 0.1 M NaCl, 0.3 M sucrose, 3 mM MgCl₂, EDTA-free Protease Inhibitor Cocktail (Roche), 0.5% Triton X-100) incubation for 5 min at RT and one CSK-T wash. The last two washes were done once with CSK and once with PBS followed by fixation with 4% paraformaldehyde (Euromedex) for 20 min at RT. Cells were once again washed with PBS and blocked for 1 h in PBS + 0.1% Tween + 5% BSA at RT. The coverslips containing the cells were incubated with 25 μl of the click reaction mix (PBS 1x, 6 nM biotin azide, 10 mM Sodium Ascorbate, and 2 mM CuSO₄) for 30 min at RT in a light-protected chamber. Cells were then washed twice in PBS + 0.1% Tween + 5% BSA followed by primary antibody incubation overnight at 4 °C (see antibodies below). The next day, the samples were subjected to the standard PLA protocol (Sigma-Aldrich Duolink) where: cells were first rinsed in 2 ml of 1X Wash Buffer A followed by 2 × 10 min incubation of coverslips in 2 ml of 1× wash buffer A on a shaker. PLA probes were prepared according to primary antibody species, vortexed, and incubated for 20 min at RT. 25 μl of probe mix was added to each coverslip and incubated for 1 h at 37 °C in a pre-heated humid chamber. For the positive control, PLA Mouse/Rabbit plus and minus probes were used for each Mouse/Rabbit antibody, separately. For negative control, only one primary antibody was used together with PLA Mouse plus and Rabbit minus probe. Cells were again rinsed in 2 ml of 1× Wash Buffer A followed by 2 × 10 min incubation of coverslips in 2 ml of 1× Wash Buffer A on a shaker before the ligation step. The ligation mix was prepared according to the manufacturer's specifications and the mix was added to the coverslip and incubated for

30 min at 37 °C in the pre-heated humid chamber. Washing was done as in previous steps with 1× wash buffer A 2×10 min, prior to the amplification reaction. The amplification mix was prepared added to the coverslips and incubated for 100 min at 37 °C in the pre-heated humid chamber. After the amplification step, coverslips were rinsed in 2 ml of 1× wash buffer B followed by 2×10 min incubation of coverslips in 2 ml of 1× Wash Buffer B on a shaker. The final wash was done using diluted 0.01× Wash Buffer B. Coverslips were let to air-dry for 5–10 min and were mounted with 7 µl ProLong Diamond (Invitrogen) onto coverslips with clear nail polish.

Images were acquired using a DM6000B upright widefield Microscope (Leica) equipped with an ×63 Plan Apochromat oil immersion objective (Leica, NA: 1.4). The fluorescence signal was recorded with bloc filters. TX2 emission was detected at 604–644 nm upon excitation between 542–582 nm. DAPI emission was detected at 445–495 nm upon excitation between 375 and 435 nm. Images were obtained with an sCMOS Orca Flash 4.0 camera (Hamamatsu). The whole system was driven by Metamorph (Molecular Devices). For 3D imaging, stacks were acquired with a z-step of 1 µm. The number of PLA spots was counted with a customized macro where the nucleus was defined by a minimum pixel size of 1500 on DAPI and a mask was generated and applied to the Z-projection to count the spots within the nucleus. The PLA spots were quantified using the ImageJ plugin Find Maxima in the Z-projection with a prominence of 2000.

Primary antibodies used for PLA were as follows: mouse anti-BRCA2 (1:500 EMD Millipore Cat. # OP95), rabbit anti-biotin (1:3000 Bethyl laboratories Cat. # BETA150-109A), mouse anti-biotin (1:3000 Jackson ImmunoResearch Cat. # AB_2339006), mouse anti-RAD51 (1:500 Novus Biologicals Cat. # NB100-148), mouse anti-PCNA (1:500 Santa Cruz Biotechnology Cat. # sc-56) and mouse anti-histone H1 (1:500 Santa Cruz Biotechnology Cat. # sc-8030).

DNA fiber assay

DNA fiber labeling scheme to visualize replication fork degradation was performed as previously described⁶⁵. Briefly, cells were labeled with 25 µM IdU, washed with warm media, exposed to 50 µM CldU, washed again with warm media, and treated with 5 mM hydroxyurea for 4 h. Cells were lysed and DNA fibers were stretched onto glass slides and then dried and fixed in methanol/acetic acid (3:1) for 10 min. The DNA fibers were denatured with 2.5 M HCl for 1 h, washed with PBS, and blocked with 2% BSA in PBS-Tween for 60 min. IdU replication tracts were revealed with a mouse anti-BrdU/IdU antibody from BD Biosciences (347580; 1:100) and CldU tracts with a rat anti-BrdU/CldU antibody from Eurobio (ABC117-7513; 1:100). The following secondary antibodies were used: Alexa fluor 488 anti-mouse antibody (Life A21241; 1:100) and Cy3 anti-rat antibody (Jackson ImmunoResearch 712-166-153; 1:100). Fibers were visualized and imaged by Carl Zeiss Axio Imager Apotome using ×40 Plan Apo 1.4 NA oil immersion objective and acquired using Zeiss Zen 3.1 software. Replication tract lengths were analyzed using ImageJ software.

DNA combing assay

DNA combing experiments were performed using a previously reported protocol¹⁶⁶ with the following modifications: Cells were plated at 2×10⁶ cells per 100 mm dish and allowed to adhere for 24 h. Subsequently, DNA was labeled for 30 min with 100 µM IdU (Sigma-Aldrich) and washed 2× with PBS followed by incubation with 100 µM CldU (Sigma-Aldrich) with or without treatment with replication stress drug/Hydroxyurea (Sigma-Aldrich), depending on the assay. For the fork restraint assays, cells were exposed simultaneously to 100 µM CldU with 0.5 mM HU for 2 h. After labeling, cells were collected with trypsin, washed with 1× PBS, and resuspended in cold 0.5× trypsin in PBS (45 µl per 100,000 cells). 500 µl of cells were transferred to a new tube, briefly heated at 42 °C, and resuspended

with 500 µl melted 2% agarose type VII (SIGMA) to make the agarose plugs. Plugs were let solidify for 20 min at 4 °C and were then digested with Proteinase K (400 mM EDTA pH 8, 10% Proteinase K, 1% Sarcosyl) at 42 °C overnight. The next day, plugs were washed 3× with TE 1× buffer. TE solution was removed and a solution containing 50 mM MES pH 5.5, 100 mM NaCl was added to the plugs that were heated at 68 °C for 20 min. Agarose plugs were then dissolved by adding 2 µl of β-agarase (NEB) and incubated at 42 °C overnight. The following day, dissolved agarose plugs were transferred to the combing machine (Genomic Vision) where DNA was combed onto silane-coated coverslips (Genomic Vision COV-002-RUO) following the manufacturer's specifications. Combed coverslips were baked for 2 h at 60 °C, denatured in denaturation buffer (25 mM NaOH, 200 mM NaCl in H₂O) for 15 min, washed 3× with 1× PBS, and dehydrated by increasing concentration of ethanol 70%, 90%, and 100% each for 5 min. For the IF staining, the coverslips were incubated with BlockAid for 15 min (Life Technologies) at RT followed by the primary anti-IdU and anti-CldU antibodies (1 h, 1:25 anti-mouse Becton Dickinson 347580 for IdU and 1:50 anti-rat Abcam ab6326 for CldU) and then incubated 1 h with the following secondary antibodies: 1:50 Alexa donkey anti-mouse 488 (Life Technologies ref. 21202), 1:50 Alexa goat anti-rat 555 (Life Technologies ref. A21434) in BlockAid (Thermo Scientific). Slides were air-dried for 5–10 min and were mounted with 7 µl mounting media (80% Glycerol and 20% PBS) and sealed with clear nail polish. Track lengths of the CldU signal (in red) were measured in Fiji⁶⁷.

S1 nuclease DNA combing Assay

As stated above for DNA combing, cells were exposed to 100 µM IdU to label replication forks, followed by 100 µM CldU with 0.5 mM HU for 2 h or left untreated. Subsequently, cells were permeabilized with 5 ml CSK buffer in 10 cm plates (10 mM PIPES, pH 6.8, 0.1 M NaCl, 0.3 M sucrose, 3 mM MgCl₂, EDTA-free Protease Inhibitor Cocktail (Roche)) at room temperature for 10 min, followed by 1 ml S1 nuclease (20 U/ml) (ThermoFisher # 18001016) in S1 buffer (30 mM sodium acetate pH 4.6, 1 mM zinc sulfate, 50 mM NaCl) for 30 min at 37 °C. Finally, cells were collected by scraping, pelleted, and resuspended in PBS (45 µl per 200,000). The following steps were the same as described in the DNA combing assay.

S1 nuclease DNA combing Assay with Olaparib treatment

Cells were treated with 10 µM Olaparib for 2 h, followed by 30 min of CldU 100 µM to label replication forks. Subsequently, cells were permeabilized and processed as described above.

Replication fork restart assay

As stated above, cells were exposed to 100 µM IdU to label replication forks, followed by 4 h 5 mM HU treatment and a second label using 100 µM CldU. The following steps were the same as described in the DNA combing assay.

HR assay

HR was performed as described³⁷. Briefly, we used a DSB-mediated gene targeting strategy with site-specific TALEN nucleases to quantify HR in cells. DLD1 BRCA2^{-/-} cells stably expressing full-length GFP-MBP-BRCA2 and the variants (C315S, S273L, and R3052W) were transfected using AMAXA technology (Lonza) nucleofector kit V (Cat. #VCA-1003) with 3 µg of the promoter-less donor plasmid (AAVS1-2A-mCherry) with or without 1 µg of each AAVS1-TALEN encoding plasmids (TALEN-AAVS1-5' and TALEN-AAVS1-3', a kind gift from Dr. Carine Giovannangeli). The day after transfection the media was changed and 48 h post-transfection the cells were trypsinized and reseeded on a 10-cm culture dish and cultured for additional 8 days. The percentage of mCherry positive cells was analyzed on a BD FACSAria III (BD Bioscience) using the FACSDiva software and data

were analyzed with the FlowJo 10.5 software (Tree Star Inc.). Viable and single cells were gated using forward scatter (FSC-A) and side scatters (SSC-S). To separate single cells from the doublets, singlets were selected using FSC-W(y-axis) plotted against FSC-A(x-axis), mCherry positive cells were detected by plotting mCherry-A(y-axis) against FSC-A(x-axis).

Metaphase spreads analysis

Cells (1×10^5) were seeded onto six-well plates on coverslips and treated with Hydroxyurea (SIGMA H8627-1G) (0.5 mM 2 h or 5 mM 5 h) and the following day was arrested in metaphase by adding 0.1 μ g/ml colcemid (ThermoFisher 15212012) for 3 h. A hypotonic shock was performed by incubating the cells with pre-warmed 16% FBS in water for 40 min. Following the hypotonic shock, the cells were fixed by adding 1 volume of methanol-acetic acid (3:1) into one volume of 16% FBS for 15 min at RT, then methanol:acetic acid (3:1) into one volume of water 5 min RT, then methanol-acetic acid (3:1) 30 min RT, and methanol-acetic acid (3:1) for 15 min 4 °C. DNA was stained with 2% Giemsa (Thermo Fisher 10092013) diluted in Gurr buffer (Thermo Fisher 10582013) for 16 min. Chromosomes were acquired either with a Leica DMRB microscope at $\times 100$ magnification and captured with a SONY DXC 930P camera or with a Zeiss Axioskop 2 plus microscope at $\times 100$ magnification and captured with a Leica DMC6200 camera. Chromosomal aberrations were manually counted using Fiji software. Around 50 metaphases were analyzed for cells of each genotype.

Anaphase bridges analysis

Cells were seeded onto six-well plates on coverslips and synchronized by a double thymidine block. Cells were treated with 2.5 mM thymidine (T1895-1G, Sigma Aldrich) for 17 h, washed once with PBS, and released into normal growth media (RPMI) for 8 h. Cells were treated again with 2.5 mM thymidine for 15 h, washed once with PBS and released into normal growth media for a total of 10 h (Control cells) or treated with HU 0.5 mM for 2 h (H8627-1G, Sigma Aldrich), washed out from the excess of HU with PBS and then released for 8 h (total release 10 h). Cells were then fixed with ice-cold methanol for 15 min at -20 °C, permeabilized with PBS-0.1% Triton (10254583, Fisher Scientific) for 15 min, and blocked with PBS-4% BSA (A4503-50G, Sigma Aldrich) overnight at 4 °C. Coverslips were stained with DAPI (268298, Merck) and mounted onto microscopy slides with Prolong Glass Antifade (P-36982, Thermo Fisher). Anaphase cells were visualized with a Zeiss Axiovert 200 M microscope for DAPI staining with a PCO edge 4.2 bi (PCO) camera and analyzed manually.

Electrophoretic mobility shift assay

DNA substrates for EMSA were purchased PAGE-purified from MWG Eurofins. The sequence of the oligonucleotides used for these assays is included in Table S1. The ssDNA substrates used in EMSA were oAC379 32 P labeled at the 5'-end. To generate the 42 bp dsDNA substrate, oAC405 was 32 P labeled at the 5'-end and annealed in a 1:1 molar ratio to oAC406. To generate the 191 bp dsDNA substrate, we used a purified PCR fragment containing the sequence encoding for the human BRCA4 fragment of BRCA2 using the plasmid pAC137 (pCMV GFP-MBP-BRC4) and oligonucleotides oAC596 and oAC597. The purified product was dephosphorylated using Antarctic phosphatase (NEB) before 32 P-labeling at the 5'-end. The proteins were incubated at the indicated concentrations with either 5 nM dsDNA (42mer), 6 nM ssDNA (dT₄₀), or 1.5 nM dsDNA (191mer) 32 P-labeled DNA substrates for 1 h at 37 °C in EMSA reaction buffer (25 mM Tris Acetate pH 7.5, 1 mM DTT, 1 mM MgCl₂, 2 mM CaCl₂). The protein-DNA complexes were resolved on 6% native polyacrylamide gels in 1xTAE buffer (40 mM Tris acetate, 0.5 mM EDTA) at 70 V for 75 min. The gels were dried and analyzed with a Typhoon PhosphorImager (Amersham Biosciences) using Image

Quant software (GE Healthcare). In all EMSAs, the ratio of DNA-protein complexes were calculated as the percentage of bound DNA compared with the free DNA.

DNA strand exchange assay

DNA substrates for strand exchange assay were purchased PAGE-purified from MWG Eurofins. The sequences of the oligonucleotides used for these assays are included in Supplementary Table 1. To generate the radiolabelled dsDNA substrate, oAC1076 was 32 P labeled at the 5'-end and annealed in a 1:1 molar ratio to oAC1077. The 3' overhang substrate was produced by annealing 32 P-labeled oAC403 (42mer 5') to oAC423 (167mer) a 1:1 molar ratio. The gapped DNA substrate was produced by annealing oAC423, oAC403, and oAC490 in a 1:1:1 ratio. RPA (100 nM) or storage buffer was pre-incubated with 668 nM (nt+bp) of 3'tail DNA or gapped DNA for 5 min at 37 °C. Then, RAD51 (380 nM) alone or with the indicated concentrations of BRCA2 were added to the mix and incubated for 5 min at 37 °C in a buffer containing 25 mM Tris Acetate pH 8.0, 1 mM DTT, 2 mM ATP, 1 mM MgCl₂, 2 mM CaCl₂, 0.1 mg/ml BSA (NEB). The reaction was started by adding 4 nM molecules of the donor template dsDNA (oAC1076 and oAC1077 1:1) and the mix was further incubated for 30 min at 37 °C. The reaction was stopped by incubation with 0.25% SDS and 0.5 mg/ml Proteinase K for 10 min. The samples were loaded on a 6% polyacrylamide gel and migrated at 70 V for 75 min. The gels were dried and analyzed with a Typhoon PhosphorImager (Amersham Biosciences) using Image Quant software (GE Healthcare). The percentage of DNA strand exchange product was calculated as labeled product divided by the total labeled input DNA in each lane.

EdU cell cycle analysis

To label replicated DNA, cells were incubated with 10 μ M EdU for 2 h. Samples were collected by trypsinization and incorporated EdU was detected using the Click-iT EdU Alexa Fluor 647 Flow Cytometry Assay Kit (Molecular Probes-Thermo Fisher Scientific) according to manufacturer's instructions. Cells were re-suspended in PBS containing 20 μ g ml⁻¹ propidium iodide (Sigma) and 10 μ g ml⁻¹ RNase A (Sigma) before samples were processed using flow cytometry (BD FACSCalibur, BD Biosciences). A number of 10,000 events were analyzed per condition using FlowJo software.

Statistical analysis

The total number of experimental replicates, mean, median, and error bars are described in the figure legends. Statistical difference was calculated using a two-way ANOVA test with Dunnett's multiple comparisons tests (Fig. 1c-f) or Tukey's test (Fig. 7b and Supplementary Fig. 7). Kruskal-Wallis test followed by Dunn's multiple comparison tests (Figs. 2a, b, 3a, b, 4b, 5ai-b, c, 6b, 7a i, ii, Supplementary Fig. 4a, c, Supplementary Fig. 5). For Fig. 4a, statistical differences were obtained using a one-way ANOVA with Dunnett's test from the mean of four experiments. For Fig. 5a ii, statistical differences were obtained using a one-way ANOVA with Tukey's on the difference of the mean CldU track from -HU vs. +HU calculated by unpaired *t*-test with Welch's correction for each cell line, as indicated in the legend. All analyses were conducted using GraphPad Prism version Mac OS X 9.4.0 (453) version.

Reporting summary

Further information on research design is available in the Nature Portfolio Reporting Summary linked to this article.

Data availability

The data generated during the current study are included in this published article and its Supplementary information files. Materials are available from the corresponding author on request. Source data are provided with this paper.

References

1. Mavaddat, N. et al. Cancer risks for BRCA1 and BRCA2 mutation carriers: results from prospective analysis of EMBRACE. *J. Natl Cancer Inst.* **105**, 812–822 (2013).
2. Howlett, N. G. et al. Biallelic inactivation of BRCA2 in Fanconi anemia. *Science (New York, NY)* **297**, 606–609 (2002).
3. Jensen, R. B., Carreira, A. & Kowalczykowski, S. C. Purified human BRCA2 stimulates RAD51-mediated recombination. *Nature* **467**, 678–683 (2010).
4. Moynahan, M. E., Pierce, A. J. & Jasin, M. BRCA2 is required for homology-directed repair of chromosomal breaks. *Mol. Cell* **7**, 263–272 (2001).
5. Carreira, A. et al. The BRC repeats of BRCA2 modulate the DNA-binding selectivity of RAD51. *Cell* **136**, 1032–1043 (2009).
6. Lomonosov, M., Anand, S., Sangrithi, M., Davies, R. & Venkitaraman, A. R. Stabilization of stalled DNA replication forks by the BRCA2 breast cancer susceptibility protein. *Genes Dev.* **17**, 3017–3022 (2003).
7. Schlacher, K. et al. Double-strand break repair-independent role for BRCA2 in blocking stalled replication fork degradation by MRE11. *Cell* **145**, 529–542 (2011).
8. Hashimoto, Y., Chaudhuri, A. R., Lopes, M. & Costanzo, V. Rad51 protects nascent DNA from Mre11-dependent degradation and promotes continuous DNA synthesis. *Nat. Struct. Mol. Biol.* **17**, 1305–1311 (2010).
9. Zellweger, R. et al. Rad51-mediated replication fork reversal is a global response to genotoxic treatments in human cells. *J. Cell Biol.* **208**, 563–579 (2015).
10. Bhat, K. P. & Cortez, D. RPA and RAD51: fork reversal, fork protection, and genome stability. *Nat. Struct. Mol. Biol.* **25**, 446–453 (2018).
11. Cong, K. et al. Replication gaps are a key determinant of PARP inhibitor synthetic lethality with BRCA deficiency. *chrome-extension://oemmnadbldboiebfnladdacbfmadadm/https://www.cell.com.insb.bib.cnrs.fr/molecular-cell/pdfExtended/S1097-2765(21)00458-5* (2021).
12. Kolinjivadi, A. M. et al. Smarcal1-mediated fork reversal triggers Mre11-dependent degradation of nascent DNA in the absence of Brca2 and stable Rad51 nucleofilaments. *Mol. Cell* **67**, 867–881.e7 (2017).
13. Quinet, A. et al. PRIMPOL-mediated adaptive response suppresses replication fork reversal in BRCA-deficient cells. *Mol. Cell* **77**, 461–474.e9 (2020).
14. Panzarino, N. J. et al. Replication gaps underlie BRCA deficiency and therapy response. *Cancer Res.* **81**, 1388–1397 (2021).
15. Wong, R. P., Petriukov, K. & Ulrich, H. D. Daughter-strand gaps in DNA replication—substrates of lesion processing and initiators of distress signalling. *DNA Repair* **105**, 103163 (2021).
16. Quinet, A., Tirman, S., Cybulla, E., Meroni, A. & Vindigni, A. To skip or not to skip: choosing repriming to tolerate DNA damage. *Mol. Cell* **37**, 5737 (2021).
17. Cantor, S. B. Revisiting the BRCA-pathway through the lens of replication gap suppression “Gaps determine therapy response in BRCA mutant cancer. *DNA Repair* **107**, 103209 (2021).
18. Branzei, D. & Szakal, B. Building up and breaking down: mechanisms controlling recombination during replication. *Crit. Rev. Biochem. Mol.* **52**, 1–14 (2017).
19. Piberger, A. L. et al. PrimPol-dependent single-stranded gap formation mediates homologous recombination at bulky DNA adducts. *Nat. Commun.* **11**, 5863–14 (2020).
20. Tagliatalata, A. et al. REV1-Pol ζ maintains the viability of homologous recombination-deficient cancer cells through mutagenic repair of PRIMPOL-dependent ssDNA gaps. *Mol. Cell* <https://doi.org/10.1016/j.molcel.2021.08.016> (2021).
21. Tirman, S. et al. Temporally distinct post-replicative repair mechanisms fill PRIMPOL-dependent ssDNA gaps in human cells. *Mol. Cell* **81**, 4026–4040.e8 (2021).
22. Yang, H., Li, Q., Fan, J., Holloman, W. K. & Pavletich, N. P. The BRCA2 homologue Brh2 nucleates RAD51 filament formation at a dsDNA–ssDNA junction. *Nature* **433**, 653–657 (2005).
23. Morimatsu, K. & Kowalczykowski, S. C. RecFOR proteins load RecA protein onto gapped DNA to accelerate DNA strand exchange: a universal step of recombinational repair. *Mol. Cell* **11**, 1337–1347 (2003).
24. Izhar, L., Ziv, O., Cohen, I. S., Geacintov, N. E. & Livneh, Z. Genomic assay reveals tolerance of DNA damage by both translesion DNA synthesis and homology-dependent repair in mammalian cells. *Proc. Natl Acad. Sci. USA* **110**, E1462–E1469 (2013).
25. Nagaraju, G. & Scully, R. Minding the gap: the underground functions of BRCA1 and BRCA2 at stalled replication forks. *DNA Repair* **6**, 1018–1031 (2007).
26. Arnaudeau, C., Lundin, C. & Helleday, T. DNA double-strand breaks associated with replication forks are predominantly repaired by homologous recombination involving an exchange mechanism in mammalian cells¹¹ Edited by J. Karn. *J. Mol. Biol.* **307**, 1235–1245 (2001).
27. Patel, K. J. et al. Involvement of Brca2 in DNA repair. *Mol. Cell* **1**, 347–357 (1998).
28. Nicolai, C., von Ehlen, A., Martin, C., Zhang, X. & Carreira, A. A second DNA binding site in human BRCA2 promotes homologous recombination. *Nat. Commun.* **7**, 12813 (2016).
29. Yang, H. et al. BRCA2 function in DNA binding and recombination from a BRCA2–DSS1–ssDNA structure. *Science (New York, NY)* **297**, 1837–1848 (2002).
30. Shimelis, H. et al. BRCA2 hypomorphic missense variants confer moderate risks of breast cancer. *Cancer Res.* **77**, 2789–2799 (2017).
31. Hucl, T. et al. A syngeneic variance library for functional annotation of human variation: application to BRCA2. *Cancer Res.* **68**, 5023–5030 (2008).
32. Chaudhuri, A. R. & Nussenzweig, A. The multifaceted roles of PARP1 in DNA repair and chromatin remodelling. *Nat. Rev. Mol. Cell Biol.* <https://doi.org/10.1038/nrm.2017.53> (2017).
33. Bryant, H. E. et al. Specific killing of BRCA2-deficient tumours with inhibitors of poly(ADP-ribose) polymerase. *Nature* **434**, 913–917 (2005).
34. Farmer, H. et al. Targeting the DNA repair defect in BRCA mutant cells as a therapeutic strategy. *Nature* **434**, 917–921 (2005).
35. Lord, C. J. & Ashworth, A. PARP inhibitors: synthetic lethality in the clinic. *Science (New York, NY)* **355**, 1152–1158 (2017).
36. Pierce, A. J., Johnson, R. D., Thompson, L. H. & Jasin, M. XRCC3 promotes homology-directed repair of DNA damage in mammalian cells. *Gene Dev.* **13**, 2633–2638 (1999).
37. Vugic, D., Ehlen, A. & Carreira, A. Monitoring homologous recombination activity in human cells. *Methods Mol. Biol. (Clifton, NJ)* **2153**, 115–126 (2021).
38. Iyer, V. N. & Szybalski, W. A molecular mechanism of mitomycin action: linking of complementary DNA strands. *Proc. Natl Acad. Sci. USA* **50**, 355–362 (1963).
39. Petruk, S. et al. TrxG and PcG proteins but not methylated histones remain associated with DNA through replication. *Cell* **150**, 922–933 (2012).
40. Petermann, E., Orta, M. L., Issaeva, N., Schultz, N. & Helleday, T. Hydroxyurea-stalled replication forks become progressively inactivated and require two different RAD51-mediated pathways for restart and repair. *Mol. Cell* **37**, 492–502 (2010).
41. Sirbu, B. M. et al. Analysis of protein dynamics at active, stalled, and collapsed replication forks. *Genes Dev.* **25**, 1320–1327 (2011).

42. Esashi, F. et al. CDK-dependent phosphorylation of BRCA2 as a regulatory mechanism for recombinational repair. *Nature* **434**, 598–604 (2005).
43. Tagliatalata, A. et al. Restoration of replication fork stability in BRCA1- and BRCA2-deficient cells by inactivation of SNF2-family fork remodelers. *Mol. Cell* **68**, 414–430.e8 (2017).
44. Carreira, A. & Kowalczykowski, S. C. BRCA2: Shining light on the regulation of DNA-binding selectivity by RAD51. *Cell Cycle (Georgetown, TX)* **8**, 3445–3447 (2009).
45. Mijic, S. et al. Replication fork reversal triggers fork degradation in BRCA2-defective cells. *Nat. Commun.* **8**, 859 (2017).
46. Schwob, E. et al. Use of DNA combing for studying DNA replication in vivo in yeast and mammalian cells. *Methods Mol. Biol. (Clifton, NJ)* **521**, 673–687 (2009).
47. Lemaçon, D. et al. MRE11 and EXO1 nucleases degrade reversed forks and elicit MUS81-dependent fork rescue in BRCA2-deficient cells. *Nat. Commun.* **8**, 860 (2017).
48. Feng, W. & Jasin, M. BRCA2 suppresses replication stress-induced mitotic and G1 abnormalities through homologous recombination. *Nat. Commun.* **8**, 525 (2017).
49. Bai, G. et al. HLTf promotes fork reversal, limiting replication stress resistance and preventing multiple mechanisms of unrestrained DNA synthesis. *Mol. Cell* **78**, 1237–1251.e7 (2020).
50. Costanzo, V. et al. An ATR- and Cdc7-dependent DNA damage checkpoint that inhibits initiation of DNA replication. *Mol. Cell* **11**, 203–213 (2003).
51. Saldivar, J. C., Cortez, D. & Cimprich, K. A. The essential kinase ATR: ensuring faithful duplication of a challenging genome. *Nat. Rev. Mol. Cell Biol.* **18**, 622–636 (2017).
52. Saada, A. A., Lambert, S. A. E. & Carr, A. M. Preserving replication fork integrity and competence via the homologous recombination pathway. *DNA Repair* <https://doi.org/10.1016/j.dnarep.2018.08.017> (2018).
53. Toledo, L. I. et al. ATR prohibits replication catastrophe by preventing global exhaustion of RPA. *Cell* **155**, 1088–1103 (2013).
54. Lai, X. et al. MUS81 nuclease activity is essential for replication stress tolerance and chromosome segregation in BRCA2-deficient cells. *Nat. Commun.* **8**, 15983 (2017).
55. Ehlen, A. et al. Proper chromosome alignment depends on BRCA2 phosphorylation by PLK1. *Nat. Commun.* **11**, 1–21 (2020).
56. Rickman, K. A. et al. Distinct roles of BRCA2 in replication fork protection in response to hydroxyurea and DNA interstrand cross-links. *Genes Dev.* **34**, 832–846 (2020).
57. Guidugli, L. et al. A classification model for BRCA2 DNA binding domain missense variants based on homology-directed repair activity. *Cancer Res.* **73**, 265–275 (2013).
58. Thakar, T. et al. Lagging strand gap suppression connects BRCA-mediated fork protection to nucleosome assembly through PCNA-dependent CAF-1 recycling. *Nat. Commun.* **13**, 5323 (2022).
59. Maya-Mendoza, A. et al. High speed of fork progression induces DNA replication stress and genomic instability. *Nature* **559**, 279–284 (2018).
60. Danford, N. Genetic toxicology, principles and methods. *Methods Mol. Biol.* **817**, 93–120 (2011).
61. Meroni, A. et al. RNase H activities counteract a toxic effect of Polymerase η in cells replicating with depleted dNTP pools. *Nucleic Acids Res.* **47**, 4612–4623 (2019).
62. Guidugli, L. et al. Functional assays for analysis of variants of uncertain significance in BRCA2. *Hum. Mutat.* **35**, 151–164 (2014).
63. Martinez, J. S. et al. BRCA2 regulates DMC1-mediated recombination through the BRC repeats. *Proc. Natl Acad. Sci. USA* **113**, 3515–3520 (2016).
64. Binz, S. K., Dickson, A. M., Haring, S. J. & Wold, M. S. Functional assays for replication protein A (RPA). *Methods Enzymol.* **409**, 11–38 (2006).
65. Lossaint, G. et al. FANCD2 binds MCM proteins and controls replisome function upon activation of S phase checkpoint signaling. *Mol. Cell* **51**, 678–690 (2013).
66. Schurra, C. & Bensimon, A. The Nucleus, Volume 2: chromatin, transcription, envelope, proteins, dynamics, and imaging. *Methods Mol. Biol.* **464**, 71–90 (2008).
67. Schindelin, J. et al. Fiji: an open-source platform for biological-image analysis. *Nat. Methods* **9**, 676–682 (2012).

Acknowledgements

We thank all members of Carreira lab for their input on this manuscript. We thank Sarah Lambert for helpful discussions on this project. We would like to acknowledge Xavier Veaute (CEA-DRF-IRCM-CIGEx) for the purification of RPA. We thank Laetitia Besse from the Cell and Tissue Imaging Facility of the Institut Curie (PICT), a member of the France BioImaging National Infrastructure (ANR-10-INBS-04), and Charlene Lasgi from the Flow Cytometry platform of Institut Curie, Orsay. This research was funded by grants from the Agence National de Recherche (ANR-17-CE12-0016), Institut National du Cancer (INCa-DGOS_8706), and Agencia Española de Investigación (MCIN/AEI) (PID2020-115977RB-I00) to A.C. and Jeunes Chercheuses (REPLIBLOCK ANR-17-CE12-0034-01) to C.R. A predoctoral Fellowship from Fondation ARC pour la recherche sur le cancer and French Ministry of Education supported D.V. A predoctoral Fellowship from Fondation pour la Recherche Médicale (FRM) supported I.D., A.M., and C.v.N. L.A.-A. was funded by an FPI Fellowship from Agencia Española de Investigación (MCIN/AEI) (PID2020-115977RB-I00). R.C. was funded by a PSL (Paris Science et Lettres) predoctoral Fellowship and R.L. was funded by Fondation ARC pour la recherche sur le cancer.

Author contributions

D.V., C.M., I.D., C.R., and A.Ca. designed the experiments; D.V., C.M.; I.D., A.M., L.A.-A., J.G.-E., R.C., R.L., C.v.N., V.B., and C.R. performed the experiments; D.V., C.M.; I.D., A.M., L.A.-A., J.G.-E., R.C., R.L., C.v.N., C.R., A.Co., and A.Ca. analyzed the data; A.Ca. wrote the manuscript with input from all the authors and A.Ca. supervised the research. Funding Acquisition, C.R., A.Co., and A.Ca.

Competing interests

The authors declare no competing interests.

Additional information

Supplementary information The online version contains supplementary material available at <https://doi.org/10.1038/s41467-023-36149-0>.

Correspondence and requests for materials should be addressed to Aura Carreira.

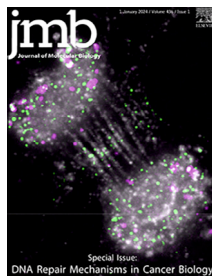
Peer review information *Nature Communications* thanks Joanna Morris and the other, anonymous, reviewer(s) for their contribution to the peer review of this work. Peer reviewer reports are available.

Reprints and permissions information is available at <http://www.nature.com/reprints>

Publisher's note Springer Nature remains neutral with regard to jurisdictional claims in published maps and institutional affiliations.

Open Access This article is licensed under a Creative Commons Attribution 4.0 International License, which permits use, sharing, adaptation, distribution and reproduction in any medium or format, as long as you give appropriate credit to the original author(s) and the source, provide a link to the Creative Commons license, and indicate if changes were made. The images or other third party material in this article are included in the article's Creative Commons license, unless indicated otherwise in a credit line to the material. If material is not included in the article's Creative Commons license and your intended use is not permitted by statutory regulation or exceeds the permitted use, you will need to obtain permission directly from the copyright holder. To view a copy of this license, visit <http://creativecommons.org/licenses/by/4.0/>.

© The Author(s) 2023



BRCA1/2 Haploinsufficiency: Exploring the Impact of Losing one Allele

Anna Minello^{1,2} and Aura Carreira^{1,2,3*}

1 - Institut Curie, PSL Research University, CNRS, UMR3348, F-91405 Orsay, France

2 - Paris-Saclay University CNRS, UMR3348, F-91405 Orsay, France

3 - Genome Instability and Cancer Predisposition Lab, Department of Genome Dynamics and Function, Centro de Biología Molecular Severo Ochoa (CBMSO, CSIC-UAM), Madrid 28049, Spain

Correspondence to Aura Carreira:*Centro de Biología Molecular Severo Ochoa (CBMSO, CSIC-UAM), Madrid, 28049, Spain. acarreira@cbm.csic.es (A. Carreira) @auracarreiralab (A. Carreira)

<https://doi.org/10.1016/j.jmb.2023.168277>

Edited by Gaorav Gupta

Abstract

Since their discovery in the late 20th century, significant progress has been made in elucidating the functions of the tumor suppressor proteins BRCA1 and BRCA2. These proteins play vital roles in maintaining genome integrity, including DNA repair, replication fork protection, and chromosome maintenance. It is well-established that germline mutations in *BRCA1* and *BRCA2* increase the risk of breast and ovarian cancer; however, the precise mechanism underlying tumor formation in this context is not fully understood. Contrary to the long-standing belief that the loss of the second wild-type allele is necessary for tumor development, a growing body of evidence suggests that tumorigenesis can occur despite the presence of a single functional allele. This entails that heterozygosity in *BRCA1/2* confers haploinsufficiency, where a single copy of the gene is not sufficient to fully suppress tumor formation. Here we provide an overview of the findings and the ongoing debate regarding BRCA haploinsufficiency. We further put out the challenges in studying this topic and discuss its potential relevance in the prevention and treatment of *BRCA*-related cancers.

© 2023 The Authors. Published by Elsevier Ltd. This is an open access article under the CC BY license (<http://creativecommons.org/licenses/by/4.0/>).

Cancer predisposition associated with BRCA1/2 mutations

Breast cancer is the predominant malignancy and the primary cause of cancer-related deaths among women worldwide.¹ In 1995, genetic linkage studies performed in familial cases led to the identification of the BRCA1 and BRCA2 genes, type 1 and type 2, *BRCA1* and *BRCA2*, respectively.^{2–5} Mutations in those genes account for approximately 30% of hereditary breast cancer cases.

During their lifetime, *BRCA1* and *BRCA2* mutation carriers have a 72% or 69% cumulative risk of developing breast cancer to age 80, respectively. The cumulative risk for ovarian

cancer to age 80 for the same population is estimated at 44% for *BRCA1* and 17% for *BRCA2* mutation carriers.⁶ In addition, bi-allelic mutations in the *BRCA1/2* genes are associated with distinct subtypes of Fanconi anemia (FA) (*BRCA2/FA-D1*, *BRCA1/FA-S*).⁷ This disease is characterized by extreme sensitivity to inter-strand crosslinking (ICL)-inducing agents like cisplatin or Mitomycin C (MMC) which is associated with bone marrow failure in childhood and cancer predisposition syndrome (reviewed in⁸).

The increased cancer risks associated with mutations in BRCA genes can be attributed to their essential roles in preserving genome integrity specifically in the homologous recombination (HR)

DNA repair pathway. HR is essential for the repair of DNA double-strand breaks (DSBs), replicative lesions such as single-strand DNA gaps (ssDNA gaps), and restarting stalled replication forks. At DSBs, BRCA1 plays a pivotal role in facilitating DNA-end resection^{9,10} while *BRCA2* operates mainly downstream facilitating the displacement of RPA and loading of the recombinase RAD51 onto the resected ssDNA.^{11–13} RAD51 assembles on ssDNA as a nucleoprotein filament which is the functional unit to promote homologous DNA pairing and strand exchange.^{14,15} When the pairing takes place with the sister chromatid as a template, this process results in error-free DNA repair.^{10,12,13,16} Furthermore, *BRCA* proteins play a critical role in the protection of stalled replication forks, where nascent DNA is exposed to nucleolytic degradation by nucleases.¹⁷ In this context, the *BRCA1-BARD1* complex promotes RAD51 recruitment,¹⁸ while *BRCA2* stabilizes RAD51 filaments onto ssDNA¹⁹, thus ensuring genome integrity during replication stress conditions.¹⁹

Replication stress induced by nucleotide depletion or the presence of obstacles ahead of the fork results in the formation of ssDNA gaps which are most prominent in cells lacking functional *BRCA1* and *BRCA2* proteins²⁰ suggesting their role in gap suppression (GS). The function of *BRCA1/2* in GS is still under study but it seems to comprise three complementary activities: ensuring replication fork arrest upon replication stress,²¹ inhibiting excessive DNA-end resection,²² and promoting the repair or filling the gaps post-replicatively by a template switch-like mechanism.^{21,23–25} Interestingly, the accumulation of these ssDNA gaps in *BRCA2*-deficient cells drives replication fork degradation by interfering with the nucleosome assembly pathway.²⁶

Which of these functions, HR, FP, or GS, are at the origin of the tumor suppressor activities of *BRCA1/2*, and therapy response in *BRCA1/2*-deficient tumors are subjects of intense investigation.^{21,23,27,28}

Mechanism of tumorigenesis associated with monoallelic mutations in *BRCA1/2*

The first evidence supporting the essential function of *BRCA1/2* as tumor suppressors came from experiments performed in mouse models. The observation that embryos lacking *Brca1/2* genes were unable to progress beyond an early stage of development strongly suggested their essential role in embryogenesis, specifically in promoting cell proliferation.^{29–32} However, subsequent studies revealed that *Brca1/2* deficiency triggered a cell cycle arrest mediated by p21,^{29,30} a downstream effector of the tumor suppressor *p53*, which down-regulates cell proliferation and induces cell death to prevent tumor formation.³³

The colocalization and physical interaction observed between the established DNA repair factor Rad51 and Brca proteins in mouse cells strongly supported the notion that *Brca1/2* were involved in DNA repair.^{34–36} Furthermore, the fact that the deficiency of Brca genes in cultured murine cells led to the presence of aberrant chromosomal structures and micronuclei,^{37,38} as well as increased sensitivity to DSB-inducing agents such as UV light and ionizing radiation,^{34,38} further pointed out a role for these proteins in preserving genome integrity. Studies in mouse cells as well as biochemical and structural work with the ortholog of *BRCA2* in *Ustilago maydis*, Brh2, and fragments of the mouse and human proteins established that BRCA proteins play a critical role in maintaining genomic stability through high-fidelity DNA repair via HR.^{10,39,40} This extensive body of evidence led to the classification of *BRCA1* and *BRCA2*, as tumor suppressors (TS).

The initial paradigm for tumor formation in TS genes emerged from the 'two-hit' model⁴¹ proposing that individuals with a mono-allelic germline mutation acquired a second mutation (second hit) in the same gene, somatically. This hypothesis was formulated for the Retinoblastoma gene (Rb)-related tumors and later extended to *BRCA1* and *BRCA2* to explain hereditary cancer susceptibility.^{42–45} However, the two-hit hypothesis was later refined to a continuous model to accommodate the fact that, in some cases, partial loss of a tumor suppressor was sufficient to promote tumorigenesis.⁴⁶

Typically, the second mutation involves the loss of the WT allele, also known as the Loss of Heterozygosity (LOH). This event refers to the somatic loss or inactivation of the remaining functional allele, leading to the absence of a functional protein. In the case of *BRCA1/2*, the mechanism of LOH is thought to arise through allelic recombination,⁴⁷ genetic rearrangements, physical deletions, somatic mitotic recombination⁴⁸ (reviewed in⁴⁹) or promoter hypermethylation (*BRCA1* only).⁵⁰ Interestingly, BRCA genes have recently been identified as common fragile sites (CFS) in the genome.⁵¹ These sites are prone to replication challenges and DNA breakage due to long repeated sequences. Replication fork stalling and subsequent error-prone repair can result in mutations or large deletions, leading to functional inactivation of the WT BRCA gene constituting another mechanism of LOH.

The mechanisms of BRCA loss have been enigmatic: On the one hand, *BRCA* deficiency resulted in cell lethality in embryos and cell cycle arrest in cultured cells and, on the other, in tumors, *BRCA* loss promoted aberrant DNA replication and unrestricted proliferation, leading to the accumulation of genetic alterations that fueled malignancy. This paradox has been partly explained by the observation that in murine cells,

the silencing of *Brca1* or *Brca2* leads to cell death unless combined with a knockout of *Tp53*.^{29,32} Later studies revealed that *TP53* loss is a common characteristic of *BRCA*-related tumorigenesis, although it is not the sole factor.^{52,53} Besides *TP53* loss, other mechanisms such as the loss of the tumor suppressor genes *RB1* or *PTEN* contribute to generating a premalignant environment in this context.⁵⁴

The combination of the mutational processes taking place in tumors results in computationally distinguishable patterns of substitutions and rearrangements known as genomic signatures. These patterns are characteristic for the different types of tumors^{55,56} including those associated with *BRCA1/2* mutations. Inactivation of *BRCA1* or *BRCA2* results in a specific mutational pattern that is commonly known as homologous recombination deficient (HRD) signature.⁵⁵ Interestingly, refined analyses can discriminate the genomic profiles of *BRCA1* vs *BRCA2*-related tumors.⁵⁷

Cells of origin for *BRCA1/2*-mutated breast cancer

BRCA1- and *BRCA2*-related tumors, while sharing similarities such as the HRD signature, they demonstrate distinct phenotypic tumor characteristics. In the case of breast cancer, these differences are evaluated based on various parameters. Firstly, tumor grade, which reflects the abnormality of cells and correlates with tumor aggressiveness. Secondly, hormonal status is based on the expression of the progesterone receptor (PR), estrogen receptor (ER), or amplification of the Her2 receptor. This is important because some treatment options vary based on the receptor expression in the tumor, with Her2-positive tumors being targeted by antibody-based therapy, and ER and PR-positive tumors benefiting from hormonal therapy. Tumors lacking the expression of all these hormonal receptors are referred to as triple-negative breast cancers (TNBC), which tend to be more aggressive and challenging to treat. Intriguingly, *BRCA1* germline mutations often result in high-grade TNBC; by contrast, *BRCA2*-associated familial tumors are generally hormone-receptor positive and medium to high-grade.⁵⁸

The presence or absence of hormone receptors is associated with the specific cell type that initiates tumor progression. Breast epithelium comprises two main cell types: luminal cells and basal or myoepithelial cells. Luminal cells, located in the inner layer near the lumen, can be further divided into secretory cells or L1 and, hormone-responsive cells, referred to as L2.^{59–60} Basal cells are found in the outer layer and possess contractile properties. Basal cells, being hormone-negative, have been identified as the most likely cell of origin for TNBC suggesting a potential effect of the

BRCA1 mutation on the basal cell compartment.^{61,62} However, recent lineage tracing analysis revealed that *BRCA1* mutations primarily affect the luminal progenitor cells, which are found in the L1 population, resulting in aberrant basal cells.^{63–64} In contrast, *BRCA2* mutation mainly affects the L2 cell population⁶²; therefore, the different cells of origin may account for the distinct characteristics observed in *BRCA1* and *BRCA2*-associated breast tumors.

Evidence of locus-specific LOH from *BRCA*-mutated tumors

The initial studies on LOH at *BRCA1/2* loci in breast tumor samples from *BRCA*-mutation carriers revealed diverse LOH patterns within and among invasive lesions; these included cases where the loss predominantly affected the mutant allele rather than the WT allele.⁶⁵ These observations suggested that LOH could play a role in the early stages of cancer development but may not be indispensable for tumor progression and maintenance. Supporting this notion, microarray-based analysis of normal breast tissue obtained from *BRCA*-mutation carriers undergoing prophylactic mastectomy showed an increased prevalence of genetic abnormalities, despite the presence of the WT allele.⁶⁶ Furthermore, the characterization of normal breast epithelium from *BRCA1* mutation carriers demonstrated a three-fold higher incidence of LOH in chromosome 17 and genomic aberrations compared to a non-carrier control group or to normal tissue from women with sporadic breast cancer.⁶⁷ These seemingly contradictory findings suggested that LOH could be a stochastic event and a consequence, rather than a causal factor, of the genomic instability associated with germline *BRCA* mutations (Figure 1).⁶⁷ In recent years, the *BRCA* haploinsufficiency hypothesis has gained momentum with the increase of genetic testing thanks to the advances in next-generation sequencing (NGS) technologies. These advances have revealed significant disparities in the frequencies of LOH between *BRCA1* and *BRCA2*-associated tumors; for example, in a cohort of 35 *BRCA2*-mutated familial breast cancers, LOH was found in 50% of cases, while in 41 *BRCA1*-mutated tumors, LOH prevalence was 90%.⁶⁸ Similarly, an analysis of LOH in hereditary ovarian cancer *BRCA1*-associated cases exhibited a 100% LOH prevalence compared to the 76% observed in *BRCA2*-related cases.⁶⁹ These differences suggest potential variations in the mechanisms of tumor formation due to *BRCA1*- or *BRCA2* mutations. In addition, the retention of the WT allele has also been observed in non-gynecological *BRCA*-associated tumors in mouse models. For instance, LOH was detected in only 37% of cell lines and xenografts derived from *BRCA2*-mutated pancreatic carcinoma.⁷⁰ Similarly, in a murine model of familial pan-

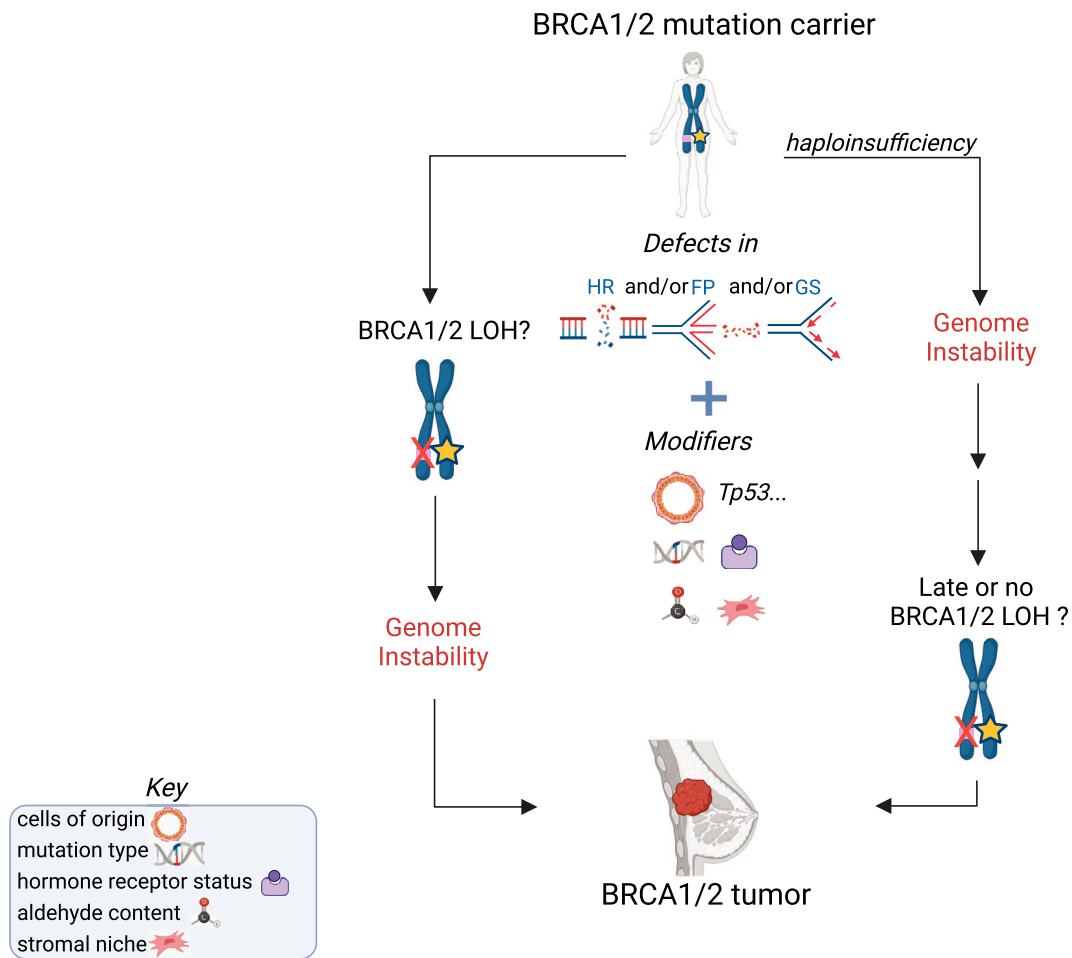


Figure 1. Possible mechanisms of tumor formation in *BRCA1/2*-mutation carriers. (Left arm) LOH may take place at an early stage (“second hit”) of tumorigenesis which would result in genome instability and lead to tumor formation. Alternatively, (right arm) haploinsufficiency may manifest early in the form of defects in one or more of the main functions of BRCA1/2 in preserving genome integrity, as indicated: HR: homologous recombination; FP: fork protection; and/or GS: gap suppression. This would instigate genome instability (including or not LOH) depending on modifiers such as the cells of origin, p53 or other tumor suppressors status, hormonal status, mutation type, presence of aldehydes or the stromal niche (see key). Figure created with BioRender.com.

creatic cancer, three out of four tumors with germline heterozygosity for a pathogenic *Brca2* mutation did not exhibit LOH at the mutation site.⁷¹ These observations have fueled research in the quest for evidence of haploinsufficiency conferred by heterozygosity of *BRCA1/2*; an effort that has not ceased as detailed below.

First molecular evidence of haploinsufficiency

The observations that some *BRCA*-related tumors retained the wild-type allele instigated the research for evidence on *BRCA1/2* haploinsufficiency in different model systems.⁷² Notably, one study found that *BRCA1*-heterozygote lymphoblastoid cell lines (LCLs) exhibited a decreased fidelity in repairing DSBs when compared to cells from non-carrier individu-

als.⁷³ Likewise, *BRCA2*-mutated LCLs exhibited elevated levels of DNA damage, even in untreated conditions, which escalated upon treatment with DNA-alkylating agents such as MMC.⁷⁴ In the same study, *BRCA2*-mutated lymphocytes increased the rate of spontaneous sister chromatid exchanges (SCEs), a readout of ongoing genomic instability. Another study examined heterozygote chicken cell lines harboring a mono-allelic *BRCA2* mutation that led to the expression of a truncated product. These cells exhibited a significant decrease in RAD51 foci formation following irradiation, along with reduced growth rate, increased cell death, and hypersensitivity to DNA-damaging agents.⁷⁵ In stark contrast, a study using human HT-29 colon cancer cells reported that the presence of a single functional *BRCA2* allele did not hinder RAD51 foci formation or compromised DNA repair capacity after irradiation.⁷⁶ In contrast, DSB repair by HR was found to be intact in mouse mammary primary cells express-

ing a truncated exon 27 *Brca2*^{+/- Δ27} whereas the homozygous mutation impaired repair.⁷⁷ These discrepancies may be in part attributed to the presence of a truncated *BRCA2* protein observed in the latter study, acting as dominant negative, or, to differences related to the cell-line model system used.

It is important to note that, *Brca*-heterozygous mice are not prone to developing breast cancer^{78,79}, while homozygous mutations often result in embryonic lethality or the development of blood tumors.^{80–82} Therefore, despite the enormous advances in the understanding of *BRCA1/2* function and tumor progression they have provided^{83,84}, results from these models may not be easily extrapolated to mimic early stages of tumor formation linked to human *BRCA1/2* mutations. A way to partially circumvent this issue came from the generation of conditional mouse models, where the concurrent tissue-specific inactivation of *Brca1* or *Brca2* and *Tp53* led to the development of breast tumors.^{83,85} Nevertheless, some *BRCA1/2*-mutated tumors do not present *Tp53* mutation raising the question of whether this is an early or necessary step in tumor development in humans.⁸⁶ Thus, the efforts to fully recapitulate the early steps of *BRCA*-related tumorigenesis in human model systems are still ongoing. One approach involves utilizing genetically modified non-tumorigenic human breast epithelial cell lines, such as MCF10A. In this setting, cells bearing a mono-allelic mutation in *BRCA1* exhibited increased genomic instability and significant deficiencies in HR repair compared to their wild-type counterparts.⁸⁷ Subsequent investigations on primary human mammary cells and fibroblasts derived from *BRCA1*-mutation carriers revealed that the HR-repair of induced DSBs was intact in these cells whereas their ability to repair replication stress-inducing lesions was attenuated.⁸⁸ Intriguingly, in both studies, the heterozygous cells showed no sensitivity to PARP inhibition.^{87,88}

One proposed model to explain the “conditional haploinsufficiency” of *BRCA1* for replication stress stems from its key function in preventing and repairing collapsed replication forks, leading to a limited availability of *BRCA1* for HR repair.⁸⁸ Similar findings were observed in primary breast epithelial cells derived from *BRCA2* mutation carriers, which displayed a weakened response to replication stress manifested in increased DNA damage after HU treatment and impaired replication checkpoint response.⁸⁹

Other strategies to investigate how cells overcome cell death and facilitate transformation have been the use of genetic screens in the context of *BRCA* deficiency. One of these genetic screens revealed that inactivating 53BP1, a DNA repair protein involved in the non-homologous end joining (NHEJ) pathway, could mirror the effect of p53 loss in rescuing proliferation defects and drug sensitivity in *Brca1* null ES cells, suggesting that

53BP1 is involved in *BRCA1*-related tumorigenesis.^{90,91} This rescue mechanism depended on the restoration of DNA-end resection (counteracted by 53BP1), required for HR. Later on, it was found that 53BP1 depletion could rescue *BRCA1* deficiency via a backup pathway driven by the ubiquitin ligase RNF168, as this factor could promote RAD51-mediated HR when *BRCA1* was absent. This activity was found to be independent of p53 status.⁹² Interestingly, the redundancy observed between *BRCA1* and RNF168 suggested that reduced levels of RNF168 or its activity could be sufficient to limit HR⁹², revealing another “conditional-haploinsufficiency” mechanism for *BRCA1*.

Emerging mechanisms of haploinsufficiency related to *BRCA1/2*

In recent years, it has become increasingly recognized that genes beyond *BRCA1/2* can modulate tumorigenesis in *BRCA*-mutated cancer. For instance, patient-derived *BRCA1*-mutant cells exhibited elevated expression of the epidermal growth factor receptor (EGFR), which could potentially explain their enhanced proliferative capacity.⁹³

One of the mechanisms proposed for tumor formation in *BRCA*-mutated cells is the impact of *BRCA1/2* mutations on hormone-signaling pathways. Notably, normal breast epithelial cells carrying a mono-allelic *BRCA1* mutation exhibit increased activity of the ER and elevated expression of the PR.⁹⁴ This can be attributed to the inhibitory role of *BRCA1* in the transcriptional activity of the ER.⁹⁵ Moreover, *BRCA1*-heterozygous cells upregulated the transcription of the *CYP1A* gene, an estrogen-metabolizing enzyme, which leads to increased DNA damage in these cells.⁹⁶ Consequently, cells with impaired *BRCA1* function display enhanced expression of hormone receptors. In addition, the heterozygosity for a germline mutation in either *BRCA1* or *BRCA2* leads to the preferential expression of a specific isoform of the PR, thereby impacting cellular differentiation.⁹⁷

An alternative proposed mechanism involves the cellular accumulation of aldehydes, leading to selective depletion of *BRCA2* via proteasomal degradation and resulting in haploinsufficiency⁹⁸; Intriguingly, other proteins within HR and FA pathways remained unaffected.⁹⁹ Aldehydes are naturally present in the environment and are also generated as by-products of cellular metabolic processes. The authors found that in cells harboring a heterozygous *BRCA2* mutation, *BRCA2* protein degradation reached a threshold where replication fork protection was defective and chromosomal aberrations followed. This “induced haploinsufficiency” could be counteracted by RNase H treatment, a nuclease that specifically degrades RNA

hybridized to DNA, suggesting that DNA-RNA hybrids were implicated in the observed phenotype. In line with these findings, *BRCA1* and *BRCA2* have been involved in the prevention and resolution of DNA-RNA hybrids^{99–101}

Finally, tissue analysis from *BRCA1*-mutation carriers uncovered how pre-cancer-associated fibroblasts (pre-CAFs) secrete pro-proliferative signals and matrix metalloproteinases promoting extracellular matrix (ECM) disassembly and contribute to cancer initiation.^{102,103} Consequently, this study highlights the role of the stromal niche in *BRCA*-related tumorigenesis.

Perspectives and implications for clinical practice

The large size and complexity of *BRCA1* and *BRCA2* proteins have challenged the study of their function ever since they were discovered nearly 30 years ago. The multiple interrelated functions they play to preserve genome integrity and the fact that they are essential in cells have also challenged researchers when inferring their function from the phenotype of cells lacking *BRCA1/2*. Understanding the mechanism of LOH and whether this is a cause or a consequence of tumor development in this setting also appears crucial in the management of *BRCA1* and *BRCA2* germline-mutated tumors. For example, recent discoveries indicate that the absence of LOH in ovarian tumors correlates with poorer overall survival when treated with platinum chemotherapy compared to those with LOH.⁶⁸ Thus, it is evident that recapitulating the early steps of tumorigenesis linked to *BRCA1/2* will be key to refining the strategies for the prevention and treatment of *BRCA*-related cancer. This will require relevant models that mimic precancerous lesions; the development of patient-derived organoid cultures¹⁰⁴ in recent years provides a suitable framework to do so.

Increasing evidence suggests that depending on the localization of *BRCA1* or *BRCA2* mutation in the sequence, their incidence in cancer and which cancer they predispose to (breast or ovarian) may change.¹⁰⁵ The variant localization also affects its impact on function, especially on HR, as it has been observed in functional assays; this in turn influences cancer risk.^{106,107} Furthermore, although both genes contribute to the development of hereditary breast tumors, mutations in *BRCA1* confer a 2-fold higher risk of developing ovarian cancer compared to *BRCA2* mutations.⁶ On the other hand, *BRCA2* mutations confer an increased risk of developing other types of cancer including male breast, pancreatic, and prostate cancer.^{70,108–110} The reasons for these differences in *BRCA1* vs *BRCA2* tumors and for the tissue specificities observed are still unclear. Nonetheless, a recent study encompassing 55 diverse tumor types sheds light on this. The authors found that for specific cancer types like

breast and ovarian, *BRCA* mutations, whether germline or somatic, correlated with tumor development and LOH.¹¹¹ Conversely, in other tissues like the lungs, *BRCA* gene mutations appeared unrelated to the process of tumor formation. Another study found that primary breast epithelial cells bearing *BRCA1* mutations exhibited genome instability and a premature senescence phenotype. Interestingly, this phenotype was found specifically in breast and not skin epithelial cells¹¹², providing clues on the tissue specificity of *BRCA1*-associated cancer. The use of xenograft models and the genomic profiling of patient-derived tumors of different origins would likely help to elucidate why only some cell lineages are affected by *BRCA* mutations.

As mentioned above, although *BRCA*-deficient cells are generally sensitive to DNA-damaging agents like PARP inhibitors and cross-linking agents (e.g., cisplatin, MMC), not all *BRCA*-related tumors exhibit a positive response to these treatments. Furthermore, many of these tumors acquire resistance to these therapies over time. Thus, many efforts are ongoing to reveal the mechanisms of therapy resistance in *BRCA1/2* mutated cancer.^{21,27,113–116} In this regard, the reported tumor *BRCA1/2* LOH heterogeneity within *BRCA1/2* tumors^{54,68} might be another source of acquired resistance. The development of single-cell NGS could be instrumental in tackling these questions and tailor cancer treatment.¹¹⁷

CRedit authorship contribution statement

Anna Minello: Conceptualization, Writing – review & editing. **Aura Carreira:** Conceptualization, Writing – review & editing, Supervision, Funding acquisition.

DATA AVAILABILITY

No data was used for the research described in the article.

DECLARATION OF COMPETING INTEREST

The authors declare that they have no known competing financial interests or personal relationships that could have appeared to influence the work reported in this paper.

Acknowledgments

We apologize to all colleagues who have made contributions in the field and could not be cited owing to space constraints.

This work was supported with funding from Institut Curie, CNRS, Matmut Assurance, Gray's

Foundation Basser Initiative, the French Breast Cancer Association “Ruban Rose”, the Worldwide Cancer Research and the Spanish Association for Cancer Research (AECC) grant 22-0222 to A. C. A. M. was supported by a French governmental fellowship and a 4th year PhD Fellowship from the French Medical Research Foundation (FRM).

Received 4 July 2023;

Accepted 8 September 2023;

Available online 14 September 2023

Keywords:

BRCA haploinsufficiency;
loss of heterozygosity;
genome instability;
cancer predisposition;
breast cancer

References

- Sung, H., Ferlay, J., Siegel, R.L., Laversanne, M., Soerjomataram, I., Jemal, A., Bray, F., (2020). Global Cancer Statistics 2020: GLOBOCAN Estimates of Incidence and Mortality Worldwide for 36 Cancers in 185 Countries. *CA Cancer J. Clin.* **71** (2021), 209–249. <https://doi.org/10.3322/caac.21660>.
- Easton, D.F., Bishop, D.T., Ford, D., Crockford, G.P., (1993). Genetic linkage analysis in familial breast and ovarian cancer: results from 214 families. The Breast Cancer Linkage Consortium. *Am. J. Hum. Genet.* **52**, 678–701.
- Wooster, R., Bignell, G., Lancaster, J., Swift, S., Seal, S., Mangion, J., Collins, N., Gregory, S., et al., (1995). Identification of the breast cancer susceptibility gene BRCA2. *Nature* **378**, 789–792. <https://doi.org/10.1038/378789a0>.
- Futreal, P.A., Liu, Q., Shattuck-Eidens, D., Cochran, C., Harshman, K., Tavtigian, S., Bennett, L.M., Haugen-Strano, A., et al., (1994). BRCA1 mutations in primary breast and ovarian carcinomas. *Science* **266**, 120–122. <https://doi.org/10.1126/science.7939630>.
- Miki, Y., Swensen, J., Shattuck-Eidens, D., Futreal, P.A., Harshman, K., Tavtigian, S., Liu, Q., Cochran, C., et al., (1994). A strong candidate for the breast and ovarian cancer susceptibility gene BRCA1. *Science* **266**, 66–71. <https://doi.org/10.1126/science.7545954>.
- Kuchenbaecker, K.B., Hopper, J.L., Barnes, D.R., Phillips, K.-A., Mooij, T.M., Roos-Blom, M.-J., Jervis, S., van Leeuwen, F.E., et al., (2017). Risks of Breast, Ovarian, and Contralateral Breast Cancer for BRCA1 and BRCA2 Mutation Carriers. *J. Am. Med. Assoc.* **317**, 2402–2416. <https://doi.org/10.1001/jama.2017.7112>.
- Howlett, N.G., Taniguchi, T., Olson, S., Cox, B., Waisfisz, Q., de Die-Smulders, C., Persky, N., Grompe, M., et al., (2002). Biallelic Inactivation of BRCA2 in Fanconi Anemia. *Science* **297**, 606–609. <https://doi.org/10.1126/science.1073834>.
- Schwartz, R.S., D’Andrea, A.D., (2010). Susceptibility Pathways in Fanconi’s Anemia and Breast Cancer. *New Engl. J. Med.* **362**, 1909–1919. <https://doi.org/10.1056/nejmra0809889>.
- Schlegel, B.P., Jodelka, F.M., Nunez, R., (2006). BRCA1 Promotes Induction of ssDNA by Ionizing Radiation. *Cancer Res.* **66**, 5181–5189. <https://doi.org/10.1158/0008-5472.can-05-3209>.
- Moynahan, M.E., Chiu, J.W., Koller, B.H., Jasin, M., (1999). Brca1 controls homology-directed DNA repair. *Mol. Cell* **4**, 511–518. [https://doi.org/10.1016/s1097-2765\(00\)80202-6](https://doi.org/10.1016/s1097-2765(00)80202-6).
- Yang, H., Li, Q., Fan, J., Holloman, W.K., Pavletich, N.P., (2005). The BRCA2 homologue Brh2 nucleates RAD51 filament formation at a dsDNA–ssDNA junction. *Nature* **433**, 653–657. <https://doi.org/10.1038/nature03234>.
- Carreira, A., Hilario, J., Amitani, I., Baskin, R.J., Shivji, M. K.K., Venkitaraman, A.R., Kowalczykowski, S.C., (2009). The BRC Repeats of BRCA2 Modulate the DNA-Binding Selectivity of RAD51. *Cell* **136**, 1032–1043. <https://doi.org/10.1016/j.cell.2009.02.019>.
- Jensen, R.B., Carreira, A., Kowalczykowski, S.C., (2010). Purified human BRCA2 stimulates RAD51-mediated recombination. *Nature* **467**, 678–683. <https://doi.org/10.1038/nature09399>.
- Sung, P., (1994). Catalysis of ATP-dependent homologous DNA pairing and strand exchange by Yeast RAD51 protein. *Science* **265**, 1241–1243. <https://doi.org/10.1126/science.8066464>.
- Hilario, J., Amitani, I., Baskin, R.J., Kowalczykowski, S.C., (2009). Direct imaging of human Rad51 nucleoprotein dynamics on individual DNA molecules. *Proc. Natl. Acad. Sci.* **106**, 361–368. <https://doi.org/10.1073/pnas.0811965106>.
- Johnson, R.D., Jasin, M., (2000). Sister chromatid gene conversion is a prominent double-strand break repair pathway in mammalian cells. *EMBO J.* **19**, 3398–3407. <https://doi.org/10.1093/emboj/19.13.3398>.
- Schlacher, K., Wu, H., Jasin, M., (2012). A distinct replication fork protection pathway connects fanconi anemia tumor suppressors to RAD51-BRCA1/2. *Cancer Cell* **22**, 106–116. <https://doi.org/10.1016/j.ccr.2012.05.015>.
- Daza-Martin, M., Starowicz, K., Jamshad, M., Tye, S., Ronson, G.E., MacKay, H.L., Chauhan, A.S., Walker, A. K., et al., (2019). Isomerization of BRCA1–BARD1 promotes replication fork protection. *Nature* **571**, 521–527. <https://doi.org/10.1038/s41586-019-1363-4>.
- Schlacher, K., Christ, N., Siaud, N., Egashira, A., Wu, H., Jasin, M., (2011). Double-strand break repair-independent role for BRCA2 in blocking stalled replication fork degradation by MRE11. *Cell* **145**, 529–542. <https://doi.org/10.1016/j.cell.2011.03.041>.
- Kolinjivadi, A.M., Sannino, V., Antoni, A.D., Zadorozhny, K., Kilkenny, M., Técher, H., Baldi, G., Shen, R., et al., (2017). Smarcal1-mediated fork reversal triggers Mre11-Dependent degradation of nascent DNA in the absence of Brca2 and stable Rad51 nucleofilaments. *Mol. Cell* **67**, 867–881.e7. <https://doi.org/10.1016/j.molcel.2017.07.001>.
- Panzarino, N.J., Kraus, J.J., Cong, K., Peng, M., Mosqueda, M., Nayak, S.U., Bond, S.M., Calvo, J.A., et al., (2021). Replication gaps underlie BRCA deficiency and therapy response. *Cancer Res.* **81**, 1388–1397. <https://doi.org/10.1158/0008-5472.can-20-1602>.
- Tirman, S., Quinet, A., Wood, M., Meroni, A., Cybulka, E., Jackson, J., Pegoraro, S., Simoneau, A., et al., (2021). Temporally distinct post-replicative repair mechanisms fill PRIMPOL-dependent ssDNA gaps in human cells. *Mol.*

- Cell* **81**, 4026–4040.e8. <https://doi.org/10.1016/j.molcel.2021.09.013>.
23. Cong, K., Peng, M., Kousholt, A.N., Lee, W.T.C., Lee, S., Nayak, S., Kraiss, J., VanderVere-Carozza, P.S., et al., (2021). Replication gaps are a key determinant of PARP inhibitor synthetic lethality with BRCA deficiency. *Mol. Cell* **81**, 3128–3144.e7. <https://doi.org/10.1016/j.molcel.2021.06.011>.
 24. Vugic, D., Dumoulin, I., Martin, C., Minello, A., Alvaro-Aranda, L., Gomez-Escudero, J., Chaaban, R., Lebby, R., et al., (2023). Replication gap suppression depends on the double-strand DNA binding activity of BRCA2. *Nat. Commun.* **14**, 446. <https://doi.org/10.1038/s41467-023-36149-0>.
 25. Nagaraju, G., Scully, R., (2007). Minding the gap: The underground functions of BRCA1 and BRCA2 at stalled replication forks. *DNA Repair* **6**, 1018–1031. <https://doi.org/10.1016/j.dnarep.2007.02.020>.
 26. Thakar, T., Dhoonmoon, A., Straka, J., Schleicher, E.M., Nicolae, C.M., Moldovan, G.-L., (2022). Lagging strand gap suppression connects BRCA-mediated fork protection to nucleosome assembly through PCNA-dependent CAF-1 recycling. *Nat. Commun.* **13**, 5323. <https://doi.org/10.1038/s41467-022-33028-y>.
 27. Chaudhuri, A.R., Callen, E., Ding, X., Gogola, E., Duarte, A.A., Lee, J.-E., Wong, N., Lafarga, V., et al., (2016). Replication fork stability confers chemoresistance in BRCA-deficient cells. *Nature* **535**, 382–387. <https://doi.org/10.1038/nature18325>.
 28. Feng, W., Jasin, M., (2017). BRCA2 suppresses replication stress-induced mitotic and G1 abnormalities through homologous recombination. *Nat. Commun.* **8**, 525. <https://doi.org/10.1038/s41467-017-00634-0>.
 29. Hakem, R., de la Pompa, J.L., Sirard, C., Mo, R., Woo, M., Hakem, A., Wakeham, A., Potter, J., et al., (1996). The Tumor Suppressor Gene Brca1 Is Required for Embryonic Cellular Proliferation in the Mouse. *Cell* **85**, 1009–1023. [https://doi.org/10.1016/s0092-8674\(00\)81302-1](https://doi.org/10.1016/s0092-8674(00)81302-1).
 30. Suzuki, A., de la Pompa, J.L., Hakem, R., Elia, A., Yoshida, R., Mo, R., Nishina, H., Chuang, T., et al., (1997). Brca2 is required for embryonic cellular proliferation in the mouse. *Gene Dev.* **11**, 1242–1252. <https://doi.org/10.1101/gad.11.10.1242>.
 31. Liu, C.Y., Flesken-Nikitin, A., Li, S., Zeng, Y., Lee, W.H., (1996). Inactivation of the mouse Brca1 gene leads to failure in the morphogenesis of the egg cylinder in early postimplantation development. *Gene Dev.* **10**, 1835–1843. <https://doi.org/10.1101/gad.10.14.1835>.
 32. Ludwig, T., Chapman, D.L., Papaioannou, V.E., Efstratiadis, A., (1997). Targeted mutations of breast cancer susceptibility gene homologs in mice: lethal phenotypes of Brca1, Brca2, Brca1/Brca2, Brca1/p53, and Brca2/p53 nullizygous embryos. *Gene Dev.* **11**, 1226–1241. <https://doi.org/10.1101/gad.11.10.1226>.
 33. Finlay, C.A., Hinds, P.W., Levine, A.J., (1989). The p53 proto-oncogene can act as a suppressor of transformation. *Cell* **57**, 1083–1093. [https://doi.org/10.1016/0092-8674\(89\)90045-7](https://doi.org/10.1016/0092-8674(89)90045-7).
 34. Sharan, S.K., Morimatsu, M., Albrecht, U., Lim, D.-S., Regel, E., Dinh, C., Sands, A., Eichele, G., et al., (1997). Embryonic lethality and radiation hypersensitivity mediated by Rad51 in mice lacking Brca2. *Nature* **386**, 804–810. <https://doi.org/10.1038/386804a0>.
 35. Scully, R., Chen, J., Plug, A., Xiao, Y., Weaver, D., Feunteun, J., Ashley, T., Livingston, D.M., (1997). Association of BRCA1 with Rad51 in Mitotic and Meiotic Cells. *Cell* **88**, 265–275. [https://doi.org/10.1016/s0092-8674\(00\)81847-4](https://doi.org/10.1016/s0092-8674(00)81847-4).
 36. Chen, J., Silver, D.P., Walpita, D., Cantor, S.B., Gazdar, A.F., Tomlinson, G., Couch, F.J., Weber, B.L., et al., (1998). Stable interaction between the products of the BRCA1 and BRCA2 tumor suppressor genes in mitotic and meiotic cells. *Mol. Cell* **2**, 317–328. [https://doi.org/10.1016/s1097-2765\(00\)80276-2](https://doi.org/10.1016/s1097-2765(00)80276-2).
 37. Tutt, A., Gabriel, A., Bertwistle, D., Connor, F., Paterson, H., Peacock, J., Ross, G., Ashworth, A., (1999). Absence of Brca2 causes genome instability by chromosome breakage and loss associated with centrosome amplification. *Curr. Biol.* **9**, 1107–S1. [https://doi.org/10.1016/s0960-9822\(99\)80479-5](https://doi.org/10.1016/s0960-9822(99)80479-5).
 38. Patel, K.J., Yu, V.P.C.C., Lee, H., Corcoran, A., Thistlethwaite, F.C., Evans, M.J., Colledge, W.H., Friedman, L.S., et al., (1998). Involvement of Brca2 in DNA Repair. *Mol. Cell* **1**, 347–357. [https://doi.org/10.1016/s1097-2765\(00\)80035-0](https://doi.org/10.1016/s1097-2765(00)80035-0).
 39. Moynahan, M.E., Pierce, A.J., Jasin, M., (2001). BRCA2 Is required for homology-directed repair of chromosomal breaks. *Mol. Cell* **7**, 263–272. [https://doi.org/10.1016/s1097-2765\(01\)00174-5](https://doi.org/10.1016/s1097-2765(01)00174-5).
 40. Xia, F., Taghian, D.G., DeFrank, J.S., Zeng, Z.-C., Willers, H., Iliakis, G., Powell, S.N., (2001). Deficiency of human BRCA2 leads to impaired homologous recombination but maintains normal nonhomologous end joining. *Proc. National. Acad. Sci.* **98**, 8644–8649. <https://doi.org/10.1073/pnas.151253498>.
 41. Knudson, A.G., (1971). Mutation and cancer: statistical study of retinoblastoma. *Proc. National. Acad. Sci.* **68**, 820–823. <https://doi.org/10.1073/pnas.68.4.820>.
 42. Collins, N., McManus, R., Wooster, R., Mangion, J., Seal, S., Lakhani, S.R., Ormiston, W., Daly, P.A., et al., (1995). Consistent loss of the wild type allele in breast cancers from a family linked to the BRCA2 gene on chromosome 13q12-13. *Oncogene* **10**, 1673–1675.
 43. Gudmundsson, J., Johannesdottir, G., Bergthorsson, J.T., Arason, A., Ingvarsson, S., Egilsson, V., Barkardottir, R. B., (1995). Different tumor types from BRCA2 carriers show wild-type chromosome deletions on 13q12-q13. *Cancer Res.* **55**, 4830–4832.
 44. Neuhausen, S.L., Marshall, C.J., (1994). Loss of heterozygosity in familial tumors from three BRCA1-linked kindreds. *Cancer Res.* **54**, 6069–6072.
 45. Smith, S.A., Easton, D.F., Evans, D.G.R., Ponder, B.A.J., (1992). Allele losses in the region 17q12–21 in familial breast and ovarian cancer involve the wild-type chromosome. *Nat. Genet.* **2**, 128–131. <https://doi.org/10.1038/ng1092-128>.
 46. Berger, A.H., Knudson, A.G., Pandolfi, P.P., (2011). A continuum model for tumour suppression. *Nature* **476**, 163–169. <https://doi.org/10.1038/nature10275>.
 47. Moynahan, M.E., Jasin, M., (1997). Loss of heterozygosity induced by a chromosomal double-strand break. *Proc. Natl. Acad. Sci.* **94**, 8988–8993. <https://doi.org/10.1073/pnas.94.17.8988>.
 48. Osorio, A., de la Hoya, M., Rodríguez-López, R., Martínez-Ramírez, A., Cazorla, A., Granizo, J.J., Esteller, M., Rivas, C., et al., (2002). Loss of heterozygosity analysis at the BRCA loci in tumor

- samples from patients with familial breast cancer. *Int. J. Cancer* **99**, 305–309. <https://doi.org/10.1002/ijc.10337>.
49. Thiagalingam, S., Foy, R.L., Cheng, K., Lee, H.J., Thiagalingam, A., Ponte, J.F., (2002). Loss of heterozygosity as a predictor to map tumor suppressor genes in cancer: molecular basis of its occurrence. *Curr. Opin. Oncol.* **14**, 65–72. <https://doi.org/10.1097/00001622-200201000-00012>.
 50. Dworkin, A.M., Spearman, A.D., Tseng, S.Y., Sweet, K., Toland, A.E., (2009). Methylation not a frequent “second hit” in tumors with germline BRCA mutations. *Fam. Cancer* **8**, 339–346. <https://doi.org/10.1007/s10689-009-9240-1>.
 51. Deshpande, M., Paniza, T., Jalloul, N., Nanjangud, G., Twarowski, J., Koren, A., Zaninovic, N., Zhan, Q., et al., (2022). Error-prone repair of stalled replication forks drives mutagenesis and loss of heterozygosity in haploinsufficient BRCA1 cells. *Mol. Cell*. <https://doi.org/10.1016/j.molcel.2022.08.017>.
 52. Crook, T., Brooks, L.A., Crossland, S., Osin, P., Barker, K. T., Waller, J., Philp, E., Smith, P.D., et al., (1998). p53 mutation with frequent novel codons but not a mutator phenotype in BRCA1- and BRCA2-associated breast tumours. *Oncogene* **17**, 1681–1689. <https://doi.org/10.1038/sj.onc.1202106>.
 53. Rhei, E., Bogomolny, F., Federici, M.G., Maresco, D.L., Offit, K., Robson, M.E., Saigo, P.E., Boyd, J., (1998). Molecular genetic characterization of BRCA1- and BRCA2-linked hereditary ovarian cancers. *Cancer Res.* **58**, 3193–3196.
 54. Martins, F.C., De, S., Almendro, V., Gönen, M., Park, S. Y., Blum, J.L., Herlihy, W., Ethington, G., et al., (2012). Evolutionary pathways in BRCA1-associated breast tumors. *Cancer Discov.* **2**, 503–511. <https://doi.org/10.1158/2159-8290.cd-11-0325>.
 55. Alexandrov, L.B., Nik-Zainal, S., Wedge, D.C., Aparicio, S.A.J.R., Behjati, S., Biankin, A.V., Bignell, G.R., Bolli, N., Borg, A., et al., (2013). Signatures of mutational processes in human cancer. *Nature* **500**, 415–421. <https://doi.org/10.1038/nature12477>.
 56. Nik-Zainal, S., Davies, H., Staaf, J., Ramakrishna, M., Glodzik, D., Zou, X., Martincorena, I., Alexandrov, L.B., et al., (2016). Landscape of somatic mutations in 560 breast cancer whole-genome sequences. *Nature* **534**, 47–54. <https://doi.org/10.1038/nature17676>.
 57. Davies, H., Glodzik, D., Morganella, S., Yates, L.R., Staaf, J., Zou, X., Ramakrishna, M., Martin, S., et al., (2017). HRDetect is a predictor of BRCA1 and BRCA2 deficiency based on mutational signatures. *Nat. Med.* **23**, 517–525. <https://doi.org/10.1038/nm.4292>.
 58. Roy, R., Chun, J., Powell, S.N., (2012). BRCA1 and BRCA2: different roles in a common pathway of genome protection. *Nat. Rev. Cancer* **12**, 68–78. <https://doi.org/10.1038/nrc3181>.
 59. Visvader, J.E., Stingl, J., (2014). Mammary stem cells and the differentiation hierarchy: current status and perspectives. *Gene Dev.* **28**, 1143–1158. <https://doi.org/10.1101/gad.242511.114>.
 60. Nguyen, Q.H., Pervolarakis, N., Blake, K., Ma, D., Davis, R.T., James, N., Phung, A.T., Willey, E., et al., (2018). Profiling human breast epithelial cells using single cell RNA sequencing identifies cell diversity. *Nat. Commun.* **9**, 2028. <https://doi.org/10.1038/s41467-018-04334-1>.
 61. Lakhani, S.R., Reis-Filho, J.S., Fulford, L., Penault-Llorca, F., van der Vijver, M., Parry, S., Bishop, T., Benitez, J., et al., (2005). Prediction of BRCA1 status in patients with breast cancer using estrogen receptor and basal phenotype. *Clin. Cancer Res.* **11**, 5175–5180. <https://doi.org/10.1158/1078-0432.ccr-04-2424>.
 62. Palacios, J., Honrado, E., Osorio, A., Cazorla, A., Sarrió, D., Barroso, A., Rodríguez, S., Cigudosa, J.C., et al., (2005). Phenotypic characterization of BRCA1 and BRCA2 tumors based in a tissue microarray study with 37 immunohistochemical markers. *Breast Cancer Res Tr.* **90**, 5–14. <https://doi.org/10.1007/s10549-004-1536-0>.
 63. Molyneux, G., Geyer, F.C., Magnay, F.-A., McCarthy, A., Kendrick, H., Natrajan, R., MacKay, A., Grigoriadis, A., et al., (2010). BRCA1 basal-like breast cancers originate from luminal epithelial progenitors and not from basal stem cells. *Cell Stem. Cell* **7**, 403–417. <https://doi.org/10.1016/j.stem.2010.07.010>.
 64. Lim, E., Vaillant, F., Wu, D., Forrest, N.C., Pal, B., Hart, A. H., Asselin-Labat, M.-L., Gyorki, D.E., et al., (2009). Aberrant luminal progenitors as the candidate target population for basal tumor development in BRCA1 mutation carriers. *Nat. Med.* **15**, 907–913. <https://doi.org/10.1038/nm.2000>.
 65. King, T.A., Li, W., Brogi, E., Yee, C.J., Gemignani, M.L., Olvera, N., Levine, D.A., Norton, L., et al., (2007). Heterogenic Loss of the Wild-Type BRCA Allele in Human Breast Tumorigenesis. *Ann. Surg. Oncol.* **14**, 2510–2518. <https://doi.org/10.1245/s10434-007-9372-1>.
 66. Rennstam, K., Ringberg, A., Cunliffe, H.E., Olsson, H., Landberg, G., Hedenfalk, I., (2010). Genomic alterations in histopathologically normal breast tissue from BRCA1 mutation carriers may be caused by BRCA1 haploinsufficiency, *Genes, Chromosom. Cancer* **49**, 78–90. <https://doi.org/10.1002/gcc.20723>.
 67. Larson, P.S., Schlechter, B.L., de las Morenas, A., Garber, J.E., Cupples, L.A., Rosenberg, C.L., (2005). Allele imbalance, or loss of heterozygosity, in normal breast epithelium of sporadic breast cancer cases and BRCA1 gene mutation carriers is increased compared with reduction mammoplasty tissues. *J. Clin. Oncol.* **23**, 8613–8619. <https://doi.org/10.1200/jco.2005.02.1451>.
 68. Maxwell, K.N., Wubbenhorst, B., Wenz, B.M., Sloover, D. D., Pluta, J., Emery, L., Barrett, A., Kraya, A.A., et al., (2017). BRCA locus-specific loss of heterozygosity in germline BRCA1 and BRCA2 carriers. *Nat. Commun.* **8**, 319. <https://doi.org/10.1038/s41467-017-00388-9>.
 69. Kanchi, K.L., Johnson, K.J., Lu, C., McLellan, M.D., Leiserson, M.D.M., Wendl, M.C., Zhang, Q., Koboldt, D. C., et al., (2014). Integrated analysis of germline and somatic variants in ovarian cancer. *Nat. Commun.* **5**, 3156. <https://doi.org/10.1038/ncomms4156>.
 70. Goggins, M., Schutte, M., Lu, J., Moskaluk, C.A., Weinstein, C.L., Petersen, G.M., Yeo, C.J., Jackson, C. E., et al., (1996). Germline BRCA2 gene mutations in patients with apparently sporadic pancreatic carcinomas. *Cancer Res.* **56**, 5360–5364.
 71. Skoulidis, F., Cassidy, L.D., Pisupati, V., Jonasson, J.G., Bjarnason, H., Eyfjord, J.E., Karreth, F.A., Lim, M., et al., (2010). Germline Brca2 heterozygosity promotes Kras (G12D) -driven carcinogenesis in a murine model of familial pancreatic cancer. *Cancer Cell* **18**, 499–509. <https://doi.org/10.1016/j.ccr.2010.10.015>.

72. Scully, R., Livingston, D.M., (2000). In search of the tumour-suppressor functions of BRCA1 and BRCA2. *Nature* **408**, 429–432. <https://doi.org/10.1038/35044000>.
73. Coupier, I., Baldeyron, C., Rousseau, A., Mosseri, V., Pagès-Berhouet, S., Caux-Moncoutier, V., Papadopoulo, D., Stoppa-Lyonnet, D., (2003). Fidelity of DNA double-strand break repair in heterozygous cell lines harbouring BRCA1 missense mutations. *Oncogene* **23**, 914–919. <https://doi.org/10.1038/sj.onc.1207191>.
74. Arnold, K., Kim, M.-K., Frerik, K., Edler, L., Savelyeva, L., Schmezer, P., Wiedemeyer, R., (2006). Lower level of BRCA2 protein in heterozygous mutation carriers is correlated with an increase in DNA double strand breaks and an impaired DSB repair. *Cancer Lett.* **243**, 90–100. <https://doi.org/10.1016/j.canlet.2005.11.041>.
75. Warren, M., Lord, C.J., Masabanda, J., Griffin, D., Ashworth, A., (2003). Phenotypic effects of heterozygosity for a BRCA2 mutation. *Hum. Mol. Genet.* **12**, 2645–2656. <https://doi.org/10.1093/hmg/ddg277>.
76. Tannenbaum, B., Mofunanya, T., Schoenfeld, A.R., (2007). DNA damage repair is unaffected by mimicked heterozygous levels of BRCA2 in HT-29 cells. *Int. J. Biol. Sci.* **3**, 402–407. <https://doi.org/10.7150/ijbs.3.402>.
77. Kass, E.M., Lim, P.X., Helgadottir, H.R., Moynahan, M.E., Jasin, M., (2016). Robust homology-directed repair within mouse mammary tissue is not specifically affected by Brca2 mutation. *Nat. Commun.* **7**, 13241. <https://doi.org/10.1038/ncomms13241>.
78. Berton, T.R., Matsumoto, T., Page, A., Conti, C.J., Deng, C.-X., Jorcano, J.L., Johnson, D.G., (2003). Tumor formation in mice with conditional inactivation of Brca1 in epithelial tissues. *Oncogene* **22**, 5415–5426. <https://doi.org/10.1038/sj.onc.1206825>.
79. Sedic, M., Kuperwasser, C., (2016). BRCA1-haploinsufficiency: Unraveling the molecular and cellular basis for tissue-specific cancer. *Cell Cycle* **15**, 621–627. <https://doi.org/10.1080/15384101.2016.1141841>.
80. Evers, B., Jonkers, J., (2006). Mouse models of BRCA1 and BRCA2 deficiency: past lessons, current understanding and future prospects. *Oncogene* **25**, 5885–5897. <https://doi.org/10.1038/sj.onc.1209871>.
81. Connor, F., Bertwistle, D., Mee, P.J., Ross, G.M., Swift, S., Grigorieva, E., Tybulewicz, V.L., Ashworth, A., (1997). Tumorigenesis and a DNA repair defect in mice with a truncating Brca2 mutation. *Nat. Genet.* **17**, 423–430. <https://doi.org/10.1038/ng1297-423>.
82. Friedman, L.S., Thistlethwaite, F.C., Patel, K.J., Yu, V.P., Lee, H., Venkitaraman, A.R., Abel, K.J., Carlton, M.B., et al., (1998). Thymic lymphomas in mice with a truncating mutation in Brca2. *Cancer Res.* **58**, 1338–1343.
83. Jonkers, J., Meuwissen, R., van der Gulden, H., Peterse, H., van der Valk, M., Berns, A., (2001). Synergistic tumor suppressor activity of BRCA2 and p53 in a conditional mouse model for breast cancer. *Nat. Genet.* **29**, 418–425. <https://doi.org/10.1038/ng747>.
84. Ludwig, T., Fisher, P., Murty, V., Efstratiadis, A., (2001). Development of mammary adenocarcinomas by tissue-specific knockout of Brca2 in mice. *Oncogene* **20**, 3937–3948. <https://doi.org/10.1038/sj.onc.1204512>.
85. Liu, X., Holstege, H., van der Gulden, H., Treur-Mulder, M., Zevenhoven, J., Velds, A., Kerkhoven, R.M., van Vliet, M.H., et al., (2007). Somatic loss of BRCA1 and p53 in mice induces mammary tumors with features of human BRCA1-mutated basal-like breast cancer. *Proc. Natl. Acad. Sci.* **104**, 12111–12116. <https://doi.org/10.1073/pnas.0702969104>.
86. Greenblatt, M.S., Chappuis, P.O., Bond, J.P., Hamel, N., Foulkes, W.D., (2001). TP53 mutations in breast cancer associated with BRCA1 or BRCA2 germ-line mutations: distinctive spectrum and structural distribution. *Cancer Res.* **61**, 4092–4097.
87. Konishi, H., Mohseni, M., Tamaki, A., Garay, J.P., Croessmann, S., Karnan, S., Ota, A., Wong, H.Y., et al., (2011). Mutation of a single allele of the cancer susceptibility gene BRCA1 leads to genomic instability in human breast epithelial cells. *Proc National Acad Sci.* **108**, 17773–17778. <https://doi.org/10.1073/pnas.1110969108>.
88. Pathania, S., Bade, S., Guillou, M.L., Burke, K., Reed, R., Bowman-Colin, C., Su, Y., Ting, D.T., et al., (2014). BRCA1 haploinsufficiency for replication stress suppression in primary cells. *Nat. Commun.* **5**, 5496. <https://doi.org/10.1038/ncomms6496>.
89. Karaayvaz-Yildirim, M., Silberman, R.E., Langenbucher, A., Saladi, S.V., Ross, K.N., Zarcaro, E., Desmond, A., Yildirim, M., et al., (2020). Aneuploidy and a deregulated DNA damage response suggest haploinsufficiency in breast tissues of BRCA2 mutation carriers. *Sci. Adv.* **6**, eaay2611. <https://doi.org/10.1126/sciadv.aay2611>.
90. Bouwman, P., Aly, A., Escandell, J.M., Pieterse, M., Bartkova, J., van der Gulden, H., Hiddingh, S., Thanasoula, M., et al., (2010). 53BP1 loss rescues BRCA1 deficiency and is associated with triple-negative and BRCA-mutated breast cancers. *Nat. Struct. Mol. Biol.* **17**, 688–695. <https://doi.org/10.1038/nsmb.1831>.
91. Bunting, S.F., Callén, E., Wong, N., Chen, H.-T., Polato, F., Gunn, A., Bothmer, A., Feldhahn, N., et al., (2010). 53BP1 inhibits homologous recombination in brca1-deficient cells by blocking resection of DNA breaks. *Cell* **141**, 243–254. <https://doi.org/10.1016/j.cell.2010.03.012>.
92. Zong, D., Adam, S., Wang, Y., Sasanuma, H., Callén, E., Murga, M., Day, A., Kruhlak, M.J., et al., (2019). BRCA1 Haploinsufficiency Is Masked by RNF168-mediated chromatin ubiquitylation. *Mol. Cell* **73**, 1267–1281.e7. <https://doi.org/10.1016/j.molcel.2018.12.010>.
93. Burga, L.N., Tung, N.M., Troyan, S.L., Bostina, M., Konstantinopoulos, P.A., Fountzilas, H., Spentzos, D., Miron, A., et al., (2009). Altered proliferation and differentiation properties of primary mammary epithelial cells from BRCA1 mutation carriers. *Cancer Res.* **69**, 1273–1278. <https://doi.org/10.1158/0008-5472.can-08-2954>.
94. King, T.A., Gemignani, M.L., Li, W., Giri, D.D., Panageas, K.S., Bogomolny, F., Arroyo, C., Olvera, N., et al., (2004). Increased progesterone receptor expression in benign epithelium of BRCA1-related breast cancers. *Cancer Res.* **64**, 5051–5053. <https://doi.org/10.1158/0008-5472.can-04-1283>.
95. Fan, S., Wang, J.-A., Yuan, R., Ma, Y., Meng, Q., Erdos, M.R., Pestell, R.G., Yuan, F., et al., (1999). BRCA1 inhibition of estrogen receptor signaling in transfected cells. *Science* **284**, 1354–1356. <https://doi.org/10.1126/science.284.5418.1354>.
96. Savage, K.I., Matchett, K.B., Barros, E.M., Cooper, K.M., Irwin, G.W., Gorski, J.J., Orr, K.S., Vohhodina, J., et al., (2014). BRCA1 deficiency exacerbates estrogen-induced DNA damage and genomic instability. *Cancer Res.* **74**,

- 2773–2784. <https://doi.org/10.1158/0008-5472.can-13-2611>.
97. Mote, P.A., Leary, J.A., Avery, K.A., Sandelin, K., Chenevix-Trench, G., Kirk, J.A., Clarke, C.L., (2004). kConFab Investigators, Germ-line mutations in BRCA1 or BRCA2 in the normal breast are associated with altered expression of estrogen-responsive proteins and the predominance of progesterone receptor A, *Genes. Chromosom. Cancer* **39**, 236–248. <https://doi.org/10.1002/gcc.10321>.
 98. Tan, S.L.W., Chadha, S., Liu, Y., Gabasova, E., Perera, D., Ahmed, K., Constantinou, S., Renaudin, X., et al., (2017). A Class of Environmental and Endogenous Toxins Induces BRCA2 Haploinsufficiency and Genome Instability. *Cell* **169**, 1105–1118.e15. <https://doi.org/10.1016/j.cell.2017.05.010>.
 99. Bhatia, V., Barroso, S.I., García-Rubio, M.L., Tumini, E., Herrera-Moyano, E., Aguilera, A., (2014). BRCA2 prevents R-loop accumulation and associates with TREX-2 mRNA export factor PCID2. *Nature* **511**, 362–365. <https://doi.org/10.1038/nature13374>.
 100. Hatchi, E., Skourti-Stathaki, K., Ventz, S., Pinello, L., Yen, A., Kamieniarz-Gdula, K., Dimitrov, S., Pathania, S., et al., (2015). BRCA1 recruitment to transcriptional pause sites is required for R-Loop-Driven DNA damage repair. *Mol. Cell* **57**, 636–647. <https://doi.org/10.1016/j.molcel.2015.01.011>.
 101. Sessa, G., Gómez-González, B., Silva, S., Pérez-Calero, C., Beaupere, R., Barroso, S., Martineau, S., Martin, C., et al., (2021). BRCA2 promotes DNA-RNA hybrid resolution by DDX5 helicase at DNA breaks to facilitate their repair. *EMBO J.* **40**, e106018. <https://doi.org/10.15252/embj.2020106018>.
 102. Noël, A., Jost, M., Maquoi, E., (2008). Matrix metalloproteinases at cancer tumor–host interface. *Semin. Cell Dev. Biol.* **19**, 52–60. <https://doi.org/10.1016/j.semcdb.2007.05.011>.
 103. Nee, K., Ma, D., Nguyen, Q.H., Pein, M., Pervolarakis, N., Insua-Rodríguez, J., Gong, Y., Hernandez, G., et al., (2023). Preneoplastic stromal cells promote BRCA1-mediated breast tumorigenesis. *Nat. Genet.* **55**, 595–606. <https://doi.org/10.1038/s41588-023-01298-x>.
 104. Sachs, N., de Ligt, J., Kopper, O., Gogola, E., Bounova, G., Weeber, F., Balgobind, A.V., Wind, K., et al., (2018). A living biobank of breast cancer organoids captures disease heterogeneity. *Cell* **172**, 373–386.e10. <https://doi.org/10.1016/j.cell.2017.11.010>.
 105. Rebbeck, T.R., Mitra, N., Wan, F., Sinilnikova, O.M., Healey, S., McGuffog, L., Mazoyer, S., Chenevix-Trench, G., et al., (2015). Association of Type and location of BRCA1 and BRCA2 mutations with risk of breast and ovarian cancer. *Jama* **313**, 1347–1361. <https://doi.org/10.1001/jama.2014.5985>.
 106. Guidugli, L., Pankratz, V.S., Singh, N., Thompson, J., Erding, C.A., Engel, C., Schmutzler, R., Domchek, S., et al., (2013). A classification model for BRCA2 DNA binding domain missense variants based on homology-directed repair activity. *Cancer Res.* **73**, 265–275. <https://doi.org/10.1158/0008-5472.can-12-2081>.
 107. Shimelis, H., Mesman, R.L.S., von Nicolai, C., Ehlen, A., Guidugli, L., Martin, C., Calléja, F.M.G.R., Meeks, H., et al., (2017). BRCA2 hypomorphic missense variants confer moderate risks of breast cancer. *Cancer Res.* **77**, 2789–2799.
 108. van Asperen, C.J., Brohet, R.M., Meijers-Heijboer, E.J., Hoogerbrugge, N., Verhoef, S., Vasen, H.F.A., Ausems, M.G.E.M., Menko, F.H., et al., (2005). Cancer risks in BRCA2 families: estimates for sites other than breast and ovary. *J. Med. Genet.* **42**, 711. <https://doi.org/10.1136/jmg.2004.028829>.
 109. T.B.C.L. Consortium, (1999). Cancer Risks in BRCA2 mutation carriers. *Jnci J National Cancer Inst.* **91**, 1310–1316. <https://doi.org/10.1093/jnci/91.15.1310>.
 110. Couch, F.J., Weber, B.L. (n.d.). BRCA2 germline mutations in male breast cancer cases and breast cancer families.
 111. Jonsson, P., Bandlamudi, C., Cheng, M.L., Srinivasan, P., Chavan, S.S., Friedman, N.D., Rosen, E.Y., Richards, A. L., et al., (2019). Tumour lineage shapes BRCA-mediated phenotypes. *Nature* **571**, 576–579. <https://doi.org/10.1038/s41586-019-1382-1>.
 112. Sedic, M., Skibinski, A., Brown, N., Gallardo, M., Mulligan, P., Martinez, P., Keller, P.J., Glover, E., et al., (2015). Haploinsufficiency for BRCA1 leads to cell-type-specific genomic instability and premature senescence. *Nat. Commun.* **6**, 7505. <https://doi.org/10.1038/ncomms8505>.
 113. Dias, M.P., Tripathi, V., van der Heijden, I., Cong, K., Manolika, E.-M., Bhin, J., Gogola, E., Galanos, P., et al., (2021). Loss of nuclear DNA ligase III reverts PARP inhibitor resistance in BRCA1/53BP1 double-deficient cells by exposing ssDNA gaps. *Mol. Cell* **81**, 4692–4708.e9. <https://doi.org/10.1016/j.molcel.2021.09.005>.
 114. Pettitt, S.J., Krastev, D.B., Brandsma, I., Dréan, A., Song, F., Aleksandrov, R., Harrell, M.I., Menon, M., et al., (2018). Genome-wide and high-density CRISPR-Cas9 screens identify point mutations in PARP1 causing PARP inhibitor resistance. *Nat. Commun.* **9**, 1849. <https://doi.org/10.1038/s41467-018-03917-2>.
 115. Guillemette, S., Serra, R.W., Peng, M., Hayes, J.A., Konstantinopoulos, P.A., Green, M.R., Cantor, S.B., (2015). Resistance to therapy in BRCA2 mutant cells due to loss of the nucleosome remodeling factor CHD4. *Genes Dev.* **29**, 489–494. <https://doi.org/10.1101/gad.256214.114>.
 116. Pettitt, S.J., Frankum, J.R., Punta, M., Lise, S., Alexander, J., Chen, Y., Yap, T.A., Haider, S., et al., (2020). Clinical BRCA1/2 reversion analysis identifies hotspot mutations and predicted neoantigens associated with therapy resistance. *Cancer Discov.* **10**, 1475–1488. <https://doi.org/10.1158/2159-8290.cd-19-1485>.
 117. Vegliante, R., Pastushenko, I., Blanpain, C., (2022). Deciphering functional tumor states at single-cell resolution. *EMBO J.* **41**, e109221. <https://doi.org/10.15252/embj.2021109221>.

At the crossroads of RNA biology, genome integrity and cancer



Summary

This article is the synthesis of the scientific presentations that took place during two international courses at Institut Curie, one on post-transcriptional gene regulation and the other on genome instability and human disease, that were joined together in their 2021 edition. This joined course brought together the knowledge on RNA metabolism and the maintenance of genome stability.

Keywords RNA; Post-transcriptional regulation; Genome instability; DNA damage; DNA repair; R-loops

Abbreviations

mRNAs	messenger RNAs
mNET-seq	mammalian Native Elongating Transcript sequencing
POINT-seq	Polymerase Intact Nascent Transcript sequencing
RNAPII	RNA Polymerase II
poly(A) tail	polyadenylate tail
CPA	Cleavage and Polyadenylation
CPF	Cleavage and Polyadenylation Factor
RBPs	RNA Binding Proteins
EJC	Exon Junction Complex
NMD	Nonsense mediated decay
NIN	Ninein
ROS	Reactive oxygen species
OOPs	Orthogonal Organic Phase separation
SG	Stress Granules
RNP	ribonucleoprotein
tRNAs	transfer RNAs
rRNAs	ribosomal RNAs
DDR	DNA damage response
PARPi	poly-ADP ribose polymerase 1 inhibitor
QIBC	quantitative imaging based cytometry
MiDAS	Mitotic DNA synthesis
OK-seq	Okazaki fragments sequencing
DSB	DNA double strand break
HR	Homologous recombination
NHEJ	Non-homologous end joining
ssDNA	Single stranded DNA
TAD	Topologically associated domain
IPA	intronic polyadenylation
UV-C	ultraviolet C
diIncRNAs	Damage-induced long non coding RNAs
DRIP	DNA-RNA immunoprecipitation

The mutual interactions between RNA metabolism and the DNA damage response have gained particular interest over the recent years and entail important clinical implications. This has led the organizers of two international courses at Institut Curie ("5th Course on Post transcriptional gene regulation" and

"3rd Course on Genome integrity and human diseases") to exceptionally join their efforts. On the one hand, the "post transcriptional gene regulation" course focuses on the study of post transcriptional regulations, from molecular mechanisms to genome wide networks. On the other, the "genome integrity and human disease" course aims to introduce basic mechanisms contributing to the maintenance of genome stability from molecular mechanisms up to omics approaches. Here, we discuss some of the highlights of this 7 day course, sponsored by Institut Curie and Société Française du Cancer, that took place in real time virtual format in April 12–20 2021.

Post-transcriptional gene regulation

Post-transcriptional regulation plays an important role in controlling gene expression by subjecting precursor of messenger RNAs (mRNAs) called pre-mRNAs to a host of maturation events (*i.e.* splicing and polyadenylation) before being exported to the cytoplasm. Pre-mRNA splicing mainly occurs co transcriptionally. The lab of Maria Carmo Fonseca (Instituto de Medicina Molecular João Lobo Antunes, PT) has contributed to determining splicing kinetics in Metazoans by using several technologies. Live cell imaging of stable transgenes showed a transcription rate of about 4 kilobases per minute and a splicing reaction lasting only for a few seconds [1]. More recently, through genome wide analyses of nascent transcripts in human cells with the mNET-seq (mammalian native elongating transcript sequencing) and POINT-seq (polymerase intact nascent transcript sequencing) techniques, her team showed that for most introns, splicing takes place co transcriptionally, immediately after the 3' splice site is transcribed by RNA polymerase II (RNAPII) [2,3]. However, for some introns splicing is delayed. These data raise questions about the molecular mechanisms underlying such different splicing kinetics, and their consequences on gene expression, alternative splicing regulation and, potentially, DNA-RNA hybrid formation and genome stability (which are discussed below). Besides splicing, another key step of pre-mRNA maturation is 3' end processing, which generally consists in-RNA cleavage at the polyadenylation site and in the addition of a polyadenylate tail (poly[A] tail), that is not encoded in DNA. This cleavage and polyadenylation (CPA) process is coupled to transcription termination. In addition, the poly(A) tail promotes the nucleo-cytoplasmic export, translation and stability of the mRNA, and is the substrate of deadenylases that trigger mRNA degradation. The lab of Lori Passmore (MRC Laboratory of Molecular Biology, Cambridge, UK) determined the molecular structure of a key multiprotein component of the yeast CPA machinery, Cleavage and Polyadenylation Factor (CPF), by using *in vitro* reconstitution

experiments, cryo-electron microscopy and X-ray crystallography [4,5]. They also determined the structural determinants of poly(A) tail recognition by two deadenylases [6]. These studies provided insights into the molecular mechanisms of CPA and deadenylation processes in yeast, with implications for human cells since most protein components of these machineries are highly conserved in humans. Moreover, both polyadenylation (e.g., FIP1L1, CPSF3/CPSF73, NUDT21/CFIm25) and deadenylation factors (e.g., CCR4-NOT complex components) have been involved in cancer [7,8]. In this context, recent work from Lori Passmore and collaborators showed that CPSF3 is a druggable node in acute myeloid leukemia and Ewing sarcoma [9].

During co-transcriptional RNA processing, RNA-binding proteins (RBPs) are deposited on transcripts, and some of them follow mRNAs into the cytoplasm and impact their fate. This is the case of the exon junction complex (EJC), a protein complex that is deposited on transcripts during splicing and promotes their nucleo-cytoplasmic export and translation. The EJC is best known for its role in triggering nonsense mediated decay (NMD) of mRNAs that have a premature stop codon located upstream of the last exon junction, which is the case of many aberrant transcripts that are produced by mutated genes or upon splicing factor mutations in diseases like cancer. About twenty years ago, Hervé Le Hir (now at Institut de Biologie of ENS, Paris, FR) discovered the EJC and its role in various processes, including NMD, mRNA export, translation and specific localization within the cytoplasm [10]. More recently, his lab showed that the EJC is localized at basal bodies during ciliogenesis in mouse neural stem cells and mediates the localization of the NIN (ninein) mRNA to centrioles, that form basal bodies and where the NIN protein plays a key function. Furthermore, EJC down-regulation impairs ciliogenesis [11]. These findings may explain the involvement of the EJC in neural stem cell division and human neurodevelopmental disorders.

Once in the cytoplasm, mRNAs are subjected to translational regulation. Alterations in the mRNA translation machinery can impact diverse cellular aspects, such as cell proliferation and metabolism. Davide Ruggero (UCSF Helen Diller Family Comprehensive Cancer Center, US) presented the activity of a general translation initiation factor, eIF4E, that binds to the "cap" structure located at the 5' end of all mRNAs. His lab showed that eIF4E is essential for translating a subset of mRNAs implicated in the regulation of intracellular ROS levels, which is critical for tumour cell survival. Interestingly, recently they demonstrated that eIF4E heterozygous mice are resistant to diet-induced obesity, suggesting that diminished eIF4E levels can promote enhanced metabolic fitness [12].

Anne Willis (MRC Toxicology Unit, University of Cambridge, UK) provided evidence that mRNA translation of ribosomal proteins and nuclear encoded mitochondrial factors is altered in malignant mesothelioma [13]. In an effort to identify RBPs involved in the cellular response to toxic injury and external stress, Anne

Willis also presented the development of experimental approaches such as Orthogonal Organic Phase Separation (OOPs) that allows to discriminate RNA-bound proteins [14]. mRNA translation is also modified upon stress induction within stress induced membrane-less organelles, so called stress granules (SG). Jeffrey A Chao (Friedrich Miescher Institute for Biomedical Research, Basel, CH) presented an elegant technique based on single molecule imaging to analyse mRNA translation in living cells. In contrast to the current model that postulates mRNA translation is inhibited in SG, he showed that translation in SG is not a rare event, and that the SG environment does not directly inhibit translation [15].

The link between cytoplasmic membrane-less ribonucleoprotein (RNP) granules and mRNA fate was presented by Dominique Weil (Institute of Biology Paris Seine, Paris, FR) who focuses on P-bodies. Her contribution in the development of a method to purify these granules enabled the characterization of RNA and protein content present in P-bodies using RNA-Seq and mass spectrometry, respectively. The comparison of the transcriptome of P-bodies before or after silencing mRNA decay or other repression factors revealed that GC content shapes mRNA storage and decay. Indeed, AU-rich and GC-rich mRNAs globally follow different decay pathways and the global GC content of mRNAs in P-bodies are closely linked to mRNA stability, translation rate, RBP and miRNA binding [16]. This study proposes an integrated view of the post transcriptional control of mRNA translation and mRNA stability.

More than just an mRNA storage compartment, P-bodies have been discovered to be implicated in a variety of polarized and non-polarized cells to compartmentalize protein synthesis. Florence Besse (Institut de Biologie Valrose, FR) has evidence that the targeting of the transcripts to their destination is operated by RNP granules which contain RNA cargo and regulatory proteins [17]. Using high resolution live imaging techniques, she showed that the targeting of mRNAs in neuronal RNP granules is a dynamic and reversible mechanism [18]. She has also found that defects in this process are linked to neurodegenerative diseases.

More than 150 chemical modifications of RNAs have recently been identified [19], which includes N6 methyladenosine (m6A), the most widespread modification on mammalian mRNAs, pseudouridine (X), ribose methylations (Nm), N1-methyladenosine (m1A), 5-methylcytidine (m5C), N-7 methylguanosine (m7G) and N-4 acetylcytidine (ac4C) among many others. These modifications harbor the potential of regulating the properties of RNAs and have emerged as critical regulators of gene expression, highlighting the importance of understanding their nature and role in biology and disease [20]. Although N4 acetylcytidine (ac4C) is possibly one of the most highly conserved mechanisms of enzymatic modification of RNA, especially in tRNAs and rRNAs, the function of this cytidine acetylation, as well as its role in biology and disease, have yet to be

elucidated [21]. Shraga Schwartz (Weizmann Institute of Science, Rehovot, IL) presented a novel chemical approach for quantitative mapping of ac4 C at single nucleotide resolution in order to study hyperthermophiles archaea. With this new insight, ac4 C appeared as an essential modification for these microorganisms to resist extreme temperatures [21].

Recent advances in the DNA damage response

Many chemotherapeutic drugs used in combination with radiotherapy kill cancer cells by damaging DNA, and many of them, target DNA replication based processes given the highly replicative nature of cancer cells. Moreover, the DNA damage response (DDR) factors and the pathways themselves are potential targets to improve anti cancer therapies. Such strategy is beautifully illustrated by the clinical use of PARP inhibitors (PARPi) that target the DNA damage sensors poly-ADP-ribose polymerase 1 and 2 (PARP1/2). Dr Matthias Altmeyer (Department of Molecular Mechanisms of Disease, University of Zurich, CH) uses quantitative imaging based cytometry (QIBC), a high-content microscopy approach to quantify the chromatin association of DDR factors and relevant parameters such as cytotoxicity according to cell cycle progression in single cells. Applying QIBC to investigate the cell response to PARPi, Dr Altmeyer revealed that these drugs have an impact outside S-phase specific DNA damage response. By testing a panel of cell lines, it was possible to predict PARPi resistance or hypersensitivity and to delineate distinct cell responses to different PARPi in a quantitative manner [22]. One deleterious consequence of failures in S-phase progression is unfinished DNA replication resulting in under-replicated regions, also known as fragile sites, when cells enter mitosis. To overcome unfinished DNA replication, a process named MiDAS (Mitotic DNA synthesis) is active in mitosis to replicate under-replicated regions using a form of break induced-replication [23]. Briefly, under-replicated DNA is cleaved by various endonucleases, generating a break from which DNA synthesis is initiated in a conservative mode, as opposed to the canonical semi conservative DNA synthesis. If MiDAS fails, 53BP1 nuclear bodies shield inherited genomic lesions from repair or degradation in G1. As a consequence of the inherited genomic lesions, the innate immune response can be activated through cGAS-TING pathway. Overall, the use of single cell experiments combined with technologies to map fragile sites and their behavior in a cell cycle specific manner provides a better description and understanding of the DDR.

Dr Chunlong Chen (Institut Curie, FR) has presented how genome-wide studies help to understand the dynamics of DNA replication in normal and challenged conditions. His lab focuses on understanding the spatio-temporal program of the human genome aiming to better understand how this program is deregulated in cancer cells or can be targeted to improve anti-cancer therapies. Deregulation of the DNA replication program threatens genome stability and is often observed in cancer cells.

Chen's team has pioneered the development of deep sequencing of Okazaki fragments (OK Seq), that mark the synthesis of the lagging strand, thus providing crucial information about replication fork directionality genome-wide [24]. His team has also developed the Repli-Seq approach that allows the timing and replication dynamics of any specific locus to be investigated [25]. Combining these approaches, Dr Chen has presented how gene transcription landscape impact on DNA replication dynamics with the emerging concept that transcription during S-phase is a source of replication stress leading to recurrent genome instability when transcription replication conflicts are not dealt with properly [26]. For example, his results have confirmed the concept that large genes embedding long-transcription units strongly delay replication completion resulting in fragile sites at which DNA synthesis is not completed before cells enter mitosis.

The most toxic DNA lesions induced by anticancer therapies are DNA double strand breaks (DSB) which are repaired either by the non-homologous end-joining (NHEJ) or homologous recombination (HR) pathway. This last pathway has been the focus of intense research since inactivation of HR (caused by BRCA1 or BRCA2 mutations for example) leads to predisposition to breast and ovarian cancers. Repair pathway choice between NHEJ and HR is under the control of several factors that prevent or favor the resection of a DSB in which single stranded DNA (ssDNA) is generated, a process essential for HR-dependent repair. The presentation of Dr Dipanjan Chowdhury (Division of Radiation and Genome Stability, Dana Farber Cancer Institute, Boston, US) highlighted a novel factor involved in the resection of DSBs, identified in a loss of function CRISPR screen. This screen was focused on the identification of factors causing PARPi resistance or platinum-based therapy in BRCA mutated cell lines. This screen led to the discovery of DYNLL1 as a novel inhibitor of DSB end-resection [27]. Mechanistically, DYNLL1 interacts with the nuclease MRE11 (which mutations cause Ataxia Telangiectasia like disorder) to impair its activity. Moreover, decrease in DYNLL1 expression in carcinomas with low BRCA1 expression reduced genomic alterations. Together, this work highlights an important new factor in DSB-repair influencing responses to cancer therapies.

The substrate of the DDR is not the naked DNA but the chromatin, which plays a pivotal role in the signalling of DSB and their repair. The team of Gaëlle Legube (CBI, Toulouse, FR) has a particular interest in understanding how chromatin folding and modifications trigger the DDR. To do so, the team has developed unique tools to induce ≈ 100 DSBs (DIVA) in cells and to analyse their signalling and repair according to the chromatin landscape [28]. The research of Legube's team previously reported that DSB within transcriptionally active regions are preferentially repaired by the HR pathway and that DSB mobility, clustering and nuclear positioning are key determinants of repair pathway choice [29–31]. More recently, her team has revealed how

chromatin folding impacts early sensing of DSBs. One of the first events at DSB sites is the phosphorylation of the histone variant H2AX by the sensor kinase ATM (mutations of which cause Ataxia Telangiectasia disorder), a histone modification known as γ H2AX. γ H2AX is visible in the form of sub-nuclear foci since this modification can spread up to 50 kb around the site of the DSB. The mechanistic insight into the rapid spreading of γ H2AX around DSB sites was missing. Gaëlle Legube presented her most recent research explaining that topologically associated domains (TAD), that are self-interacting genomic regions, are pivotal to establish the early steps of the DDR. TAD boundaries assist in the establishment of γ H2AX via one-sided cohesion-mediated loop extrusion on both sides of the DSB [32]. Taken together, she proposes that TADs are functional units of the DDR to establish γ H2AX chromatin domains that promote DSB signalling and repair foci.

The links between DNA damage and RNA biology

It is now well established that DNA damage widely impacts gene expression at the level of transcription, but also at multiple post-transcriptional levels [33]. In particular, Martin Dutertre (Institut Curie, FR) showed that alternative splicing is widely regulated in cancer cell response and resistance to genotoxic anticancer agents, such as topoisomerase inhibitors [34-36]. In recent years, many genes have been found to contain alternative polyadenylation sites within annotated introns, and their use generates so-called intronic polyadenylation (IPA) isoforms with alternative last exons. Martin Dutertre showed that IPA isoforms are widely regulated by camptothecin and doxorubicin (topoisomerase I and II inhibitors, respectively) but with different genome-wide patterns: mainly, down-regulation events in the case of doxorubicin, and equal proportions of up- and down-regulation events in the case of camptothecin [35]. He also presented data showing the widespread regulation of IPA isoforms by cisplatin, another genotoxic anticancer agent. IPA isoform regulation is enriched in genes related to the DDR, cell cycle and cell death, and he identified IPA isoforms that impact cell sensitivity to genotoxic agents. In addition, while the regulation of IPA isoforms has been mainly studied at the level of transcript synthesis, splicing and polyadenylation, he presented unpublished genome-wide analyses of their cytoplasmic regulation and of their translation status, by using 3'-seq (RNA-seq focused on the 3' end of polyA+ RNA) on subcellular compartments and polysome fractions. These analyses reveal diverse fates and translational outcomes of IPA isoforms. Finally, he discussed the increasing evidence for reciprocal links between pre-mRNA 3' end processing (cleavage and polyadenylation) and genome stability [37].

The regulation of gene expression at multiple levels by DNA-damaging agents has been particularly characterized in the case of ultraviolet C (UV-C) irradiation. Jesper Svejstrup (University of Copenhagen, DK) showed, by using genome-wide

GRO-seq analyses, that UV-C cell irradiation causes an inhibition of transcription elongation within 45 min. This is followed by an inhibition of transcription initiation within 2 to 4 hours due to RNAPII degradation. Finally, transcription restarts between 12 and 24 hours after irradiation thanks to RNAPII recovery, which is compromised in Cockayne syndrome B cells [38]. His lab also showed by RNA-seq analysis that elongation inhibition by UV-C irradiation is accompanied by an increase in the relative levels of IPA versus full-length mRNA isoforms in many long genes. In the *ASCC3* gene, IPA generates a transcript isoform with a non-coding function that antagonizes the function of the *ASCC3* protein-encoded by the full-length mRNA in transcription recovery following UV-C irradiation [39]. Jesper Svejstrup and his collaborators found that the *ASCC3* protein is also involved in the management of translational stress due to ribosome collisions [40]. Recently, they discovered that collided ribosomes are coactivators of cGAS, a sensor of cytosolic DNA that activates interferon-stimulated genes and thereby the innate immune response [41]. This finding may be relevant to understand inflammation caused by viral infections.

The links between genome stability and RNA biology are not limited to post transcriptional gene regulation by DNA damage. Indeed, in the last decade, non-coding RNAs have emerged as pivotal players in the maintenance of genome stability in response to DNA damage (see also next section). Dr Fabrizio d'Adda di Fagagna (IFOM, Milano, IT) has made major discoveries in this field by establishing that DSBs are actively transcribed by RNAPII although some details of this mechanism remain to be elucidated [42]. His team has proposed that RNAPII is recruited to DSB to generate ncRNAs named damage induced long non-coding RNAs (dilncRNAs) that are important to foster DSB signaling and DDR foci by a liquid phase-separation process [43]. The inhibition of dilncRNAs using antisense oligonucleotides (called AOS) lead to site-specific inhibition of the DDR, affecting DSB repair by NHEJ and HR. These results bring about the concept that DSB-induced transcription is essential to fully activate the DDR. Moreover, the use of telomere specific AOS to inhibit the DDR induced by telomere shortening restored tissue homeostasis in animal models, providing a potential clinical option to treat diseases associated to accelerated aging [44,45]. Finally, Dr Fabrizio d'Adda di Fagagna presented his recent work on the mechanism of recruitment of RNAPII to DSBs: he showed that RNAPII recruitment requires the MRN complex which cleaves the dsDNA providing an entry point for RNAPII binding and transcription initiation [46]. Monika Gullerova (University of Oxford, UK) has also contributed to describe how ncRNAs are generated at DSBs. Her lab showed that in human and mouse cells, a fraction of the endoribonuclease Dicer—which is best known for its cytoplasmic role in microRNA processing—is present in the nucleus, phosphorylated upon DNA damage, recruited to DSBs, and processes damage induced dsRNA

[47,48]. Furthermore, she showed that Dicer depletion delays the DDR by impaired recruitment of repair factors MDC1 and 53BP1 [48]. She presented novel work pertaining to a novel noncanonical pathway of ncRNA processing by Dicer. RNA-containing structures such DNA-RNA hybrids or ribonucleotide insertions have recently emerged as essential players in the maintenance of genome integrity. RNA in the form of R-loops is the subject of study of Fred Chédin lab (UC Davis, US). These 3-stranded nucleic acid structures are composed of a DNA-RNA hybrid and a displaced ssDNA strand which form co transcriptionally. R-loops have physiological roles such as transcription regulation but may also impose pathological consequences for the cell. The Chedin lab has pioneered several high-throughput technologies based on DRIP (DNA-RNA immunoprecipitation) such as DRIP-seq and DRIPc-seq to map R-loops at the single molecule level in the mammalian genome using the RNA-DNA hybrid specific antibody S9.6. Using these technologies, they have found that there are around 300 R-loops/per cell and that R-loops are on average \approx 300 bp in size. Chedin focused

his talk on the physiological role of R-loops: these functions include helping to pause the RNA pol II as well as transcription termination. Interestingly, he introduced the concept that these structures can transiently absorb or relax negative super-coiling which in turn may impact promoter activation and/or replication origin firing. Super helicity also drives R-loop formation; thus, the dynamic formation and resolution of R-loops may contribute to the regulation of gene expression genome wide acting as an epigenetic mark [49,50]. R-loops can be a source of genome instability in particular in the context of replication, the focus of Karlene Cimprich team (Stanford University, USA). In their lab, they recently developed a technique based on DRIPseq called qDRIP which allows not only strand specific mapping of DNA-RNA hybrids as DRIPc-seq but facilitates the comparison of the DNA-RNA hybrid content between different biological conditions using synthetic DNA-RNA hybrids as internal standards [51]. Although most laboratories have studied R-loops in the nuclear compartment, one of Cimprich's lab most surprising recent findings is the presence of

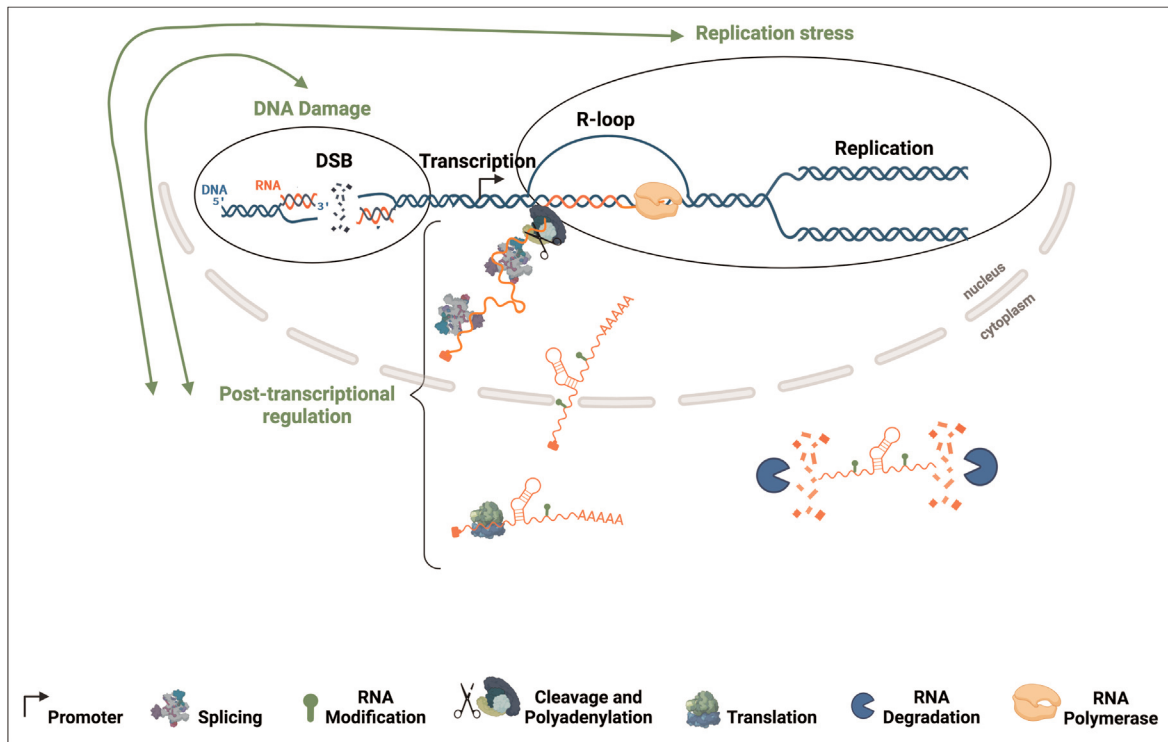


FIGURE 1
Reciprocal links between RNA biology and genome integrity. Some RNA molecules are produced at sites of double-strand DNA breaks and promote the recruitment of repair factors. R-loops, which are made of DNA-RNA hybrids and a displaced DNA strand, are involved in transcription-replication conflicts, leading to replication stress and DNA damage. Defects in pre messenger RNA splicing and cleavage/polyadenylation, which are generally coupled to transcription, can favor DNA damage. DNA damage signaling widely impacts post-transcriptional steps of gene expression, including RNA splicing, cleavage/polyadenylation, modification, export, localization, translation and degradation, all of which contribute to the regulation of genes involved in the DNA damage response (DDR). DNA is depicted in blue and RNA in orange. DSB, double-strand DNA break (Created with BioRender.com).

R-loops also in the cytoplasm. The role of these R-loops, how they form and why is currently under investigation.

Contributing to the question of the origin of R-loops tackled by Chedin and Cimprich labs; Benoit Palancade (Institut Jacques Monod, FR) described a series of elegant experiments performed in the yeast *S. cerevisiae* model system to demonstrate that R-loops form preferentially in intron-less genes and reciprocally, intronic sequences protect from R loop formation [52]. These findings have led his team to hypothesize that introns protect from genome instability. In his talk, Benoit Palancade also brought up one of the conundrums in the field that is whether DNA-RNA hybrids are an obstacle or a necessary intermediate for DSB repair: He discussed that nascent RNA at DSBs may serve as a template for repair by HR in a process he describes as transcription associated recombination (TAR); whereas other labs have shown that the accumulation of DNA RNA hybrids during transcription can have deleterious consequences for genetic integrity, as mentioned above. This conundrum was further discussed by Aura Carreira (Institut Curie, FR). Her lab recently focused on the RNA helicase DDX5, a novel partner of the breast cancer susceptibility protein BRCA2. Her team found that BRCA2 and DDX5 localize at DNA RNA hybrids at induced DSBs of actively transcribed regions. Using a missense variant of BRCA2 detected in breast cancer patients that reduces the association between the two proteins, they could show that BRCA2 and DDX5 cooperate to resolve DNA-RNA hybrids at DSBs whereas in cells bearing the variant repair by HR is delayed [53]. Thus, in this scenario, DNA-RNA hybrids appear to be deleterious for repair by HR.

In conclusion, this course has underscored the multiple and reciprocal links between RNA biology and genome integrity (figure 1). Indeed, DNA damage and replication stress widely impact gene expression and RNA metabolism at multiple post-transcriptional levels. Conversely, post transcriptional regulation of DDR genes impacts genome integrity; moreover, RNA processing-which is extensively coupled to transcription and chromatin-is involved in both the generation and repair of DNA damage. The study of these links is a recently expanding field that enhances our understanding of genome biology (by integrating genome expression, replication and integrity) and sheds new light on the molecular mechanisms of cancer development and therapy.

Disclosure of interest: the authors declare that they have no competing interest.

References

- [1] Martin RM, Rino J, Carvalho C, Kirchhausen T, Carmo Fonseca M. Live cell visualization of pre mRNA splicing with single molecule sensitivity. *Cell Rep* 2013;4:1144-55. <http://dx.doi.org/10.1016/j.celrep.2013.08.013>.
- [2] Nojima T, Gomes T, Grosso ARF, Kimura H, Dye MJ, Dhir S, et al. Mammalian net seq reveals genome wide nascent transcription coupled to rna processing. *Cell* 2015;161:526-40. <http://dx.doi.org/10.1016/j.cell.2015.03.027>.
- [3] Sousa Luís R, Dujardin G, Zukher I, Kimura H, Weldon C, Carmo Fonseca M, et al. Point technology illuminates the processing of polymerase associated intact nascent transcripts. *Mol Cell* 2021;81:1935-50. <http://dx.doi.org/10.1016/j.molcel.2021.02.034>.
- [4] Casañal A, Kumar A, Hill CH, Easter AD, Emsley P, Degliesposti G, et al. Architecture of eukaryotic mRNA 3' end processing machinery. *Science* 2017;358:1056-9. <http://dx.doi.org/10.1126/science.aao6535>.
- [5] Hill CH, Boreikait V, Kumar A, Casañal A, Kubik P, Degliesposti G, et al. Activation of the endonuclease that defines mrna 3' ends requires incorporation into an 8 subunit core cleavage and polyadenylation factor complex. *Mol Cell* 2019;73:1217-31. <http://dx.doi.org/10.1016/j.molcel.2018.12.023>.
- [6] Tang TTL, Stowell JAW, Hill CH, Passmore LA. The intrinsic structure of poly (A) RNA determines the specificity of Pan2 and Caf1 deadenylases. *Nat Struct Mol Biol* 2019;26:433-42. <http://dx.doi.org/10.1038/s4159401902279>.
- [7] Nourse J, Spada S, Danckwardt S. Emerging roles of rna 3' end cleavage and polyadenylation in pathogenesis, diagnosis and therapy of human disorders. *Biomolecules* 2020;10:915. <http://dx.doi.org/10.3390/biom10060915>.
- [8] Chalabi Hagkarim N, Grand RJ. The regulatory properties of the Ccr4-not complex. *Cells* 2020;9:2379. <http://dx.doi.org/10.3390/cells9112379>.
- [9] Ross NT, Lohmann F, Carbonneau S, Fazal A, Weihofen WA, Gleim S, et al. CPSF3 dependent pre-mRNA processing as a druggable node in AML and Ewing's sarcoma. *Nat Chem Biol* 2020;16:50-9. <http://dx.doi.org/10.1038/s4158901904241>.
- [10] Hir HL, Saulière J, Wang Z. The exon junction complex as a node of post transcriptional networks. *Nat Rev Mol Cell Biol* 2016;17:41-54. <http://dx.doi.org/10.1038/nrm.2015.7>.
- [11] Kwon OS, Mishra R, Safieddine A, Coleno E, Alasseur Q, Faucourt M, et al. Exon junction complex dependent mRNA localization is linked to centrosome organization during ciliogenesis. *Nat Commun* 2021;12:1351. <http://dx.doi.org/10.1038/s4146702121590w>.
- [12] Conn CS, Yang H, Tom HJ, Ikeda K, Oses Prieto JA, Vu H, et al. The major cap binding protein eIF4E regulates lipid homeostasis and diet induced obesity. *Nat Metab* 2021;3:244-57. <http://dx.doi.org/10.1038/s4225502100349z>.
- [13] Grosso S, Marini A, Gyuraszova K, Voorde JV, Sfakianos A, Garland GD, et al. The pathogenesis of mesothelioma is driven by a dysregulated translatome. *Nat Commun* 2021;12:4920. <http://dx.doi.org/10.1038/s41467021251737>.
- [14] Villanueva E, Smith T, Queiroz RML, Monti M, Pizzinga M, Elzek M, et al. Efficient recovery of the RNA bound proteome and protein bound transcriptome using phase separation (OOPS). *Nat Protoc* 2020;15:2568-88. <http://dx.doi.org/10.1038/s4159602003442>.
- [15] Mateju D, Chao JA. Stress granules: regulators or by-products? *FEBS J* 2021;15821. <http://dx.doi.org/10.1111/febs.15821>.
- [16] Courel M, Clément Y, Bossevain C, Foretek D, Vidal Cruchez O, Yi Z, et al. GC content shapes mRNA storage and decay in human cells. *ELife* 2019;8:e49708. <http://dx.doi.org/10.7554/eLife.49708>.
- [17] Pushpalatha KV, Besse F. Local translation in axons: when membraneless rnp granules meet membrane bound organelles. *Front Mol Biosci* 2019;6:129. <http://dx.doi.org/10.3389/fmolb.2019.00129>.
- [18] Formicola N, Heim M, Dufourt J, Lancelot AS, Nakamura A, Lagha M, et al. Correction: tyramine induces dynamic RNP granule remodeling and translation activation in the Drosophila brain. *ELife* 2021;10:e70755. <http://dx.doi.org/10.7554/eLife.70755>.
- [19] Boccaletto P, Machnicka MA, Purta E, Piłkowskij P, Bagiński B, Wirecki TK, et al. Modomics: a database of RNA modification pathways. 2017 update. *Nucleic Acids Res* 2018;46:D303-7. <http://dx.doi.org/10.1093/nar/gqx1030>.

- [20] Schwartz S. Cracking the epitranscriptome. *RNA* 2016;22:169–74. <http://dx.doi.org/10.1261/rna.054502.115>.
- [21] Sas Chen A, Thomas JM, Matzov D, Taoka M, Nance KD, Nir R, et al. Dynamic RNA acetylation revealed by quantitative cross evolutionary mapping. *Nature* 2020;583:638–43. <http://dx.doi.org/10.1038/s4158602024182>.
- [22] Michelenaj, Lezaja A, Teloni F, Schmid T, Imhof R, Altmeyer M. Analysis of PARP inhibitor toxicity by multidimensional fluorescence microscopy reveals mechanisms of sensitivity and resistance. *Nat Commun* 2018;9:2678. <http://dx.doi.org/10.1038/s41467018050319>.
- [23] Lezaja A, Altmeyer M. Dealing with DNA lesions: when one cell cycle is not enough. *Curr Opin Cell Biol* 2021;70:27–36. <http://dx.doi.org/10.1016/jceb.2020.11.001>.
- [24] Petryk N, Kahli M, d'Aubenton Carafa Y, Jaszczyszyn Y, Shen Y, Silvain M, et al. Replication landscape of the human genome. *Nat Commun* 2016;7:10208. <http://dx.doi.org/10.1038/ncomms10208>.
- [25] Brison O, El Hilali S, Azar D, Koundrioukoff S, Schmidt M, Nähse V, et al. Transcription mediated organization of the replication initiation program across large genes sets common fragile sites genome-wide. *Nat Commun* 2019;10:5693. <http://dx.doi.org/10.1038/s41467019136745>.
- [26] Promonet A, Padioulet I, Liu Y, Sanz L, Biernacka A, Schmitz AL, et al. Topoisomerase 1 prevents replication stress at R loop enriched transcription termination sites. *Nat Commun* 2020;11:3940. <http://dx.doi.org/10.1038/s41467020178582>.
- [27] He YJ, Meghani K, Caron MC, Yang C, Ronato DA, Bian J, et al. DYNLL1 binds to MRE11 to limit DNA end resection in BRCA1 deficient cells. *Nature* 2018;563:522–6. <http://dx.doi.org/10.1038/s41586-018-06705>.
- [28] Clouaire T, Rocher V, Lashgari A, Arnould C, Aguirrebengoa M, Biernacka A, et al. Comprehensive mapping of histone modifications at dna double strand breaks deciphers repair pathway chromatin signatures. *Mol Cell* 2018;72:250–262.e6. <http://dx.doi.org/10.1016/j.molcel.2018.08.020>.
- [29] Aymard F, Aguirrebengoa M, Guillou E, Javierre BM, Bugler B, Arnould C, et al. Genome wide mapping of long range contacts unveils clustering of DNA double strand breaks at damaged active genes. *Nat Struct Mol Biol* 2017;24:353–61. <http://dx.doi.org/10.1038/nsmb.3387>.
- [30] Marnef A, Cohen S, Legube G. Transcription coupled DNA double strand break repair: active genes need special care. *J Mol Biol* 2017;429:1277–88. <http://dx.doi.org/10.1016/j.jmb.2017.03.024>.
- [31] Marnef A, Finoux AL, Arnould C, Guillou E, Daburon V, Rocher V, et al. A cohesin/HUSH and LINC-dependent pathway controls ribosomal DNA double strand break repair. *Genes Dev* 2019;33:1175–90. <http://dx.doi.org/10.1101/qad.324012.119>.
- [32] Arnould C, Rocher V, Finoux AL, Clouaire T, Li K, Zhou F, et al. Loop extrusion as a mechanism for formation of DNA damage repair foci. *Nature* 2021;590:660–5. <http://dx.doi.org/10.1038/s4158602103193z>.
- [33] Dutertre M, Lambert S, Carreira A, Amor Guéret M, Vagner S. DNA damage: RNA binding proteins protect from near and far. *Trends Biochem Sci* 2014;39:141–9. <http://dx.doi.org/10.1016/j.tibs.2014.01.003>.
- [34] Dutertre M, Sanchez G, De Cian MC, Barbier J, Dardenne E, Gradou L, et al. Cotranscriptional exon skipping in the genotoxic stress response. *Nat Struct Mol Biol* 2010;17:1358–66. <http://dx.doi.org/10.1038/nsmb.1912>.
- [35] Dutertre M, Chakrama FZ, Combe E, Desmet FO, Mortada H, Polay Espinoza M, et al. A recently evolved class of alternative 3' terminal exons involved in cell cycle regulation by topoisomerase inhibitors. *Nat Commun* 2014;5:3395. <http://dx.doi.org/10.1038/ncomms4395>.
- [36] Tanaka I, Chakraborty A, Saulnier O, Benoit Pilven C, Vacher S, Labiod D, et al. ZRANB2 and SYF2-mediated splicing programs converging on ECT2 are involved in breast cancer cell resistance to doxorubicin. *Nucleic Acids Res* 2020;48:2676–93. <http://dx.doi.org/10.1093/nar/qkz1213>.
- [37] Dutertre M, Sfaxi R, Vagner S. Reciprocal links between pre messenger RNA 3' end processing and genome stability. *Trends Biochem Sci* 2021;46:579–94. <http://dx.doi.org/10.1016/j.tibs.2021.01.009>.
- [38] Tufegdović Vidaković A, Mitter R, Kelly GP, Neumann M, Harreman M, Rodríguez Martínez M, et al. Regulation of the RNAPII pool is integral to the DNA damage response. *Cell* 2020;180:1245–61. <http://dx.doi.org/10.1016/j.cell.2020.02.009>.
- [39] Williamson L, Saponaro M, Boeing S, East P, Mitter R, Kantidakis T, et al. UV irradiation induces a non-coding RNA that functionally opposes the protein encoded by the same gene. *Cell* 2017;168:843–55. <http://dx.doi.org/10.1016/j.cell.2017.01.019>.
- [40] Juszkiewicz S, Speldewinde SH, Wan L, Svejstrup JQ, Hegde RS. The ASC 1 complex disassembles collided ribosomes. *Mol Cell* 2020;79:603–614.e8. <http://dx.doi.org/10.1016/j.molcel.2020.06.006>.
- [41] Wan L, Juszkiewicz S, Blears D, Bajpe PK, Han Z, Faull P, et al. Translation stress and collided ribosomes are co activators of cGAS. *Mol Cell* 2021;81:2808–22. <http://dx.doi.org/10.1016/j.molcel.2021.05.018>.
- [42] Michelini F, Pitchiaya S, Vitelli V, Sharma S, Gioia U, Pessina F, et al. Damage induced lncRNAs control the DNA damage response through interaction with DDRNAs at individual double strand breaks. *Nat Cell Biol* 2017;19:1400–11. <http://dx.doi.org/10.1038/ncb3643>.
- [43] Pessina F, Giavazzi F, Yin Y, Gioia U, Vitelli V, Galbiati A, et al. Functional transcription promoters at DNA double strand breaks mediate RNA driven phase separation of damage response factors. *Nat Cell Biol* 2019;21:1286–99. <http://dx.doi.org/10.1038/s4155601903924>.
- [44] Aguado J, Sola Carvajal A, Canela V, Revéchon G, Ong PF, Jones Weinert CW, et al. Inhibition of DNA damage response at telomeres improves the detrimental phenotypes of Hutchinson–Gilford Progeria syndrome. *Nat Commun* 2019;10:4990. <http://dx.doi.org/10.1038/s41467019130183>.
- [45] Di Micco R, Krizhanovsky V, Baker D, d'Adda di Fagnagna F. Cellular senescence in ageing: from mechanisms to therapeutic opportunities. *Nat Rev Mol Cell Biol* 2021;22:75–95. <http://dx.doi.org/10.1038/s4158002000314w>.
- [46] Sharma S, Anand R, Zhang X, Francia S, Michelini F, Galbiati A, et al. MRE11 RAD50 NBS1 complex is sufficient to promote transcription by rna polymerase II at double strand breaks by melting DNA ends. *Cell Rep* 2021;34:108565. <http://dx.doi.org/10.1016/j.celrep.2020.108565>.
- [47] Burger K, Gullerova M. Nuclear re localization of Dicer in primary mouse embryonic fibroblast nuclei following DNA damage. *PLoS Genet* 2018;14:e1007151. <http://dx.doi.org/10.1371/journal.pgen.1007151>.
- [48] Burger K, Schlackow M, Potts M, Hester S, Mohammed S, Gullerova M. Nuclear phosphorylated Dicer processes double stranded RNA in response to DNA damage. *J Cell Biol* 2017;216:2373–89. <http://dx.doi.org/10.1083/jcb.201612131>.
- [49] Chedin F, Benham CJ. Emerging roles for R loop structures in the management of topological stress. *J Biol Chem* 2020;295:4684–95. <http://dx.doi.org/10.1074/jbc.REV119.006364>.
- [50] Ginno PA, Lott PL, Christensen HC, Korfi I, Chédin F. R Loop formation is a distinctive characteristic of unmethylated human cpG island promoters. *Mol Cell* 2012;45:814–25. <http://dx.doi.org/10.1016/j.molcel.2012.01.017>.
- [51] Crossley MP, Bocek MJ, Hamperl S, Swigut T, Cimprich KA. qDRIP: a method to quantitatively assess RNA–DNA hybrid formation genome wide. *Nucleic Acids Res* 2020;48:e84. <http://dx.doi.org/10.1093/nar/qkaa500>.
- [52] Bonnet A, Grosso AR, Elkaoutari A, Coleno E, Presle A, Sridhara SC, et al. Introns protect eukaryotic genomes from transcription associated genetic instability. *Mol Cell* 2017;67:608–621.e6. <http://dx.doi.org/10.1016/j.molcel.2017.07.002>.
- [53] Sessa G, Gómez González B, Silva S, Pérez Calero C, Beaupere R, Barroso S, et al. BRCA2 promotes DNA RNA hybrid resolution by DDX5 helicase at DNA breaks to facilitate their repair. *EMBO J* 2021;40. <http://dx.doi.org/10.15252/emboj.2020106018>.

Biswendu Biswas¹, Rady Chaaban¹, Shrena Chakraborty¹,
Alexandre Devaux¹, Ana Luisa Dian¹, Anna Minello¹, Jenny Kaur Singh¹,
Stephan Vagner, Patricia Uguen, Sarah Lambert, Martin Dutertre,
Aura Carreira

CNRS UMR 3348 Genome integrity, RNA and Cancer, Institut Curie,
University Paris-Saclay, 91401 Orsay, France

Correspondence: Patricia Uguen, CNRS UMR 3348 Genome integrity,
RNA and Cancer, Institut Curie, University Paris-Saclay, 91401 Orsay,
France

patricia.uguen@curie.fr
¹Equal contribution.

Received 20 December 2021
Accepted 21 February 2022
Available online: 18 May 2022

<https://doi.org/10.1016/j.bulcan.2022.02.014>